



# Thermoelectric Heat Recovery from Low Temperature Exhausts of Steel Processes

(THERELEXPRO)

*FINAL REPORT*

**Thermoelectric Heat Recovery from Low Temperature Exhausts of Steel Processes  
(THERELEXPRO)**

European Commission

Directorate-General for Research and Innovation

Directorate D - Industrial Technologies

Unit D.4 — Coal and Steel

Contact Hervé Martin

E-mail [RTD-PUBLICATIONS@ec.europa.eu](mailto:RTD-PUBLICATIONS@ec.europa.eu)

European Commission

B-1049 Brussels

Manuscript completed in 2019.

This document has been prepared for the European Commission however it reflects the views only of the authors, and the Commission cannot be held responsible for any use which may be made of the information contained therein.

More information on the European Union is available on the internet (<http://europa.eu>).

Luxembourg: Publications Office of the European Union, 2019

PDF

ISBN 978-92-79-98329-0

ISSN 1831-9424

doi: 10.2777/56474

KJ-NA-29-536-EN-N

© European Union, 2019.

Reuse is authorised provided the source is acknowledged. The reuse policy of European Commission documents is regulated by Decision 2011/833/EU (OJ L 330, 14.12.2011, p. 39).

For any use or reproduction of photos or other material that is not under the EU copyright, permission must be sought directly from the copyright holders.

All pictures, figures and graphs © RINA Consulting - Centro Sviluppo Materiali S.p.A., RFSR-CT-2013-00029 THERELEXPRO

European Commission

# Research Fund for Coal and Steel

## **Thermoelectric Heat Recovery from Low Temperature Exhausts of Steel Processes (THERELEXPRO)**

Ugo Chiarotti  
Valerio Moroli, Roberto Piancaldini, Fernando Menchetti,  
Fabio Nazzi, Massimiliano Gabriele  
**RINA Consulting - Centro Sviluppo Materiali S.p.A.**  
Via di Castel Romano 100, 00128 Roma - Italy

Juan José Arribas Ramirez  
**Arcelor Mittal España S.A.**  
Residencia La Granda s/n, 33418 Gozón (Asturias) – Spain

Min Gao, Jorge-García Cañadas, Tanuj Singh  
**Cardiff University**  
Newport Road 30-36, CF24ODE Cardiff – United Kingdom

Loris Bianco, Alberto Viotto, Giulia Baracchini, Daniele Gaspardo  
**Ferriere Nord S.p.A.**  
Via Zona Industriale Fraz. Rivoli, 33010 Osoppo (Udine) – Italy

Frank Mintus, Jacques Soons  
**VDEh-Betriebsforschungsinstitut**  
Sohnstrasse 65, 40237 Dusseldorf - Germany

Grant Agreement RFSR-CT-2013-00029  
01/07/2013 – 30/06/2016

### **Final report**

Directorate-General for Research and Innovation

## **Table of contents**

1	Final Summary .....	7
2	Scientific and technical description of the results .....	15
2.1	Objectives of the project .....	15
3	Description of activities and discussion .....	17
3.1	WP1 - Development, improvement and implementation of devices and modules .....	17
3.1.1	Task 1.1 - Development, characterization and implementation of thermoelectric devices/modules (all partners) .....	17
3.1.1.1	Identification of heat source and heat sink (all partners) .....	17
3.1.1.2	Prototype A: heat source and heat sink (CSM, FENO) .....	18
3.1.1.3	Prototype B: heat source and heat sink (AME, BFI) .....	20
3.1.1.4	Identification of prototypes general design (all partners) .....	27
3.1.1.5	Prototype A: general design (CSM, FENO) .....	27
3.1.1.6	Prototype B: general design (AME, BFI) .....	28
3.1.1.7	Selection of thermoelectric modules and components (CSM, CU, BFI) .....	33
3.1.1.8	Thermoelectric module design theory (CU) .....	35
3.1.1.9	Theoretical model at given $\Delta T$ (CU) .....	35
3.1.1.10	Theoretical model at given thermal input Q (CU) .....	37
3.1.1.11	Theoretical study to use the prototype A in the range 100°C-350°C (CSM, FENO) .....	38
3.1.1.12	Theoretical study to use the prototype B in the range 150°C-350°C (AME, BFI) .....	41
3.1.2	Task 1.2 - Development of tools for control and monitoring (CSM, CU, BFI) .....	42
3.1.2.1	Prototype A: tools for control and monitoring (CSM, FENO) .....	42
3.1.2.2	Prototype B: tools for control and monitoring (AME, BFI) .....	43
3.2	WP 2 - Construction of laboratory lab-scale "test bed" and laboratory tests .....	44
3.2.1	Task 2.1 - Construction of laboratory lab-scale "test bed" (CSM, CU, BFI) .....	44
3.2.1.1	Design and construction of CSM laboratory "test bed" (CSM) .....	44
3.2.1.2	Design and construction of Cardiff University laboratory "test bed" (CU) .....	46
3.2.1.3	Design and construction of BFI laboratory "test bed" (BFI) .....	49
3.2.2	Task 2.2 - First laboratory test of the thermoelectric prototypes (CSM, CU, BFI) .....	50
3.2.2.1	Prototype A: hydraulic pressure test (CSM) .....	50
3.2.2.2	Prototype A and B: thermoelectric module test (CU) .....	51
3.2.2.3	Prototype A: TEM electric power vs. load pressure (CSM) .....	53
3.2.2.4	Prototype B: electric power vs. modules pressure (torque) and thermal interface material (BFI) .....	54
3.2.2.5	Prototype B: electric power vs. electric resistance load (BFI) .....	55
3.2.2.6	Prototype B: electric power vs. module temperature difference (BFI) .....	56
3.2.2.7	Prototype A: final functional tests .....	58
3.2.2.8	Prototype B: final functional tests .....	58
3.3	WP3 - Analysis of the modules and identification of their structural weakness .....	59
3.3.1	Task 3.1 - Identification of the equipment weakness points (CSM, CU) .....	60
3.3.1.1	Maximum module compression test (CSM) .....	60
3.3.1.2	Different constructive methods of $\text{Bi}_2\text{Te}_3$ modules: advantages and disadvantages (CU) .....	60
3.3.1.3	Effect of exposure to increased temperatures (BFI) .....	62
3.3.2	Task 3.2 - Identification of the technological improvements (CSM, CU, BFI) .....	63
3.3.2.1	Hot side heat exchanger: thermal paste and graphite foil (BFI) .....	63
3.3.2.2	Electric power consumption optimization and electric load matching (CSM, CU) .....	64
3.3.3	Task 3.3 - Design of the final specifications (CSM, CU, BFI) .....	65
3.3.3.1	Prototype A: design of the final specifications (CSM, FENO) .....	65
3.3.3.2	Prototype B: design of the final specifications (AME, BFI) .....	67
3.4	WP4 - Design, construction and plant installation of the full-scale thermoelectric system .....	68
3.4.1	Task 4.1 - Final configuration of thermoelectric systems modules (all partners) .....	69
3.4.1.1	Final configuration of prototype A (CSM, FENO, CU) .....	69
3.4.1.2	Final configuration of prototype B (AME, BFI, CU) .....	69
3.4.2	Task 4.2 - Plant installation of the full-scale thermoelectric system (all partners) .....	71
3.4.2.1	Installation of prototype A at Ferriere Nord (CSM, FENO) .....	71
3.4.2.2	Installation of prototype B at Arcelor Mittal España (AME, BFI) .....	73

<b>3.5 WP5 – Execution of full-scale test and analysis of the thermoelectric system .....</b>	<b>75</b>
<b>3.5.1 Task 5.1 – On-line full-scale tests of the thermoelectric system prototypes (AME, FENO, CSM, BFI) .....</b>	<b>75</b>
<b>3.5.1.1 Prototype A: on-line full-scale test description (CSM, FENO).....</b>	<b>75</b>
<b>3.5.1.2 Prototype B: on-line full-scale test description (BFI, AME) .....</b>	<b>76</b>
<b>3.5.2 Task 5.2 – Assessment of the thermoelectric system performance (AME, FENO, CSM, BFI, CU) ...</b>	<b>78</b>
<b>3.5.2.1 Prototype A: data analysis and results obtained during on-line test (CSM, FENO).....</b>	<b>78</b>
<b>3.5.2.2 Prototype B: data analysis and results obtained during on-line test (BFI, AME).....</b>	<b>83</b>
<b>3.5.3 Task 5.3 – Estimation of the electricity production cost (CSM, AME, CU, FENO) .....</b>	<b>90</b>
<b>3.5.1.3 Method of electric energy cost calculation (CSM) .....</b>	<b>90</b>
<b>3.5.1.4 Comparison with different competing technologies (CSM, CU).....</b>	<b>92</b>
<b>3.5.4 Task 5.4 – Environmental benefits analysis (CSM, AME, CU, FENO) .....</b>	<b>96</b>
<b>3.5.2.3 Classification of thermoelectric materials (CSM, CU).....</b>	<b>96</b>
<b>3.5.2.4 Thermoelectric materials and their Earth's crust abundance (CSM, CU).....</b>	<b>98</b>
<b>3.5.2.5 Thermoelectric generators and their environmental impact (CSM, CU).....</b>	<b>100</b>
<b>3.5.2.6 Life Cycle Assessment (LCA) (all partners).....</b>	<b>101</b>
<b>3.6 WP6 – Coordination and dissemination.....</b>	<b>102</b>
<b>3.6.1 Project management and description of the activities (all partners).....</b>	<b>102</b>
<b>3.6.2 Result dissemination (all partners) .....</b>	<b>102</b>
<b>3.6.3 Result exploitation (all partners).....</b>	<b>102</b>
<b>Table of symbols .....</b>	<b>103</b>
<b>List of figures .....</b>	<b>105</b>
<b>List of tables .....</b>	<b>109</b>
<b>List of acronyms and abbreviations .....</b>	<b>111</b>
<b>List of references.....</b>	<b>113</b>
<b>Appendices .....</b>	<b>115</b>
<b>Annex A.1.....</b>	<b>115</b>
<b>Deliverable D1.1: Procedure of manufacturing the thermoelectric systems prototypes (CU): .....</b>	<b>115</b>
<b>A.1.1 Procedure of manufacturing the thermoelectric systems prototypes.....</b>	<b>115</b>
<b>Annex A.2.....</b>	<b>119</b>
<b>Deliverable D1.2: Description of the tools for modules control and monitoring (CSM, CU, BFI) .....</b>	<b>119</b>
<b>A.2.1 Prototype A: description of the tools for modules control and monitoring .....</b>	<b>119</b>
<b>A.2.2 Prototype B: description of the tools for modules control and monitoring .....</b>	<b>122</b>
<b>Annex A.3.....</b>	<b>125</b>
<b>Deliverable D2.1: Design of the lab-scale test bed (CSM, CU, BFI).....</b>	<b>125</b>
<b>A.3.1 Design of CSM lab-scale test bed .....</b>	<b>125</b>
<b>A.3.2 Design of CU lab-scale test bed .....</b>	<b>127</b>
<b>A.3.3 Design of BFI lab-scale test bed .....</b>	<b>129</b>
<b>Annex A.4.....</b>	<b>133</b>
<b>Deliverable D2.2: Description of lab-scale performance test results (CSM, CU, BFI) .....</b>	<b>133</b>
<b>A.4.1 CSM lab-scale performance test results.....</b>	<b>133</b>
<b>A.4.2 Cardiff University lab-scale performance test results.....</b>	<b>133</b>
<b>A.4.3 BFI lab-scale performance test results .....</b>	<b>137</b>
<b>Annex A.5.....</b>	<b>139</b>
<b>Deliverable D3.1: Weaknesses analysis of thermoelectric devices and the causes/mechanisms of degradation/failures (CSM, CU, BFI) .....</b>	<b>139</b>
<b>A.5.1 CSM weakness analysis .....</b>	<b>139</b>
<b>A.5.2 Cardiff University weakness analysis .....</b>	<b>139</b>
<b>A.5.3 BFI weakness analysis.....</b>	<b>144</b>
<b>Annex A.6.....</b>	<b>145</b>
<b>Deliverable D3.2: Description of the technological solutions to be implemented for improving the reliability and the performance of the systems (CSM, CU, BFI) .....</b>	<b>145</b>
<b>A.6.1 CSM identification of technological improvements (CSM) .....</b>	<b>145</b>
<b>A.6.2 Cardiff University identification of technological improvements (CU) .....</b>	<b>146</b>

A.6.3	BFI identification of technological improvements (BFI) .....	147
<i>Annex A.7</i>	.....	149
<b>Deliverable D3.3: Description of the final configuration of the thermoelectric modules (CSM, CU, BFI)</b>		149
A.7.1	Prototype A: thermoelectric modules assembling and characteristics.....	149
A.7.2	Prototype B: thermoelectric modules assembling and characteristics.....	151
<i>Annex A.8</i>	.....	153
<b>Deliverable D4.1: Design of the final configuration of the thermoelectric system (all partners)</b> .....		153
A.8.1	Prototype A: final configuration.....	153
A.8.2	Prototype B: final configuration.....	154
<i>Annex A.9</i>	.....	157
<b>Deliverable D4.2: Description of the activities for the plant test set up (all partners)</b> .....		157
A.9.1	Prototype A: set up of the TEG at plant site.....	157
A.9.2	Prototype B: set up of the TEG at plant site.....	159
<i>Annex A.10</i>	.....	163
<b>Deliverable D5.1: Description of the full-scale test results (AME, FENO, CSM, BFI)</b> .....		163
A.10.1	Prototype A: full-scale test results table.....	163
A.10.2	Prototype B: full-scale test results table.....	163
<i>Annex A.11</i>	.....	165
<b>Deliverable D5.2: Thermoelectric system performance analysis (AME, FENO, CSM, CU)</b> .....		165
A.11.1	Prototype A: performance analysis table .....	165
A.11.2	Prototype B: performance analysis table.....	165
<i>Annex A.12</i>	.....	167
<b>Deliverable D5.3: Thermoelectric system economic viability analysis (AME, FENO, CSM, CU)</b> .....		167
<i>Annex A.13</i>	.....	171
<b>Deliverable D5.4: Thermoelectric system environmental benefit analysis (AME, FENO, CSM, CU)</b> .....		171
<i>Annex A.14</i>	.....	185
<b>Deliverable D6.1: Description of the activities carried out in disseminating the results of the project (all partners)</b> .....		185



## **1 Final Summary**

This research focused on improving thermoelectric technology to recover waste heat (<350°C) from steel plants and convert it into electricity.

Thermoelectric generators have the ability of directly converting heat into electricity when a heat flux passes through them. Therefore, a complete thermoelectric generator system requires a hot source to provide the heat flux, and a cold sink to discharge the heat from the system.

The main objective of the project was to investigate the technical and economic performance of two power generators based on thermoelectric devices (TEG) installed in steel plants. The first prototype (prototype A) has been designed with the aim of recovering the waste heat from hot water in off-gas cooling system of an electric furnace, while the second (prototype B) has been designed with the objective of recovering waste thermal radiation energy from the surfaces of hot steel products.

Prototype A has been manufactured at CSM laboratories (Rome, Italy) and installed at Ferriere Nord plant in Osoppo (Italy). Prototype B has been manufactured at BFI laboratories (Dusseldorf, Germany) and installed at Arcelor Mittal plant in Gijon (Spain). Cardiff University (UK) participated actively in the design and modeling of both prototypes.

Figure 1.1 and Figure 1.2 show photographs of the locations in two plants selected to perform the on-line test.



**Figure 1.1** – Ferriere Nord plant, Italy



**Figure 1.2** – Arcelor Mittal plant, Spain

### **WP1 – Development, improvement and implementation of devices and modules**

Task 1.1: Prototype A was designed to work in a situation where the heat flux is obtained from an industrial water-cooling system. This scenario is very common at steel plants, where large amount of thermal energy has to be dissipated using dedicated cooling systems. These systems normally work with flowing fluids, usually water, at relative low temperature (< 100°C). Therefore, prototype A has been designed to use the fluids of a temperature below 100°C as the heat source. Theoretical calculations have also been carried out to check the working conditions at higher temperatures.

Prototype B was designed to work in a situation where the available heat is obtained from thermal energy radiated from surfaces of high temperature steel products that move around various places in the plant during different treatments. As this energy is available in the form of radiation, it can be only partially captured. Consequently, in this case, although the heat source has very high temperature, the heat flux through thermoelectric generator is limited, resulting in much lower temperature produced on the hot side of the thermoelectric module (generally <250°C).

The research program started with selecting suitable heat sources and heat sinks at the two industrial plants.

For Prototype A, due to the heat source was the cooling water of the EAF off-gas, it was necessary to define the exact location of the thermoelectric generators and the exact distance between the heat source and the generators, both of which have significant effect on the generator design. The temperatures of the heat source and the cold sink have been monitored over the whole testing period. The average temperature of the heat source is 78.7°C with the highest temperature of 90.6°C and the cold sink temperature that is controlled by the water taken from a well is in a range between 10°C and 14°C.

For Prototype B, three possible heat sources at Arcelor Mittal plant were analysed, which include 1) wire rods at the cooling table, 2) slabs in the cooling yard after continuous casting and 3) hot strip mill. Based on practicality, the temperature range of the heat source and the data from pyrometer measurements, the best heat source suitable for this application was identified to be the wire rods and the best position was the fixed lateral panels of the cooling tables. Although the cover panels have also been considered as a possible installation position, it is deemed unsuitable because of lower temperatures due to cooling by fans. From measurements at the selected positions, it has been determined, during a stationary process condition, that the maximum surface temperature was in the range of 120°C-190°C. The cold side of the thermoelectric generator was cooled using industrial water.

The design of each prototype was carried out after the hot source and the cold sink were chosen. Figure 1.3 and Figure 1.4 show the general layouts of the two developed thermoelectric generation systems.

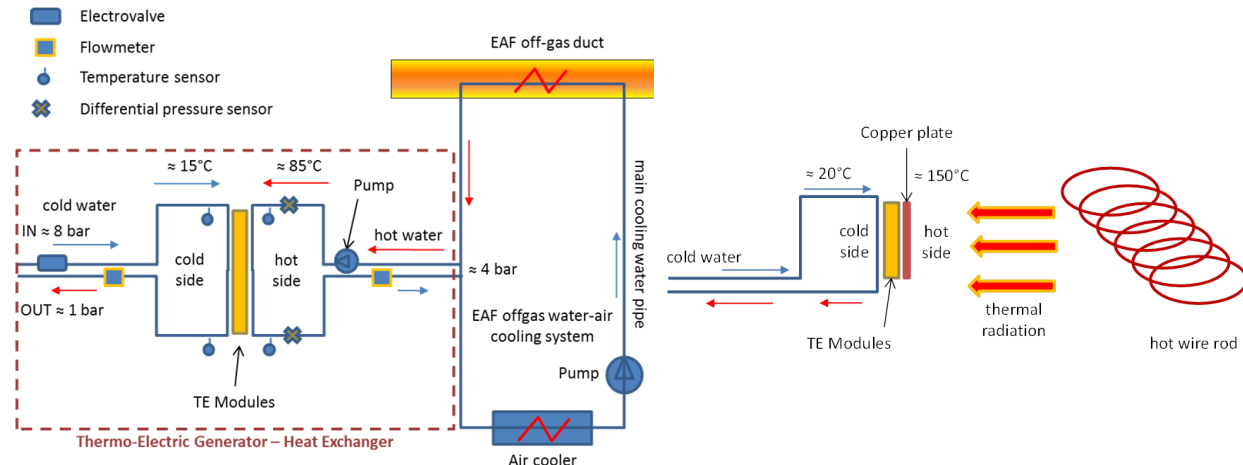


**Figure 1.3 – General layout of Prototype A**

**Figure 1.4 – General layout of Prototype B**

In Prototype A, the hot water was tapped from the main cooling water pipe of the EAF off-gas cooling system at a pressure of about 4 bars. It was pumped through the hot side of the thermoelectric generator and then return back to the main pipe. The pipeline section and a high efficiency pump were accurately chosen to reduce as much as possible electric pump consumption. The cold water from a well was supplied to the cold side of thermoelectric generator by an external pumping system with high pressure (8 bars), which was discharged at atmospheric pressure. The electric consumption of the pumping system was estimated and the fluid into the cold side was regulated using an electro-valve remotely controlled. Several measurement devices were installed on the thermoelectric generator, including two flow meters, a differential pressure meter and several temperature and voltage sensors. All the measured data were displayed on-line via specific graphical interfaces and then stored for further off-line analysis.

Prototype B was constructed using a number of thermoelectric modules sandwiched between a copper plate and aluminium plates with water channels. The copper plate serves as the absorber to capture the thermal energy radiated from the hot wires when they pass through the wire mill bed. The water channels, cooled by industrial water, enable the cooling of the TEMs cold side. The copper plate could be connected or not connected with the cooling table (side guard panel along the cooling conveyor system). BFI developed different prototypes, tested in laboratory, with different connection configurations.

Cardiff University committed to the development of theoretical models to assist design of the thermoelectric generators. A first thermoelectric model was developed assuming constant temperature gradient across the thermoelectric module. This occurs when the temperature at the hot and cold sides can be maintained constant, such as in the case of Prototype A. A second thermoelectric model was established assuming constant heat flux across the thermoelectric modules, suitable for modelling Prototype B. Both the models concluded that there is no need to go for long thermoelements lengths.

CSM and BFI investigated the possibility to apply the developed thermoelectric generators under higher temperature gradients in respect to the values envisaged by the original design.

This calculation demonstrated that an increase of 66% in the hot side temperature (from 75°C to 125°C) of Prototype A results in an increase of 90% in the electric power (from 71 kW to 135 kW). This is due to an increase in the overall efficiency of the system at higher temperature differences.

A similar benefit can also be obtained for prototype B. BFI showed a promising method to increase as much as possible the temperature of the hot side. The new system should be based on an actuator controlled by a temperature measurement, which moves back and forth the whole thermoelectric modules to reach the optimal distance in respect to the hot source.

Task 1.2: The controlling and monitoring tools were designed and constructed for both prototypes that have been used during the on-line tests.

### **WP2 – Construction of laboratory lab-scale “test bed” and laboratory tests**

Task 2.1: In order to verify the performances and limits of the designs, CSM, CU and BFI set up three laboratory testing facilities and built respective system to test the main prototype components. To simulate hot source and cold sink, both hot/cold water and radiation systems have been put in operation.

Hot and cold water circuit have been realised to simulate as much as possible the operative plant working conditions. Cardiff University developed a specific “test bed”, mainly for thermoelectric module characterisation.

BFI developed specific test-beds to simulate high radiation flux on the hot side of Prototype B. A small thermal radiation test bed was constructed using a ceramic plate heater, which was used to investigate a single thermoelectric module. For investigating Prototype B that consists of multiple thermoelectric modules, a larger test bed was constructed, which consists of eight porous burners (8 – 25 kW each) providing thermal radiation to a laterally installed thermoelectric generator, similar to the one planned for the full scale tests at Arcelor Mittal España plant site.

Task 2.2: CSM, Cardiff and BFI developed respective laboratory tests specifically set up to perform the required tests on components and the whole thermoelectric systems.

CSM carried out laboratory tests to verify the capability of the water circuit that can tolerate high hydraulic pressure, high temperature exposition and heavy load pressure on the thermoelectric modules, together with electric test of the thermoelectric generator and general working function prior to the shipment to the plant.

Cardiff University characterised the performances of all thermoelectric modules, acquired by the partners during the whole project, under different operative conditions. This provides experimentally validated data for choosing the suitable modules for the systems and set up benchmark to system development.

BFI performed several electric lab tests of prototype B, including measurement of the electric power in function of module pressure (torque), thermal interface materials, electric resistance load, and module temperature differences. Additional functional tests of the whole system prior to the shipping of the prototype were also performed.

### **WP3 – Analysis of the modules and identification of their structural weakness**

Task 3.1: Weakness points of the thermoelectric modules have been identified in terms of maximum applicable pressure and temperature. Cardiff University studied advantages and disadvantages of different constructive methods.

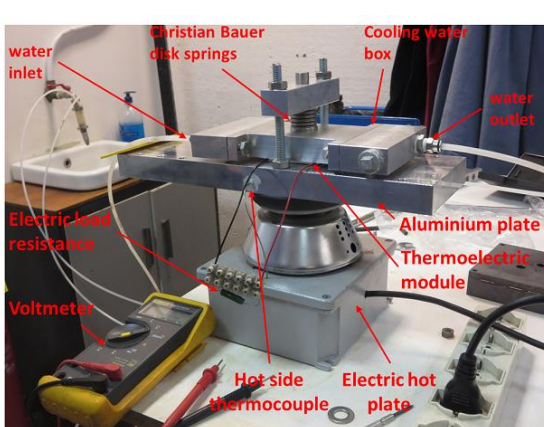


**Figure 1.5 – Prototype A lab test**

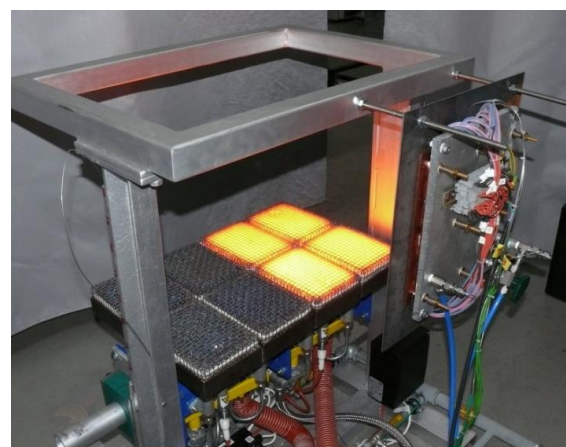


**Figure 1.6 – Prototype B lab test**

Task 3.2: CSM and BFI identified different technological improvements by means of specific laboratory tests (Figure 1.5 and Figure 1.6). BFI tested different methods to increase the heat transfer to the thermoelectric modules and CSM studied the problem of the optimum electric load matching.

Task 3.3: specifications of the two prototypes have been finally established and selected.

#### **WP4 – Design, construction and plant installation of the full scale thermoelectric system**

Task 4.1: After completing the laboratory tests of each component, prototypes A and B, have been assembled into their final configuration.

Prototype A was basically a multi-pass counter-flow heat exchanger, made of 6 horizontal water boxes of cold water and 5 horizontal water boxes of hot water. 6 thermoelectric modules were inserted between each alternating cold and hot water boxes. This gives a total of 10 layers of the thermoelectric modules, consisting a total of 60 thermoelectric modules (6 column x 10 rows) in the whole system. With this configuration it was designed to produce about 40 to 60 W (of gross power), which is in reasonable agreement with the experimental data obtained during the on-line tests. Figure 1.7 shows a photograph of the main part of the thermoelectric generator where thermoelectric modules are heated and cooled by the flowing water.

Prototype B was assembled into a sandwich configuration using three layers. The external layer (the hot side) was made of a copper plate for capturing thermal radiation energy. The intermediate layer contains 20 thermoelectric modules (4 column x 5 rows). The cold layer was made of an aluminium plate with channels cooling water. Two generators of such design were constructed. It was designed to obtain a power output of 50 – 60 W at temperature difference of 95°C between the hot and cold side of the thermoelectric modules. Figure 1.8 shows a photograph of Prototype B in its final configuration.

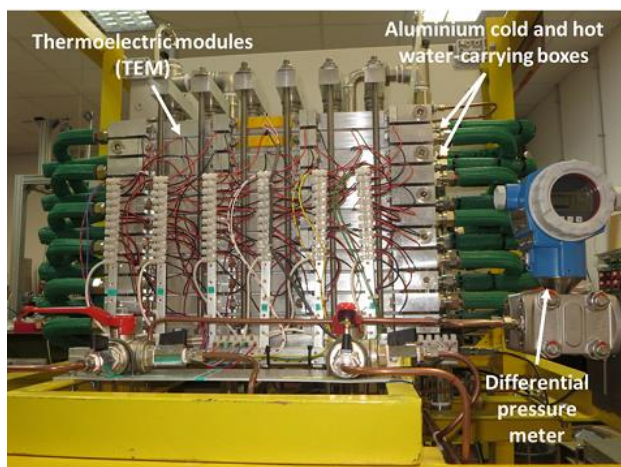


**Figure 1.7** – Prototype A

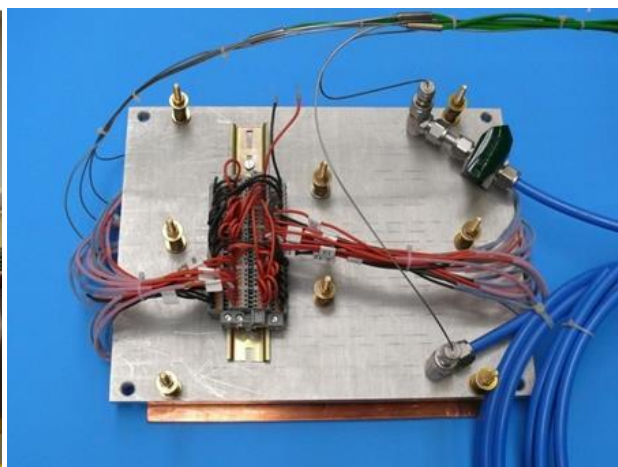


**Figure 1.8** – Prototype B

Task 4.2: after completing the laboratory tests, Prototypes A and B were shipped to the plant sites and installed at selected locations and prepared for the on-line tests (see Figure 1.9 and 1.10).

#### **WP5 – Execution of full-scale test and analysis of the thermoelectric systems**

Task 5.1: On-line tests of Prototypes A and B were performed to verify the various performances of the TEG devices under different working conditions.

In particular for Prototype A, the flow rate of the hot and cold water and the electric load impedance variations were monitored. A load resistor of  $3 \Omega$  was connected to each column (made of 10 thermoelectric modules) of this thermoelectric generator. It was not possible to control the temperature of hot and cold water as they were defined by the plant condition (for the hot water) and by the season (for the cold water). However, the cold water was practically constant during the whole test period (11-12°C), and the temperature variation of the hot water was sufficiently slow, which permit CSM to gather enough data and operative information.

Similarly, the following parameters were measured during on-line tests of Prototype B: the cooling water flow, the temperatures of cooling water at inlet and outlet, the temperatures at cold and hot side of TE modules, the voltage, current, electrical resistance and electrical power. The data were

recorded in time intervals of every 5 seconds. The matched load resistance of  $6 \Omega$  was determined during the commissioning and the value was used over the whole period of full-scale tests.



**Figure 1.9** – Prototype A at plant site

**Figure 1.10** – Prototype B at plant site

Task 5.2: The analysis of the performance for both systems have been carried out.

Performance results of the on-line test of Prototype A were:

- ✓ At standard conditions Prototype A worked as an heat exchanger which transfer about 6500 W of thermal energy from the hot source to the cold sink producing about 40 W of electric power.
- ✓ Considering the TEG as a heat engine, with a distance of the hot and cold source from the TEG unit of about 50 m (as in the case under study), the measured electric conversion efficiency of Prototype A was 0.3 % (40 W produced by the thermoelectric modules and 20 W consumed by the pumps).
- ✓ Prototype A shows an electric energy conversion efficiency of about 0.61% when no energy is required to pump the water.

Performance results of the on-line test of Prototype B were:

- ✓ Generated electricity increased rapidly with increasing hot side temperature.
- ✓ The maximum power output was  $\sim 50$  W for generator 1 and  $\sim 25$  W for generator 2.
- ✓ The efficiency of the Prototype B generators was in the range of 0,4 and 2,8 % depending on the temperature.

Due to a damage of Prototype B caused by an unexpected overheating, the on-line test at AME had to be stopped after several weeks.

Task 5.3: Every electric power producer has the serious problem in understanding, before building a new industrial plant, what is the cost of the produced electricity for a given type of plant. The problem may seem deceptively simple to solve, but it is not. In fact, the real cost of electricity produced by a given plant derives from many factors, some of them absolutely unpredictable and highly variable during the lifetime of the production plant.

In this task, the Levelized Cost of Electricity (LCOE) is used as an economic indicator of the developed Prototypes. The LCOE yields the discounted average cost of the produced electric energy for a specified power plant, expressed in €/kWh. It can also be considered as the price at which the produced electric energy must be sold to obtain parity between the revenue and the expenditure accumulated at the end of the plant lifetime, assuming the constancy of the quantity and the production costs.

The LCOE formula used in the present report was taken from *Fraunhofer ISE*, November 2013. Applying this formula using the data from the literature some competing electric energy production technologies have been compared with the LCOE calculated for the two developed prototypes.

The final result based on the assumed data, was:

- Prototype A: 10 years of operation, net electricity 175 kWh/Y -> LCOE = 4.12 €/kWh
- Prototype A: 20 years of operation, net electricity 175 kWh/Y -> LCOE = 3.61 €/kWh
- Prototype B: 10 years of operation, net electricity 175 kWh/Y -> LCOE = 3.50 €/kWh

- Prototype B: 20 years of operation, net electricity 175 kWh/Y -> LCOE = 3.24 €/kWh

Task 5.4: Although almost all of electrically conductive materials exhibit thermoelectric properties to some extent, only a very limited number of materials are more suitable to be employed for energy conversion applications.

Raw material cost per kilogram along with the thermoelectric figure of merit, ZT, have been reported, together with the price per kilogram versus crustal abundance of elements, and the figure of merit, ZT versus crustal abundance.

The trend observed indicates that the elements that are less abundant are more expensive.

The fact that some thermoelectric materials are increasingly being used in other fields too, such as the case of Te in photovoltaic technology, makes their price volatile. The price of Te increased from \$ 22/kg in 2004 to around \$ 440/kg at the beginning of 2011. On the other hand, there has been only 25% increase in the global production of Te.

Despite of the problems and low abundance of  $\text{Bi}_2\text{Te}_3$ , it is the most suitable material around room temperatures due to its better performance (ZT). The rest of competitors around  $ZT \approx 1$  are useful at higher temperature ranges.

Unfortunately  $\text{Bi}_2\text{Te}_3$  is rated as acutely toxic and hence requires proper disposal. It is estimated that 40% tellurium is used in photovoltaic industry and 30% in thermoelectric power generation and cooling modules. Recycling of Te is growing gradually, photovoltaic industry produced around ~7% of total Te production in 2010 through recycling. According to official US statistics, nearly all alloys containing Bi were recycled in 2012 and contributed to 10% of US's Bi consumption.

Life cycle assessment (LCA) is a standardized international technique used to better understand and address environmental protection and impacts associated with product manufacturing and consumption.

OpenLCA software (version 1.5.0) has been used to model the inventory analysis and the impact assessment. All the data used in this study was from the ELCD (European reference Life Cycle Database) 3.2 database.

LCA analysis has been carried out considering a production of a set of 2750 TEGs of Prototype A, corresponding to an electric power of 55 kW. This number has been calculated assuming to discharge into the cold sink 18 MW of heat energy, as required by the EAF off-gas cooling system. For comparison reasons, it is also assumed that Prototype B has the same electric power (55 kW). Because both prototypes have the same average power, Prototype B was considered to require a production set of 2750 TEGs.

Based on these assumptions, the inventory of the materials required to manufacture a single TEG has been estimated and then filled into the OpenLCA software for the LCA calculation.

The "inventory results" showed a large difference in energy consumption (energy input) for the two prototypes. This is caused by the large amount of steel (50 kg and 1.83 kg) and aluminium (50 kg and 6.93 kg) used to manufacture Prototype A and Prototype B, respectively. This gap is related to the dimension of the two systems (e.g., a heavy frame is used in Prototype A). For the same reason, also Earth "water" and "air" consumption of prototype A exceed more than about 60% and 70% the consumption of prototype B.

Concerning the outputs, the inventory results showed a similar conclusion that the emission caused by the production of Prototype A is approximately 70% higher than that caused by the production of Prototype B.

Concerning the "impact results", it can be noted that the first four "impact categories" are the same, and in the same order. They are: marine and aquatic ecotoxicity, depletion of abiotic resources (fossil fuels), climate change and human toxicity.

Marine and aquatic toxicity is caused by release of hydrogen fluoride (HF) into the seawater.

Depletion of fossil fuel resources has the same flow sources for both prototypes but different distribution. Prototype A production has the same contribution from hard coal (34%), natural gas (33%) and almost the same from crude oil (28%); instead, Prototype B production shows high depletion of crude oil (60%) and lower depletion for natural gas (22%) and hard coal (13%).

Climate change is caused mainly by carbon dioxide emission, both for prototype A (91%) and prototype B (89%). It is important to note that figures refer to the manufacture of TEG systems, and not to greenhouse gases emission during electric power production. In terms of carbon footprint for electricity generation, both the thermoelectric systems have zero emissions, because both the systems do not produce any gas emission. However, of course, there is a carbon footprint during the production and installation of the TEG systems. Considering these figures, it is possible

to obtain the carbon footprint for electricity production for Prototype A (69 gCO<sub>2</sub>eq/kWh) and Prototype B (21 gCO<sub>2</sub>eq/kWh).

Toxicity for humans is caused mainly by dioxins dispersion in water and air, and by hydrogen fluoride dispersion in air. Dioxins dispersion has an impact of 84% for Prototype A and 74% for prototype B of the total kg of 1.4-Dichlorobenzene equivalents emissions. Hydrogen fluorides have an impact of 7.78% in the case of Prototype A and 13.45% in the case of Prototype B.

The above findings show that Prototype A production has more impact on the environment than Prototype B production for equal electric power generation. This is caused by a greater weight of Prototype A compared with Prototype B. In terms of greenhouse emission, both prototypes can be considered low-carbon renewable power production systems. Concerning emission of toxic material into the environment, it is to be noted that electric power production through thermoelectric generators produces toxic materials, differently by other power plants, only during the generators manufactory phase, and not during the operative period. Therefore, assuming that every power plant has comparable impact during the manufacture phase, TEGs must be considered as a green technology similar to wind, hydro or solar production and much better, for this impact category, than production methods based on combustion technologies.

No recommendation can be made to prefer one or the other prototype. In fact they have been designed to operate in two completely different conditions, involving their own advantages and disadvantages. Prototype A works as a cooler able to contemporarily cool water and produce electric energy. Prototype B works as an heat recovery system able to convert waste radiation energy into electric energy. Therefore the two prototypes have different objectives and cannot be recommended for the use with one against the other.

### ***Conclusions***

This research have produced a large amount of data that is essential for future studies. However, both prototypes developed in this project are not yet cost-effective to be employed for electricity production on industrial scale.

This high cost of electricity production is very sensitive in the steel industry because the price of electricity available to the steel plants is lower than in other industries.

The results of this research demonstrated that the thermoelectric systems are able to produce electricity using waste heat from steel plants and more importantly it can, produce "net electricity" under proper circumstances. They are suitable, in the near future, for small electric energy production.

In terms of greenhouse emission, both prototypes can be considered low-carbon renewable power production systems, with 69 and 21 gCO<sub>2</sub>eq/kWh carbon footprint.

To lower the electricity cost produced by thermoelectric systems at low temperatures, it is not very beneficial by focusing only on developing low-cost alternatives for Be<sub>2</sub>Te<sub>3</sub>. The cost benefit by such approaches is too small to be practically useful. Instead, developing new thermoelectric materials with significantly improved thermoelectric figure-of-merit is necessary.

On the other hand, it is more beneficial to investigate system optimisation that incorporates the existing thermoelectric materials, such as Bi<sub>2</sub>Te<sub>3</sub>, with the structures or components in a system employed at specific industrial plants. This would reduce the costs of assembly and installation at the end user and allow the optimization of heat exchange in the overall thermoelectric system.



## **2 Scientific and technical description of the results**

### **2.1 Objectives of the project**

The project objective is to investigate the technical and economic performance of thermoelectric power generators for waste thermal energy harvesting at steel plants. This target has been achieved by analysing the data obtained from two on-site thermoelectric power generators (Prototype A and B). Prototype A was designed with the aim of recovering waste heat from hot water of an industrial cooling system, while Prototype B was designed with the objective of recovering waste thermal radiation energy from hot surfaces.

Prototype A was developed at CSM laboratory (Italy) and installed at Ferriere Nord plant (Italy). Prototype B has been developed at BFI laboratory (Germany) and installed at Arcelor Mittal plant in Gijon (Spain).

Laboratory tests and theoretical models have been also developed to evaluate different module designs and the effective economic and environmental sustainability of the thermoelectric power generation technology.



### **3 Description of activities and discussion**

#### **3.1 WP1 - Development, improvement and implementation of devices and modules**

WP1 objectives are:

- Identification of heat source and heat sink at the steel plants
- Identification of the general design of the prototypes
- Selection of thermoelectric modules and auxiliary components
- Theoretical study of operating the prototypes at higher temperature ranges
- Development of tools for prototype control and monitoring

##### **3.1.1 Task 1.1 - Development, characterization and implementation of thermoelectric devices/modules (all partners)**

This first task was devoted to a preliminary analysis of the available conditions at industrial plants. Particular attention was paid to the identification of the heat sources and heat sinks, which determines all the subsequent design of the thermoelectric power generators.

###### **3.1.1.1 Identification of heat source and heat sink (all partners)**

As a first step, the design of a thermoelectric power generator requires to identify both the heat source and heat sink. In general, the entire electric power generation system will be more efficient if the heat source and the heat sink can provide the maximum temperature difference possible and if they are close one to each other. Therefore, their selection is crucial.

Going into more detail, we can distinguish three main components for each side.

At the hot side: the "heat source", a "heat carrier", used to transport the heat from the hot source to the TEG, and a "component" used to transfer and distribute the heat from the heat carrier to the hot side of the thermoelectric modules.

For the cold side: a "component" is used to transfer and distribute the heat from the cold side of the thermoelectric modules to a "heat carrier". A "heat carrier", used to transport the heat from the TEG to the "heat sink". All these components have to be selected and defined for each thermoelectric device.

Prototype A represents an application where the available heat is obtained from an industrial water-cooling system. This scenario is very common in steel plants where large quantities of thermal energy have to be disposed by dedicated cooling systems. These systems usually employ flowing fluids, generally water, at relative low temperature (< 100°C).

It was decided to use the water of an Electric Arc Furnace (EAF) off-gas cooling system as the heat source for Prototype A. Fortunately, this hot water is also very clean and therefore it was decided to directly use it as the heat fluid to the thermoelectric generator. Therefore, the water of the cooling system works both as "heat source" and as "heat carrier", i.e. used to transport the heat from the hot source to the TEG.

This case is not very common because generally the industrial fluids cannot be used directly to pass through the thermoelectric generator due to existence of possible impurities. For example, it is very common, at industrial plants, to use seawater or partially treated water as cooling fluid. In this case it is not recommended to use the same fluid to go through the thermoelectric generators.

The direct use of the industrial water allows improving the overall efficiency of the thermoelectric generator. In fact, this solution allows eliminating the heat exchanger between the primary hot fluid of the heat source and the fluid used within the thermoelectric generator. This is equivalent to say that the efficiency of this heat exchanger is 1.

Prototype B represents an application where the available heat is obtained from thermal radiation emitted by high temperature steel products that move all around the plant during the passages between the required different treatments. As this energy is available as radiant energy, it can only be partially captured. Consequently, in this case, although the "heat source" showed very high temperature, the component in contact with the thermoelectric module, present much low temperature (generally <250°C). Therefore, it is not defined as high temperature thermoelectric energy. In this case, thermoelectric materials suitable for low temperature applications can be used. Arcelor Mittal have studied several possible heat sources of radiant energy at steel plants as reported in the following paragraph.

### **3.1.1.2 Prototype A: heat source and heat sink (CSM, FENO)**

Prototype A was installed at Ferriere Nord steel plant. Figure 3.1.1.2.1 shows the EAF off gas duct (i.e. the thermoelectric generator heat source) and the water air cooler (WAC) of this plant. The cooling water was selected as hot source heat carrier.



**Figure 3.1.1.2.1** – FENO, EAF off gas duct and water air cooler.

Well water, available not far from the heat source, has been selected as the heat sink and carrier.

The main characteristics of the fluids have been analysed. The results of the analysis are shown in Table 3.1.1.2.1. The water used in the off-gas cooling system is demineralized water with a low content of calcium, which is an important property for the hot side of the TEG system, which may be affected by calcium deposition in the narrow ducts.

<b>FENO hot heat source and heat carrier characteristics</b>	
Circuit type	closed circuit
Flow type	demineralized water
Temperature [°C]	70 - 90
Flow rate [m³/h]	2200 – 2800 (max)
Pressure [bar]	3.9 – 4.2
pH [20°C]	9 – 10
Water hardness [ppm CaCO <sub>3</sub> ]	10 – 30
<b>Cold heat sink and heat carrier characteristics</b>	
Circuit type	open circuit
Flow type	well water
Temperature [°C]	13 -15
Flow rate [m³/h]	2
Pressure [bar]	4.5
pH [20°C]	7.85
Water hardness [ppm CaCO <sub>3</sub> ]	280 - 300

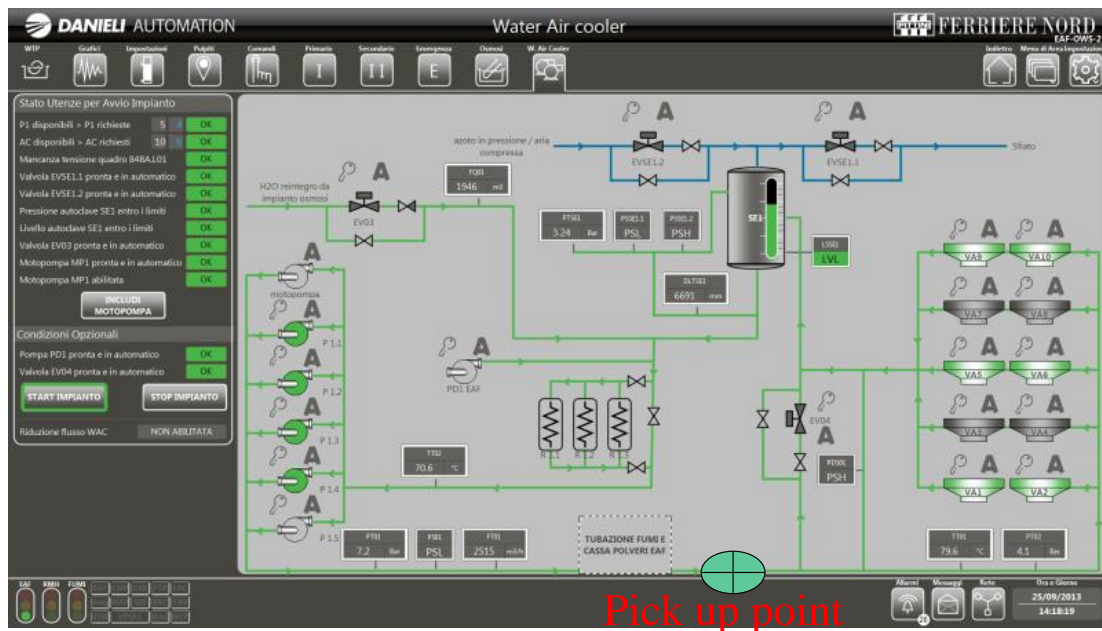
**Table 3.1.1.2.1** - FENO, hot source and cold sink heat carrier characteristics

Figure 3.1.1.2.1 shows a picture of the EAF off gas duct and the path of the hot water pipeline from the main pipe towards the TEG location (red line).



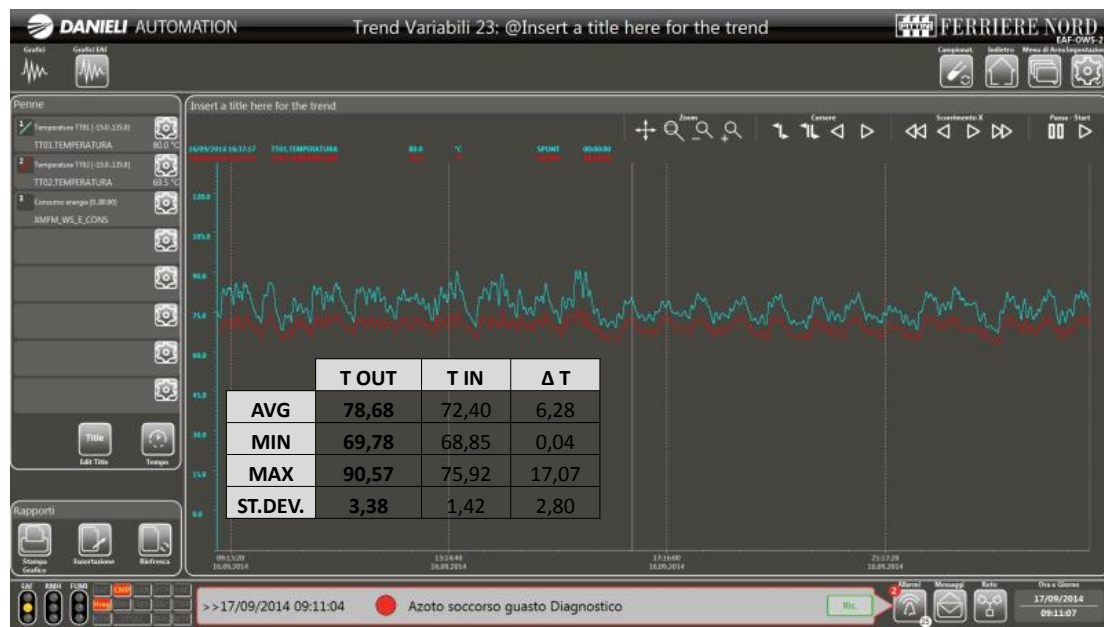
**Figure 3.1.1.2.2** - FENO, EAF off-gas duct and pipe path

Figure 3.1.1.2.3 shows the water air cooler plant scheme and the position of the hot water pick up point, close to the entrance of the air cooler. The water temperature, at the entrance and at the exit of the furnace, has been monitored.



**Figure 3.1.1.2.3** – FENO, Water Air Cooler scheme and pick-up point

Figure 3.1.1.2. 4 shows the trend of the measured hot water temperature. During the monitored period the higher temperature, at the pickup point, was 90.6°C and the average value 78.7°C.



**Figure 3.1.1.2. 4 – FENO, water temperature trend at the air cooler.**

In addition, the cold water, used as heat sink, has been monitored. Figure 3.1.1.2.5 shows the measured temperature annual trend which was ranging between 10°C and 14°C.

While the hot water temperature can be considered very low, at the limit of the possibilities for producing electrical energy from a thermoelectric device, the cold water values are quite suitable and in line with the better expected values.

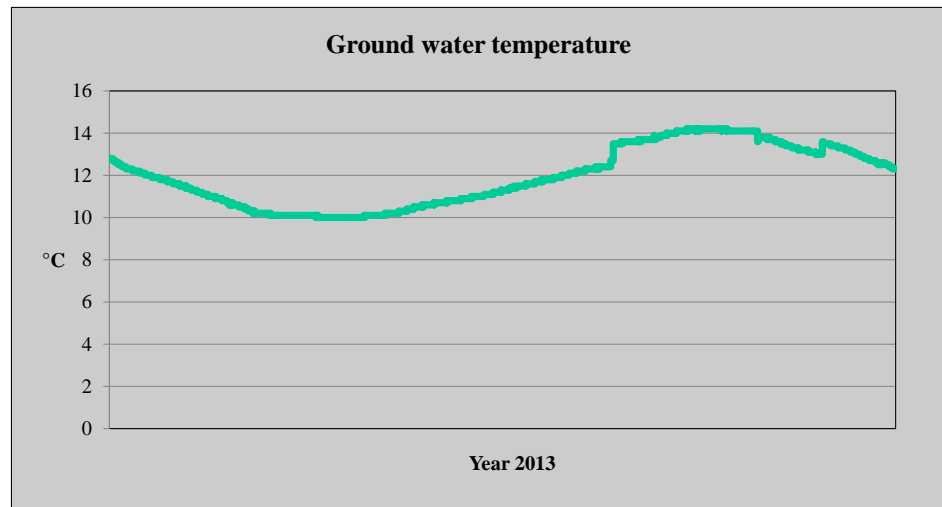


**Figure 3.1.1.2.5 – FENO, heat sink temperature monitoring**

### 3.1.1.3     **Prototype B: heat source and heat sink (AME, BFI)**

Concerning Prototype B, three possible heat sources have been identified at AME steel plant:

1. The wire rod at the cooling table (Figure 3.1.1.3.1)
2. The slabs in the cooling yard after continuous casting (Figure 3.1.1.3.2)
3. The hot strip mill (Figure 3.1.1.3.3)



**Figure 3.1.1.3.1** – AME, wire rod as hot source



**Figure 3.1.1.3.2** – AME, slabs in cooling yard as hot source



**Figure 3.1.1.3.3** – AME, hot strip mill as hot source

For this type of thermoelectric devices, the radiation emitted by the heat source is captured by a metal plate (TEG plate) and then transferred to the thermoelectric modules. Thus, in this case, heat is transported from the heat source to the TEG by means of radiation. The TEG plate serves as a way to capture and distribute the heat to the hot side of the thermoelectric modules.

Employing pyrometer measurements the average temperatures of the heat sources described above were determined (heat source temperature measurements were done at those positions in the process line, where the industrial demonstrator could be installed according to the plant supervisor). The results of this analysis are reported in Table 3.1.1.3.1. It was decided, due to both practical reasons and the large temperature range of the heat source (that allows the thorough study of the influence of this parameter) that the best position for Prototype B installation is the cooling table.

AME hot heat source temperature data	
Wire rod temperature [°C]	900 - 250
Slabs in cooling yard [°C]	600
Hot strip [°C]	150-200

**Table 3.1.1.3.1** - AME, hot source temperature measurement

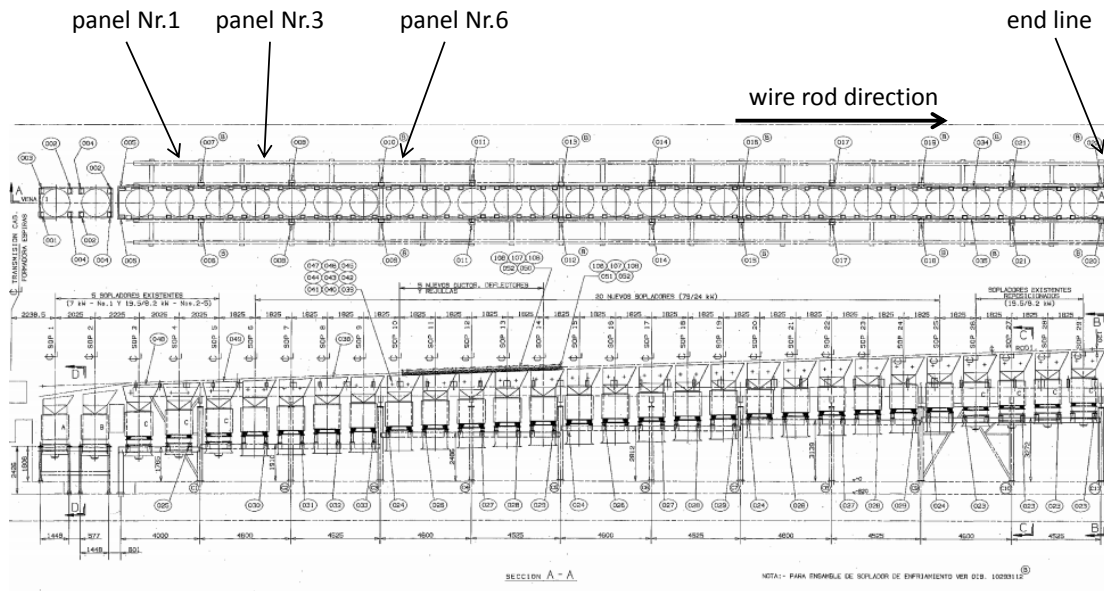
Two possible positions for the TEG plates have been identified: the cover panels (Figure 3.1.1.3.4) and the fixed lateral panels (Figure 3.1.1.3.5) of the cooling table, where panels are a section of a cooling table. Both of these positions allow capturing the heat from the wire rod. For construction simplicity the fixed lateral panels have been preferred and selected for the prototype B installation.



**Figure 3.1.1.3.4** – AME, cover panels of the cooling table conveyor



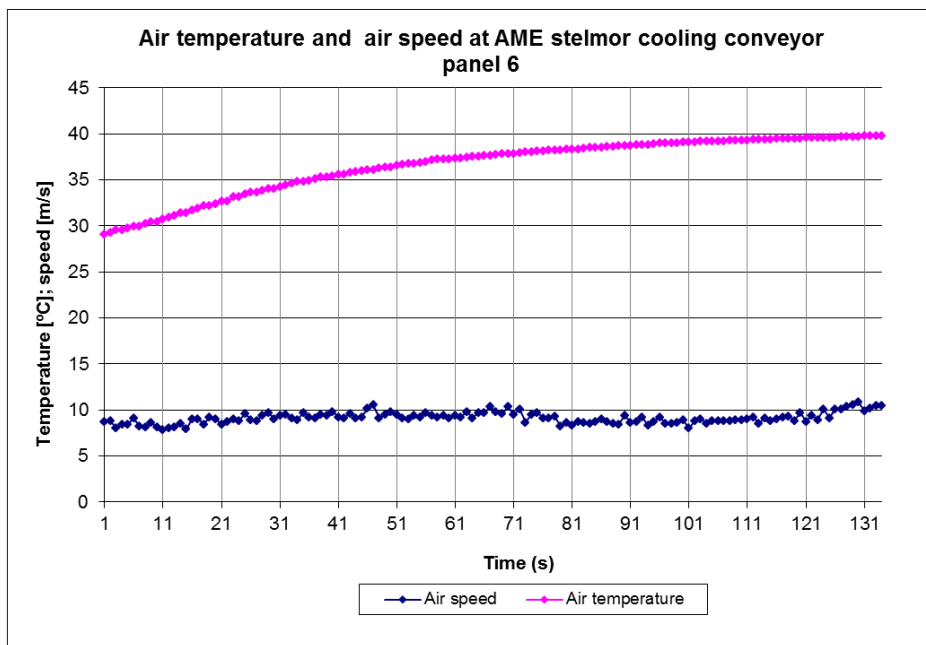
**Figure 3.1.1.3.5** – AME, fixed lateral panels of the cooling table conveyor



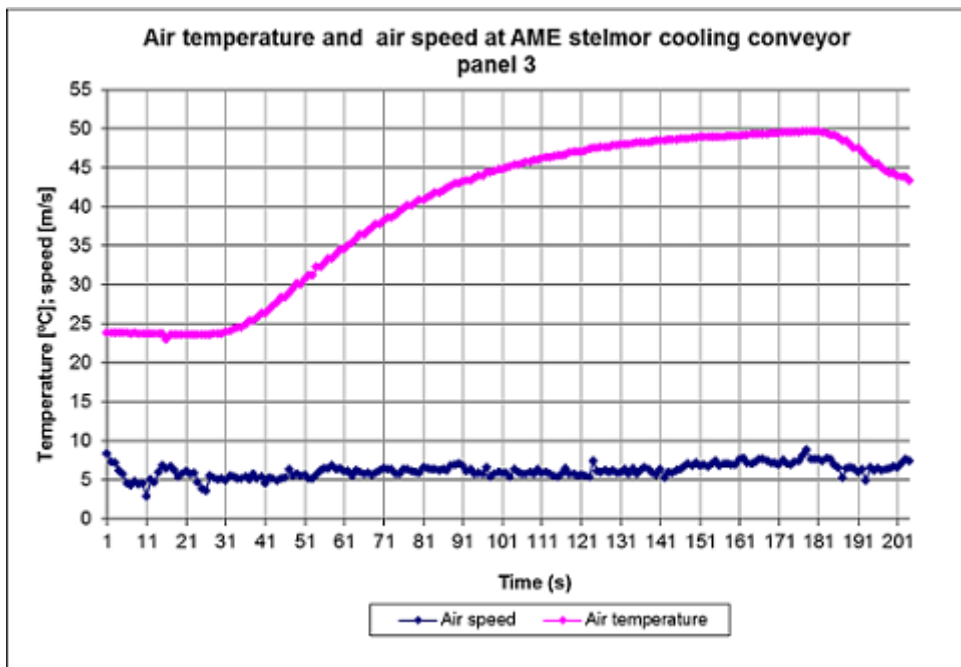
**Figure 3.1.1.3.6 – AME, cooling table conveyor layout**

Figure 3.1.1.3.6 shows the AME plant cooling table conveyor layout and the panels selected for Prototype B positioning (panels 1, 3, 6).

Temperature and speed measurements of the hot air from the cooling fan have been measured by AME at panel 3 and 6. These measurements have been carried out using thermocouples and a Pitot tube positioned about one meter over the wire rod during the wire cooling process. Figure 3.1.1.3.7 and Figure 3.1.1.3.8 show the results of these measurements, revealing that the air temperature at panel 3 does not exceed 50°C, which is very close to where the hot wire enters the cooling line (at panel 1, see layout in Figure 3.1.1.3.6).



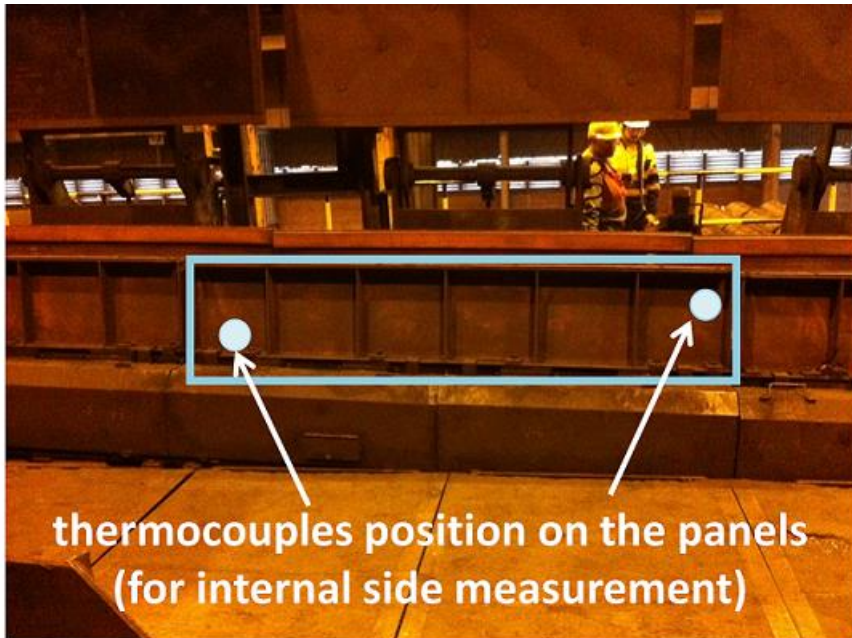
**Figure 3.1.1.3.7 - AME, air temperature and air speed at panel 6**



**Figure 3.1.1.3.8 – AME, air temperature and air speed at panel 3**

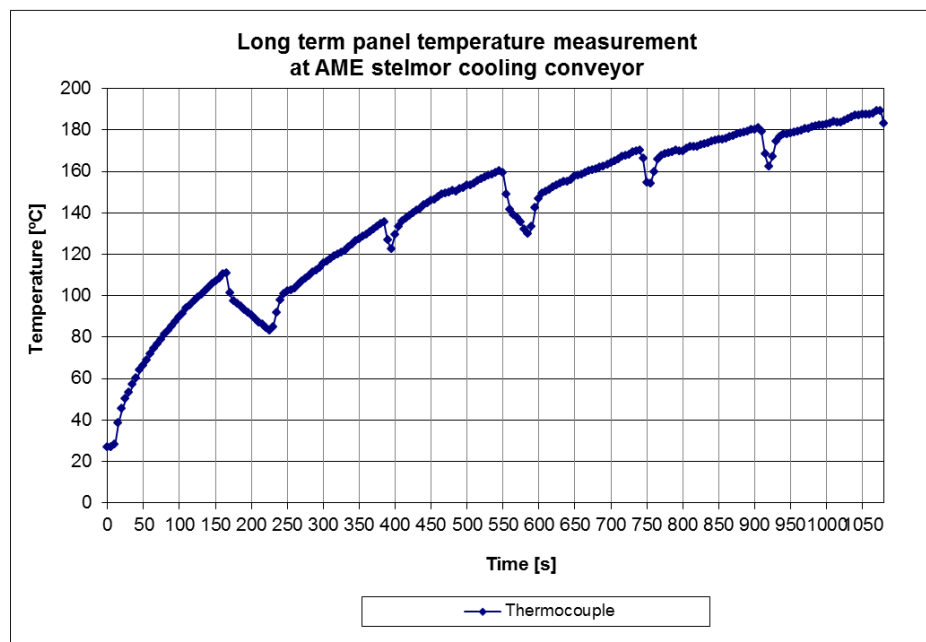
Clearly, because of the low temperature ( $50^{\circ}\text{C}$ ) of the cooling air, it will tend to cool the TEG plate. Therefore the choice of positioning the TEG panel at the side panels is better than at the cover panels, where the effect of heating as a result of radiation would be diminished by forced convection by the cooling air.

Temperature measurements of the inside panel surfaces have been carried out using thermocouples (positions exemplary shown in Figure 3.1.1.3.9) fixed at the steel plates. Four panels, panel 1, 3, 6 and the end panel) have thus been studied.



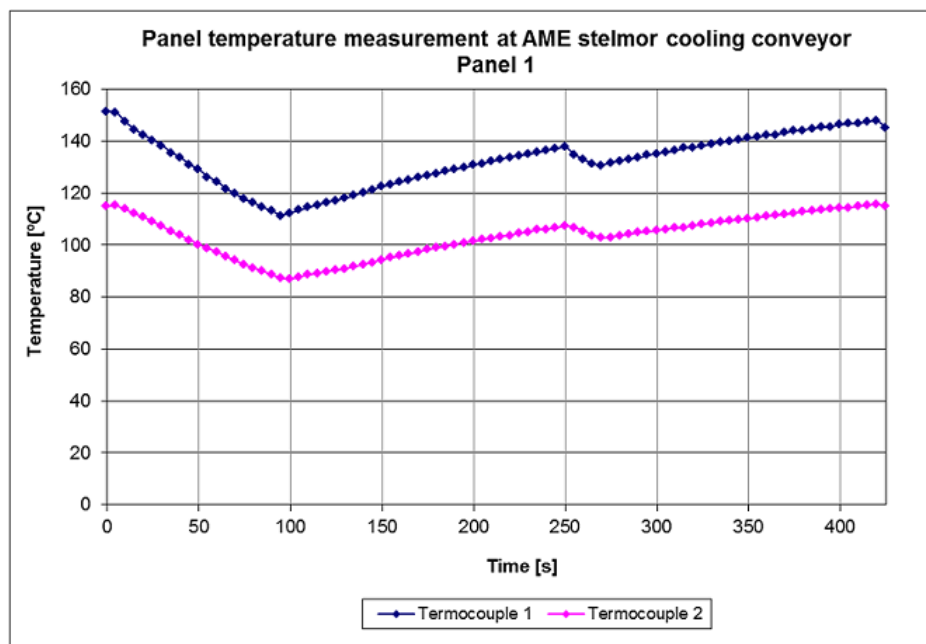
**Figure 3.1.1.3.9 - AME, position of the thermocouple for the internal side measurements**

Figure 3.1.1.3.10 shows the initial step of the process (cooling table 6), covering the first seventeen minutes and about six wire rod treatments. As can be seen in this figure, the panel's inside surface is cold ( $26^{\circ}\text{C}$ ) at the beginning of the process; but gradually heated to reach a maximum temperature between  $150^{\circ}\text{C}$  and  $190^{\circ}\text{C}$ . Obviously, the rate of the temperature increase ( $dT_{\text{surface}}/dt$ ), decreases as more wires are processed.



**Figure 3.1.1.3.10 – AME, long term panel measurement (internal side)**

Figure 3.1.1.3.11 and Figure 3.1.1.3.12 show temperature measurements at panel 1 and the end panel in more detail, measured with thermocouples at two different heights, around 300 mm, of the same panel.



**Figure 3.1.1.3.11 – AME, panel temperature measurement in two points**

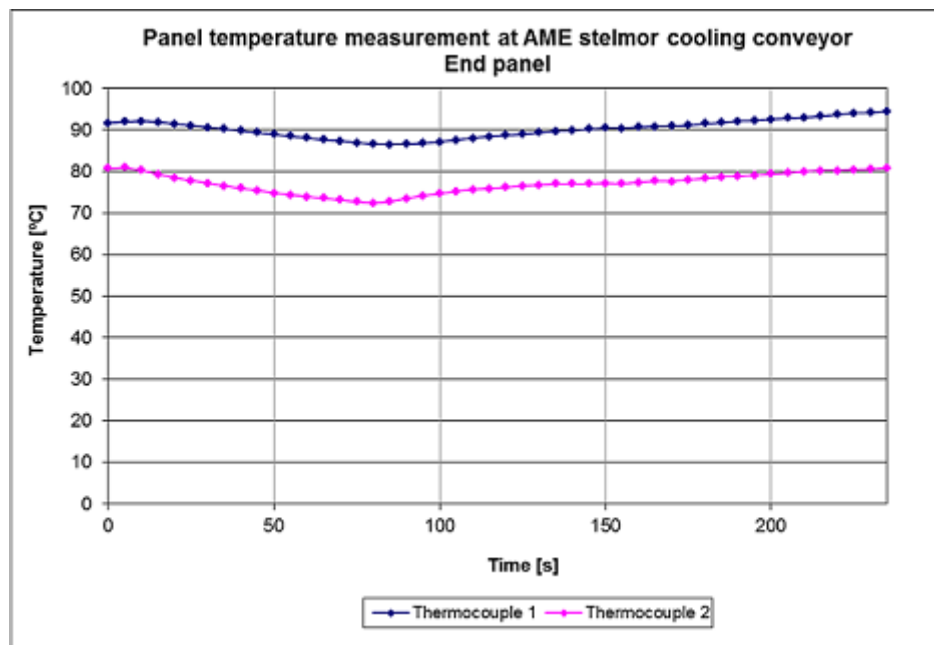


**Figure 3.1.1.3.12** – AME, panel temperature measurement in two points

Other measurements of the internal side of the panels have been carried out using an infrared thermo-camera at panel 3 (Figure 3.1.1.3.13). Thus, setting the surface emissivity at 0.9, an average temperature in the range 163°C-186°C was measured, close to the measurements performed using the thermocouples. Figure 3.1.1.3.14 shows the same panel (panel 3) measured with an instrument set for line temperature measurement. This figure shows that the two maximum average temperatures occur at LI02 and LI03. This is probably caused by a partial shielding of the radiation on the line below, where a horizontal bar is part of the panel construction. It is therefore important to note, as in any phenomenon dominated by electromagnetic radiation, that it is necessary to avoid as much as possible any shielding of the source radiation. Also the role of the forced convection may be a possible explanation of this particular phenomenon.

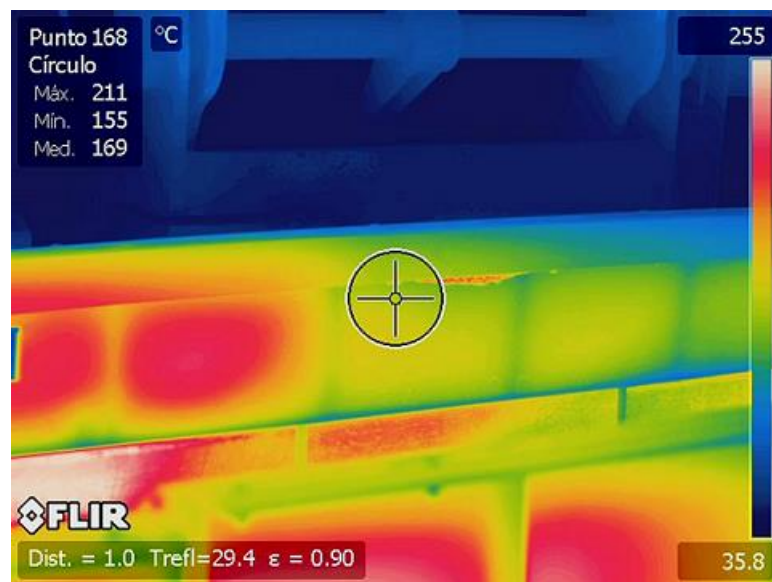


**Figure 3.1.1.3.13** – AME, panel temperature measurement with IR thermo-camera

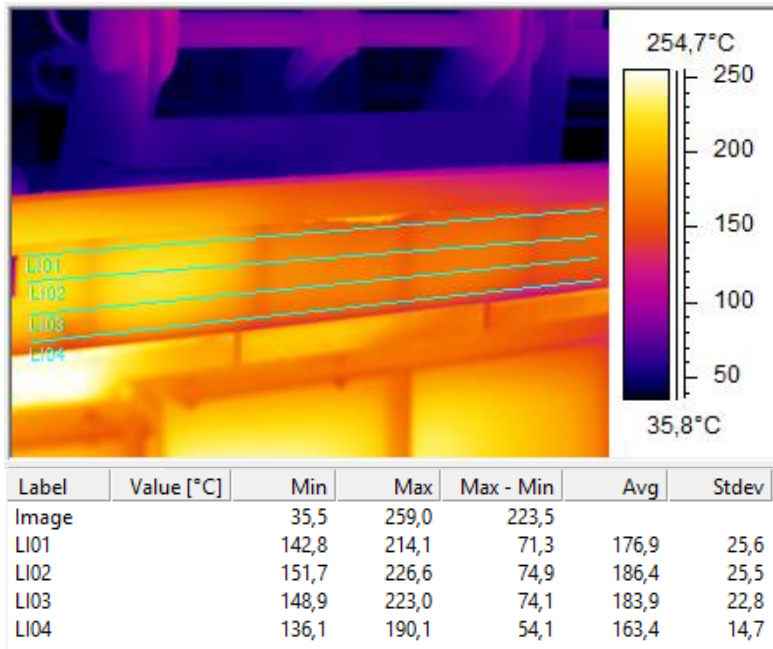


**Figure 3.1.1.3.14** – AME, four line temperature measurement with IR thermo-camera

From the measurement, it was possible to verify, during a stationary process condition, that the maximum inside panels surface temperature (for a panel close to the entrance of the cooling table conveyor) was in the range of 120°C-190°C.

Of course, it must be considered that when Prototype B is installed, the equilibrium temperature of the TEG plate strongly depended on the heat flow through the TE module towards the heat sink. Therefore, the effective temperature of the TEG hot side could be significantly different.

As heat sink of the thermoelectric generator, industrial water has been used. The cooling water was then discharged into the sewage system.

### 3.1.1.4 Identification of prototypes general design (all partners)

After defining the hot source and the cold sink, it was possible to start the general design of each prototype. As already mentioned, the distance of the heat source and the heat sink are both important parameters for the project that influence the overall efficiency of the system. It is clear that in order to transfer heat from the hot source to the thermoelectric module and from the thermoelectric module to the cold sink, in certain cases, it is needed to put in motion a heat carrier (for example gas or liquid). In this case it is therefore required to consume energy for the movement of the heat carrier. This energy is lost by the overall system and then reduces the total efficiency.

This fact is particularly important at low heat source temperatures, due to the low efficiency of thermoelectric modules. In fact, in order to generate 1 kW<sub>e</sub> of electrical energy (assuming the thermoelectric generator has a conversion efficiency of 1%), it is necessary to transfer from the hot source to the cold sink 100 kW<sub>t</sub> of thermal energy., This involves putting in motion large masses or requiring very high radiated power.

As already said, the two prototypes were designed to operate using two completely different energy sources: Prototype A uses thermal energy from the cooling water at low temperature and Prototype B uses radiant energy from hot surfaces.

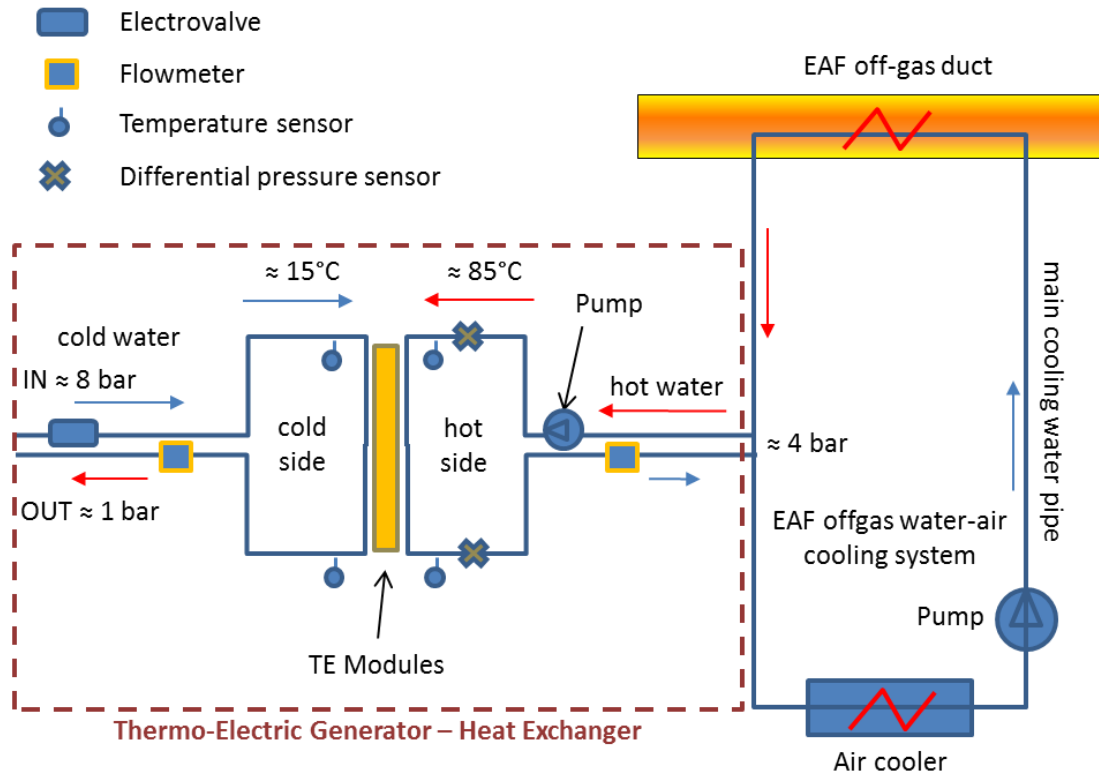
### 3.1.1.5 Prototype A: general design (CSM, FENO)

Figure 3.1.1.5.1 shows the general layout of Prototype A.

The figure shows that the hot water is tapped from the main cooling water pipe of the EAF off-gas cooling system, at a pressure of about 4 bars, prior to the air cooler. Then, it is fluxed into the TEG hot side and successively injected again into the main pipe. A high efficiency pump is used to flux the hot water. The overall power energy required to flow the hot water is obtained measuring the electric power consumption of the water pump.

The cold water is supplied by an external pumping system with high pressure (8 bars) and discharged at atmospheric pressure. The flux into the cold side is regulated using an electro-valve

remotely controlled. The overall power required to flow the cold water is calculated from the flow rate and the estimated pressure drop.



**Figure 3.1.1.5.1** - Prototype A, general layout

For this kind of systems, it is generally necessary to have a pumping system for both the hot and cold water circuits. Therefore, one of the objectives of the on-line tests is to find the optimal flow rate of the hot and cold water to maximize the production of useful electrical energy, i.e. the energy produced by the thermoelectric modules minus that consumed by the two pumping circuits. For Prototype A, to obtain the maximum production of energy it was appropriately adjusted the two flow rates of the hot and cold water by means of the regulation of the pump power and the electro-valve aperture.

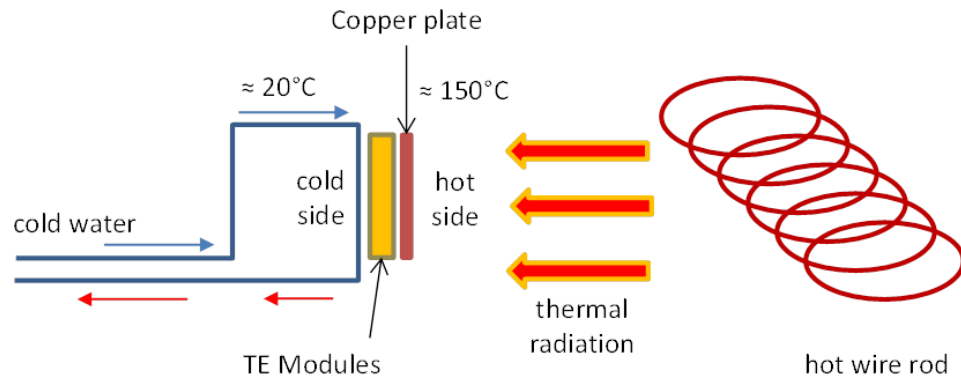
To maintain the highest possible temperature difference between the sides of the thermoelectric modules, it is necessary to reduce as much as possible the linear length of the TEG system. Therefore, it was decided that Prototype A should be arranged in short horizontal layers of thermoelectric modules overlapped each other with a maximum of six thermoelectric modules for each horizontal layer. The thermoelectric modules should be then sandwiched between aluminium boxes with internal circulation of the hot and cold water.

More details on the design of TEG final configuration can be found in Sec. 3.3.3 (Task 3.3 – Design of the final specifications), Annex A.7 (Deliverable D3.3 – Description of the final configuration of the thermoelectric modules) and Annex A.8 (Deliverable D4.1 – Design of the final configuration of the thermoelectric systems).

### 3.1.1.6 Prototype B: general design (AME, BFI)

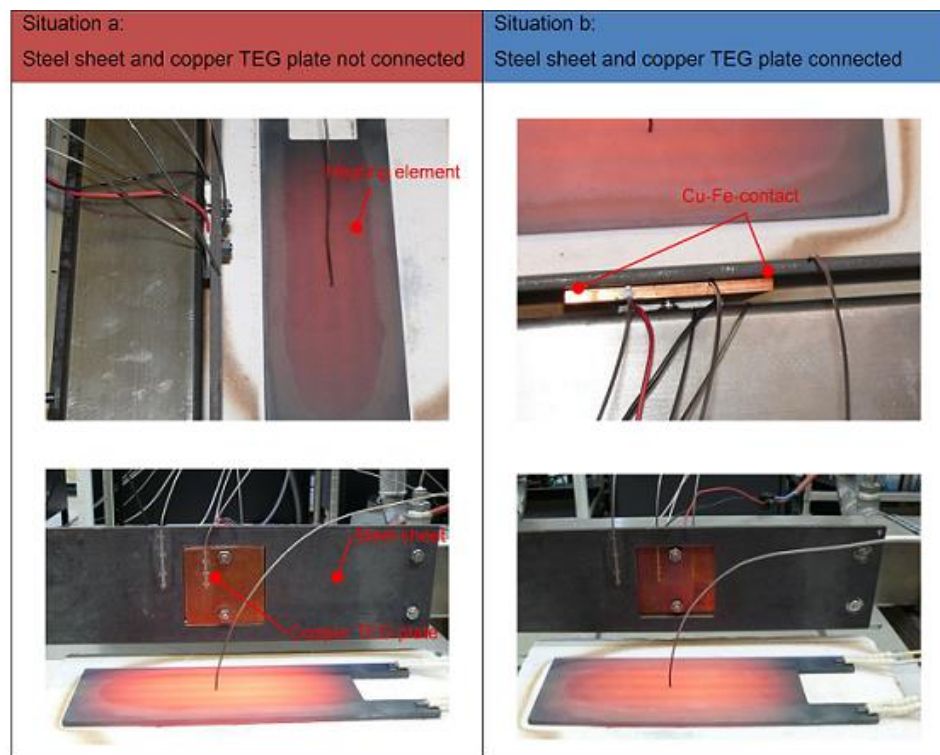
The second thermoelectric generator was developed by BFI and AME for installation at the AME steel plant. This prototype, named Prototype B, is formed by a group of thermoelectric modules locked between a copper plate and aluminium plates with grooves. The copper plate has the objective of capturing, as much as possible, the thermal radiation from the hot wires when they transit into the wire mill. The grooves, cooled by water flow, have the objective of cooling the TEMs cold side. The copper plate can be connected or not connected with the cooling table.

Figure 3.1.1.6.1 shows the general layout of this TEG system.

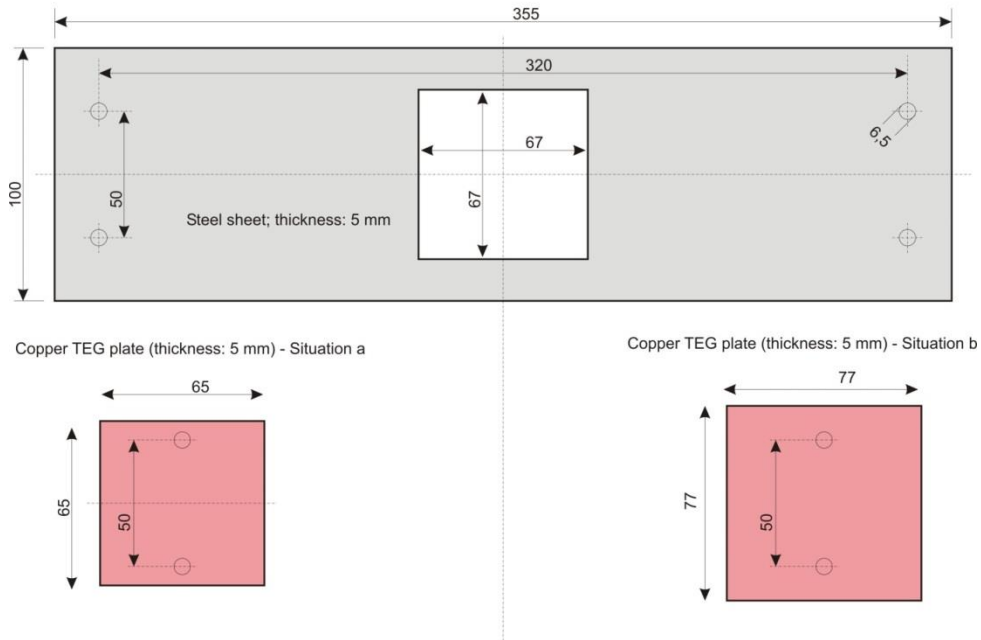


**Figure 3.1.1.6.1** General layout of Prototype B.

Figure 3.1.1.6.2 shows two kinds of setups tested at BFI laboratories. In situation a, shown by the pictures in the left column of Figure 3.1.1.6.2, no connection existed between the copper TEG plate and the steel sheet (simulating the cooling table). In situation b, at the right column of the same figure, steel and copper were connected (contact area  $1.440 \text{ mm}^2$ , see also Figure 3.1.1.6.3).

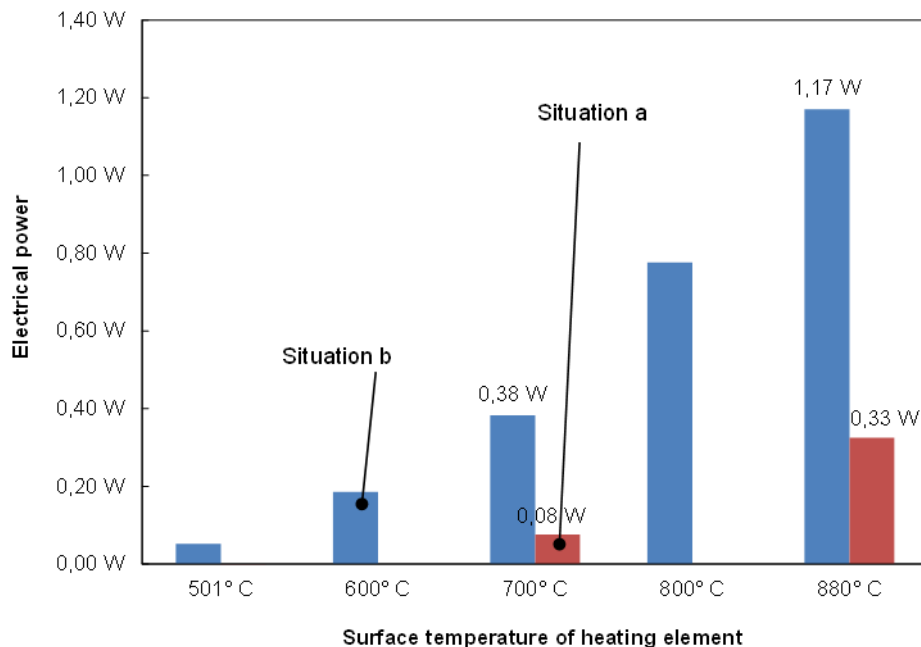


**Figure 3.1.1.6.2** Two possible configurations of Prototype B.



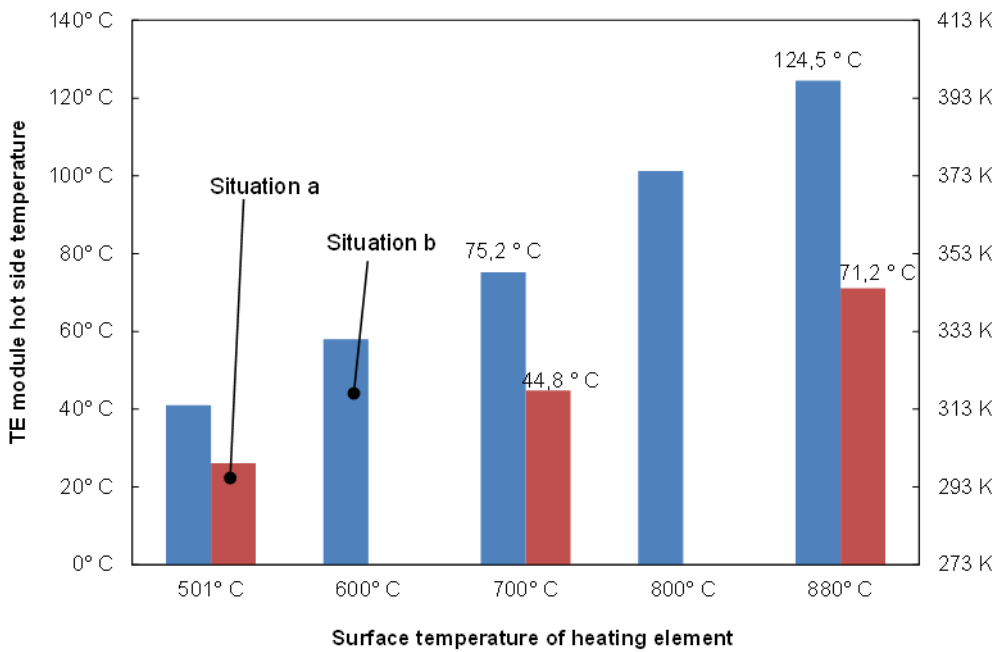
**Figure 3.1.1.6.3** - Prototype B, copper TEG plate and steel sheet geometries

Figure 3.1.1.6.4 shows the effect of the configuration on the amount of power, produced by the TE module (one TE module, supplier 2, see Sec. 3.1.1.7), as a function of the surface temperature of the heating element.



**Figure 3.1.1.6.4** - Electrical power as a function of surface temperature of the heating element, situation a and situation b

Clearly visible is the reduced power generation in situation a. This can be explained by the absence of heat transported from the steel sheet to the TE module hot side (via the copper TEG plate). In situation b, this heat transport mechanism, conductivity, is guaranteed for because of the connection made between steel sheet and the copper TEG plate. This produces an increased surface temperature, both at the hot (Figure 3.1.1.6.5) and cold (Figure 3.1.1.6.6) sides of the module, for situation b (net  $dT_{\text{module}}$  increase).



**Figure 3.1.1.6.5** - TE module hot side temperature as a function of surface temperature of the heating element at situations a and b

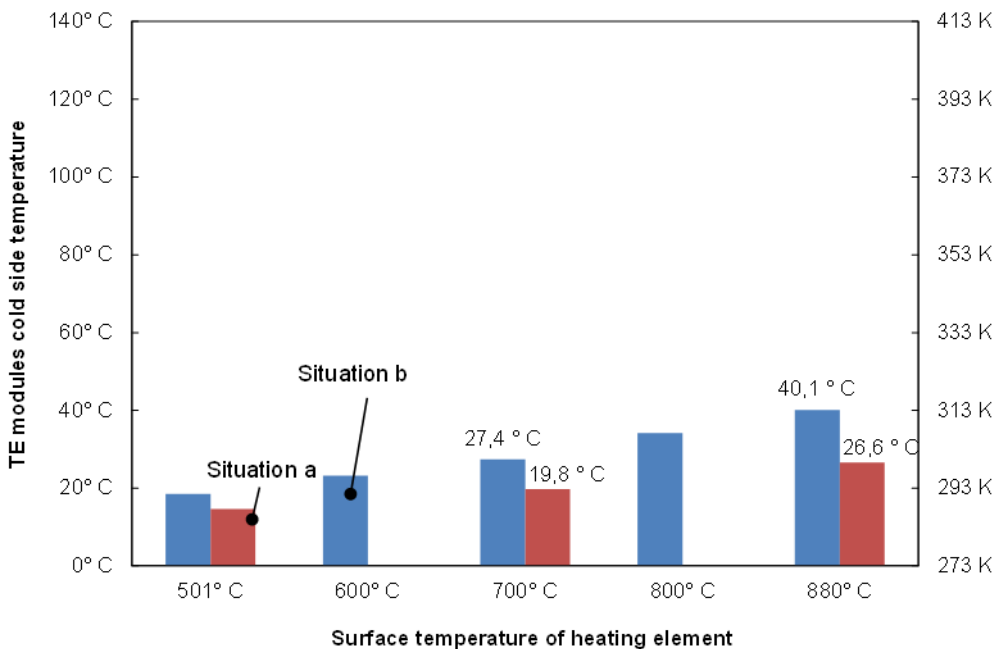


**Figure 3.1.1.6.6** - TE module cold side temperature as a function of surface temperature of the heating element for situations a and b

The maximum conversion efficiency ( $\Phi$ ) of a thermoelectric module (neglecting contacts influence and assuming same thermoelectric properties for n and p-type materials) can be calculated using:

$$\Phi = \frac{T_H - T_C}{T_H} \cdot \frac{\sqrt{1 + Z\bar{T}} - 1}{\sqrt{1 + Z\bar{T}} + T_C/T_H} \quad \text{Eq.3.1.1.6.1}$$

where  $T_H$  = temperature of hot side;  $T_C$  = temperature of cold side ;  $\bar{T} = (T_H + T_C)/2$ ;  $Z$ = figure of merit ( $=\alpha^2\sigma/\lambda$ ).

Table 3.1.1.6.1 shows the efficiency calculations, using Eq.3.1.1.6.1, for BFI trials where the heating element surface temperature was set at 700 °C.

<b>Variable definition</b>	<b>Symbol</b>	<b>Unit</b>	<b>Ref.</b>	<b>Situation a</b>	<b>Situation b</b>
Hot temperature	$T_H$	[K]	Figure 3.1.1.6.5	318	348
Cold temperature	$T_C$	[K]	Figure 3.1.1.6.6	293	301
Dimensionless figure of merit (estimated)	ZT	[-]	-	0.9	0.9
Electric power	$P_e$	[W]	Figure 3.1.1.6.4	0.08	0.38
Conversion efficiency (calculated)	$\Phi$	[-]	-	0.013	0.023
Calculated hot side heat power (calculated)	$\dot{Q}_H$	[W]	-	6.1	16.5

**Table 3.1.1.6.1** – Prototype B, TE power production properties using a heating element with a surface temperature of 700°C

Furthermore, as the conversion efficiency is defined by:

$$\Phi = \frac{P_e}{\dot{Q}_H} \quad \text{Eq.3.1.1.6.2}$$

(where  $P_e$  is the electric power produced by the TE module;  $\dot{Q}_H$  is hot side heat flow)

It is possible to obtain:

$$\dot{Q}_H = \frac{P_e}{\Phi} \quad \text{Eq.3.1.1.6.3}$$

Therefore the hot side heat flow ( $\dot{Q}_H$ ) can be calculated from conversion efficiency definition using Eq.3.1.1.6.3 as the electric power and the conversion efficiency are known.

The last row of Table 3.1.1.6.1 shows the calculated hot side heat flow rate calculated from Eq.3.1.1.6.3.

It can be concluded, for a surface temperature of the heating element of 700°C, that there is a 182% increase of the incident heat flow at the hot side of the module as a result of the surface contact that is realized in situation b. Table 3.1.1.6.2 shows the efficiency calculations for BFI trials where the heating element surface temperature was set at 880°C. In this case, it can be observed that there is a 111 % heat flow increase in  $Q_H$  as a result of the surface contact that is realized in situation b.

Therefore, although the TE module hot side incident heat flow digressively increases upon increasing radiation, the relevance of a heat capacity (in this case the steel sheet connected to the TE module) becomes evident.

<b>Variable definition</b>	<b>Symbol</b>	<b>Unit</b>	<b>Ref.</b>	<b>Situation a</b>	<b>Situation b</b>
Hot side temperature	$T_H$	[K]	Figure 3.1.1.6.5 Figure 3.1.1.6.6	344	398
Cold side temperature	$T_C$	[K]	Figure 3.1.1.6.6	300	313
Dimensionless figure of merit (estimated)	ZT	[-]		0.95	0.95
Electric power	$P_e$	[W]	Figure 3.1.1.6.4	0.33	1.17
Conversion efficiency (calculated)	$\Phi$	[-]		0.023	0.039
Calculated hot side heat power (calculated)	$\dot{Q}$	[W]		14.4	30.4

**Table 3.1.1.6.2** – Prototype B, TE power production properties at a surface temperature of the heating element of 880°C.

### **3.1.1.7 Selection of thermoelectric modules and components (CSM, CU, BFI)**

An important chapter of TEG design concerns the choice of the characteristics of thermoelectric modules. The research efforts to achieve new high efficiency (large ZT) thermoelectric materials have been persistent since the 1950s. During the past decade, new bulk materials, such as lead antimony silver telluride (LAST) and its alloys, including skutterudites, have appeared. These materials show improved ZT, but are only feasible for high-temperature operations. At relatively near room temperature (0° to 250°C),  $\text{Bi}_2\text{Te}_3$ -based (bismuth telluride) materials, with a peak  $\text{ZT} \approx 1$ , still dominate [1].

Despite being expensive and scarce, no other materials are available to operate efficiently in the room temperature range nowadays. During the last 3 years, conducting polymers have appeared as a possible alternative to  $\text{Bi}_2\text{Te}_3$  [2]. However, they are still far in performance and present poorer stability and lifetime. In addition, MgAgSb-based materials have been recently reported [3] with similar properties to  $\text{Bi}_2\text{Te}_3$ , but they are still at a very early stage and only p-type elements have been identified so far.

CSM, CU and BFI have acquired  $\text{Bi}_2\text{Te}_3$  thermoelectric modules, commercially available, from different suppliers for lab-test and on-line trials.

CSM has chosen the largest thermoelectric modules available on the market (62 x 62 mm) to reduce as much as possible the overall dimension of the whole device, with a total module thickness of 4 mm and maximum operating temperature of 250°C. BFI was oriented towards 40 x 40 mm modules with a maximum thickness of 3.9 mm (7.1mm for a Multi Stage Module) and a maximum operating temperature of approximately 250°C, but purchased a 62 mm x 62mm x 4 mm module as well.

Table 3.1.1.7.1 shows the TE modules purchased in the present research by BFI (supplier from 1 to 5) and by CSM (supplier 6). They were not necessarily purchased from the companies that manufacture them; in fact, most of them were purchased from intermediaries. Not all suppliers added complete product specifications to their products, some of them only characterised the product for its operation in Peltier mode.

However, in general, it seems that there are no large performance differences among the different suppliers. Specific laboratory tests have been carried out to verify TE modules performances under certain conditions. The results of these tests are reported in Sec. 3.2.2.2.

An important constructive difference of  $\text{Bi}_2\text{Te}_3$  modules have been observed by CU during the tests. The explanation of these differences and advantages/disadvantages is reported in Sec. 3.3.1.2.

<b>Supplier</b>	<b>Price [€/Module]</b>	<b>T max [°C]</b>	<b>Country of origin</b>	<b>Seebeck coefficient of the module [V/K]</b>	<b>Dimension L x W x H [mm]</b>	<b>Maximum electrical power according to product specification at <math>T_H, T_C, dT</math> [°C]</b>
1	~ 56,00	200	Cuba	n.a.	40 x 40 x 7.1	Peltier characteristics specified only
2	~ 18,20	200	Russia	0.050	40 x 40 x 3.8	Peltier characteristics specified only
3	~ 26,70	225	Russia	0.054	40 x 40 x 3.4	n.a.
4	~ 30,40	200	China	0.053	40 x 40 x 3.5	19 W at 200, n.a., n.a.
5	~ 92,80	250	UK	0.052	62 x 62 x 4	25,5 W at 250, 30, 220
6	~ 37,44	250	UK	0.052	62 x 62 x 4	28,3 W at 250, 30, 220

**Table 3.1.1.7.1** - TE modules purchased in the project

A typical  $\text{Bi}_2\text{Te}_3$  module produces about 1 - 5 W of electricity for a temperature gradient of 100°C. This power output decreases not linearly when reducing the temperature gradient (Figure 3.1.1.7.1).

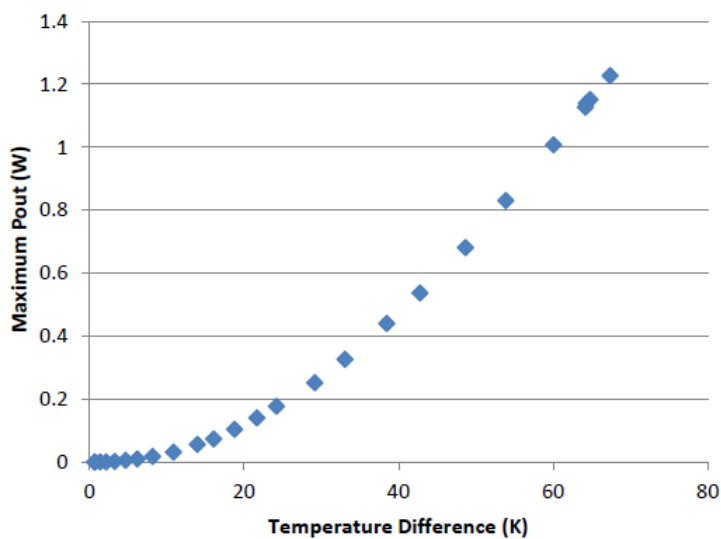


**Figure 3.1.1.7.1** - Typical  $\text{Bi}_2\text{Te}_3$  based TE modules electric power output

For example, it is expected for Prototype A that each thermoelectric module will produce 0.8-1 W at a temperature gradient of about 60°C (see also Sec. 3.3.3.1), but the same component is able to produce about 5 W for a temperature gradient of 110°C.

Another important aspect to keep in mind during the design of a TEG device is the coupling between the thermoelectric module and the "component" used to capture and distribute the heat (for example the aluminium boxes for prototype A and the copper plate for prototype B).

In general, to increase the overall efficiency of the TEG system, it is required to increase as much as possible the heat flow exchanged between the TE modules and the "components" (both on the hot and cold side). This can be obtained by increasing the contact surface between the two parts. Therefore, it is required to increase the forces between the two parts and to introduce a soft material (or grease), with high thermal conductivity, which fills the gaps (removing air) at the junction between the two rigid surfaces.

Pressed graphite sheets are generally a suitable solution. However, other materials, less expensive, can be used as well. A study involving the use of different materials has been carried out by BFI and is discussed in Sec. 3.3.2.1.

### **3.1.1.8 Thermoelectric module design theory (CU)**

The design of a thermoelectric device is very important in order to optimise its performance. CU is committed in the project to the development of theoretical models to assist with the module design. These models can be used both to improve the module design for thermoelectric generator objectives and also to support the general design of the system prototypes.

Table 3.1.1.8.1 reports the definitions of the variables used in the following theoretical models.

<b>Symbol</b>	<b>Variable Definition</b>
$\alpha$	Seebeck coefficient
$\Delta T$	temperature difference across the module
$\Phi$	conversion efficiency
$\lambda$	thermal conductivity of the thermoelement
$\lambda_c$	thermal conductivity of the contact layer
$\rho$	electrical resistivity of the thermoelement
$\rho_c$	electrical resistivity of the contact layer
$A$	cross-sectional area of thermoelement
$l$	length of the thermoelement
$l_c$	thickness of the contact layer
$K$	total thermal conductance of both n- and p-type thermoelements
$N$	number of thermoelements in a module
$P_{out}$	power output delivered to the load
$R_L$	electrical resistance of the electric load
$R_{TEM}$	electrical resistance of the module
$T_C$	cold side temperature
$T_H$	hot side temperature

**Table 3.1.1.8.1** - Model variables definitions

### **3.1.1.9 Theoretical model at given $\Delta T$ (CU)**

A first thermoelectric model can be obtained when the temperature gradient across the thermoelectric module is considered fixed. This occurs if the temperature at the hot and cold sides can be maintained constant, for example using temperature controllers or similar methods. However, in most of the practical situations it is more common that the device operates under a fixed heat flux and temperature variations occur during operation. This case will be also described later on.

Assuming a thermoelectric module as the one shown in Figure 3.1.1.9.1 and for a given  $\Delta T$ , it is possible to calculate exactly the power output delivered to the load ( $P_L$ ) and the conversion

efficiency ( $\phi$ ) of a single module. The conversion efficiency is defined as the ratio between the maximum power output delivered to the load and the heat flux absorbed at the hot side of the device.

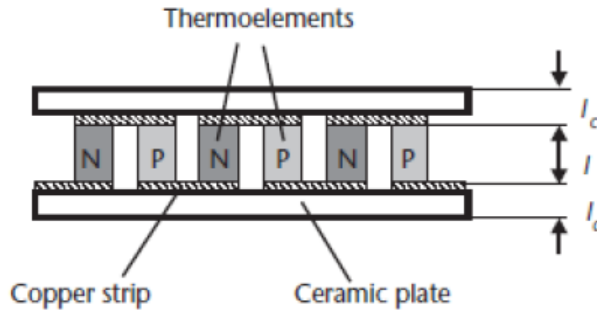


**Figure 3.1.1.9.1** - Cross sectional view of a thermoelectric module

Below, the formulas for  $P_L$  and  $\Phi$  when  $\Delta T$  is considered constant are given.

$$P_L = \frac{s}{(1+s)^2} \frac{\alpha^2}{\rho} \frac{NA \Delta T^2}{(n+l) \left(1 + 2r \frac{l_c}{l}\right)^2} \quad \text{Eq.3.1.1.9.1}$$

$$\phi = \frac{\frac{\Delta T}{T_H}}{\left(1 + 2r \frac{l_c}{l}\right)^2 \left(2 - \frac{1}{2} \left[\frac{\Delta T}{T_H}\right] + \left[\frac{4}{Z T_H}\right] \left[\frac{l+n}{l+2r l_c}\right]\right)} \quad \text{Eq.3.1.1.9.2}$$

Where:  $s = \frac{R_L}{R_{TEM}}$ ;  $n = 2 \frac{\rho_c}{\rho}$ ;  $r = \frac{\lambda_c}{\lambda}$ ;  $Z = \frac{\alpha^2}{R_{TEM} K}$

Figure 3.1.1.9.2 reports the result of the simulations for the power output and efficiencies using above equations. It is shown how the power output per unit area, at a given  $\Delta T$ , has a maximum close to 1 mm of the thermoelement length and then decreases exponentially. On the other hand, the efficiency keeps increasing at higher thermoelement lengths but reaching a constant trend after few mm. For this reason a compromise between efficiency and power output is usually followed and typical thicknesses employed are around 1-2 mm.

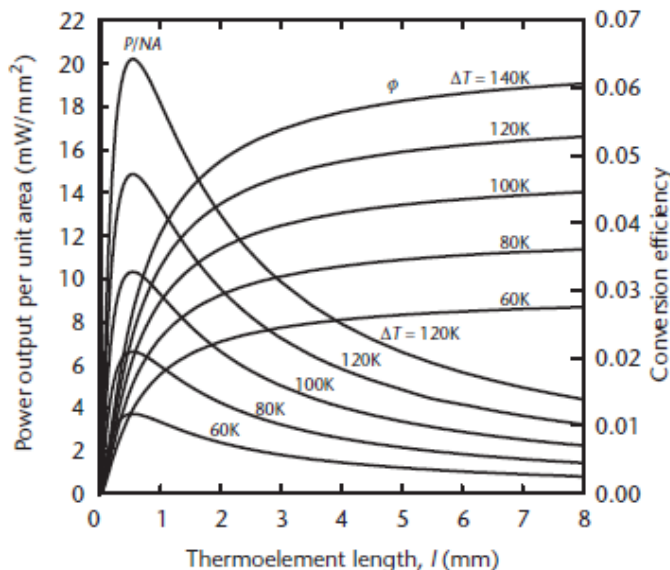


**Figure 3.1.1.9.2** - Thermoelectric model results for given  $\Delta T$

### 3.1.1.10 Theoretical model at given thermal input $Q$ (CU)

Similarly as in the previous model, the thermal input of a module can be fixed, and consequently the power output calculated. Figure 3.1.1.10.1 shows this situation.

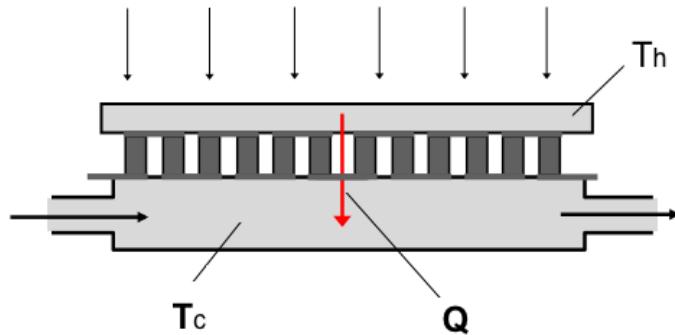


**Figure 3.1.1.10.1** - Thermoelectric module subject to a given thermal input

Below are the formulas for  $P_L$  and  $\Phi$  when the thermal flux  $\dot{Q}$  is constant are given.

$$P_L = \frac{s}{(1+s)^2} \frac{Z}{(1+Z T_M)^2} \frac{\dot{Q}^2 l^2}{\lambda A (n+l) \left(1 + 2r \frac{l_c}{l}\right)^2} \quad \text{Eq. 3.1.1.10.1}$$

$$\Phi = \frac{s}{(1+s)^2} \frac{Z}{(1+Z T_M)^2} \frac{\dot{Q} l^2}{\lambda A (n+l) \left(1 + 2r \frac{l_c}{l}\right)^2} \quad \text{Eq. 3.1.1.10.2}$$

Where:  $s = \frac{R_L}{R_{TEM}}$ ;  $n = 2 \frac{\rho_c}{\rho}$  ;  $r = \frac{\lambda_c}{\lambda}$  ;

$$Z = \frac{\alpha^2}{R_{TEM} K}; T_M = \frac{(1+2s) T_H + T_C}{2 (1+s)^2}$$

Figure 3.1.1.10.2 shows the result of the simulation for a given thermal flux  $\dot{Q}/A = 600 \text{ W/m}^2$ .

From the simulations it is clear that there is no need to go for long lengths, as the power output saturates. Furthermore, if a fixed length is considered, at larger cross-sectional areas of the elements, the power output is lower due to the decrease of  $\Delta T$ . This indicates that at smaller amount of thermoelectric elements (less number of modules) the power output is enhanced.

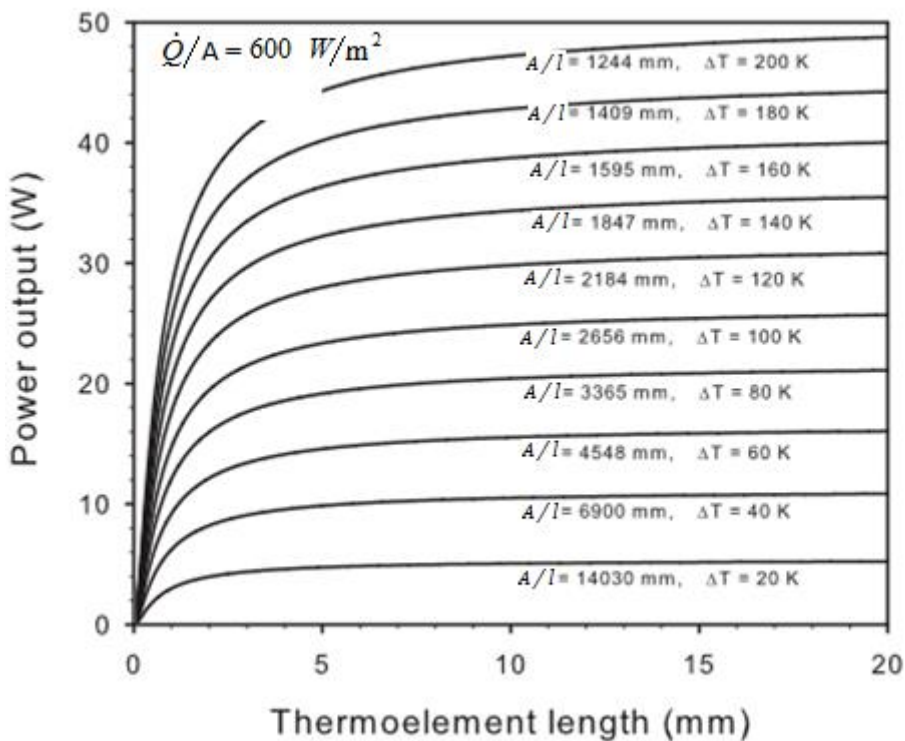


**Figure 3.1.1.10.2** - Thermoelectric model results for given thermal flux (600 W/m<sup>2</sup>)

### 3.1.1.11 Theoretical study to use the prototype A in the range 100°C-350°C (CSM, FENO)

From Eq.3.1.1.9.1 it is possible to calculate the electric power output of a thermoelectric module. Assuming constant its physical properties, this equation shows that the electric power varies with the square of the temperature difference between the hot source and the cold sink.

For the case of prototype A the cold water comes from a well, close to the plant, and its temperature cannot be reduced. Therefore, the only possibility to raise the TEG power is to increase the hot source temperature.

EAF off-gas flowing into the main duct has a temperature of around 1000°C-1200°C, at the exit of the furnace after air infiltration, and drop down to about 600°C in the duct section where it is cooled by the water air cooling system. In principle, it is possible to raise the temperature of the cooling water. Of course, there are two main limitations: the first one is related with the cooling plant design and the second with steam formation into the piping.

Every industrial plant is designed for specific operative conditions and cannot work outside these conditions without a revision of its certification and in particular, for pressurized plant, is required to satisfy the European Pressure Equipment Directive (PED). For example, assuming that is possible to obtain a new plant certification maintaining the operating water temperature 70°C below the water saturate steam temperature (this fact must be verified under the specific plant certification conditions), Table 3.1.1.11.1 shows the maximum temperature of the hot source as a function of the maximum available pressure in the pipeline.

At present, Ferriere Nord EAF water air cooling system works with a maximum operating pressure of 7 barG and a maximum working temperature of 100°C.

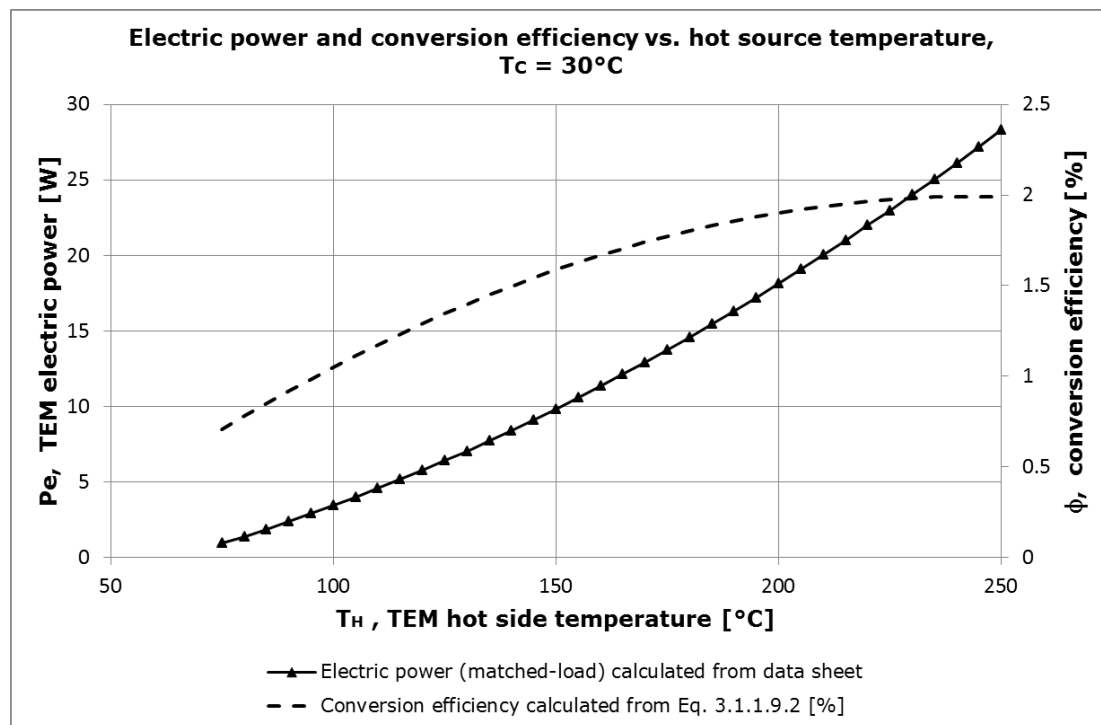
Table 3.1.1.11.1 shows that it is possible to raise the temperature of the water up to 120°C-130°C changing some safety components (and plant certifications) without any substantial change of the pipeline material.

Operative water temperature [°C]	Operative duct pressure [barG]	Saturate steam temperature [°C]
95	6	165
100	7	170
105	8	175
110	9	180
114	10	184
118	11	188
122	12	192

**Table 3.1.1.11.1** – Operative water temperature in the pipeline with a safety temperature gap of 70°C

On the basis of the above, it can be considered reasonable to adapt the cooling system to maintain the cooling water at a maximum temperature of around 120°C and make it available as the hot source of the TEG system. Higher temperatures are also achievable but it requires substantial changes to the plant and substantial additional costs.

From Eq.3.1.1.9.2 it is possible to estimate the conversion efficiency of a thermoelectric module as a function of the hot source temperature.



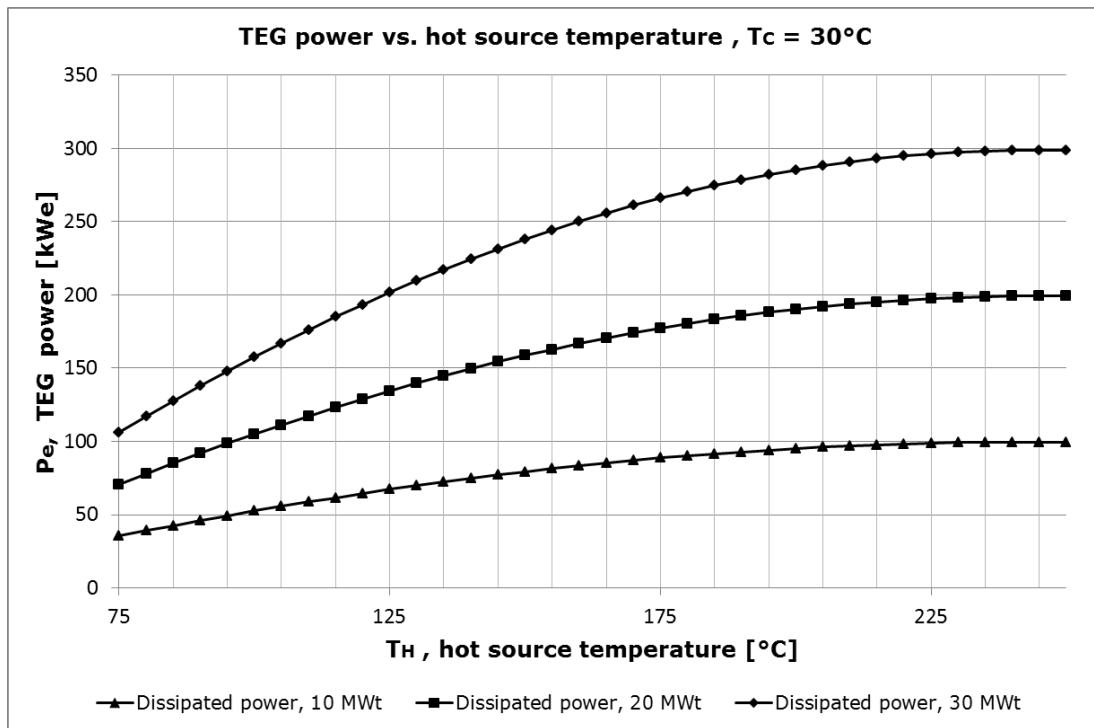
**Figure 3.1.1.11.1** – Prototype A, electric power and conversion efficiency of one TEM vs. hot side temperature (cold side temperature =30°C)

Figure 3.1.1.11.1 shows the efficiency trend for the thermoelectric module used in prototype A (European Thermodynamics® GM250-127-28-10). In this figure the electric power of one TEM has been obtained from the graph "Matched Load Output Power v. Hot side temperature for various fixed cold sides" reported into the manufacturer datasheet, while the conversion efficiency has been obtained using the physical parameters reported in the same manufacturer datasheet (see Table 3.1.1.11.2).

Symbol	Unit	Value
N	[-]	126
A	[mm <sup>2</sup> ]	6.25
r	[-]	0.2
l <sub>c</sub>	[mm]	1.95
l	[mm]	0.7
$\alpha_n$	[ $\mu$ V/K]	$0.001530736*T^2 - 1.08058874*T - 28.338095$
$\alpha_p$	[ $\mu$ V/K]	$-0.003638095*T^2 + 2.74380952*T - 296.214286$
$\sigma_n$	[S/m]	$(0.01057143*T^2 - 10.16048*T + 3113.71429)*10^2$
$\sigma_p$	[S/m]	$(0.015601732*T^2 - 15.708052*T + 4466.38095)*10^2$
$\lambda_n$	[W/(mK)]	$0.0000334545*T^2 - 0.023350303*T + 5.606333$
$\lambda_p$	[W/(mK)]	$0.0000361558*T^2 - 0.026351342*T + 6.22162$

**Table 3.1.1.11.2 – Prototype A, TEM parameters**

From Figure 3.1.1.11.1 it can be calculated the electric power supplied by a whole TEG system as a function of the total thermal power supplied to the TEG system for each temperature of the hot source, assuming a total conversion efficiency of the whole system as a fraction of the conversion efficiency of the TE module.



**Figure 3.1.1.11.2 – TEG power vs. hot source temperature for different thermal power cooling plant (TEMs cold side temperature = 30°C)**

One of the objectives of this project is to exactly evaluate the value of the fraction of energy lost in the conversion of the thermal power from the hot source into electricity. This value will be determined experimentally, but for a simplified calculation it can be assumed to be 0.5, i.e. exactly half of the thermoelectric modules conversion efficiency.

Figure 3.1.1.11.2 shows the calculated electric power supplied by a TEG as a function of temperature of the hot source (hot water) for some hypothesized total thermal power supplied to

the TEG system, i.e. dissipated power from the plant cooling system. For example, assuming that the plant cooling system has to dissipate 20 MW<sub>t</sub> of thermal power (close to Ferriere Nord EAF cooling system plant), this figure shows that it is possible to produce about 71 kW<sub>e</sub> of electric power (see squared dots) with the TEG using a hot source temperature of 75°C, or 135 kW<sub>e</sub> using a hot thermal source temperature of 125°C. From the same figure the maximum number of required thermoelectric modules can be obtained. The maximum number of TEMs can be calculated by means of the conversion efficiency as the energy lost in the energy conversion is known. Once the number of TEM required is known, it is also possible to calculate the price of the TEG and therefore evaluate its possible economic benefit.

### **3.1.1.12 Theoretical study to use the prototype B in the range 150°C-350°C (AME, BFI)**

Alloys based on bismuth telluride can be used at temperatures up to 250°C [1]. There are other materials which can be suitable at higher temperatures, such as skutterudites, and PbTe-based alloys as shown in Figure 3.1.1.12.1. We would like to remark here (before comparing the performance of different materials based on ZT values) that when ZT values are measured at different set temperatures, a small T difference around this set temperature (usually a difference around 10 °C) is used. Thus, under actual operating conditions, where the material operates in a wide T range (instead of just few degrees around a set temperature) an average ZT in the operating T range should be considered.

It can be observed (see Figure 3.1.1.12.1) that for the T range between room temperature and 350 °C, Bi<sub>2</sub>Te<sub>3</sub> alloys show a higher average ZT than the other alternatives (skutterudites, PbTe-based alloys, etc.). A performance similar to Bi<sub>2</sub>Te<sub>3</sub> is achieved by skutterudites at T>200°C. At lower temperatures, a ZT higher than 0.8 could be considered for Bi<sub>2</sub>Te<sub>3</sub>, whereas skutterudites show values between 0.5 and 0.8. This fact points out that although better ZT values than Bi<sub>2</sub>Te<sub>3</sub> can be achieved by skutterudites at higher temperatures, the difference is not that significant to balance the poorer performance at the lowest temperatures.

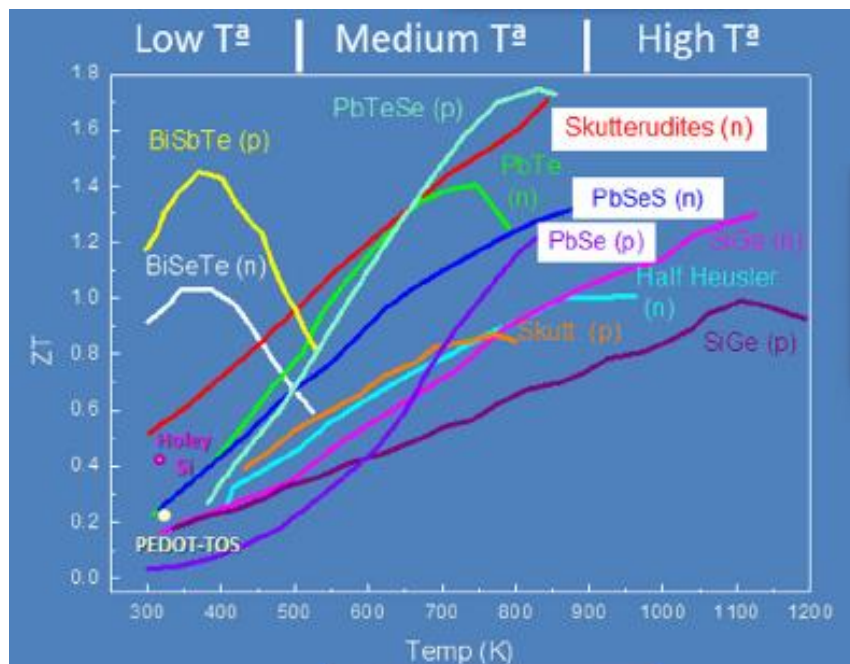


**Figure 3.1.1.12.1 – ZT of state of the art thermoelectric materials vs. temperature.**

In addition, the technology for module fabrication is more advanced and well established for Bi<sub>2</sub>Te<sub>3</sub> than the other materials, and due to this the whole device performance is expected to be better and more reliable.

As the dimension of the power production facility can decrease upon increasing efficiency, the specific costs for power production can also decrease. Ideally, thermoelectric generators should be positioned (in the case of TE module heated by means of radiation) in the way for the highest possible hot side temperature to be reached. An actuator, controlled by a temperature measurement, could be used to reach the optimum distance between hot material and the TE generator, see Figure 3.1.1.12.2.

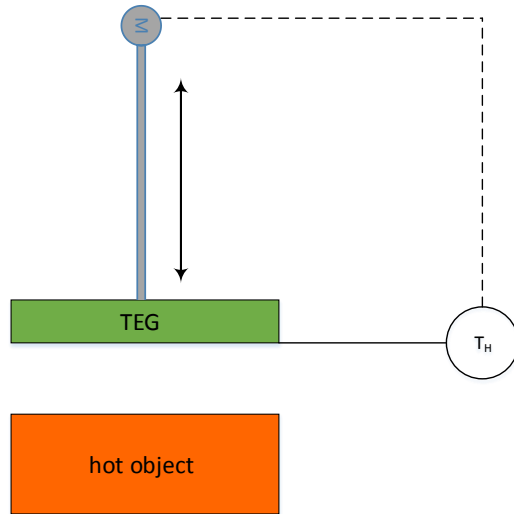


**Figure 3.1.1.12.2** – Example of a regulation system to obtain the optimal distance from the radiation hot source

### 3.1.2 Task 1.2 - Development of tools for control and monitoring (CSM, CU, BFI)

Prototype A and B have been equipped with several sensors and control devices with the objective of both optimising and verifying the performances of the developed generators. The following paragraphs describe these control systems in detail.

#### 3.1.2.1 Prototype A: tools for control and monitoring (CSM, FENO)

Prototype A generates electricity depending on the temperature difference at the TEM sides and on the flow rates at the water circulation circuits. A temperature difference increase, between the TEM sides, increases the produced electricity (see Figure 3.1.1.7.1). Similarly, an increase of the water flow rates increases the cooling/heating capacity of the water boxes and hence the temperature difference across the TEMs. In fact, the increase of the water flow lowers the temperature difference between the water boxes extremities, making it more similar at the different positions.

Therefore, prototype A has been equipped with four thermoresistance sensors positioned at the water inlet and outlet of thermoelectric modules. During the on-line test the water temperature cannot be regulated, because depends on the available water supply, but can be measured and data gathered on the PC.

Two inverters control both the pump of the hot water closed circuit and the electro valve of the cold water open circuit. These controls regulate the heat input (at the hot side) and heat removed (at the cold side) of the TEMs respectively. The inverters use, as a reference, the measurement of the water flow rate obtained by two flowmeters (see Figure 3.1.1.5.1).

By the regulation of the flow rate it is possible to verify the real conversion efficiency of the system at different operating conditions.

Figure 3.1.2.1.1 shows parts of the control and monitoring software interfaces developed.

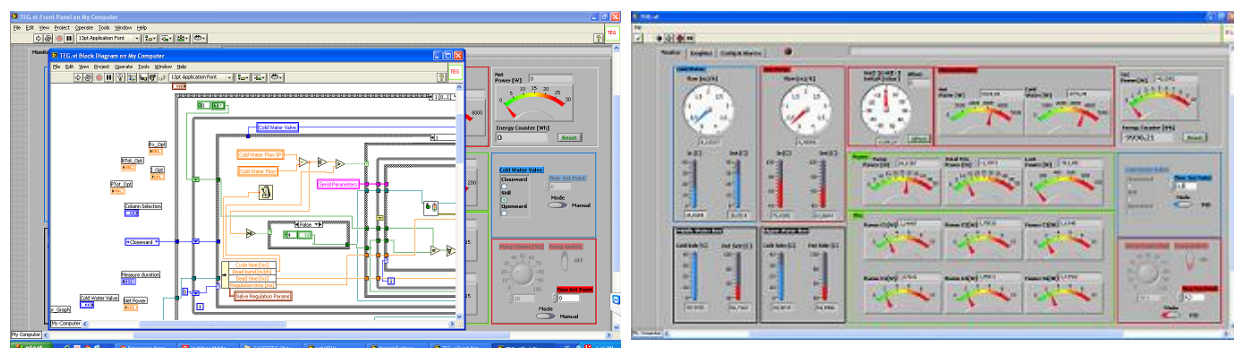


**Figure 3.1.2.1.1** - Prototype A: on line control and monitoring software & interface

In order to measure the efficiency ( $\phi_A$ ) of Prototype A, the following equation has been used:

$$\phi_A = \frac{P_e}{\dot{Q}_H} \quad \text{Eq. 3.1.2.1.1}$$

where  $P_e$  = electric power produced by the TEG;  $\dot{Q}_H$  = thermal power to the TEMs.

$P_e$  has been measured using the following equation:

$$P_e = \frac{V^2}{R_L} \quad \text{Eq. 3.1.2.1.2}$$

where  $V$  is the voltage generated by the TEG (measured by an Analog I/O module) and  $R_L$  is the load resistance (defined by the electric circuit design).

$\dot{Q}_H$  was calculated using the following equation:

$$\dot{Q}_H = \dot{m}_H c_p \Delta T_H \quad \text{Eq. 3.1.2.1.3}$$

where  $\dot{m}_H$  is the hot side water mass flow rate (measured by the hot water volume flow rate measurement system multiplied by the water density),  $c_p$  the specific heat capacity of the water,  $\Delta T_H$  is the temperature variation of the hot water between the inlet and the outlet of the TEG hot water circuit (measured by the pair of thermoresistances).

More details on the monitoring and control system layout and sensors description (in terms of type and characteristics) are reported in Annex A.2 (Deliverable D1.2 – Description of the tools for modules control and monitoring).

### 3.1.2.2 Prototype B: tools for control and monitoring (AME, BFI)

In order to be able to determine the efficiency ( $\phi_B$ ) of Prototype B, the following equation has been considered:

$$\phi_B = \frac{P_e}{\dot{Q}_H} \quad \text{Eq.3.1.2.2.1}$$

where the electrical power ( $P_e$ ) and the thermal input at the hot side ( $\dot{Q}_H$ ) need to be determined.

Introducing the following equation:

$$P_e = \dot{Q}_H - \dot{Q}_C - \dot{Q}_{loss} \quad \text{Eq.3.1.2.2.2}$$

where  $\dot{Q}_C$  is the thermal power extracted from the TEG cold side by the heat sink,  $\dot{Q}_{loss}$  is the system loss thermal power (heat losses).

Assuming no heat losses ( $\dot{Q}_{loss} = 0$ ), the thermal power to the hot side can be determined by:

$$\dot{Q}_H \sim P_e + \dot{Q}_C \quad \text{Eq.3.1.2.2.3}$$

Therefore, from Eq.3.1.2.2.1 and Eq.3.1.2.2.3 (assuming no heat losses):

$$\phi_B \leq \frac{P_e}{P_e + \dot{Q}_C} \quad \text{Eq.3.1.2.2.4}$$

In order to estimate the conversion efficiency, it is necessary to measure  $P_e$  and  $\dot{Q}_C$ .

The electric power generated by Prototype B can be obtained by:

$$P_e = V I \quad \text{Eq.3.1.2.2.5}$$

where  $V$  (input signal for MeasX data acquisition system) and  $I$  (measured by Minipan 352V) are the voltage and current generated by the TEG respectively.

Thermal power from the TEG cold side to the heat sink can be obtained by:

$$\dot{Q}_C = \dot{m}_C c_p \Delta T_C \quad \text{Eq.3.1.2.2.6}$$

where:

- $m_C$  equals the cooling water mass flow through the heat sink that can be calculated by multiplication of the magnetic-inductive flow measurement value and the cooling water density (assumed here  $1000 \text{ kg m}^{-3}$ ),
- $c_p$  is the cooling water specific heat capacity (here  $4.182 \text{ J kg}^{-1} \text{ K}^{-1}$ ),
- $\Delta T_C$  is the temperature increase of cooling water as a result of the heat flow from the TE module to the heat sink. The most accurate temperature measurements, two Pt100-resistance temperature sensors, have been selected here.

In addition to these measurements, a variable load resistance (range:  $0 \Omega - 800 \Omega$ ) will be used when testing Prototype B at the AME hot wire mill. Type K thermocouples allow the temperature measurement of the individual components that form the TE generator (e.g. copper plate, panel, (cold side) heat exchanger). One of the parameters that has to be monitored constantly is the temperature at the hot side of the TE module, since exposure to too high temperatures can wreck the TE module (see Sec. 3.3.1.3). Thermal conductive paste is always used at the junctions of two surfaces to reduce thermal contact resistances.

Sensors description (in terms of type and characteristics) and their position within Prototype B are reported in Annex A.2 (Deliverable D1.2 – Description of the tools for modules control and monitoring).

## **3.2 WP 2 - Construction of laboratory lab-scale "test bed" and laboratory tests**

WP2 objectives are:

- Fabrication and installation of a lab-scale "test-bed",
- Execution of labs tests in order to check the performance and reliability of modules and components.

### **3.2.1 Task 2.1 - Construction of laboratory lab-scale "test bed" (CSM, CU, BFI)**

In order to verify the performances and limits of prototypes and components, CSM, CU and BFI set up three laboratories equipped with systems able to test the main prototypes components. To simulate the hot source and the cold sink both hot/cold water and radiation systems have been put in operation. These set-ups are named "test beds". Furthermore, the "test beds" have been equipped with different measurement systems needed to run the tests. The following paragraphs report a description of how the test bed has been set up and a description of the tests carried out.

#### **3.2.1.1 Design and construction of CSM laboratory "test bed" (CSM)**

Three types of laboratory tests have been carried out at CSM laboratories and consequently the following three different lab scale test beds have been prepared:

- Lab scale test bed for the hydraulic pressure test.
- Lab scale test bed for single TEM electric power and maximum compression verification.
- Lab scale test bed for TEG on-line readiness test.

#### **Lab-scale test bed for hydraulic pressure test**

CSM-Ferriere Nord thermoelectric generator has been designed to work with hot and cold liquid fluids, therefore each TE module is sandwiched between two water boxes. The foreseen pressure in the water boxes, as designed, was expected to be 4-6 bar for the hot water circuit and 4-8 bar for the cold water circuit. Therefore, each water box and connection has been designed and tested to work under a pressure of 10 bars.

Figure 3.2.1.1 shows a scheme of the lab-scale test bed set up used to verify the liquid sealing of the water boxes and the connectors. All the tests were positive, and TEG components have perfectly withstood the 10 bar pressure without showing any leak.

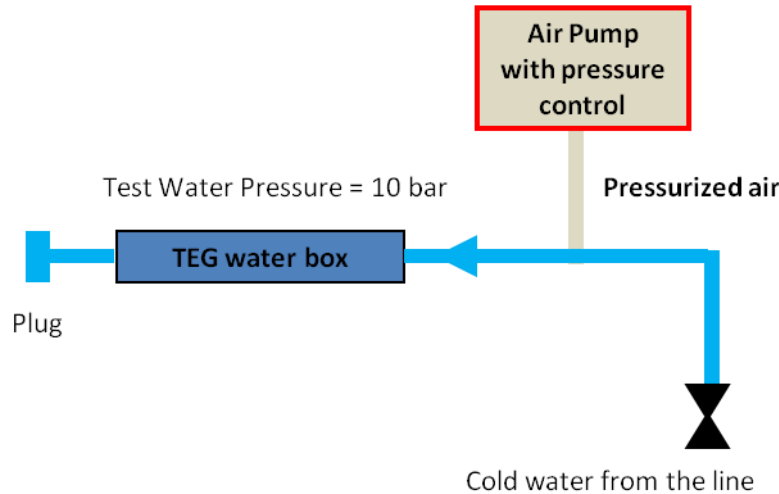


**Figure 3.2.1.1.1** – Lab-scale test bed for the hydraulic pressure test

#### **Lab-scale test bed for single TEM electric power and maximum compression verification**

This lab-scale test bed is designed for measuring the electric power produced by a single TE module under different pressure and heating conditions. A single TE module has been sandwiched between a water box, flowing cold water from the net, and an aluminium plate, heated by a small electric hot plate with an electronic temperature regulation system. Over the cold water box a set of Christian Bauer Disk Spring was applied giving the possibility to regulate and monitor the total pressure applied to the thermoelectric module.

Figure 3.2.1.1.2 shows the layout of this lab-scale test bed set up. The temperature of the cold water was measured using a portable thermometer and the values obtained were in the range of 17-20 °C. The water flow rate was regulated by a manual control valve. The temperature of the aluminium plate was measured by a thermocouple and controlled by the small electric furnace with electronic set-up system.

The objective of this test was to measure the TE module matched-load resistance under variable operating conditions, to verify the produced current under different TEM compression loads, and the maximum compression load applicable.

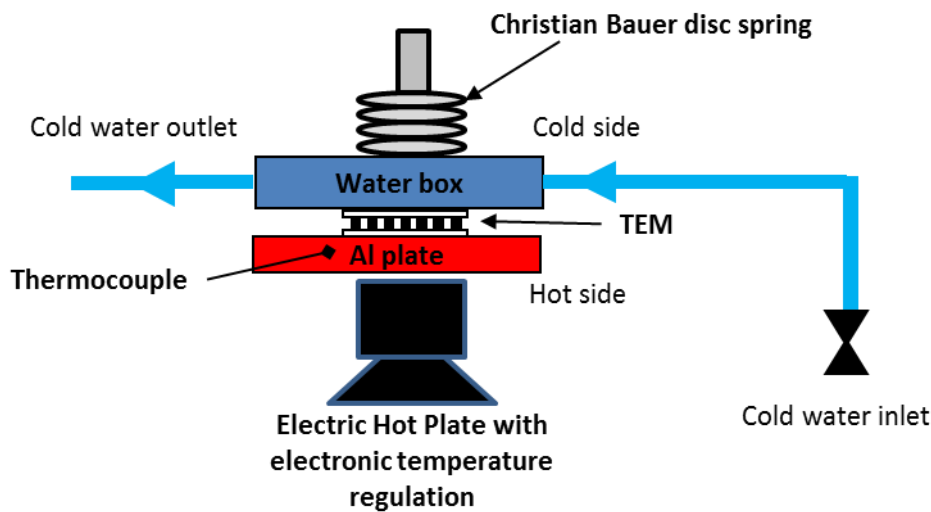


**Figure 3.2.1.1.2** - Lab scale test bed for single TEM test

#### **Lab-scale test bed for TEG on-line readiness test**

This lab-scale test bed is designed to test the overall thermoelectric generator "Prototype A" in order to have it ready for the on-line application at Ferriere Nord plant.

Figure 3.2.1.1.3 shows the lay out of this lab-scale test bed.

The hot water is heated up by three electrical heaters connected in series, supplying each one around 1500 W of thermal power. The electrical heaters have been un-regulated to reach the maximum temperature possible working under safe conditions. Working with the TEG cold side cooled by cold water flow, the lab-scale test bed was able to supply the TEG with hot water at a temperature of about 85°C, at stationary conditions. To circulate the hot water into the lab-scale test bed the same pump that will be used for the on-line tests was used. At the end of the mid-term report period, the hot and cold water flow meters were installed but they were not already ready for data acquisition. Therefore, during the first laboratory test it was measured the temperature of the cold and hot water, the pump power consumption and the power output of the TEG.

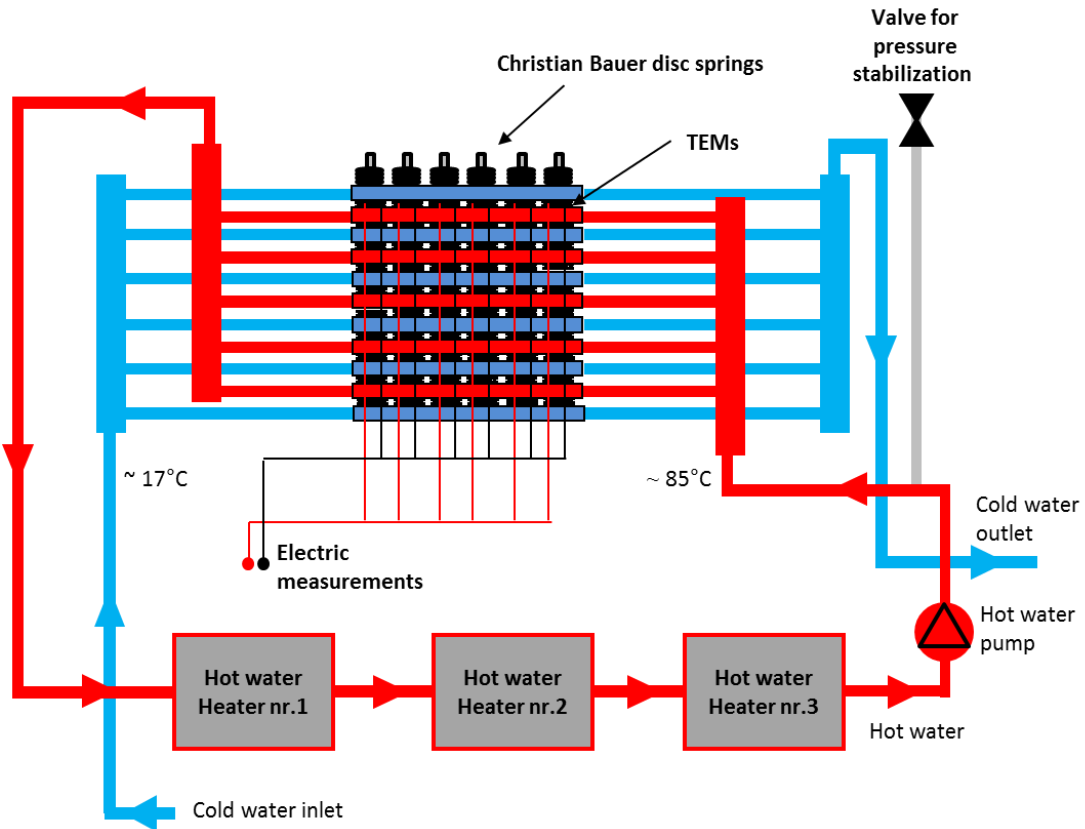


**Figure 3.2.1.1.3 – Lab-scale test bed for TEG on-site readiness test**

Laboratory “test bed” photos and components characteristics are reported at Annex A.3 (Deliverable D2.1 – Design of the lab-scale test bed).

### 3.2.1.2     *Design and construction of Cardiff University laboratory “test bed” (CU)*

#### **Lab-scale test bed**

A lab-scale test bed was designed and constructed at the School of Engineering, Cardiff University. The purpose of the test bed was to characterise the performances of thermoelectric modules, and analyse their performance in terms of the maximum power output, conversion efficiency, effective ZT, and matched load resistance under operating conditions.

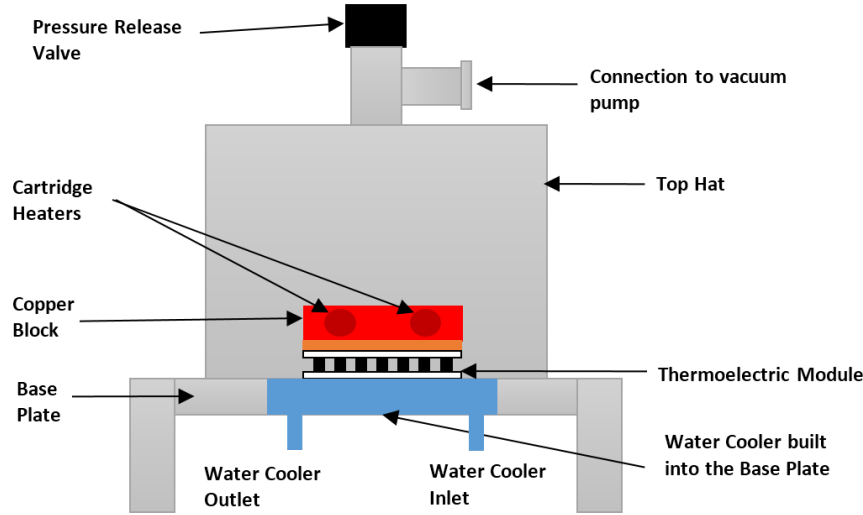


**Figure 3.2.1.2.1** - Schematic diagram of module characterisation set-up

The main components of the test bed are shown in Figure 3.2.1.2.1, which include:

- *Vacuum Chamber* - The vacuum chamber is the main component of the test bed that allows experiments to be conducted under vacuum so that the effect of convection heat loss can be eliminated. It is made up of two parts; the top hat and the base plate. The top hat is made up of aluminium and it consists of connections for the vacuum pump hose and pressure release valve. The base plate is made up of a thick aluminium plate with a built-in liquid heat exchanger, which is connected to a temperature controlled water recirculation unit.
- *Heat Source* - In order to measure the performances of a thermoelectric module, a temperature difference is required to be established across the module. This is achieved by attaching a heat source on the top side of the thermoelectric module and pumping away the heat from the cold side. The heat source comprises of a copper block of length and width same as the module to be tested. Cartridge heaters, two or three depending upon the size of the module, are inserted into the copper block. These heaters are connected to a variable transformer so that the amount of heat supplied, hence the temperature, can be controlled.
- *Cold Source/Cold Water Recirculation unit* - The cold water recirculation unit is a Neslab GP-200 Constant Temperature Bath, which provide temperature controlled cooling water to the heat exchanger on the base plate of the vacuum chamber. The unit consists of a heater, circulation pump, stainless steel bath, and a temperature controller.
- *Temperature sensors* - K-type thermocouples are used to determine the temperature of hot and cold sides. The thermocouples are connected to a thermocouple data logger.
- *Vacuum Pump* - A 2-stage pump system, consisting of a rotary vane and a turbomolecular pump, is used to achieve vacuum in the chamber with a pressure down to  $1 \times 10^{-5}$  torr.
- *Potentiostat* - The thermoelectric module is connected to an Autolab PGSTAT302N Potentiostat for I-V (current-voltage) curves measurements, which enables determination of the maximum power output and module resistance, and other relevant thermoelectric properties.

#### **Lab-scale power generator**

A lab scale power generator was designed to analyse the behaviour of a number of modules connected in series or parallel (Figure 3.2.1.2.2).

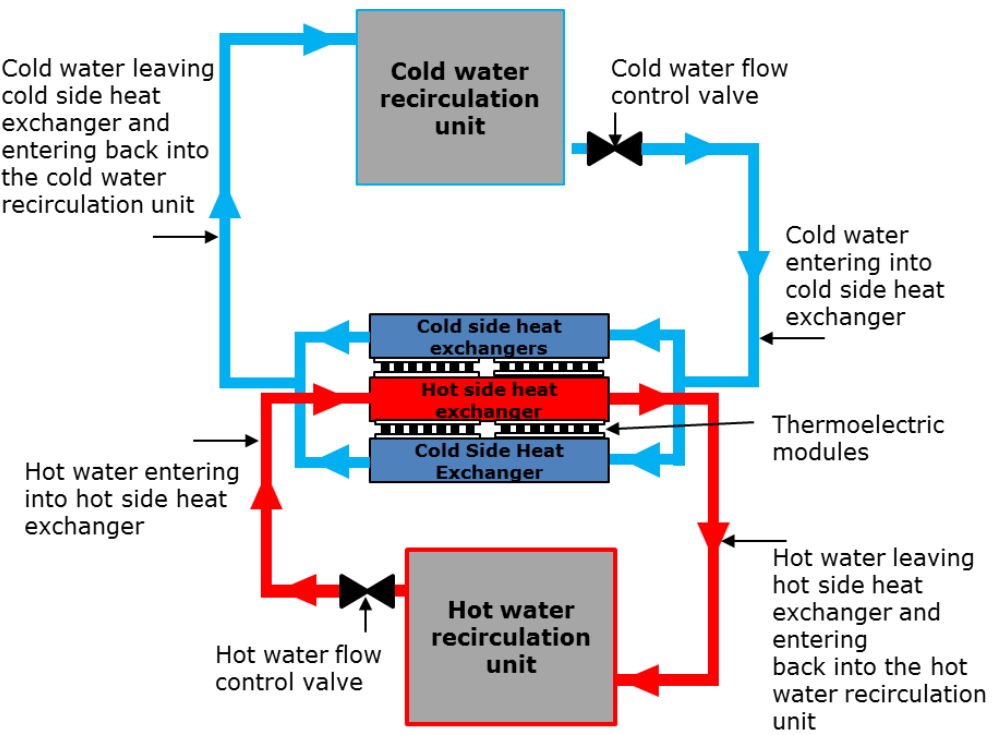


**Figure 3.2.1.2.2** - Schematic of Lab Scale Power Generator developed by CU

Main components of the power generator include:

- *Hot Water Recirculation unit* - The Hot Water Recirculation unit is a *HTC-1200 Recirculating Heater*, which is designed to provide a continuous flow of heated fluid at a constant flow rate and temperature. The unit consists of a stainless steel reservoir, a pump, a heater with a high temperature limit device, and a digital temperature controller.
- *Cold Water Recirculation unit* - The Cold Water Recirculation unit is the same as used in the test bed.
- *Hot and Cold Side Heat Exchangers* - There are two cold side heat exchangers and one hot side heat exchanger in the configuration, as shown in the figure 3.2.1.2.3. The heat exchangers are made up of copper and have inlet and outlet connections for fluid supply.
- *Thermoelectric Modules* - There can be up to eight thermoelectric modules used in the power generator; four modules are placed on each side of the hot side heat exchanger. The modules are sandwiched between the hot and cold side heat exchangers in a way that the hot side heat exchanger is common for all the modules, as shown in the Figure 3.2.1.2.3.

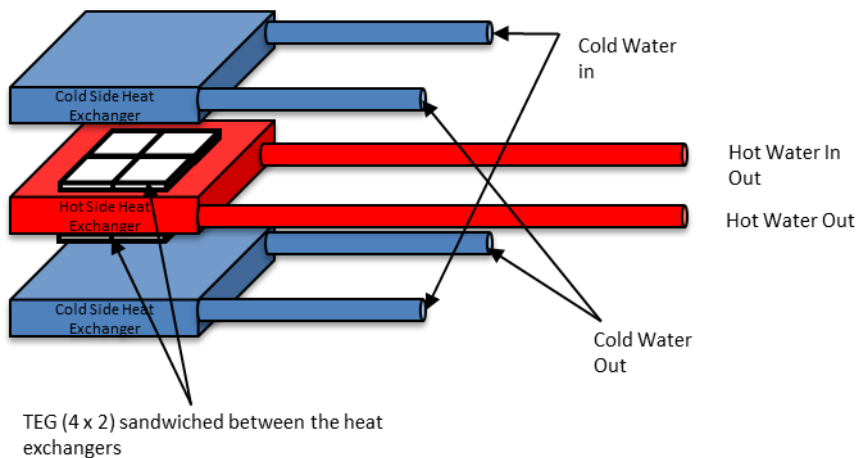


**Figure 3.2.1.2.3** - Schematic of Cold and Hot Side Heat Exchangers and Thermoelectric modules in CU's Lab Scale Power Generator

Figure 3.2.1.2.4 shows power output from CU's Lab Scale Power Generator as a function of temperature difference, operating with eight  $40 \times 40 \text{ mm}^2$  TE modules connected in series. The

tests were conducted at matched-load condition. The cold side temperature was maintained at 293 K. Laboratory "test bed" photos and components characteristics are reported at Annex A.3 (deliverable D2.1 – Design of the lab-scale test bed).

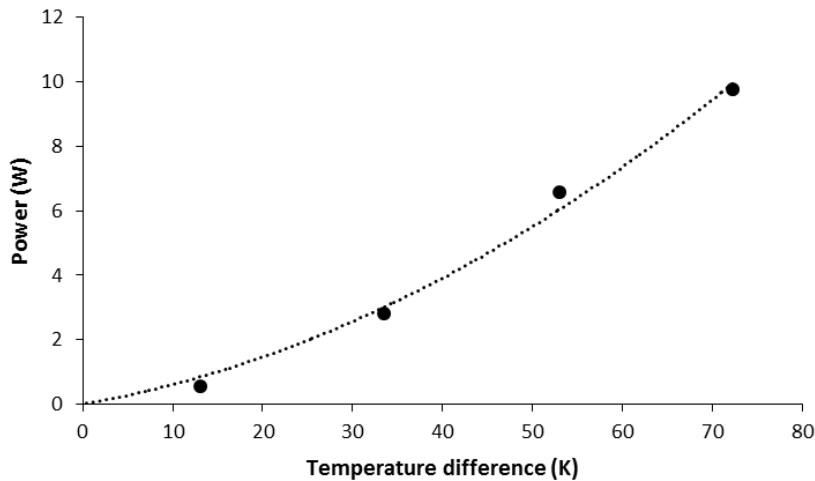


**Figure 3.2.1.2.4** - Power output from CU's Lab Scale Power Generator at various temperature difference at matched-load condition

### 3.2.1.3     ***Design and construction of BFI laboratory "test bed" (BFI)***

The BFI laboratory test-bed objectives are:

1. characterize the selected TE *modules* in a near-industrial environment
2. quantify the influence of non-module related aspects of the TE *generator* like heat exchanger surface area and external load.

Thus two test beds were constructed. One to test single TE modules and the other one to test the function of the entire prototype B.

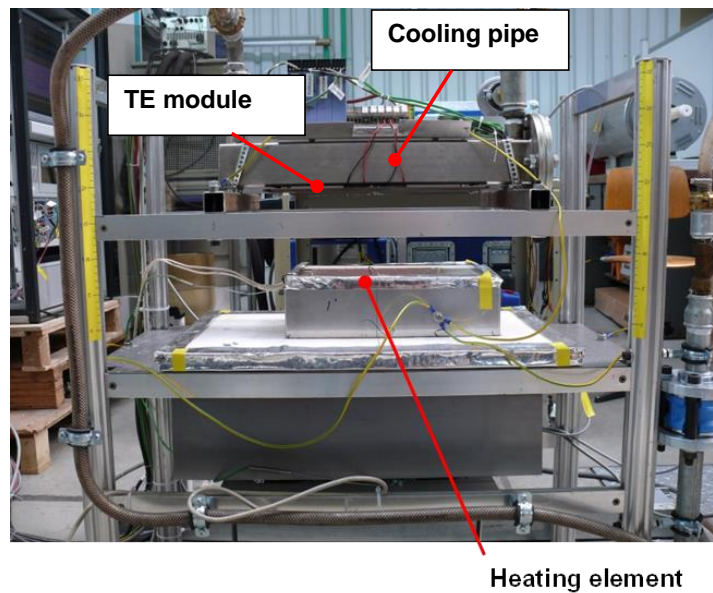


**Figure 3.2.1.3.1** - BFI testing facility for single TEM modules

The test bed for single TE modules consists of a ceramic heater plate as heat source and a water cooled square pipe. It is shown in Figure 3.2.1.3.1. The TE modules could be fixed at the cooling pipe by a copper plate and positioned in different configurations near to the heat source. Thus the investigation of the influence of temperature level of the waste heat source can be determined.

Figure 3.2.1.3.2 shows the testing facility for the entire prototype B. It consists of eight porous burners (8 – 25 kW each) and one lateral installed generator, like it is planned for the full scale tests at Arcelor Mittal Espana plant site.

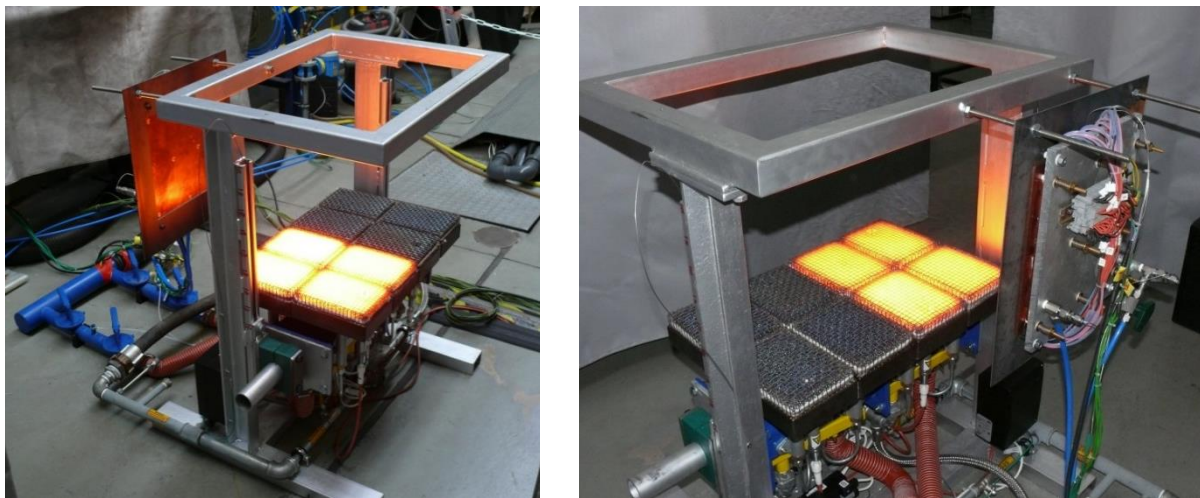


**Figure 3.2.1.3.2 - BFI testing facility for functionally tests of Prototype B**

Results obtained from the test-bed experiments enabled to design the prototype B system, with which the full-scale industrial tests at AME have been done.

Laboratory “test bed” photos and components characteristics are also reported in deliverable D2.1.

### **3.2.2 Task 2.2 - First laboratory test of the thermoelectric prototypes (CSM, CU, BFI)**

#### **3.2.2.1 Prototype A: hydraulic pressure test (CSM)**

With the objective to verify the water sealing of prototype A, the hydraulic test bed, shown in Figure 3.2.1.1.1, has been set up and tests carried out.

The water boxes have been filled with fresh water (Figure 3.2.2.1.1) and then connected with a pressure calibrator (Figure 3.2.2.1.2). The pressure of the water was successively increased up to 10 bar verifying the presence of possible water leaks.

These experiments have shown the capability of the water boxes connections to maintain a pressure of 10 bars without any pressure reduction for more than one hour. Therefore the water boxes can be considered adequately designed for the TEG working conditions.

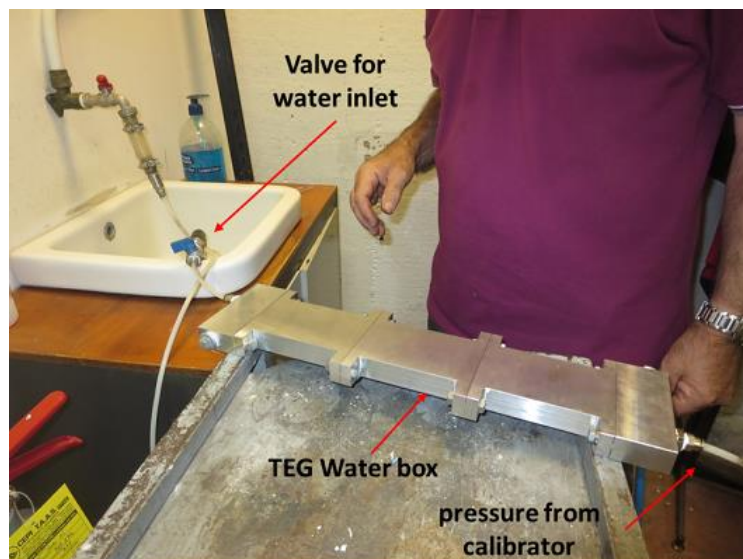


**Figure 3.2.2.1.1 – Water box hydraulic test**



**Figure 3.2.2.1.2 – Manual pressure calibrator**

### 3.2.2.2    *Prototype A and B: thermoelectric module test (CU)*

The module characterisations were carried out in vacuum on the test bed described in Sec. 3.2.1.2. The aim of the experiments was to assess the performance of TE modules at various operating conditions. This allows finding the maximum power output, electrical resistance and figure of merit at the different conditions. Tests were conducted at various temperature differences ( $\Delta T$ ): 10 K, 20 K and 50 K. The internal resistance of the module (matched-load resistance) can also be determined from these measurements. The TE module delivers maximum power output to a load when the value of the load resistance is equal to the internal resistance of the module.

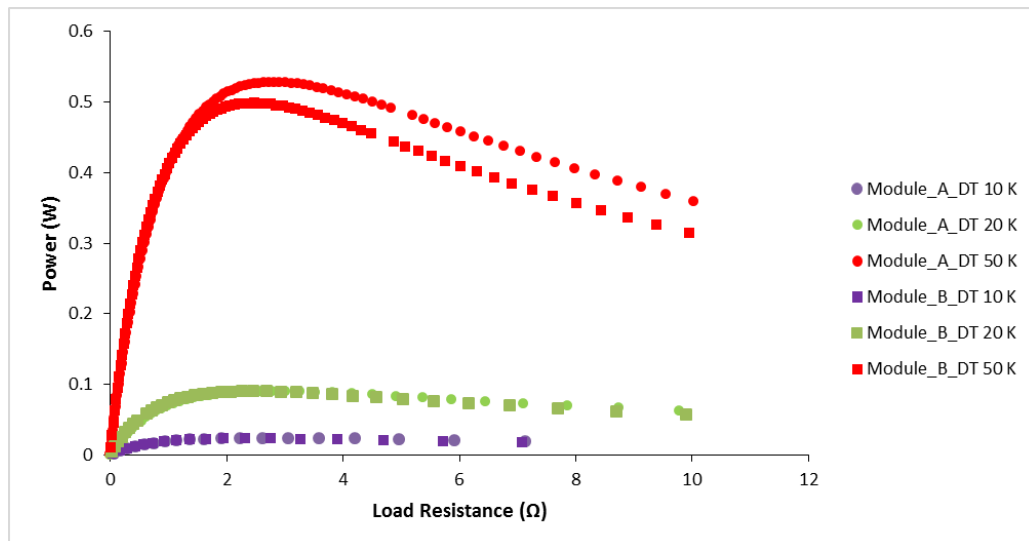


**Figure 3.2.2.2.1 - Power Generation at some temperature differences for samples A and B**

Figure 3.2.2.2.1 shows the power output generated by two modules, A and B, as a function of the load resistance for different temperature differences. A constant temperature difference was maintained across the module while performing each test as a function of load resistance. The figure of merit (ZT) was also determined using the current-voltage curves. The ZT of sample A was found to be higher than sample B, as shown in Figure 3.2.2.2.2.

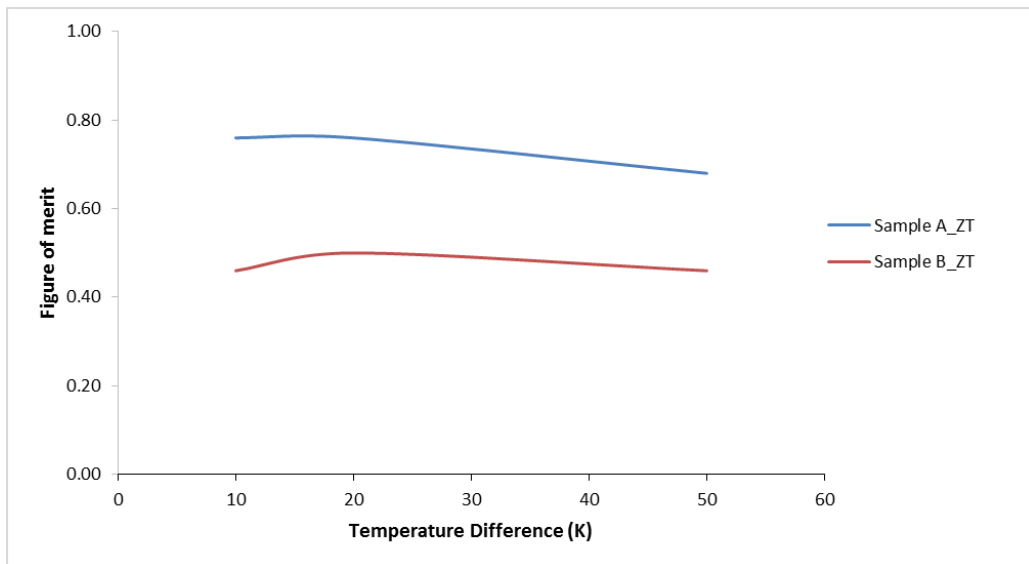


**Figure 3.2.2.2.2-** Figure of Merit (ZT) at different temperature differences for samples A and B

#### **Characterization of CSM modules**

Three TE modules were provided by CSM for characterization. The modules, procured from European Thermodynamics (UK) were  $62 \times 62 \text{ mm}^2$  and consisted of 254 thermoelements. They were sealed by silicone sealant at all the sides.

Figure 3.2.2.2.3 above shows the open circuit voltage ( $V_{oc}$ ) at 50 K constant temperature difference for three different cases; Case 1:  $V_{oc}$  without pressure, Case 2:  $V_{oc}$  with pressure and Case 3: Theoretical  $V_{oc}$ . The  $V_{oc}$  was found to be low, 0.47 V. On application of pressure on the module, the open circuit voltage was observed to increase but was still below the theoretical value of  $V_{oc}$ . A detailed analysis on performance of this module has been provided in Sec. 3.3.1.2.

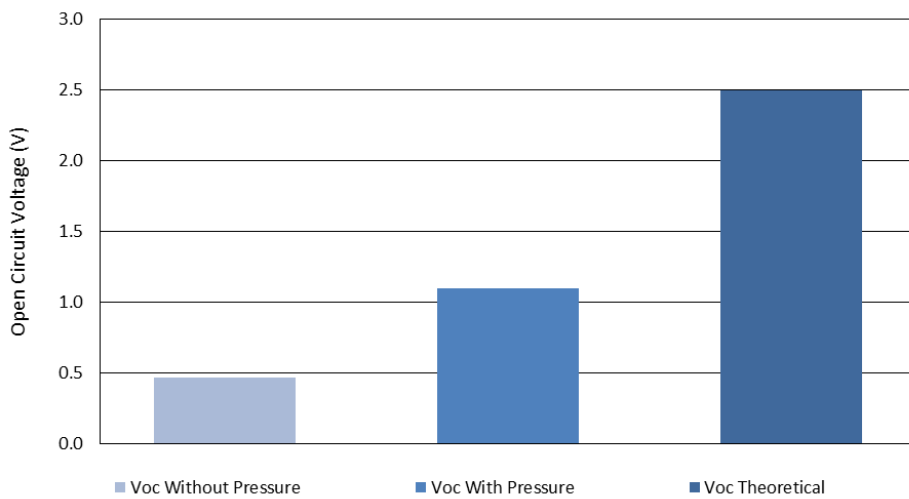


**Figure 3.2.2.3 -** Characterization results of CSM modules- Open circuit voltage comparison for different cases.

#### **Characterization of BFI modules**

The modules provided by BFI were characterized. Figure 3.2.2.4 shows the maximum power outputs as a function of the temperature difference for six TE modules from different suppliers. The fitting to a parabolic expression (dotted lines) is also shown. All modules have a ceramic size of  $40 \times 40 \text{ mm}^2$  except for the one supplied by RS, which has a ceramic area of  $62 \times 62 \text{ mm}^2$ . As expected, the module RS generates the largest power output due to the large area. However, it is the module Eureca\_A that produces the largest power per unit area, while the module PSI produces the lowest.

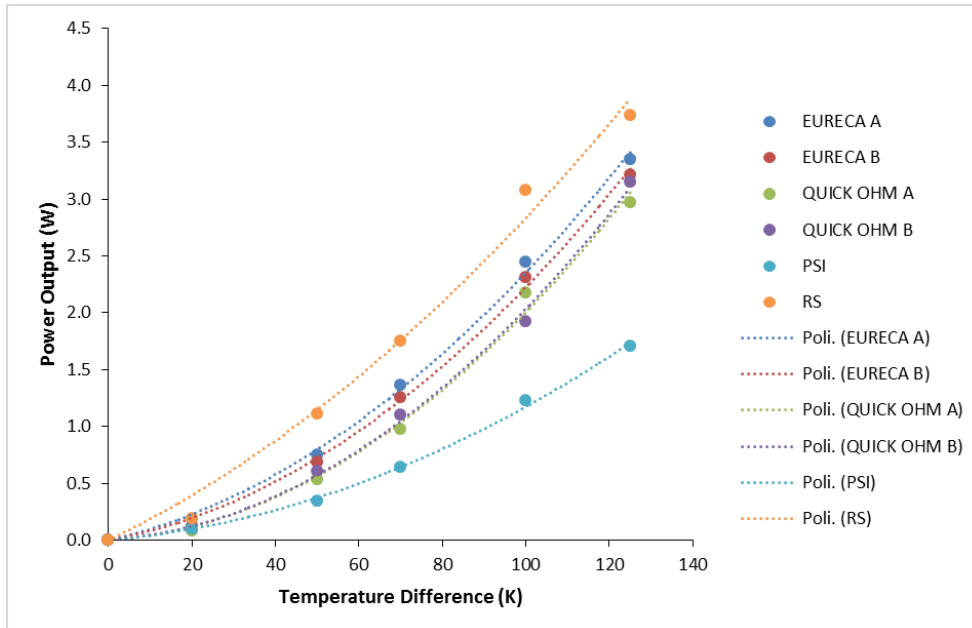


**Figure 3.2.2.2.4** - The power output as a function of temperature difference for modules of different suppliers

### 3.2.2.3 Prototype A: TEM electric power vs. load pressure (CSM)

By means of the lab-scale test bed shown in Figure 3.2.1.1.2 and Figure 3.2.2.3.1, some of the TE modules (see characteristics in Table 3.1.1.7.1 supplier 6) have been tested at different load pressures and cooling water fluxes. The temperature of the hot side was stabilized to 90°C measured at the aluminium plate.

The first test was carried out to define the TEM matched-load resistance under a standard condition fixed to a pressure around 0.8 N/mm<sup>2</sup> and an intermediate cooling water flow rate (unfortunately, during these tests the cooling water flow rate measurement system was not operative yet and a precise value could not be provided). The measured matched-load resistance, under these conditions, was 0.33 Ω for a single TEM.

Then, setting the load resistance to 0.33 Ω, it was measured the TEM electric power varying the load pressure with two different cooling flow rates (high and low).

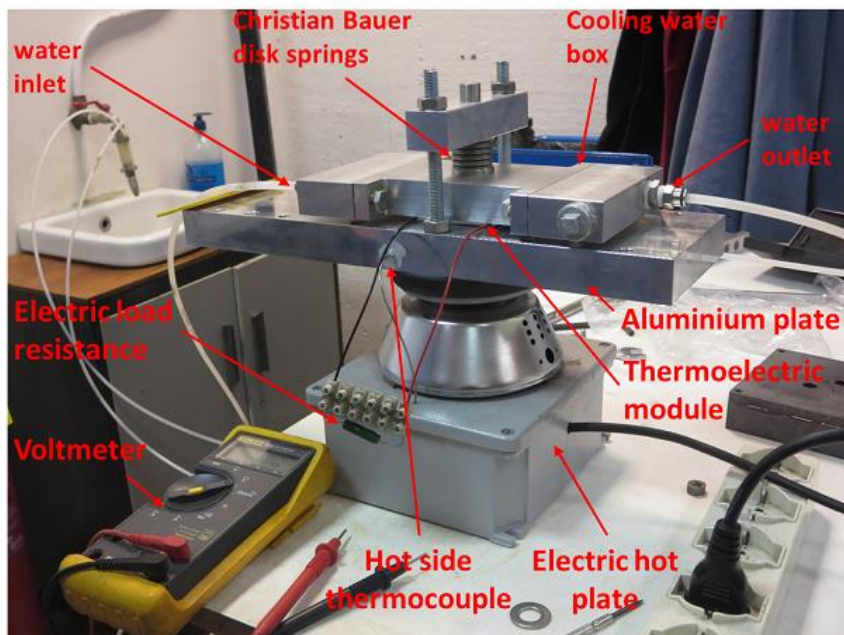


**Figure 3.2.2.3.1** – Laboratory testing device: power vs. load pressure test

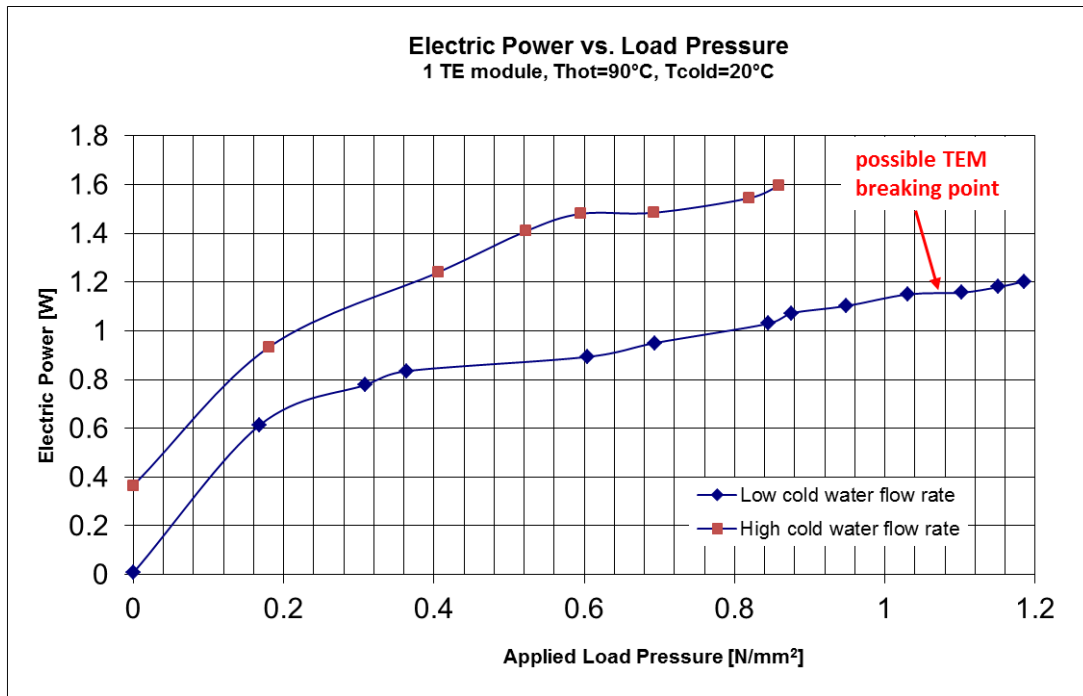


**Figure 3.2.2.3.2 – TEM electric power vs. load pressure test**

Figure 3.2.2.3.2 shows the results of the tests. From this figure it can be observed both the importance of the cooling flow rate and the pressure applied to the TEMs.

The maximum power produced by a single TE module under these conditions was 1.6 W, in agreement with supplier's specifications.

It should be noted that thermoelectric modules are not exactly identical one each other due to their fabrication process. Therefore, it is normal to observe certain differences on their electrical performance. In addition, the establishment of the thermal contacts during the setup of each module can also introduce additional variations.

Figure 3.2.2.3.2 also shows the thermoelectric module breakage test that will be discussed in Sec. 3.3.1.1.

#### 3.2.2.4     **Prototype B: electric power vs. modules pressure (torque) and thermal interface material (BFI)**

Figure 3.2.2.4.1 shows a close up of two TE modules positioned between the heat sink and the copper plate (in the test-bed configuration for single TE modules - see also Figure 3.2.1.3.1 - where the copper plate was positioned parallel to the heating element). Clearly visible is the bending of the copper plate when 15 Nm torque was applied to the screws. This resulted in a non-complete contact between the surfaces of the module and their corresponding heat exchangers.

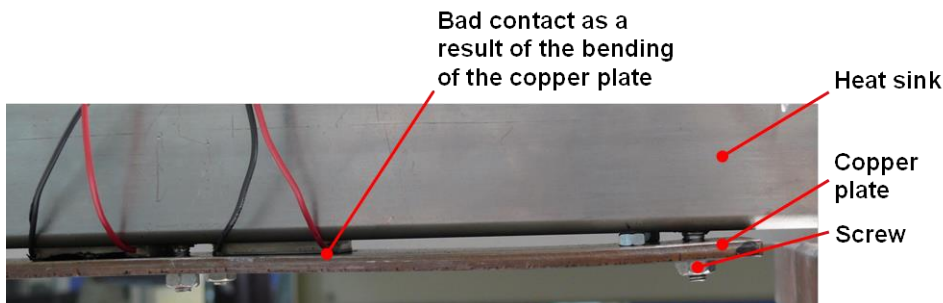


**Figure 3.2.2.4.1 – 15 Nm torque applied to screws that push (via copper plate) TE modules to heat sink**

Figure 3.2.2.4.2 shows the power generation and the TE module temperature difference as a function of the applied torque on the screws shown in Figure 3.2.2.4.1. At increased torques, the  $\Delta T$  module increases as a result of the decreased heat flow as a result of the diminishing contact. Thus, the power generated by the TE modules also decreases. Conclusion is that the bending of

and thus, a bad contact between the copper plate and the TE modules, has to be avoided for the final configuration of prototype B.

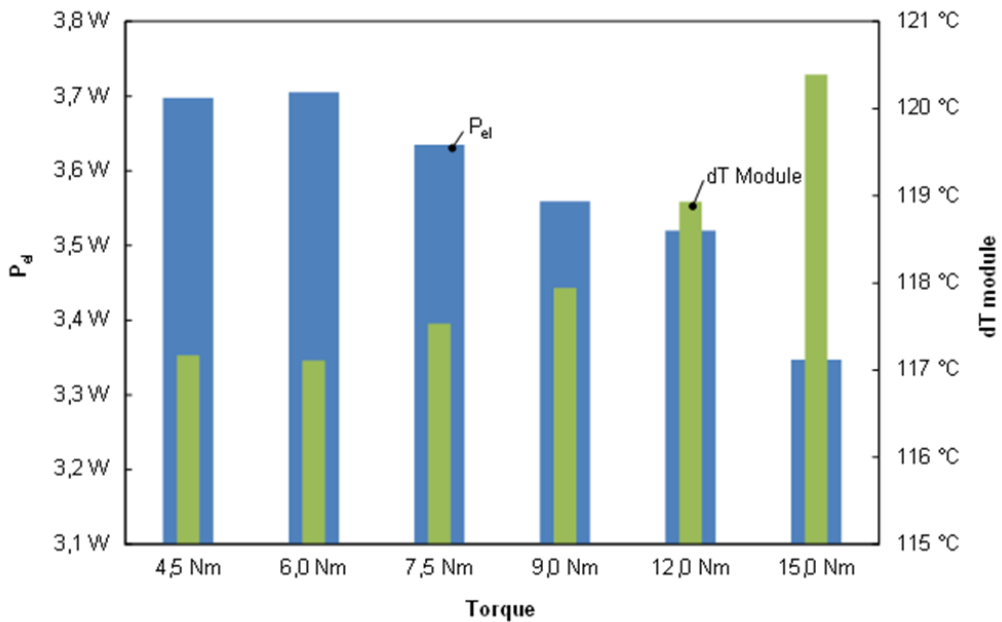
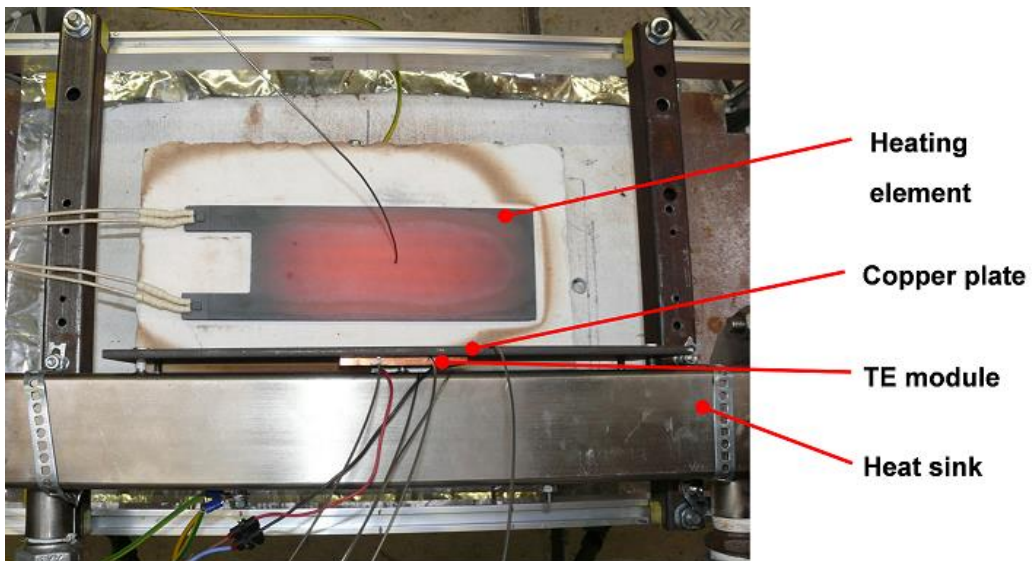


**Figure 3.2.2.4.2** - Power output and  $\Delta T_{\text{module}}$  as a function of the applied torque on screws as shown in Figure 3.2.2.4.1 (two TE module, supplier 2)

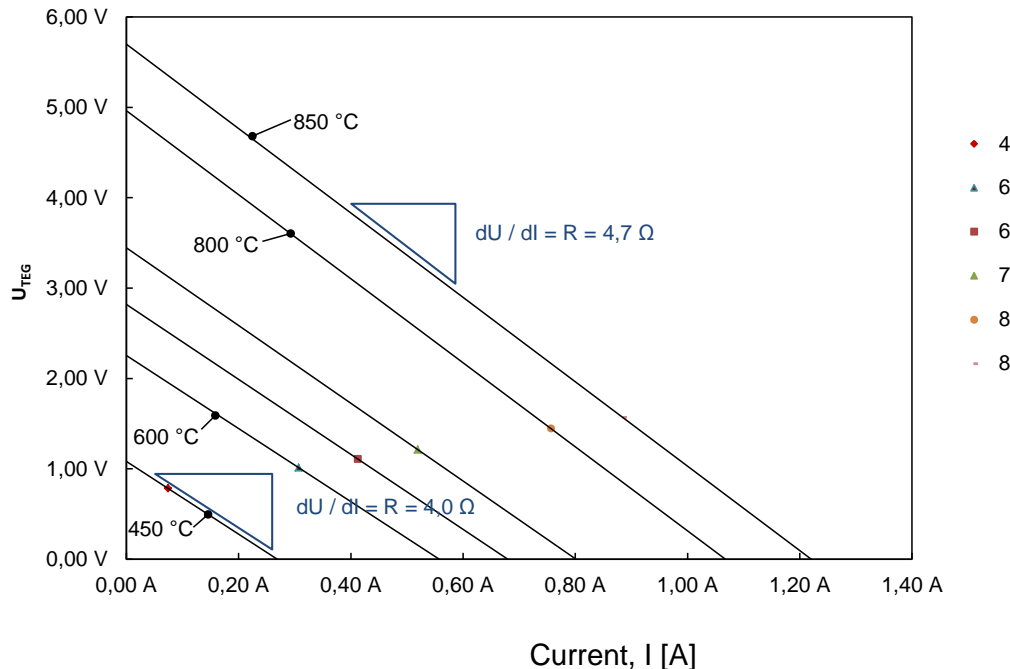
### 3.2.2.5 Prototype B: electric power vs. electric resistance load (BFI)

Figure 3.2.2.5.1 shows the test-bed set-up (at the test bed for single TE modules) and Figure 3.2.2.5.2 the corresponding V-I results of tests with supplier 2 modules (see Table 3.1.1.7.1 - TE modules purchased in the project) at different temperatures of the heating element ( $T_{\text{HE}}$ ).

The (linear) V-I relationship was determined by measuring the open circuit voltage ( $V_{\text{OC}}$ ) and V and I at a load resistance ( $R_L$ ) of approximately  $1 \Omega$ . As  $T_{\text{HE}}$  increases, thus increasing the TEM temperature difference, the power output of the module also increases. From these curves, the internal resistance,  $R_i$ , of the TE module (at any value of  $R_L$ ) can be determined from the slope of the V-I relation. As shown in Figure 3.2.2.5.2,  $R_i$  increases with increasing  $T_H - T_C$ .



**Figure 3.2.2.5.1** – Prototype B test bed set-up



**Figure 3.2.2.5.2 – Laboratory V-I test results (supplier 2)**

Because the power output of the TE module is at its maximum when  $R_i = R_L$ ,  $R_L$  should be controlled when non-steady state conditions occur. The external load that has been purchased by BFI (see Annex A2.3) can be manually controlled ( $0 \Omega - 40 \Omega$  /  $40 \Omega - 800 \Omega$ ), nevertheless not automatically (outside the scope of the project).

Figure 3.2.2.5.3 shows the effect of  $R_L$  on the power output of the TEM (supplier 4) at a temperature of the heating element of 700°C (graphite foil was used between surfaces of TE module and heat exchangers). Maximum TEG power is achieved when operating at  $R_L \sim 4 \Omega$ .

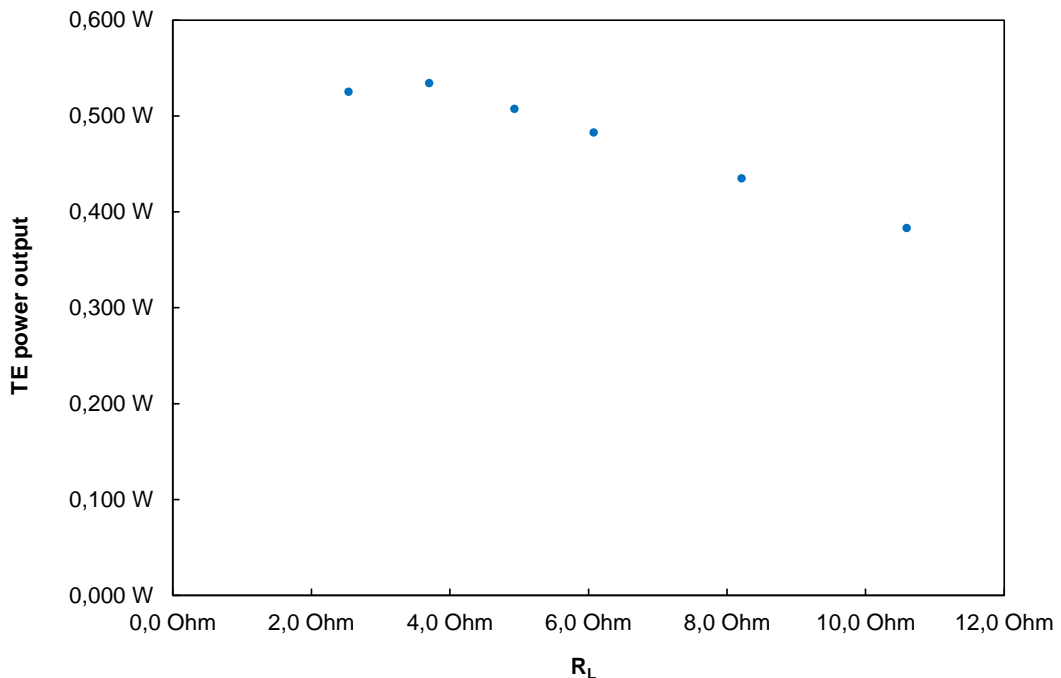


**Figure 3.2.2.5.3 - TE power output as a function of the load resistance ( $R_L$ )**

### 3.2.2.6 Prototype B: electric power vs. module temperature difference (BFI)

Figure 3.2.2.6.1 shows the generated electrical power ( $P_{TEG}$ ) and module temperature difference ( $dT_{module}$ ) as a function of the temperature of the heating element (test-bed configuration as shown in Figure 3.2.1.3.1). Both increase progressively with increasing temperature of the heating

element. This is obvious since the specific radiation  $M$  progressively increases with increasing temperature of a (grey) object:

$$M = \epsilon \sigma T^4$$

**Eq. 3.2.2.6.1**

Where  $\epsilon$  is the emission coefficient and  $\sigma$  is the Stefan-Boltzmann constant ( $5,67 \cdot 10^{-8} \text{ W/m}^2\text{K}^4$ ).

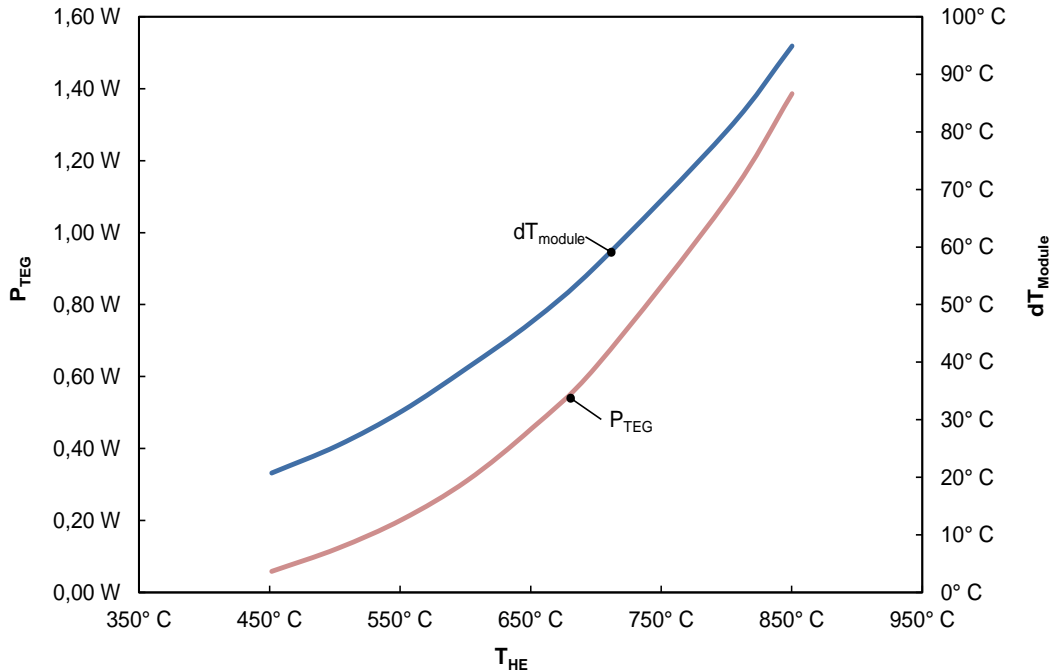


**Figure 3.2.2.6.1** - TE power output and  $\Delta T_{\text{module}}$  as a function of the temperature of the heating element (one TE module, supplier 2)

Figure 3.2.2.6.2 shows the electrical output and the efficiency (calculation as described in Sec. 3.1.2.2) as a function of the temperature difference across the module. As  $\Delta T_{\text{module}}$  increases, both power and efficiency increase.

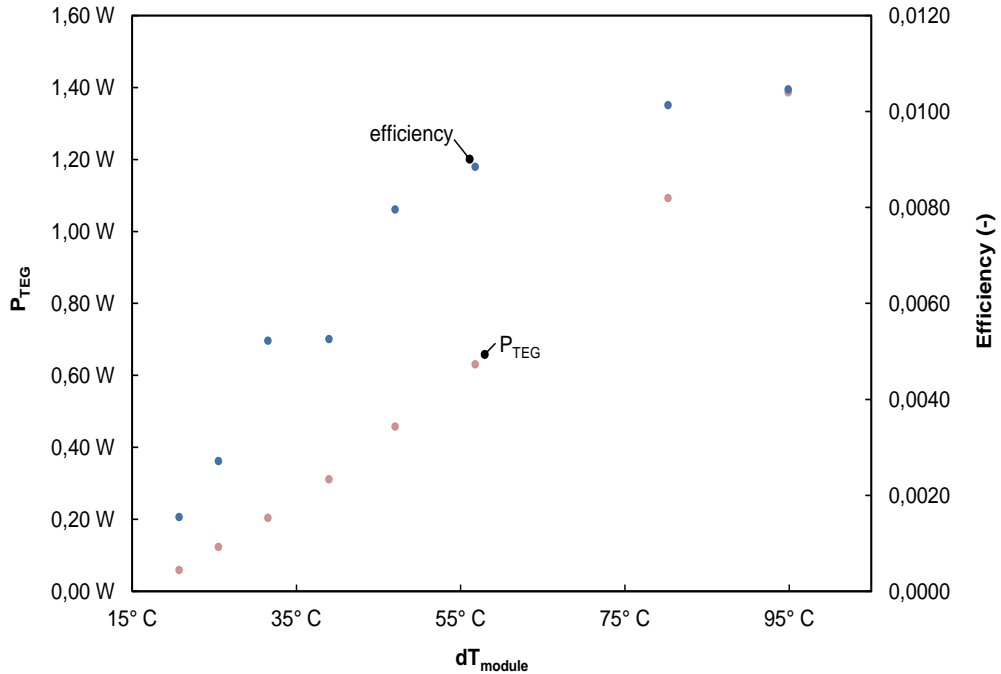


**Figure 3.2.2.6.2** - TE power output as function of  $\Delta T_{\text{module}}$  (one TE module, supplier 2)

Obviously, as the specific investment cost of the installation decrease with increasing efficiency, the highest  $\Delta T_{\text{module}}$  should be aimed for. This needs to be taken into account when selecting the panel of the cooling table conveyor where prototype B will be installed, although some flexibility is

present as the panels can be re-positioned using cranes. Thus, the panel with the prototype B demonstrator can be moved upstream of the cooling table line (where the temperature of the hot wire rod is higher) if too small  $\Delta T_{\text{module}}$  values are observed.

### **3.2.2.7    Prototype A: final functional tests**

CSM completed the mechanical and electrical assembly of prototype A in June 2015, while software was ready in December. Therefore prototype A was ready for plant installation at the end of December 2015.



**Figure 3.2.2.7.1 – Prototype A during final laboratory set up**

Figure 3.2.2.7.1 shows prototype A after the final assembling at CSM laboratory during the final tests prior to the installation at Ferriere Nord plant. These tests concerned: water leakage detections, power generation using external water electric heaters, acquisition system verification.

### **3.2.2.8    Prototype B: final functional tests**

BFI finished the assembly of both generators of prototype B in September 2015. Subsequent functionality tests of the prototype were done at BFI testing facility in Düsseldorf (see Figure 3.2.1.3.2 ).

The functional tests included:

- Leakage and functional test
- Determination of the pressure drop of the cooling water
- Determination of the ideal load resistance
- Recording of V-I and P-I curves (variation of load resistance between 1 and 15 Ohm)

Results were:

- No leakages
- Max. power production at a load resistance of  $\sim 5$  Ohm
- No significant influence of cooling water supply (200 – 600 l/h) on the power production
- No significant influence of contact pressure of the TE modules (400 – 560 N) on the power production
- Results of generator No. 2 are in good accordance to the test results of single TE modules (see Sec. 3.2.2.6)
- Power production of generator No. 1 is lower than expected from the test results of single TE modules

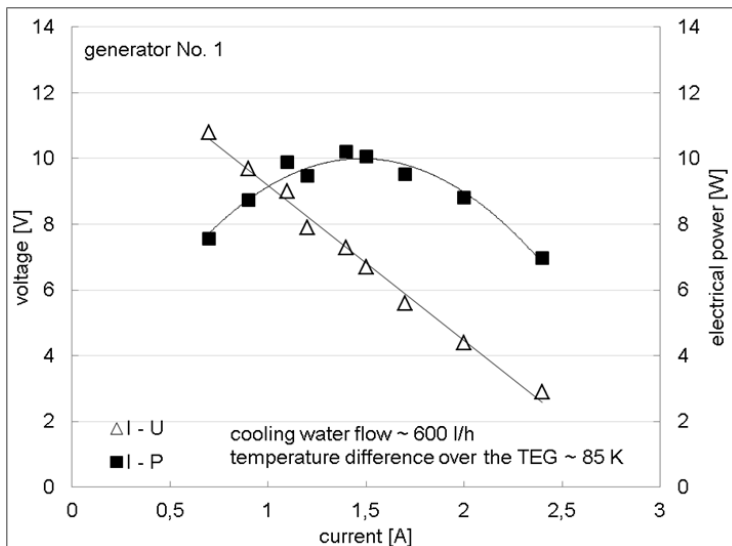


**Figure 3.2.2.8.1** – Prototype B: V-I and P-I characteristic curves of generator No. 1 recorded at the BFI testing facility

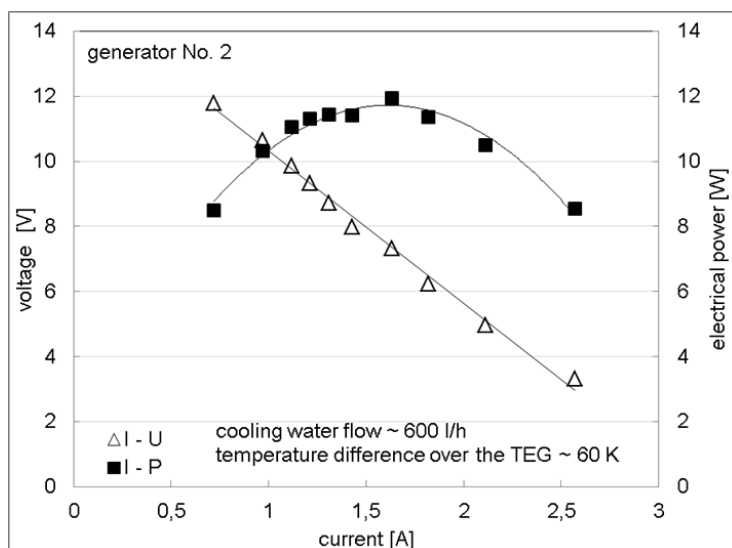


**Figure 3.2.2.8.2** – Prototype B: V-I and P-I characteristic curves of generator No. 2 recorded at the BFI testing facility

Figure 3.2.2.8.1 and Figure 3.2.2.8.2 show, as a result of the investigation of prototype B at the test bed with the porous burners, the V-I and P-I characteristic curves of the generators. While generator No. 2 reached a maximum power of 12 W at a temperature difference of approximately 60 K, the maximum power of generator No. 1 was just 10 W at a temperature difference of approximately 85 K. Reasons could be: improved contact between the TE modules and the copper plates of generator No. 2 by using more screws and more heat-conductive paste and improved performance of TE modules in generator No. 2 due to manufacturing differences.

### 3.3 WP3 – Analysis of the modules and identification of their structural weakness

WP3 objectives are:

- Identify apparatus weakness points and degradation causes during normal operation
- Identify technological improvements
- Finalise the prototypes specifications of the thermoelectric systems for steel plant applications.

### **3.3.1 Task 3.1 - Identification of the equipment weakness points (CSM, CU)**

#### **3.3.1.1 Maximum module compression test (CSM)**

The laboratory test, performed at low cold water cooling flow rate (see Figure 3.2.2.3.2), was carried on up to the breakage of the thermoelectric module. Since during the test the thermoelectric module was sandwiched between the aluminium plates, it was not possible to verify exactly the pressure applied to the module when it broke down. However, it was clear (on the basis of sequential checks) that it broke after a load pressure of 1 MPa. It was observed that the TE modules broke at the ceramic plate of the hot side and, in despite of this, it continued to supply current without any performance reduction after breakage.

This experiment confirmed that the breaking point of the thermoelectric module is around 1 MPa. Although the thermoelectric module continues to operate even after the fracture of the ceramic plate, it was decided not to apply a load pressure greater than 1 MPa during the TEG assembling. The value of 1 MPa is the same recommended by the manufacturer of the modules.

Figure 3.3.1.1.1 shows the thermoelectric module after the breaking test. It can be observed that only the ceramic plate was damaged while the TEM resulted completely safe. As can be seen from Figure 3.2.2.3.2 the maximum load pressure applied to this TEM was 1.2 MPa.

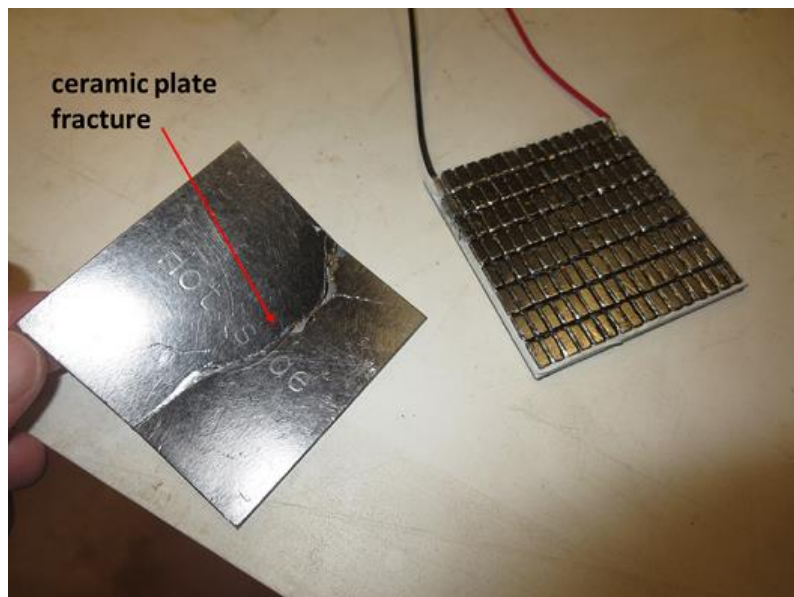


**Figure 3.3.1.1.1 – TE module after maximum compression test**

#### **3.3.1.2 Different constructive methods of $\text{Bi}_2\text{Te}_3$ modules: advantages and disadvantages (CU)**

A thermoelectric generator consists of n-type and p-type semiconductors connected electrically in series by highly conducting metal stripes and sandwiched between thermally conducting but electrically insulating plates. These plates are usually made up of ceramic. The cross sectional view of a typical thermoelectric module is shown in Figure 3.1.1.9.1. It appears that the modules investigated in this project were fabricated using two different methods.

##### ***Traditional manufacturing method***

Most of commercially available modules are manufactured using a traditional method, which involves soldering of thermoelements on metallized ceramic substrates on both the hot and cold side, as shown in the Figure 3.3.1.2.1.

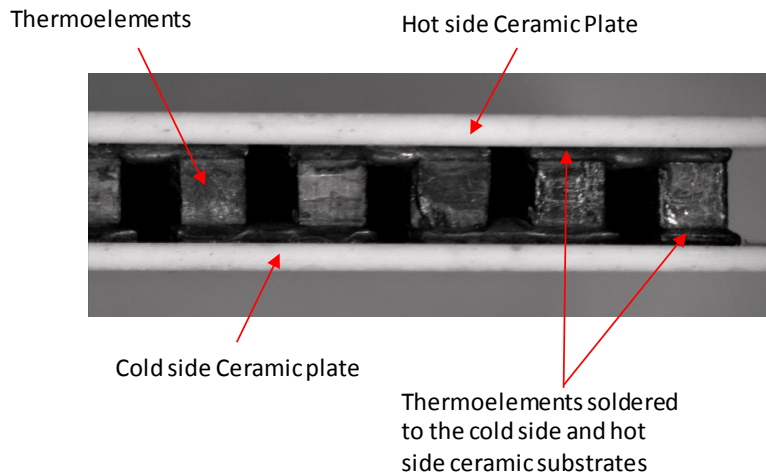


**Figure 3.3.1.2.1** - Module manufactured by traditional manufacturing method

#### **Non-traditional manufacturing method**

This method has come under notice recently. It involves soldering of the thermoelements to the metallised ceramic on the cold side only, whereas on the hot side, the elements are soldered to copper strips (metal interconnector) which are not fixed on to the top ceramic. The silicone sealant holds the top ceramic plate. To ensure a good thermal contact between the hot side copper strips and the top ceramic plate, a graphite sheet is placed between the copper strips and ceramic plate

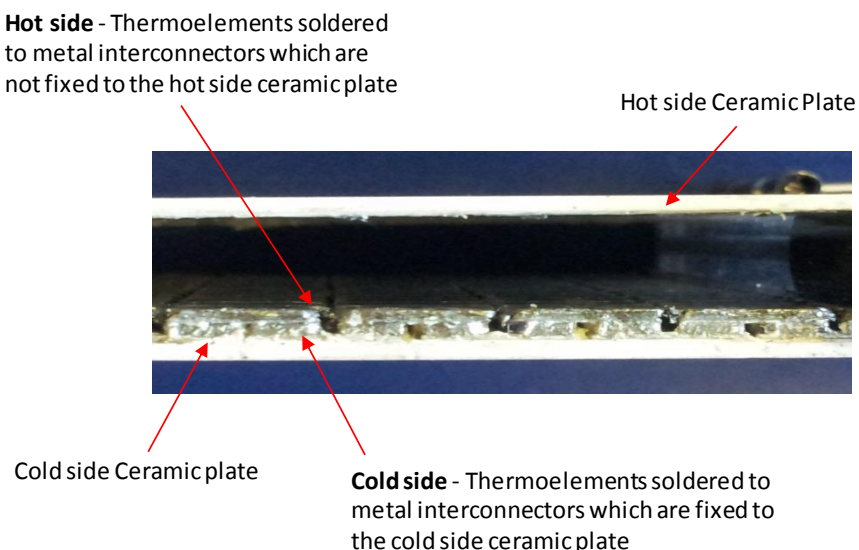


**Figure 3.3.1.2.2** - Module manufactured by non-traditional manufacturing method

Figure 3.3.1.2.2 shows a module manufactured using non-traditional method. It can be seen that the thermoelements are only soldered to one ceramic plate, whereas the other ceramic plate is placed on the top of the metal contact strips rather than soldered.

#### **Performance analysis of the two manufacturing techniques**

An investigation was carried out to analyse the performance of modules manufactured by traditional and non-traditional methods.

The module manufactured using non-traditional method was procured from European Thermodynamics (UK). The dimensions of the module are 62mm x 62mm x 3.7mm. It consists of 254 thermoelectric elements and was sealed by silicone sealant at all the sides.

The module manufactured with the traditional method has the dimensions of 40mm x 40mm x 3.4mm and consists of 254 thermoelements. The module was not sealed.

Figure 3.3.1.2.3 shows a comparison of the open-circuit voltages obtained from the two modules fabricated using traditional and non-traditional methods, respectively. The operating temperature difference during the test was maintained constant at 50 K.

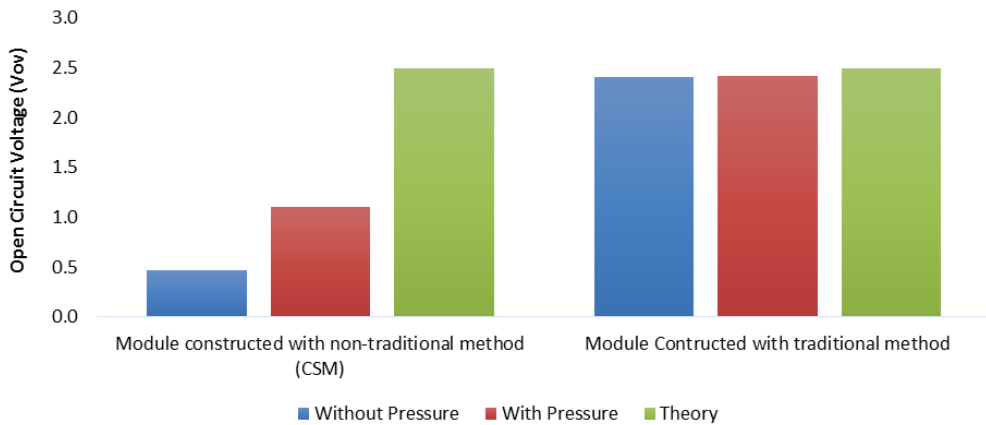


**Figure 3.3.1.2.3** - Comparison of the open-circuit voltage generated by modules fabricated using traditional and non-traditional methods.

The open circuit voltage ( $V_{oc}$ ) of the module manufactured using non-traditional method was observed to be 0.6 V, which is significantly lower than the theoretical value. By applying pressure to the module, the  $V_{oc}$  is increased significantly but still below the theoretical value calculated based on the value of Seebeck Coefficient ( $\alpha$ ) of  $180 \mu\text{VK}^{-1}$ , 254 thermoelements (N) and 50 K temperature difference ( $\Delta T$ ), using the equation:  $V_{oc} = N\alpha\Delta T$ .

On the other hand, the module manufactured using traditional method produced  $V_{oc}$  which is in agreement with the theoretical value, as shown in Figure 3.3.1.2.3. The module showed no effect on the  $V_{oc}$  under the pressure.

To conclude, the performance of the module manufactured using non-traditional method was poor and requires very high pressure due to the fact that the hot side is not soldered to the top ceramic plate, which is held in place by the silicone sealant. Under the application of pressure the heat transferred is increased and hence, the load voltage obtained is higher. The non-traditional module design is aimed at reducing the thermal stress and improving the reliability of modules when operated at high temperature. However, the disadvantage of this design is that it requires huge pressure to ensure a good thermal contact.

### 3.3.1.3 Effect of exposure to increased temperatures (BFI)

A correct determination of the temperature of the hot side of the module is required in order to be able to guarantee a long operating live. Figure 3.3.1.3.1 shows a TE module that has been exposed to too high temperatures. Clearly visible is that the solder that connects the wire to the module has melted, thus taking the TE generator (modules are connected in series) out of operation.

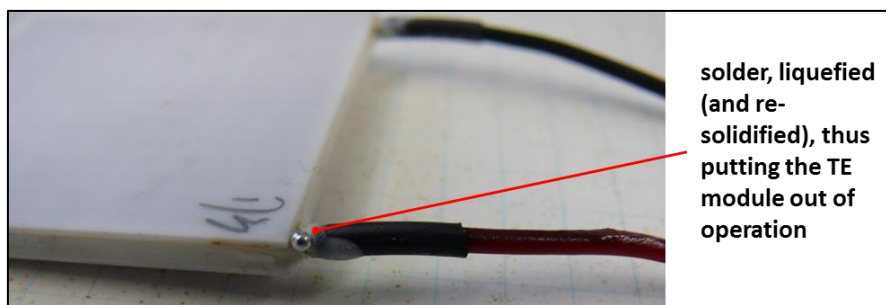


**Figure 3.3.1.3.1** – Thermoelectric module exposed to high temperature

Figure 3.3.1.3.2 shows a type K thermocouple clamped in a groove of the (copper) hot side plate that was used in the BFI-test-bed. The fact that no heat sink compound was used at the very first tests could be the reason for the too low temperature measurement, thus exposing the module to too high temperatures. It should also be noted that some module suppliers define the maximum

operating temperature of their products by the melting temperature of the solder. This in fact means that the maximum operating temperature of the modules should *not* be reached.

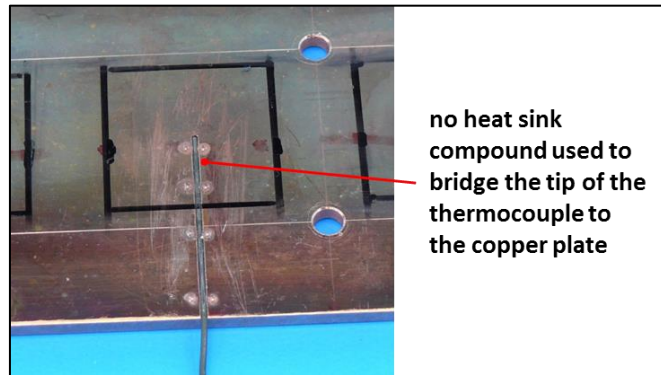


**Figure 3.3.1.3.2 – type K thermocouple clamped in the hot side**

Since it would not make sense to determine the TE hot side temperature of all the modules and taking into account the above observations, attention needs to be paid to which module of prototype B is measured. It comes naturally, that this should be done on the module that will be exposed to the highest temperature. Considering the results of the thermo-camera (see Figure 3.1.1.3.14), a TE module should be selected that will have a position on LIO<sub>2</sub>, showing the highest temperature over the height of the panel, of course close to where the hot wire is coming from (see Figure 3.1.1.3.13, note the temperature increase of approx. 40°C on the left surface of one of the vertical bars that are on the panels).

### **3.3.2 Task 3.2 - Identification of the technological improvements (CSM, CU, BFI)**

#### **3.3.2.1 Hot side heat exchanger: thermal paste and graphite foil (BFI)**

In order to increase heat transport to (from heat source) and from (to heat sink) the module surfaces, two different conditions have been tested. Figure 3.3.2.1.1 shows (from the left) a 'clean' TE module surface, a TE module covered with a thermal conductive paste (Al<sub>2</sub>O<sub>3</sub> compound, heat conductivity: 2,9 W/mK) and a TE module covered with graphite foil (thickness: 125 µm; heat conductivity: 16 W/mK).

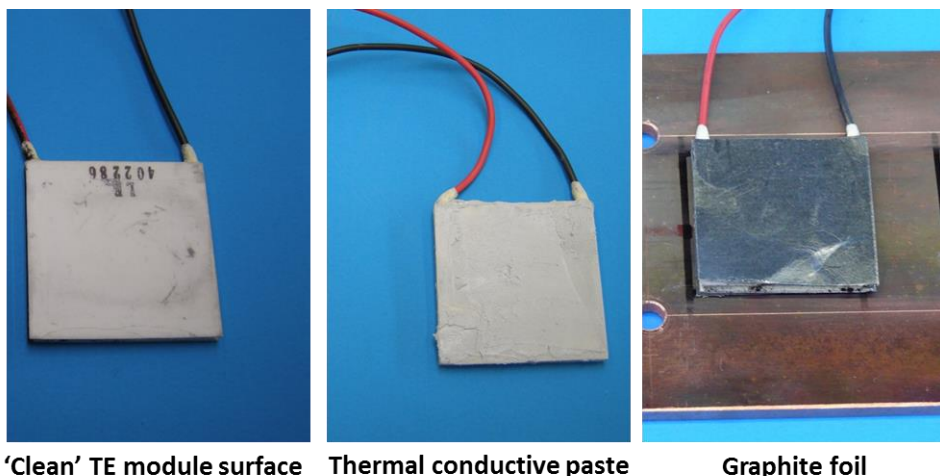


**Figure 3.3.2.1.1 - Clean and covered TE module surfaces**

Figure 3.2.2.5.1 shows the set-up of the test-bed with the ceramic heater and Figure 3.3.2.1.2 the corresponding experimental results (V-I relation) that have been achieved when operating the heating element to a temperature of 750 °C. Clearly visible is the increased performance (despite the lower heat conductivity of the thermal paste compared to that of the graphite foil) when using the thermal paste between the TE module and the copper plate and the heat sink. All other tested TE modules showed the same power output improvement when using the thermal conductive paste.

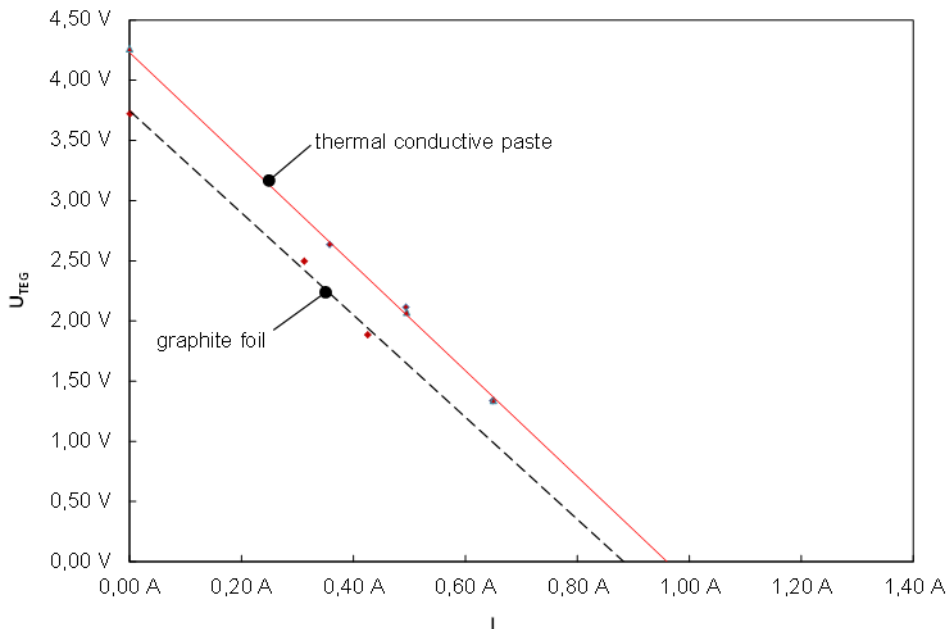


**Figure 3.3.2.1.2** - V-I relation for TE module (supplier 2) that were tested with graphite foil and thermal conductive paste

### 3.3.2.2 Electric power consumption optimization and electric load matching (CSM, CU)

CSM has realized laboratory tests to verify the electrical characteristics of the apparatus. In particular it was added a potentiometer able to change the load resistance of a single column of TEMs from  $2.5 \Omega$  up to  $3.5 \Omega$ , in order to verify the optimum load resistance and the deviation between the assumed impedance and the optimal one (see Figure 3.3.2.2.1).

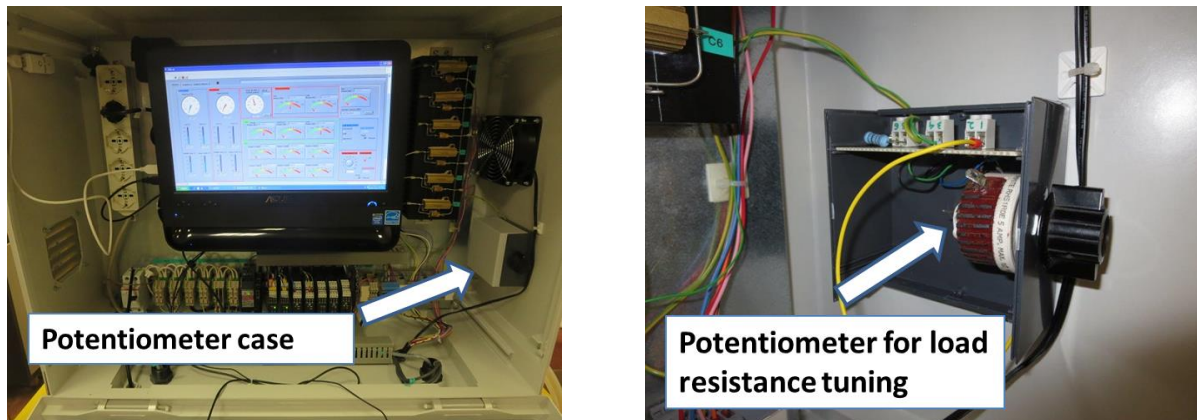


**Figure 3.3.2.2.1** – Potentiometer for the tuning of the TEG load resistance

These tests showed that the maximum power of the single TEMs column is obtained with a load resistance ranging between  $2.7 \Omega$  and  $3.1 \Omega$ , and also a small dependence of the power with load resistance variation below  $0.6 \Omega$ . This fact confirmed that the chosen load resistance of  $3.0 \Omega$  was correctly defined. Furthermore it showed a maximum reduction of the generated power, due to unmatched load, approximately lower than 1% of the total power for each column.

Figure 3.3.2.2.2 shows another test used to characterise the TEMs behaviour of the device. In this case it was measured the open circuit voltage (points on the ordinate of the figure) of each TEMs, and the short circuit voltage and current by closing each TEMs on a digital meter (these points are not on the abscissa due to the digital meter impedance) at  $0.3 \text{ m}^3/\text{h}$  of flow rate for both hot and cold water circuit. Using this technique it was possible to measure two points of the TEMs V-I characteristic curve (linear) and consequently to calculate the P-I characteristic curve (parabolic). It can be observed that module 01 (TEM 01) located on the upper side of the TEG column 1 (similarly for the bottom side of the TEG column – not showed in the graph) works at very different

conditions respect to the other TEMs of the column. This fact is caused by a much better cooling of the upper and bottom TEMs which have the cold side cooled by a double cold water flow rate.

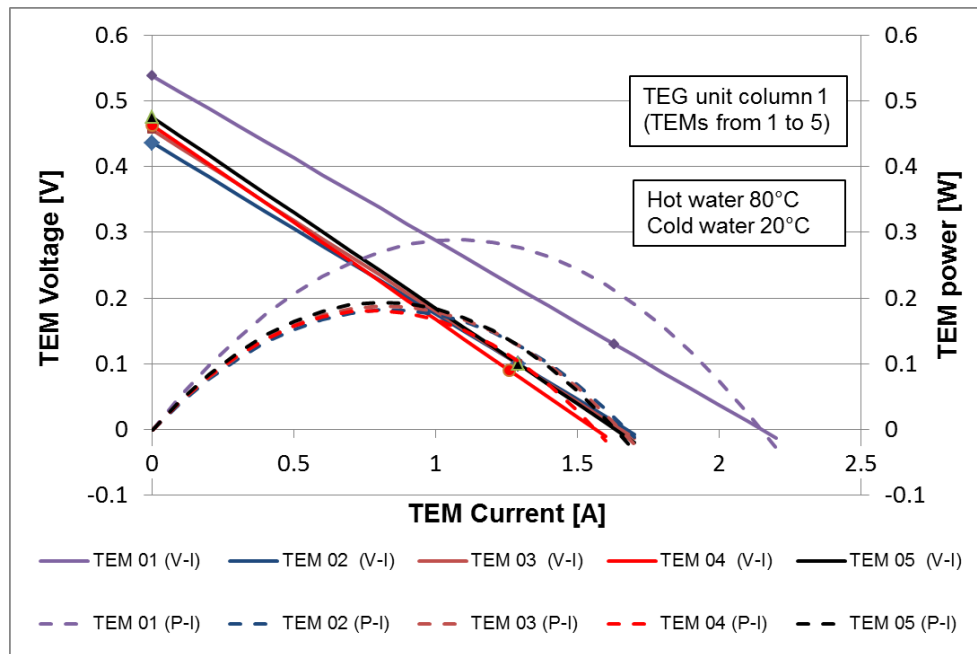


**Figure 3.3.2.2.2 – Prototype A: V-I and P-I characteristic curves of column 1, TEMs 1 to 5.**

### 3.3.3 Task 3.3 - Design of the final specifications (CSM, CU, BFI)

#### 3.3.3.1 Prototype A: design of the final specifications (CSM, FENO)

On the basis of the general layout defined at Sec. 3.1.1.5 the final design of the prototype A and the final specifications were produced.

The design of this type of system is very complex and inevitably requires to be performed in repeated steps. The first step concerns the definition of some parameters, defined by local conditions, including for example (in the case of prototype A) the distance between the source of the hot water and the place where the generator is positioned.

Successively, a simplified model must be adopted and, on the basis of its calculations, new variables can be calculated. By repeating all these steps subsequently, a suitable design can be obtained.

In the case of prototype A it was assumed that each module of the TEG was working between two water boxes which have the same surface of the modules and a temperature obtained as the average between the calculated inlet and outlet temperatures of the hot and cold side of the water boxes.

Assuming the hot and cold flow rates and the cross-section of the tubes of the hot and cold hydraulic circuits (see Figure A.2.1.1), it is possible to calculate the pressure drop and consequently the water flow velocity inside the water boxes. Then, by using the hot and cold water velocity, the thermal conductivity and the cross sectional areas of each part of a single TEM, it is possible to calculate the energy balance between the inlet and outlet thermal flow through the TEMs, and therefore the water outlet temperatures of the hot and cold water boxes.

Figure 3.3.3.1.1 shows the result of this simplified model. In this simulation has been considered an inlet cold water temperature of 10°C with a flow rate of 1.5 m<sup>3</sup>/h, and an inlet hot water temperature of 85°C with a flow rate of 1 m<sup>3</sup>/h. From the model output each thermal drop through into the thermoelectric device can be obtained. Under the considered conditions the thermal drop across the thermoelectric module is 42°C.

Th_inlet	Th_outlet				
85.00	78.61	°C	Th_water	water	
	72.83	°C	Th_Al	aluminium	
	70.84	°C	Th_film	film grafite	
	70.24	°C	Th_Tem	TEM	
	28.20	°C	Tc_Tem	TEM	
	27.60	°C	Tc_film	film grafite	
	25.60	°C	Tc_Al	aluminium	
10.00	15.93	°C	Tc_water	water	
Tc_inlet	Tc_outlet				
<b>Hot water flow rate [m<sup>3</sup>/h] =</b>		1.00			
<b>Cold water flow rate [m<sup>3</sup>/h] =</b>		1.50			
<b>Calculated TEM ΔT [°C] =</b>		42.04			

**Figure 3.3.3.1.1** - Prototype A, simplified model for TEG design

This model also gives the knowledge of the temperature profile across the thermoelectric modules and therefore the possibility to calculate the electric power produced by the whole thermoelectric generator. If the result of the model, for example in terms of total electric power, is not satisfactory, it is possible to modify the parameters that are not linked to the local conditions and employing an iterative method to find a better configuration of the TEG.

It is important to note that during the design of the TEG unit it was required to select both the pump characteristics and pipe sections, on the basis of the desired flow rates. Consequently the velocity of the fluids have to work in a range between a maximum and a minimum value, depending on the circuit components. In fact, an excessive flow rate leads to an energy lost, due to friction in the pipeline. On the other hand a low flow rate reduces the TEG heat exchange capability and its temperature uniformity, resulting in lower electric conversion performance. Therefore, it is important to design carefully all the components of the system (including the pipeline), to obtain a balance between advantages and disadvantages. In the case of the present device the desired water flow rate was fixed at 1 m<sup>3</sup>/h, both for the hot and cold circuit (as a design specification), and as a consequence of this choice, the components of the whole device were selected.

Table 3.3.3.1.1 shows the prototype A final specifications obtained by the procedure explained above.

On the basis of the results obtained by the simplified model the final TEG configuration was then manufactured considering ten horizontal layers (rows) and six thermoelectric modules for each horizontal layer (columns). Therefore, the total number of thermoelectric modules was 60. With this configuration, assuming a power of 1 W for each thermoelectric module, it is possible to produce about 40-60 W (gross electric power, i.e. excluding the power required for water pumping).

Springs have been used to correctly set the pressure over the thermoelectric modules, which have to be strongly pressed to increase their efficiency. Obviously, they cannot be pressed too much because they can break.

The basic electrical connection of the thermoelectric modules was made in series in groups of vertical columns. In any case, prototype A provides flexibility to change the electrical connections obtaining different solutions. The electric connections have been carefully chosen, because they can influence significantly the general performance of the TEG system.

Prototype A controls the electric power output by modifying the hot and cold water flow rates. In fact, by regulating the water flow rate the temperature gradient between the two sides of the TE modules can be modified and consequently the electric power generation.

Variable description	Unit	Value
Hot water temperature	[°C]	85
Cold water temperature	[°C]	10
Thermoelectric module hot side temperature	[°C]	70
Thermoelectric module cold side temperature	[°C]	28
Hot water flow rate	[m <sup>3</sup> /h]	1
Cold water flow rate	[m <sup>3</sup> /h]	1.5
Average electric power for a thermoelectric module	[W]	0.8
Number of thermoelectric modules	[W]	60
Thermoelectric generator electric power	[W]	48
Hot water pump electric power consumption	[W]	10
Cold water pump electric power consumption	[W]	10
Aluminium water boxes	-	-

**Table 3.3.3.1.1 – Prototype A final main specifications**

### 3.3.3.2     **Prototype B: design of the final specifications (AME, BFI)**

Based on the BFI test results shown in Figure 3.3.3.2.1 (V-I relation) and Figure 3.3.3.2.2 (P-I relation, from trend line form Figure 3.3.3.2.1), TE modules of supplier 2 have been selected for the prototype B design (the test-bed set-up for single TE modules shown in Figure 3.2.2.5. 1 was used). Not only did the TE modules of supplier 2 achieve the highest power output at a temperature of the heating element of 750°C, but they are also the cheapest (< 20 € whereas all the other modules cost > 26 €).

For prototype B design calculations, it was assumed that the TE modules produce 1.4 W each (see also V-I relations shown in Sec. 3.2.2.5 at T<sub>HE</sub> = 850°C; corresponding to T<sub>H</sub> - T<sub>C</sub> ~ 95°C). In order to be able to produce at least 50 W, it was decided to design the prototype B with 40 modules. Assuming the conversion efficiency of prototype B as 1%, i.e. Φ<sub>B</sub> = 0.01, by Eq.3.1.2.2.1 can be calculated the thermal power extracted by the hot heat source ( $\dot{Q}_H$ ):

$$\dot{Q}_H = \frac{P_e}{\Phi_B} \quad \text{Eq. 3.3.3.2.1}$$

Furthermore, assuming no heat losses and P<sub>e</sub> <<  $\dot{Q}_C$  (thermal power extracted from TEG cold side), by Eq.3.1.2.2.3 can be obtained:

$$\dot{Q}_C \sim \dot{Q}_H = \frac{P_e}{\Phi_B} \quad \text{Eq. 3.3.3.2.2}$$

Using this formula, the maximum heat flow extracted by the heat sink of prototype B can be calculated, that is about 5 kW. For additional details considering prototype B, see Sec. 3.4.1.2.

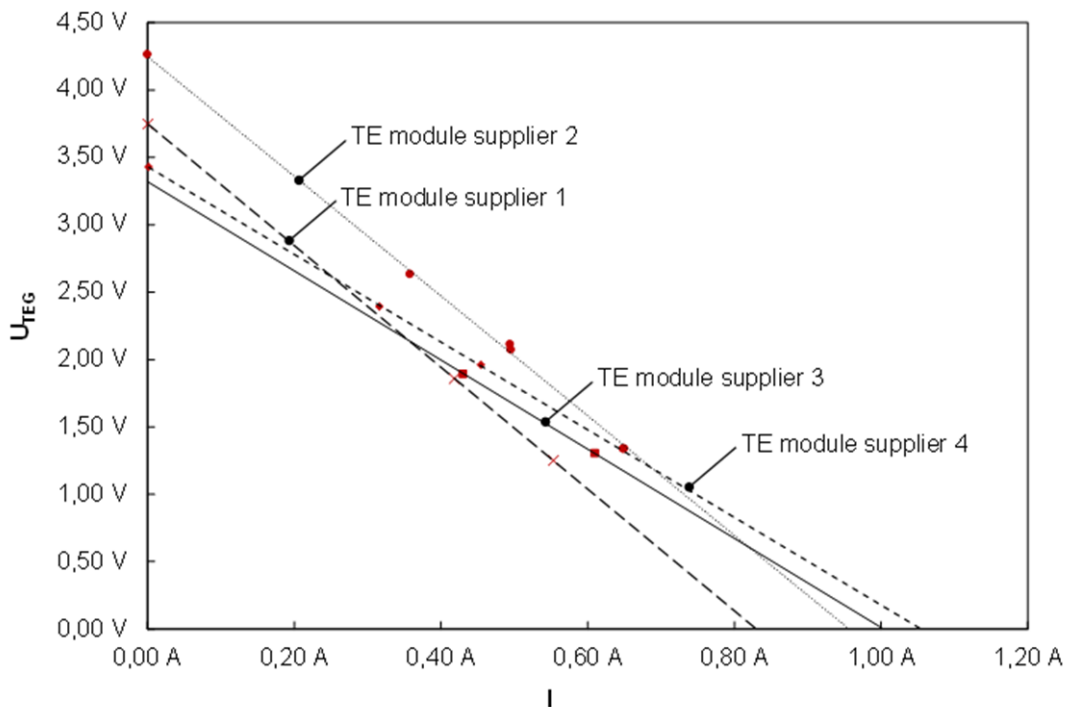


**Figure 3.3.3.2.1** - V-I relations at  $T_{HE} = 750^\circ C$

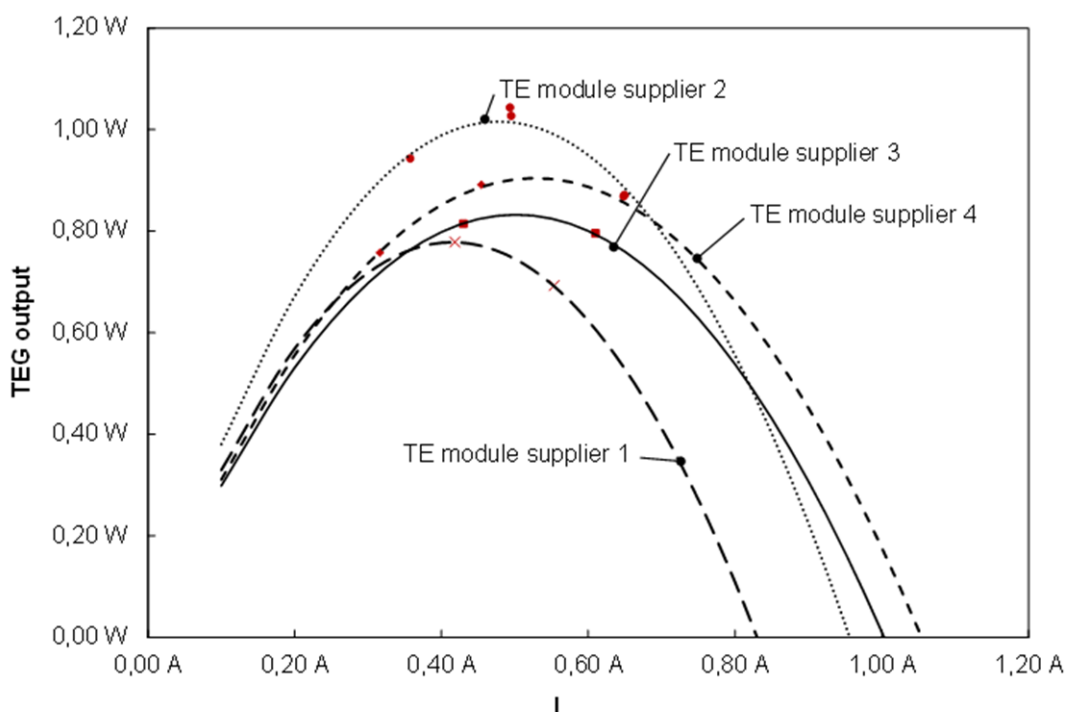


**Figure 3.3.3.2.2** - P-I relations at  $T_{HE} = 750^\circ C$

### 3.4 WP4 – Design, construction and plant installation of the full-scale thermoelectric system

WP4 objectives are:

- Design, construction and assembling of prototypes for full scale on-line tests
- Installation of the systems at the steel plant sites and connect them with both the hot source and the cold sink

### **3.4.1 Task 4.1 - Final configuration of thermoelectric systems modules (all partners)**

#### **3.4.1.1 Final configuration of prototype A (CSM, FENO, CU)**

The final configuration of the prototype A has required a compromise between the need to reduce as much as possible the length of a cooling box (to have the minimum temperature decrease in the horizontal direction) and an acceptable height of the whole TEG (for TEG stability, but also to avoid an excessive pressure on the TEMs below).

Therefore, it was decided to manufacture a TEG made of 10 horizontal layers where each layer is composed of a group of six in plane thermoelectric modules (see also Sec. 3.3.3.1 and Deliverable D3.3).

Figure 3.4.1.1.1 shows a picture of the prototype A in its final configuration and ready for the on-site installation finalised in January 2016.

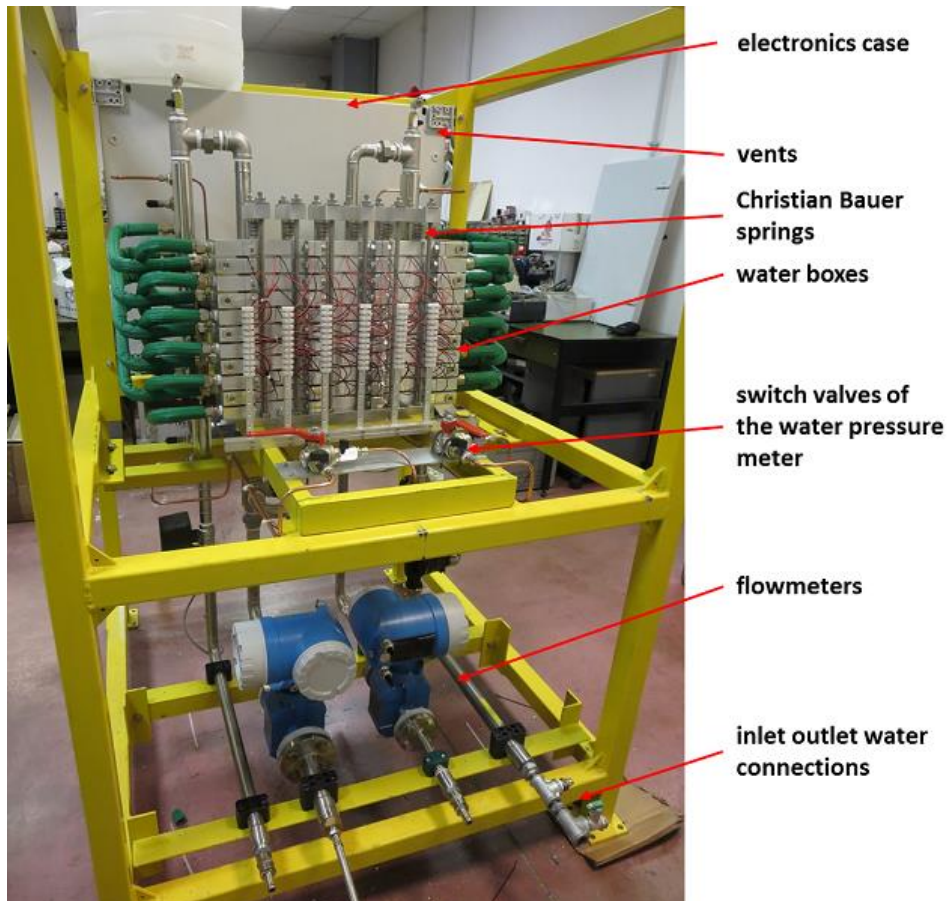
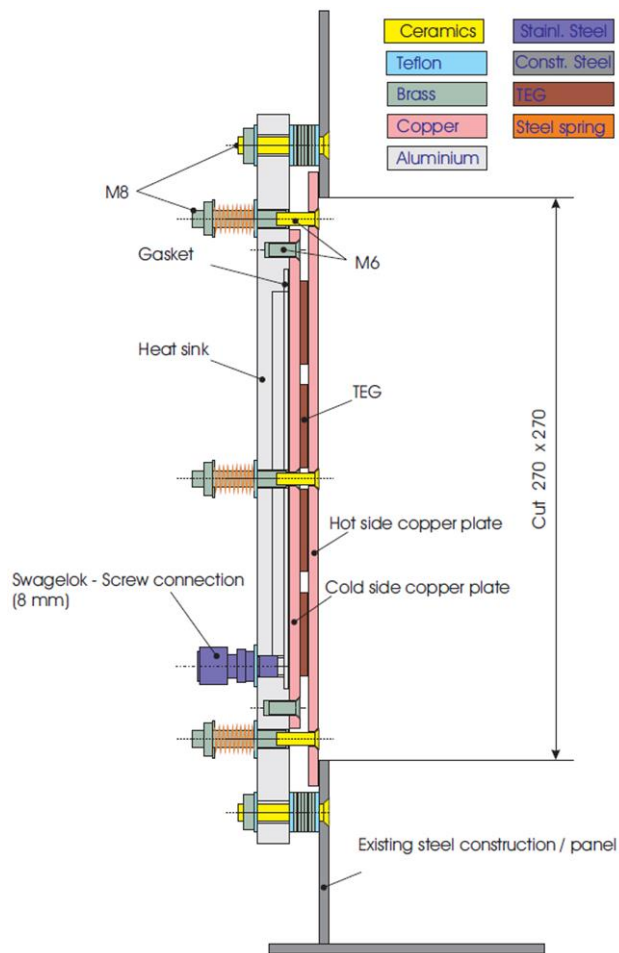


**Figure 3.4.1.1.1** - Prototype A, in its final configuration

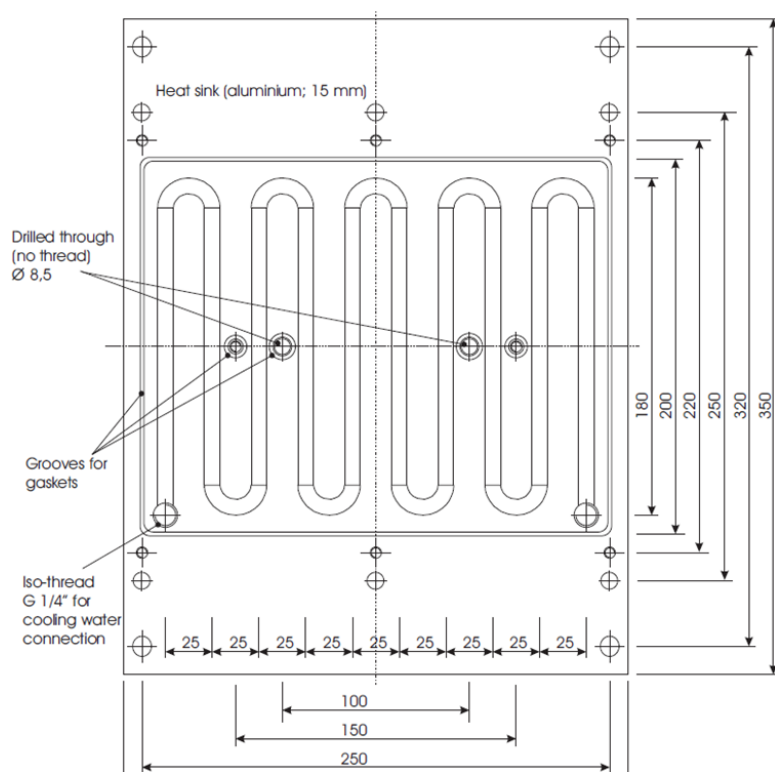
#### **3.4.1.2 Final configuration of prototype B (AME, BFI, CU)**

Figure 3.4.1.2.1 shows a side view of one of two generators of prototype B (consisting of 4 rows of 5 modules) as it was installed in the steel panels of the AME cooling bed conveyor. In order to improve the heat flow to and from the thermoelectric modules (1) copper plates were used on either side of the modules and (2) the hot side copper plate is in contact with the steel structure (the panel). Heat transport at thermal bridges (connections are required to (1) apply pressure (spring-controlled) on the hot and cold side of the modules and (2) attach the prototype B generator onto the panel) ceramic/teflon bolting systems were used.

Figure 3.4.1.2.2 shows a front view of the aluminium heat sink of 1 TE generator of the prototype B. Cooling water (water quality requirements have not been defined) flows, in open circuit, through a  $\sim 1,8$  m groove (groove surface perpendicular to cooling water flow:  $64 \text{ mm}^2$ ). A rubber gasket guarantees that cooling water does not leave the heat sink where it is in contact with the cold side copper plate.



**Figure 3.4.1.2.1** - Design of 1 (of 2) TE generator of the prototype B



**Figure 3.4.1.2.2** - Front view of the Al-heat sink of 1 (of 2) TEG of the prototype B

Table 3.4.1.2.1 lists all other prototype B design parameters.

Design parameter	Value	Remarks
Specific power output (W)	1,4	Required $dT_{\text{module}}$ : 95°C
Amount of TE modules / generator	20	4 rows, each row counting 5 modules
Amount of generators	2	The prototype B consists of two generators
Heat energy to heat sink	5,6 kW	Assumed 1% efficiency
Cooling water flow rate (sum: for both generators)	0,27 kg/s (~ 1,0 m <sup>3</sup> /h)	$dT_{\text{cooling water}}$ : 5°C; $dT_{\text{cooling water}} = \dot{Q} / \dot{m} \cdot c_p$
Cooling water velocity in 8 mm · 8 mm groove (in aluminium heat sink) for cooling water.	2,1 m/s	Considering the flow of cooling water, the generators are connected in parallel

**Table 3.4.1.2.1** - Prototype B design parameters

BFI finished the assembly of both generators of prototype B in September 2015. Subsequent functionality tests of prototype B were done at a BFI testing facility in Düsseldorf. Figure 3.2.1.3.2 shows the testing facility. It consists of eight porous burners (8 – 25 kW each) and one lateral installed generator, like it is planned for the full scale tests at Arcelor Mittal Espana plant site. Results are described in Sec. 3.2.2.8.

### **3.4.2 Task 4.2 - Plant installation of the full-scale thermoelectric system (all partners)**

#### **3.4.2.1 Installation of prototype A at Ferriere Nord (CSM, FENO)**

Ferriere Nord identified a service building, not far from the main duct of the EAF cooling system, to place prototype A. About 50 meters of pipeline was installed to connect the TEG with the hot heat source. The hot water pipeline was thermally insulated and it was calculated that, assuming a flow rate of 1 m<sup>3</sup>/h, the temperature loss should be less than 1°C from the main duct to the TEG device (this result was successively confirmed by on site measurements).

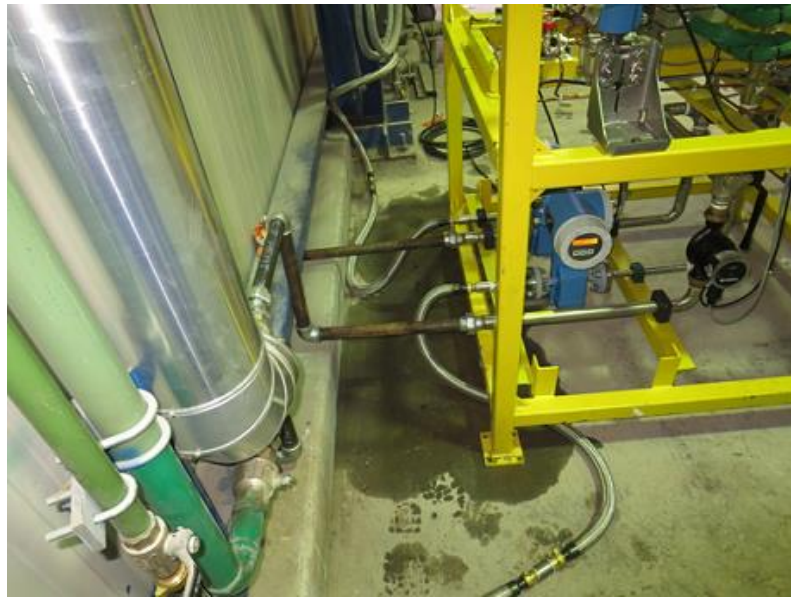
After a delay caused by software problems, finally prototype A was ready for final installation at plant site and it was transferred from CSM lab in Rome to Ferriere Nord plant in Osoppo (Udine). No other problems were encountered and on-line trials started correctly in January 2016.

Figure 3.4.2.1.1 and Figure 3.4.2.1.2 show the TEG device at the terminal point of the new pipe lines inside the service building, both for the hot and cold water supply.

Figure 3.4.2.1.3 shows the picking up point of the hot water from the main duct of the EAF cooling system. This figure shows also the required valves to disconnect the two hydraulic circuits.

To minimise the water friction, and hence the energy spent by the pumping system, it was chosen a pipe section of 1.5" (DN 40mm). The choice of the pipe section is very important for the overall energy balance, mainly for long distances. Therefore, the designer has to consider that a larger section reduces the friction, lowering the electric power losses for the pumping, but increases the travel time of the water into the pipe line, increasing the temperature losses and consequently reducing the whole system efficiency. Therefore, the choice of the section of the pipe must be adopted carefully.

Other pictures of prototype A installed at steel plant building are showed in Deliverable D4.2.



**Figure 3.4.2.1.1** – Prototype A connections with EAF plant hot and cold water



**Figure 3.4.2.1.2** – Prototype A installed at Ferriere Nord plant

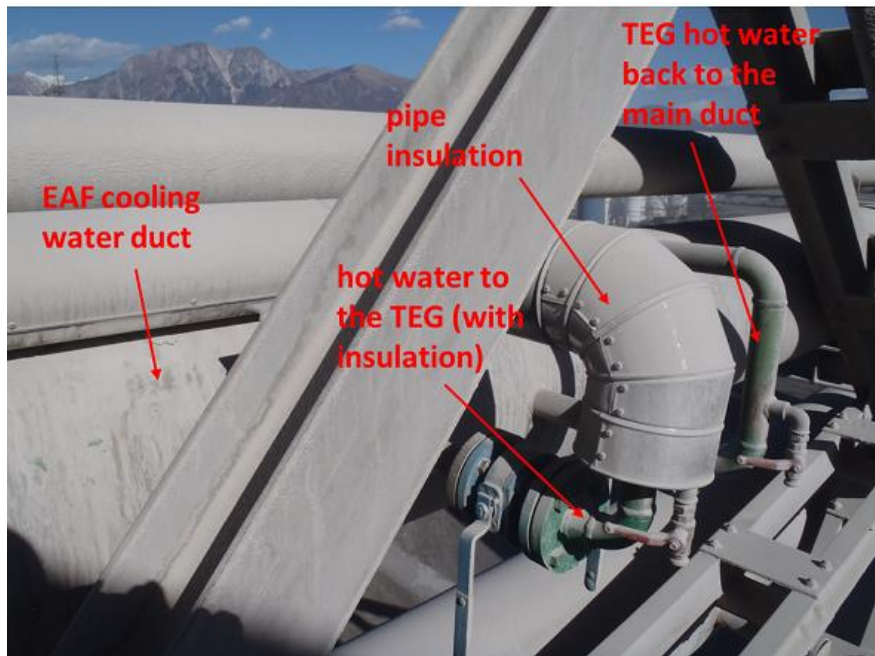


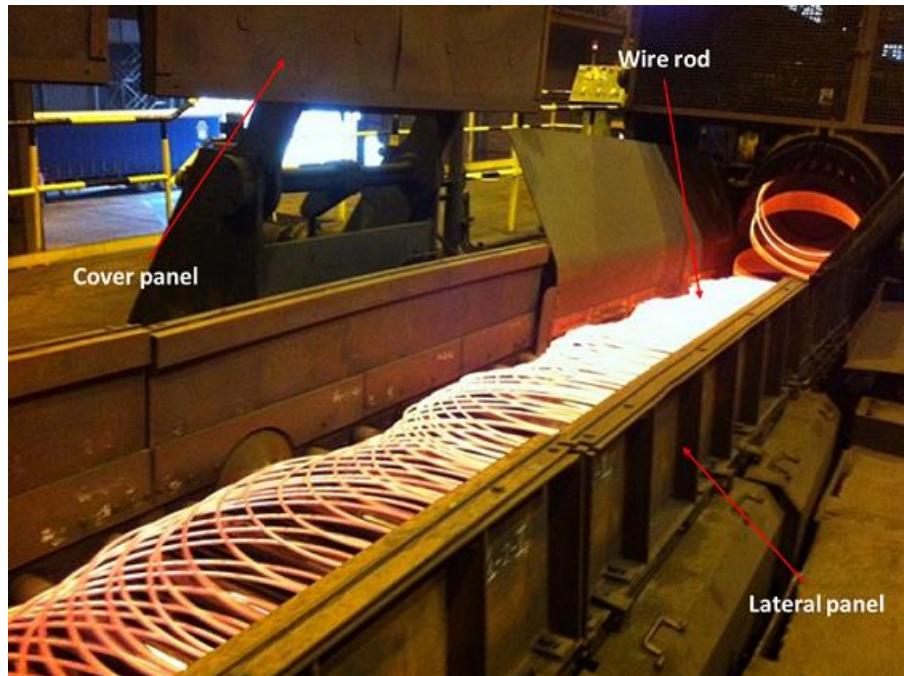
**Figure 3.4.2.1.3** - Prototype A, hot water connection with EAF off-gas cooling water duct

#### **3.4.2.2 Installation of prototype B at Arcelor Mittal España (AME, BFI)**

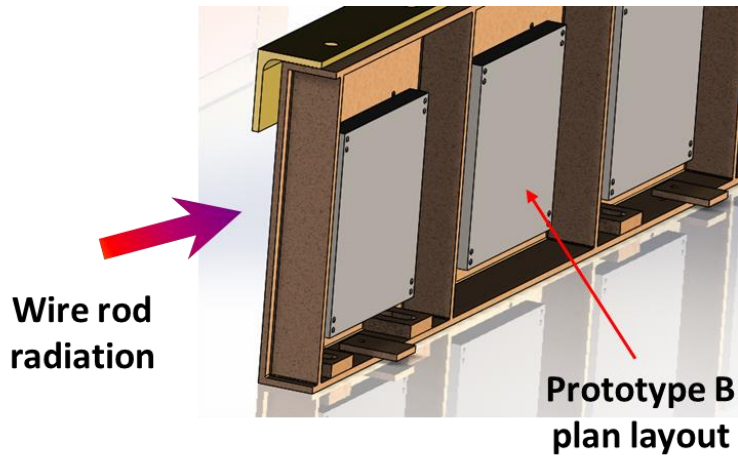
After finishing the functional tests, BFI carried the prototype and the appendant equipment (data acquisition system, load resistance, tubes, wiring etc.) to Arcelor Mittal plant site in Gijon. The installation of the prototype on a side panel of the cooling table and commissioning was done in the beginning of October 2015 by AME and BFI staff.

Figure 3.4.2.2.1 shows the selected cooling table plant area where prototype B was installed.

Figure 3.4.2.2.2 shows a drawing of prototype B generators on a side panel of the AME cooling table.



**Figure 3.4.2.2.1** - Prototype B at installation plant area



**Figure 3.4.2.2.2** – Prototype B, drawing of side panel at the AME cooling table

The generators were initially installed at the fourth panel of the cooling table (distance to the hot wire inlet approximately 8 m) to avoid overheating of the generators (maximum allowed temperature of the TE modules' hot side approximately 200°C)

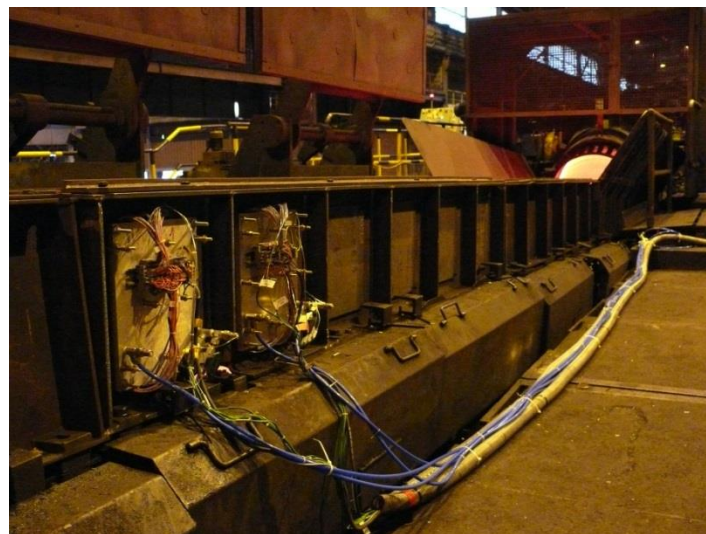


**Figure 3.4.2.2. 3** – Prototype B, general overview of layout at AME plant

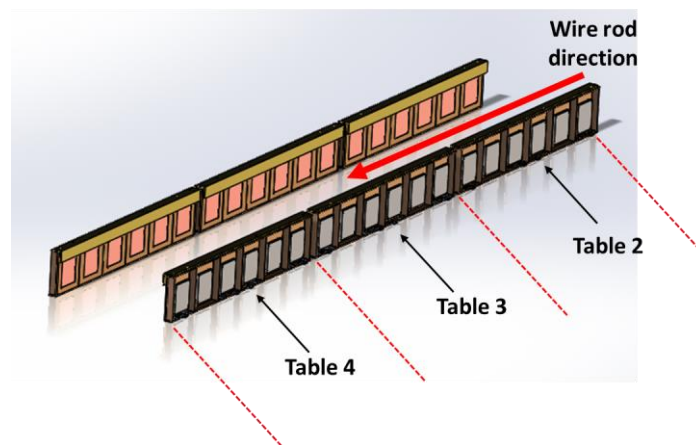


**Figure 3.4.2.2. 4** - Prototype B, possible multiple installation

Figure 3.4.2.2. 3 shows the installed generators of prototype B, the wiring and the cooling water tubes. Other pictures of the prototype B installation can be found in Deliverable D4.2.

Figure 3.4.2.2. 4 shows a possible multiple installation of prototype B at the cooling table plant (not foreseen in the present research program).

### **3.5 WPS – Execution of full-scale test and analysis of the thermoelectric system**

#### **3.5.1 Task 5.1 – On-line full-scale tests of the thermoelectric system prototypes (AME, FENO, CSM, BFI)**

##### **3.5.1.1 Prototype A: on-line full-scale test description (CSM, FENO)**

On-line full-scale test of prototype A was started in January 2016 at Ferriere Nord plant in Osoppo and continued for more than three months. The thermoelectric prototype was remotely controlled from CSM in Rome and performed different working tests.

During the period of test the hot water temperature, coming from the EAF off-gas cooling system, ranged from 70°C to 85°C, and the cold water between 10°C and 12°C (winter time).

Figure 3.5.1.1.1 shows the TEG interface developed to control on-line the variables and their trends. Using this interface it was possible to monitor several data, such as: the flow rate of hot and cold water, inlet and outlet temperatures of hot and cold water, water pressure drop of the hot or cold water circuit, external temperature of the aluminium water boxes, produced electric current and power in various points of the electric circuit.

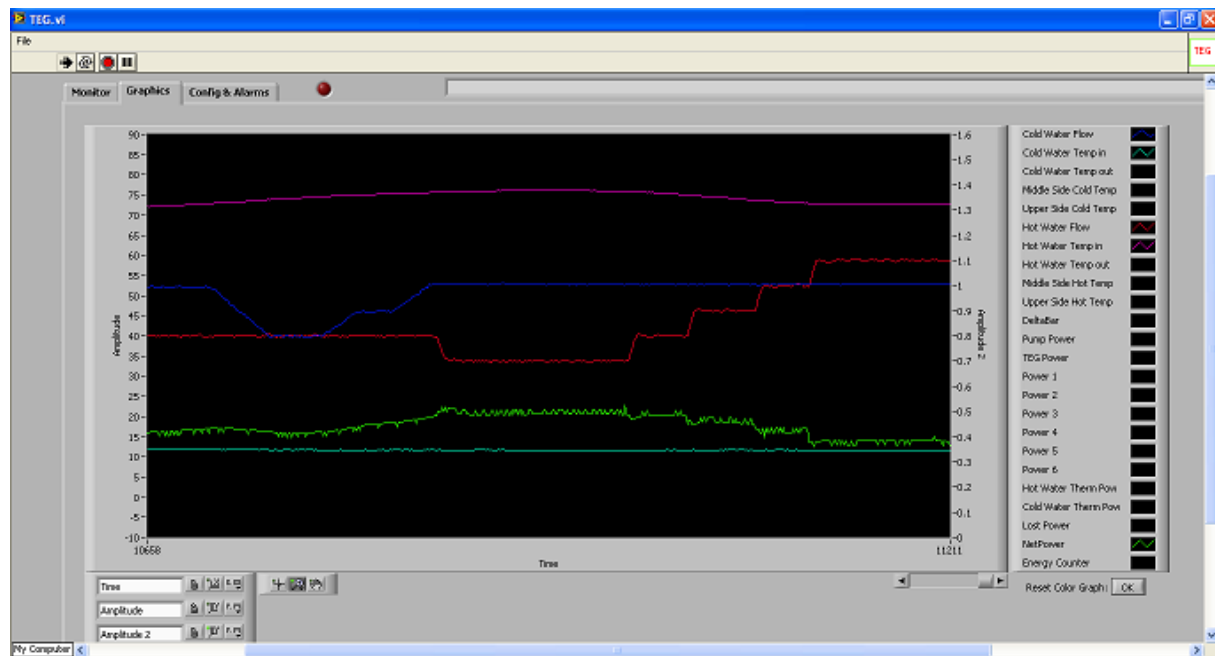


**Figure 3.5.1.1.1** – Snapshot of measured data during on-line tests of Prototype A

Figure 3.5.1.1.2 shows a screenshot of the control interface during the test. From this interface it was possible to have an immediate vision of the process. In particular, the top right shows the "net power", i.e. the difference between the power produced by the thermoelectric generators and the power used to flow the water into the whole system. This value is a direct measure of the capability of the whole thermoelectric generator system.

Tests were performed mainly to verify the different performances of the TEG device under different working conditions, in particular, the variation of the flow rate of hot and cold water, and the variation of electric load impedance.

It was not possible to control the temperatures of hot and cold water as they were determined by the plant condition (for the hot water) and by the season (for the cold water). However, the temperature of the cold water was practically constant during the whole test period, and the change in hot water temperature was sufficiently slow. This permits CSM operators to gather enough data and required information as it was a constant value.

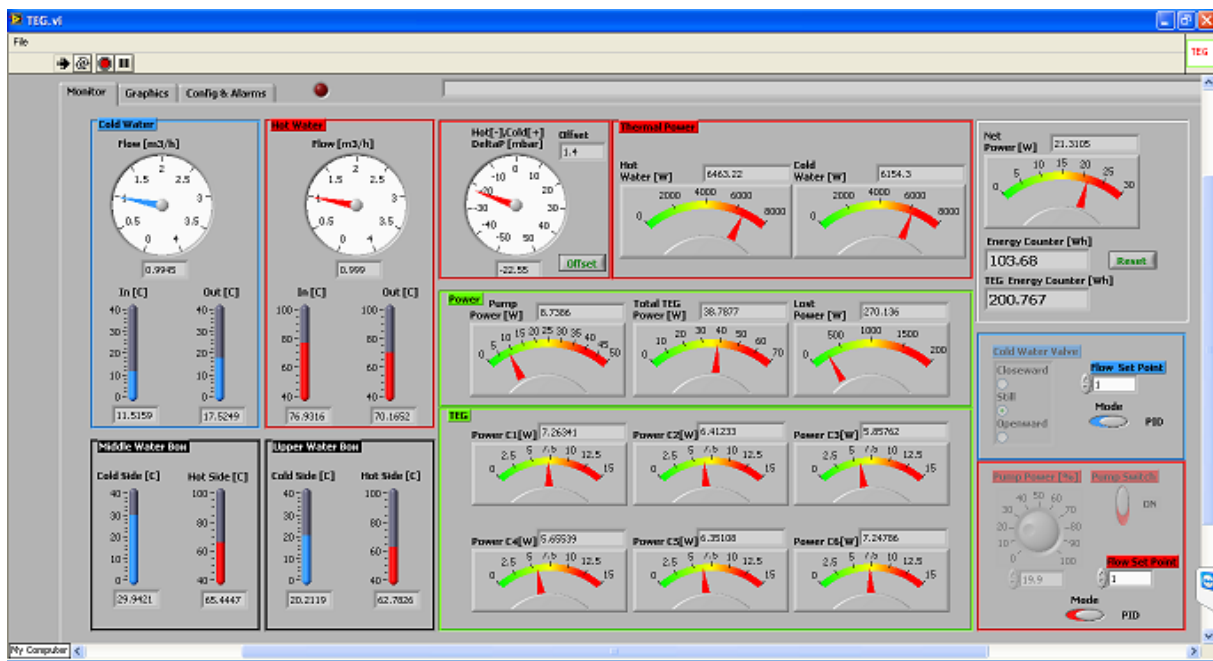


Figure 3.5.1.1.2 – Prototype A, control interface

### 3.5.1.2 Prototype B: on-line full-scale test description (BFI, AME)

The full-scale tests of Prototype B at AME plant site were carried out from beginning of October to mid of November 2015. Measured data of the generators were: cooling water flow, temperature of cooling water inlet and outlet, cold side and hot side temperature of TE modules 1, 13 and 20 (No. 20 only at generator No. 2), voltage, current, electrical resistance and electrical power.

The data were recorded at intervals of every 5 seconds. During the commissioning an ideal load resistance of 6 Ohm was detected. Thus, this value was used during the whole time of the full-scale tests. During the tests, the set up was controlled by AME staff regularly.

After a several days of testing, it turned out that the temperature of the hot side of the TE modules was very low at the selected position in the panels of the cooling table (maximum temperature difference over the TE modules approximately 55 – 70 K), so that the generators reached a maximum power of just 9 W each. Thus, it was decided to change the position of the generators closer to the wire inlet. This was done on October 15<sup>th</sup> by AME staff during a standstill of the plant. The generators were installed in the front of the 3<sup>rd</sup> panel of the cooling table. Thereafter the maximum power of the generators increased up to approximately 19 W, at a temperature difference over the TE modules of 109 K (generator No. 1) and 82 K (generator No. 2).

Since the emissivity of the surface of the copper plates is very low ( $\epsilon \sim 0.04$ ) the copper plates were painted black to increase the heat transfer. Initially generator No. 2 was blacked on October 23<sup>rd</sup>. Figure 3.5.1.2.1 shows the front view of prototype B with the copper plate of generator No. 2 painted black.

From October 23<sup>rd</sup> to 29<sup>th</sup> the data acquisition system was out of order. The failure was fixed on October 29<sup>th</sup> by AME staff.

After collecting data with one blacked generator and one untreated, generator No. 1 was blacked on November 10<sup>th</sup>. Figure A.9.2.5 in Deliverable D4.2 shows the front view of prototype B with both copper plates of the generators painted black.

On November 13<sup>th</sup> the data acquisition of generator No. 2 showed a current of 0 A and thus an electrical power of 0 W. The wires and connections of generator No. 2 were checked by AME staff, but no damage was detected.

On November 17<sup>th</sup> the data acquisition of both generators showed unrealistic values for all measurements (temperatures, current, voltage, power). The wires and connections of both generators were checked by AME staff, but no damage was detected. Neither a restart of the data acquisition system showed better values. The evaluation of the data recorded in front of the system failure showed, that the hot side temperature of the TE modules rose to more than 300°C for several minutes, see Figure 3.5.1.2.2 and Figure 3.5.1.2.3. Since the maximum allowed temperature of the TE modules is approximately 200°C a damage of several or all modules was most likely. Further a flaking of the black paint was detected especially at generator No. 1, see Figure 3.5.1.2.4. Thus the full-scale tests were abandoned. A detailed failure and damage analysis

of prototype B was carried out by BFI staff, when the prototype was back at the BFI in Düsseldorf. This was done in early 2016.



**Figure 3.5.1.2.1** - Front view of prototype B, copper plate of generator No. 2 painted black, copper plate of generator No. 1 not painted

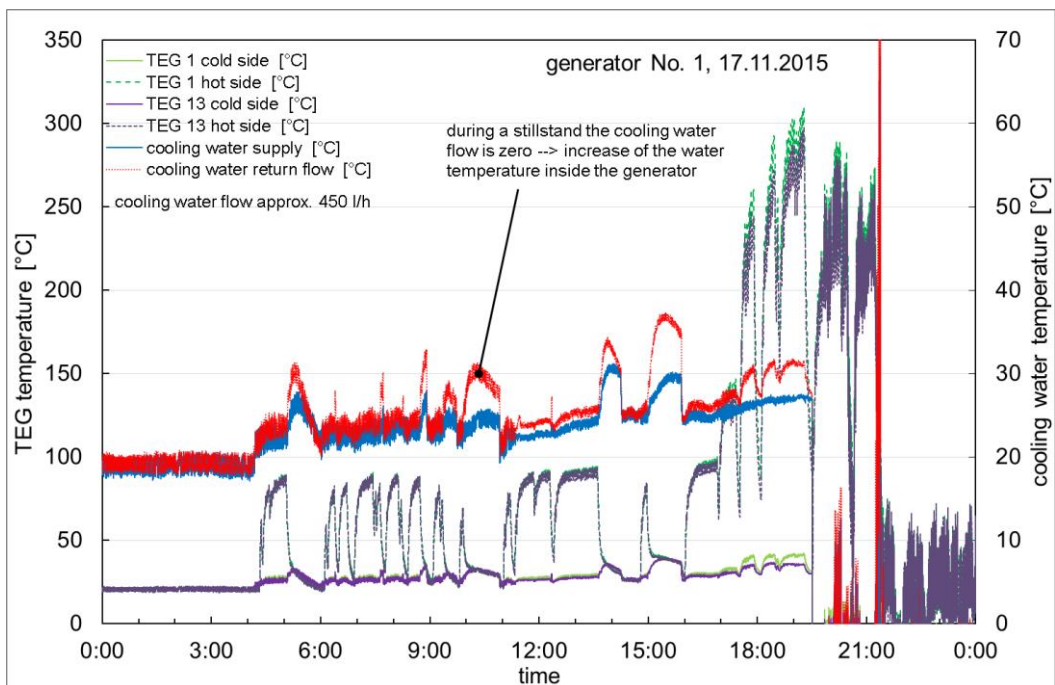


**Figure 3.5.1.2.2** - Measured temperature profile for generator No. 1 on November 17<sup>th</sup>, most likely overheating of the TE modules from approximately 17:30 to 19:30; unusable data after 19:30

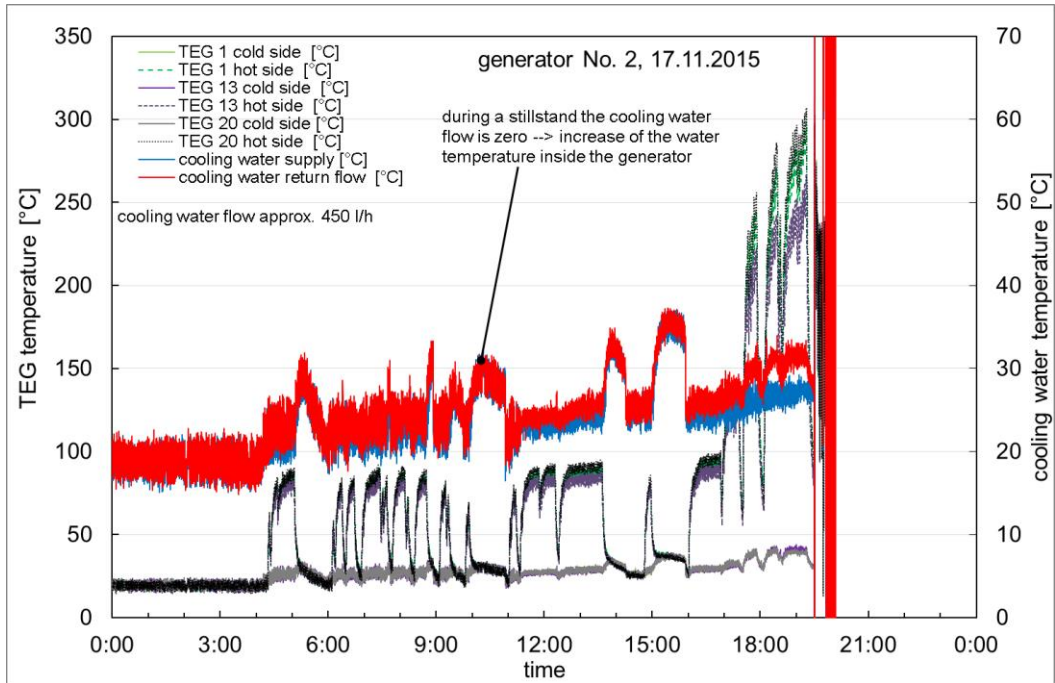


**Figure 3.5.1.2.3** - Measured temperature profile for generator No. 2 on November 17<sup>th</sup>; most likely overheating of the TE modules from approximately 17:30 to 19:30; unusable data after 19:30



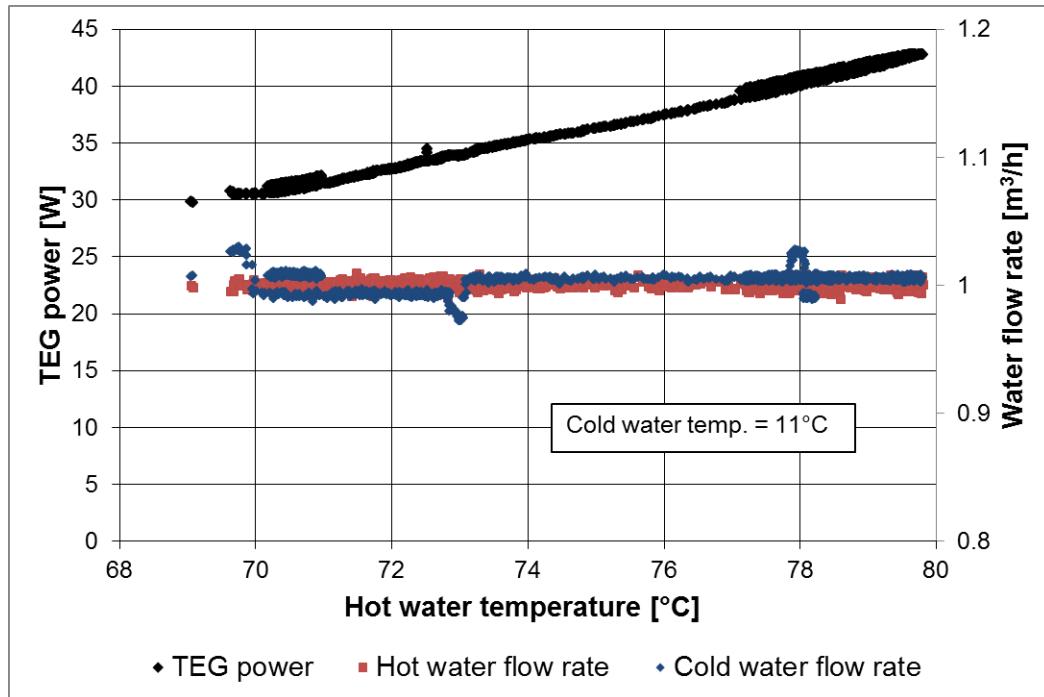
**Figure 3.5.1.2.4** - Flaking of the black paint from the generators

### 3.5.2 Task 5.2 – Assessment of the thermoelectric system performance (AME, FENO, CSM, BFI, CU)

#### 3.5.2.1 Prototype A: data analysis and results obtained during on-line test (CSM, FENO)

The first objective of the on-line tests was to verify the TEG power trend as a function of the inlet hot water temperature at a constant cold water temperature. Fortunately the cold water was effectively constant (11°C) for the whole test period, and then it was required only to wait the correct hot water temperature coming from the furnace. The results of this test are shown in Figure 3.5.2.1.1. In the same figure is also reported the measure of hot and cold water flow rate that was set to 1 m<sup>3</sup>/h for each flows. A strong linear dependence of the TEG power with respect to hot water temperature has been observed. This result is a direct consequence of the similar behaviour shown by the thermoelectric elements. This result is also important because it shows that the power output of these power production systems can be easily controlled through the control of the cold and hot water flow rate. Therefore, hot and cold water affect directly the overall performance of these devices.

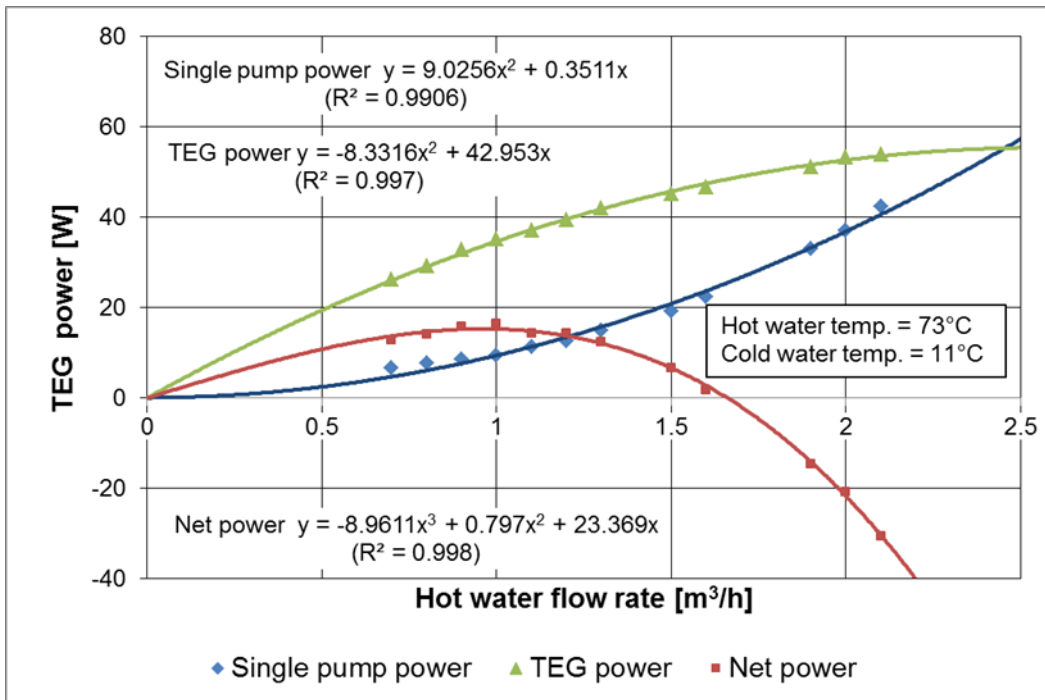
It is also possible to control the flow rate of hot and cold water independently, but this approach unnecessarily complicates the results interpretation. Thus it was decided to design a system working with the same flow rate for both the hot and cold water. Certainly, it is also possible to investigate situations in which the two flow rates are different, but this requires further study. In any case, it is advisable to perform this type of test under laboratory conditions because in the plant the water temperatures cannot be controlled conveniently..



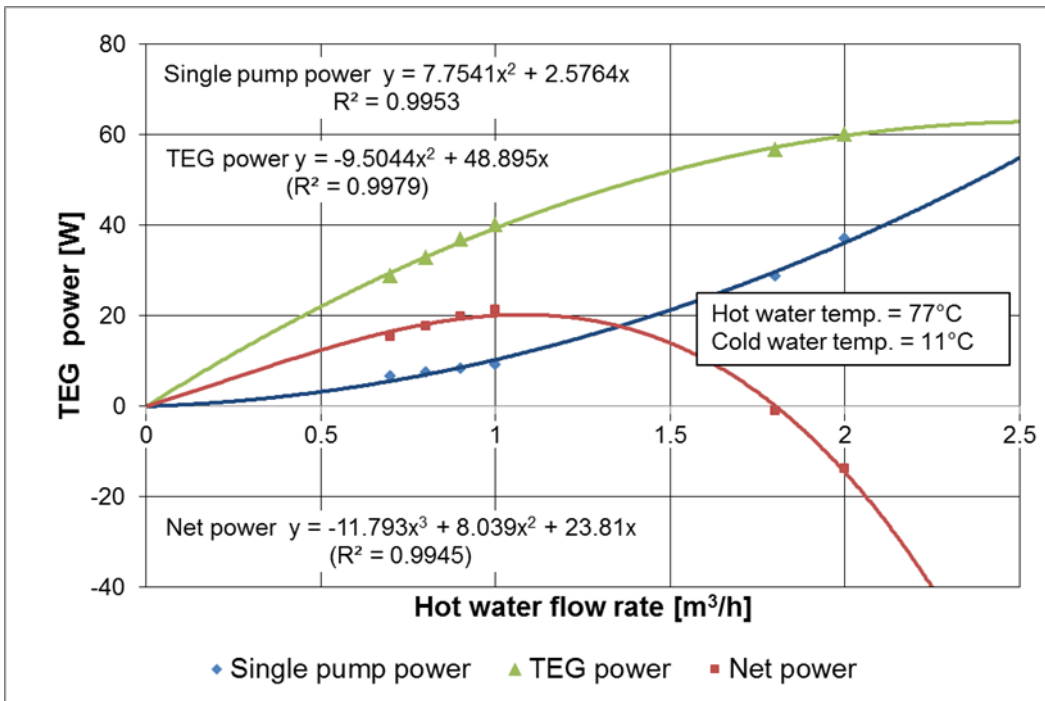
**Figure 3.5.2.1.1** – Prototype A, electric power versus hot water temperature

Figure 3.5.2.1.2 and Figure 3.5.2.1.3 show measured data obtained during on line trials. The figures show the electric power produced by TEG (green markers) and the simultaneous pump power consumption (blue markers), as a function of the hot water flow rate. For each point of the graph, the cold water flow rate was set to the same value as the hot water flow rate, and under two different inlet hot water temperature conditions (73°C and 77°C). These graphs show that both the TEG power production and the pump power consumption have a parabolic dependence on the flow rate of hot and cold water (but with a different sign on the  $x^2$  term). Because the device requires two water circuits (hot and cold), the net power has been calculated as the difference between the produced TEG power and the double of the consumed pump power measured on the hot water circuit.

It can be observed that the system is able to produce net power for a flow rates up to 1.6-1.8 m<sup>3</sup>/h. At higher values the pumps have power consumption higher than the TEG power production. Moreover, the maximum net power was obtained at about 1 cubic meter per hour, as required by the design specifications. This confirms the proper overall equipment sizing under the foreseen plant conditions.



**Figure 3.5.2.1.2** - Power production and power consumption ( $T_{hot}=73^\circ\text{C}$ )



**Figure 3.5.2.1.3** - Power production and power consumption ( $T_{hot}=77^\circ\text{C}$ )

The Maximum Power Point (MPP) [4] of each column, i.e. the point at which a column of TEMs delivers the maximum electrical power, was measured modifying manually the external resistance load of each column from 2.5 to 3.5  $\Omega$ . These tests showed that the chosen resistance load of 3  $\Omega$  for a single column, sets the system working point close to the MPP for each operational condition. It should be noted that it is also possible to connect the TEMs in series along the horizontal rows, instead of the columns. As the heat exchanger has a counter-flow configuration, the TEMs in this case could perceive to have the same temperature difference. This configuration requires further investigation.

Other tests were performed to verify the behaviour of each column. The open circuit voltage, the voltage with the fixed column resistance load (working point) and the current and voltage drop through the digital tester were measured for each TEM of each column. Using these values the

voltage-current (V-I) characteristic curve (linear) and the power-current (P-I) characteristic curve (parabolic) were calculated. Figure 3.5.2.1.4 shows the two characteristic curves for five TEMs of the first column. Also from these data it is possible to verify that each TEM works very close to its own MPP confirming a good sizing of the selected resistance load.

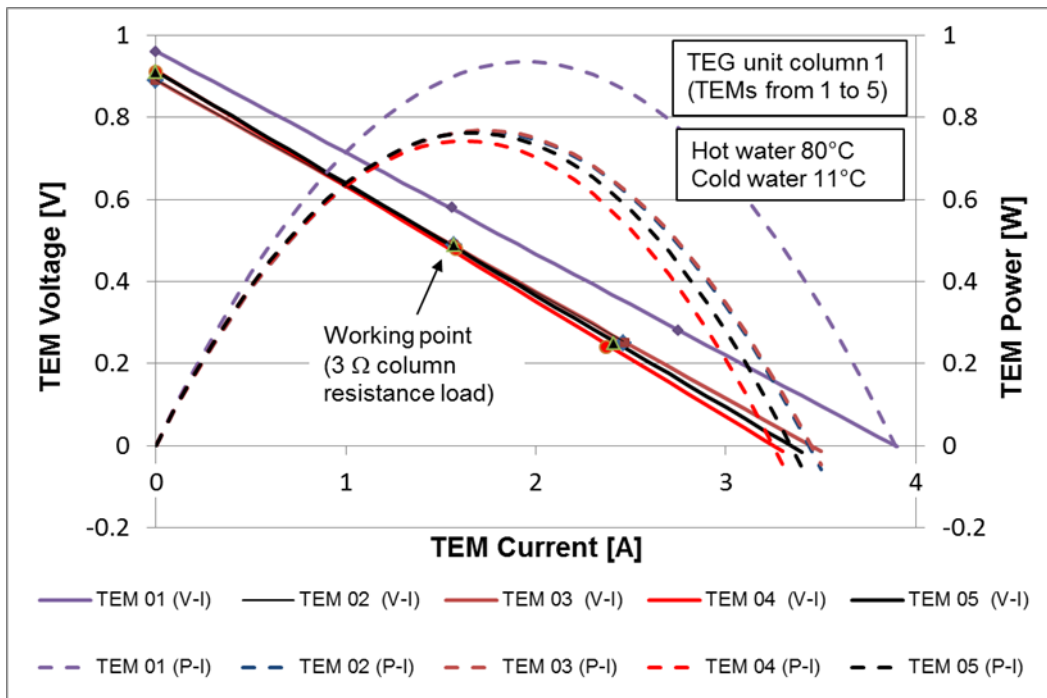


**Figure 3.5.2.1.4** - Characteristic curves (V-I) and (P-I) of five TEMs of the first TEG column

Table A.11.1.1 (Deliverable D5.2) shows the measured TEG unit performance at standard conditions. In this condition the TEG unit works as a heat exchanger which transfers about 6500 W of thermal energy from the hot source to the cold sink producing about 40 W of electric power.

The "lost thermal power" shown in Table A.11.1.1 is calculated as the difference between the measured power that enters, and the measured power that exits, from the TEG device. The first being the thermal power lost by the hot water crossing the TEG device, and the latter being the sum of the thermal power absorbed by the cold water crossing the TEG device and the produced electricity. This value shows a loss of power mainly caused by pipeline thermal dissipation.

This fact confirm that a better design, possibly carried out using thermoelectric elements directly incorporated into the structure of the heat exchanger, will lead to better efficiency reducing pipelines radiation.

Considering the TEG as a heat engine, the device shows an electric energy conversion efficiency of about 0.61%. This low efficiency is both caused by the actual thermoelectric module efficiency and by the simple counter current design of the thermoelectric generator. In fact, can be observed that the original temperature gap between the hot and cold water of 65.4 °C (=76.9°C hot source -11.5 °C cold sink) drops down, in the real device, to an effective 35.5 °C (=65.4°C hot source -29.9 °C cold sink) between the aluminium water boxes, that is probably a good average value of the real temperature gap received by the thermoelectric modules. In the same conditions, assuming the ZT figure of merit equal to one, the theoretical efficiency [5] is 3.47% and 1.88% respectively. Therefore, in the best case, and by using a better design, i.e. obtained through a reduction of the TEG structural sections, and then reducing the thermal barriers between the thermoelectric modules, it can be expected to double or triple the electric conversion efficiency.

In any case, the energy spent to move the hot and cold fluids cannot be neglected in a real device. Assuming the distance of the hot and cold source from the TEG unit of about 50 m (as for the case study), it was measured a pumping power for hot water circulation (both for connection and TEG pipes) of 8.7 W and therefore for both circuits of approximately 17.4 W. As a consequence, the measured actual electric conversion efficiency of the developed TEG unit, under the described working conditions, is about 0.33 %.

It is also interesting to note that doubling both the source and the sink distance from 50 m to 100 m also doubles approximately the pumping power required to move the water into the pipeline. In such situation, the TEG unit produces an amount of electric energy equal to that is needed to move the water. So it can be stated that, if the source and the sink are located less than 100 meters away from the TEG unit, it acts as a heat exchanger that requires no energy for its own

operation. However, it should be also considered that the use of control instrumentation and power converters causes a further electric consumption, thus reducing the overall efficiency

### **Weakness and failure analysis of prototype A**

After finishing the on-line test, Prototype A was sent back to CSM laboratories in Rome. It was disassembled and all components of the device were checked. No particular damage was observed.

The problem of limestone deposits is one of the main problems for this type of equipment. In fact, from the side of the cold water flow, the water is drawn from a well and, therefore, could be rich in calcium. The temperature rise, if excessive, could generate a continuous deposit of calcium on the tubes and water boxes surfaces, which, after a long time, could create a barrier that prevents the passage of heat. This phenomena can drastically reduce the efficiency of the whole thermoelectric device. For this reason, it is necessary to take in account the cold water hardness in relation to the temperature rise reached during its passage inside the TEG system.

The internal pipe surfaces of Prototype A did not show any residual limestone after dismantle. However, Prototype A worked on-line only for a few months, while in a production system it should operate for years. Therefore this problem must be better investigated in the future with longer in situ tests.

Figure 3.5.2.1.5 shows the disassembling of prototype A. Figure 3.5.2.1.6 shows small damages on the carbon surface of the thermoelectric modules caused by sticking on the water box. This damage is not considered alarming because it occurs during disassembling. Figure 3.5.2.1.7 shows three thermoelectric module stick on the water box.

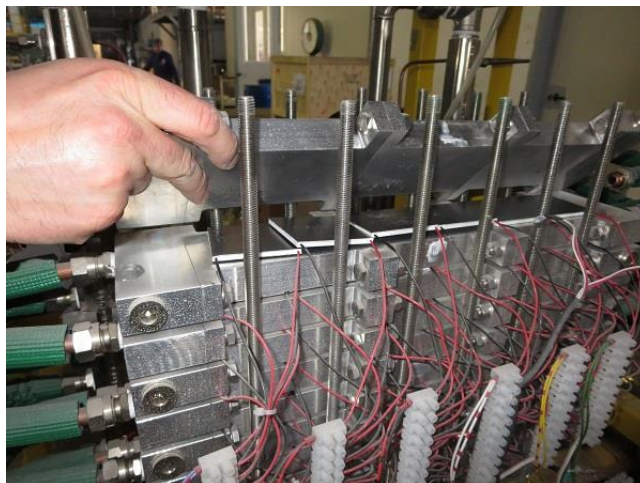


**Figure 3.5.2.1.5 – Disassembling of prototype A**



**Figure 3.5.2.1.6 – Small damages on the thermoelectric modules caused by sticking**

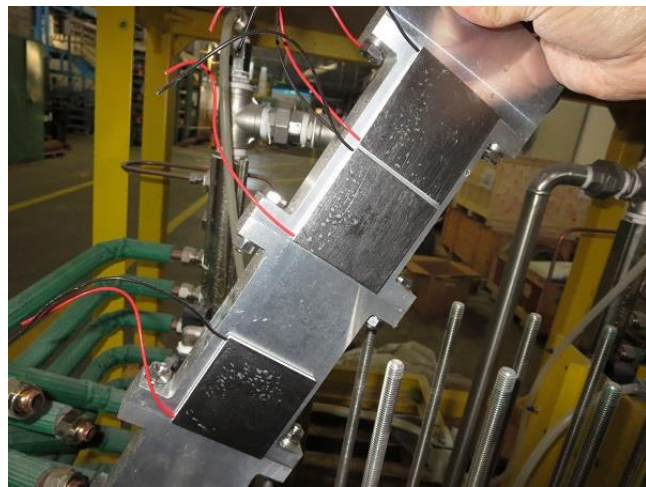
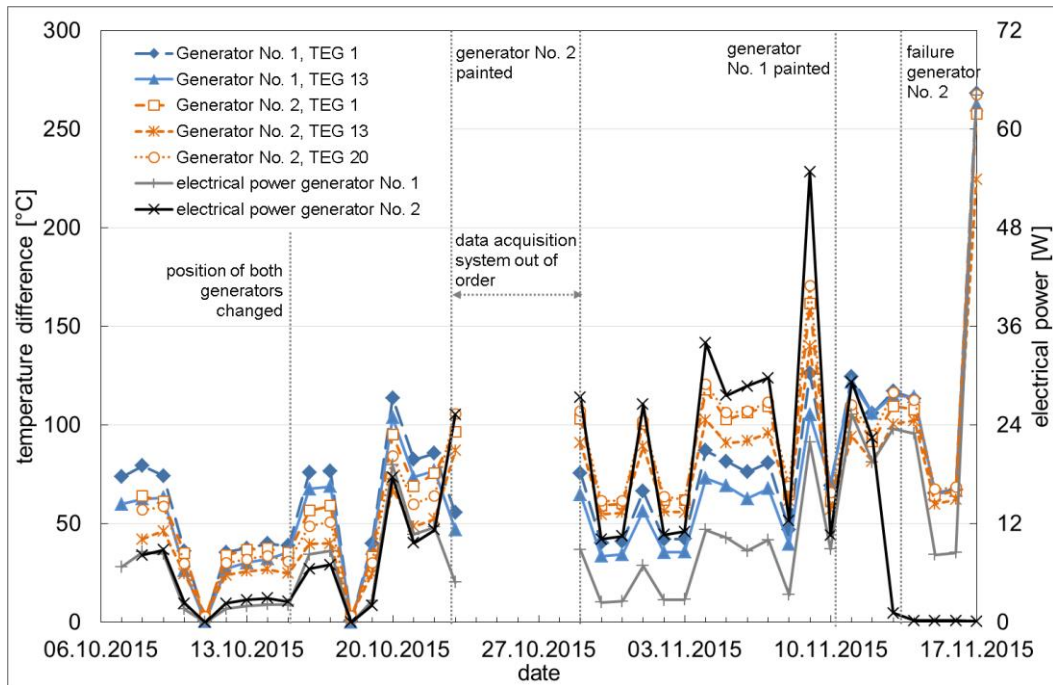


**Figure 3.5.2.1.7 – Some thermoelectric modules stick on the water box**

### 3.5.2.2    **Prototype B: data analysis and results obtained during on-line test (BFI, AME)**

Usable data were recorded from October 7<sup>th</sup> until November 17<sup>th</sup> and analyzed. The maximum temperature difference over the TE modules was approximately 170°C. On November 17<sup>th</sup> the hot side temperature of the TE modules increased for a short time up to 300°C. This caused damage to the generators or data acquisition system, so that thereafter no usable data were available anymore (see also Sec. 3.5.1.2). A detailed damage analysis was done in the beginning of 2016.

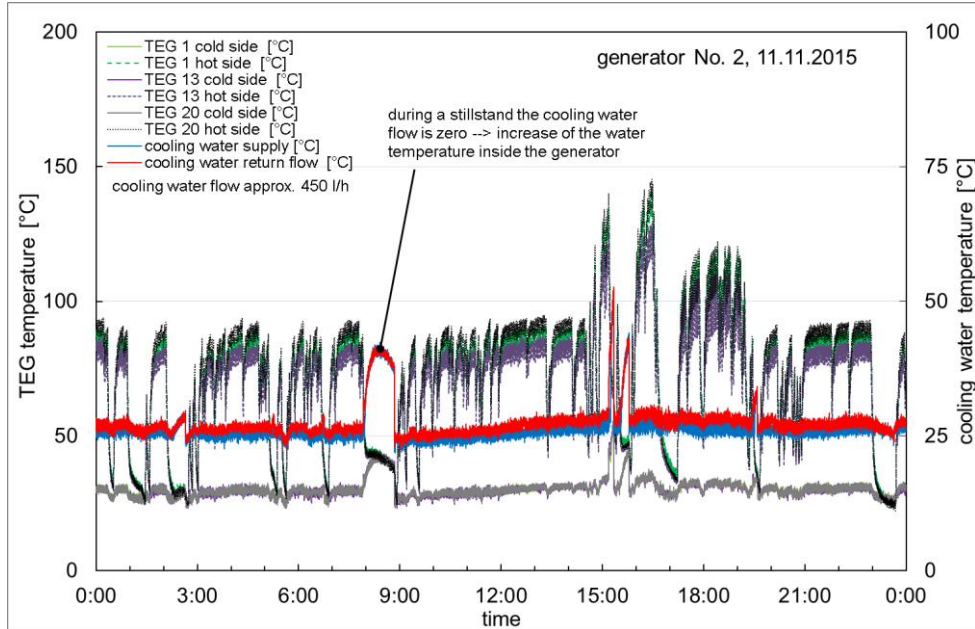
Figure 3.5.2.2.1 shows the measured maximum temperature difference of TE modules and the electrical power of both prototype B generators over the whole testing period.



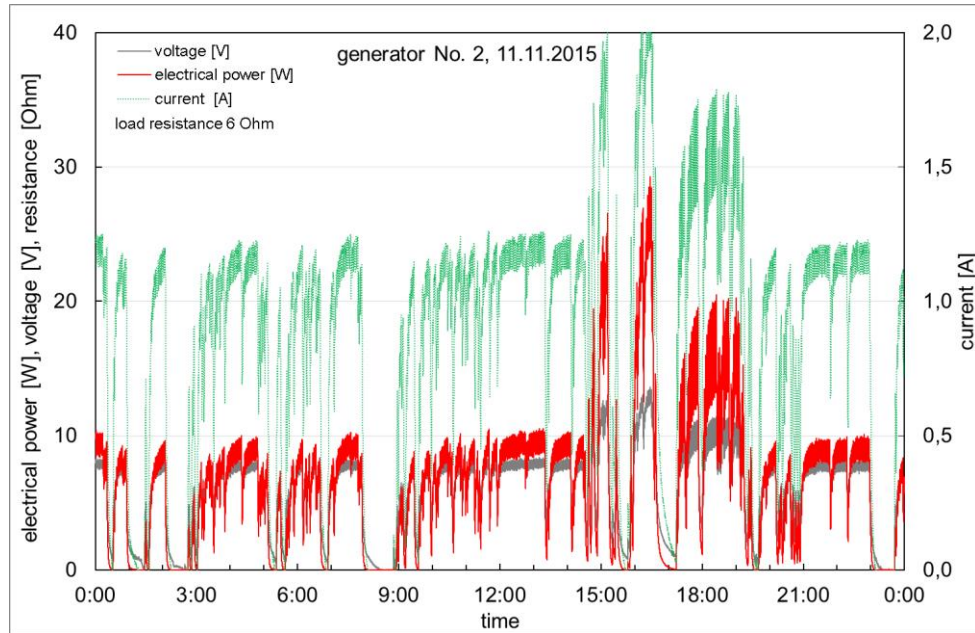
**Figure 3.5.2.2.1 - Maximum measured temperature difference of selected TE modules from both generators during the full scale tests at AME plant site**

It is found that the blackening of the hot generator surface resulted in a substantial increase in the achievable performance by up to 200%. While the electrical power of both generators was similar in the period from October 7<sup>th</sup> to 23<sup>rd</sup>, the power of generator No. 2 increased considerably after its blacking on October 23<sup>rd</sup>. After blacking generator No. 1 on November 10<sup>th</sup> the electrical power of both generators was similar again. On November 13<sup>th</sup> the data acquisition of generator No. 2 showed a current of 0 A and thus an electrical power of 0 W. A damage of the generator or the data acquisition system could not be detected.

Due to the production, the daily temperature profiles show a highly discontinuous temperature difference over the TE modules and thus a discontinuous electrical power of the generators, see Figure 3.5.2.2.2 and Figure 3.5.2.2.3. Varying waste heat streams arise due to various products with different wire diameters, lengths and materials and thus the achievable performance of prototype B was highly discontinuous, which is reflected both in the daytime and the long-term data. During longer standstills of the plant, the cooling water supply to the generators was stopped automatically. Thus an increase of the cooling water temperature inside the generators occurred by absorbing residual heat (see Figure 3.5.2.2.2) during standstill periods.

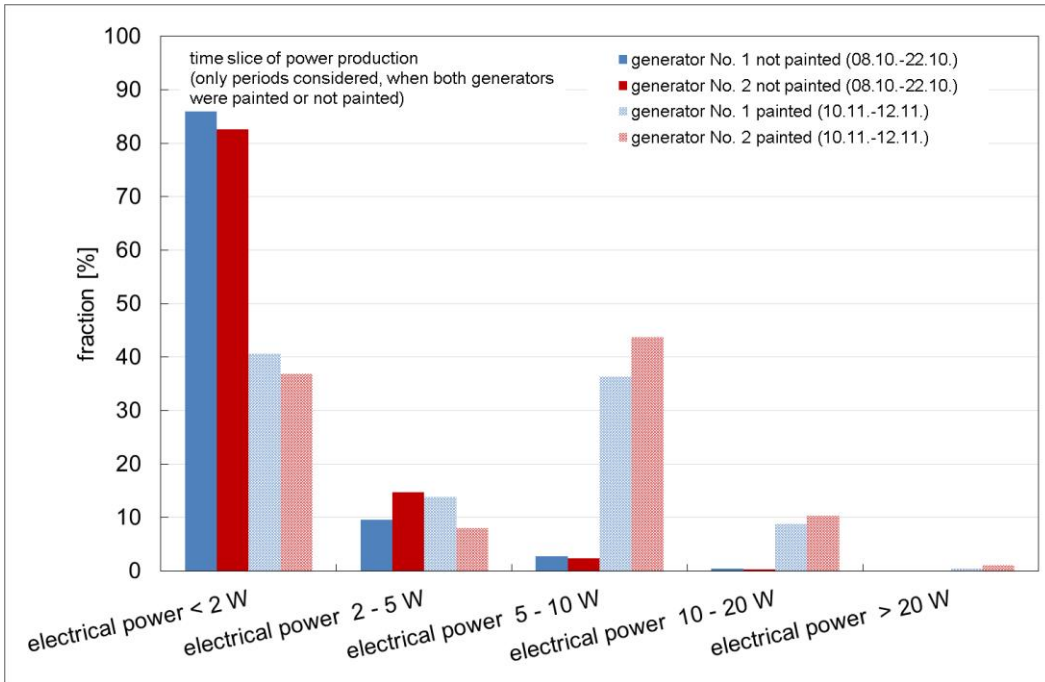


**Figure 3.5.2.2.2** - Measured temperature profile for generator No. 2 on November 11<sup>th</sup>



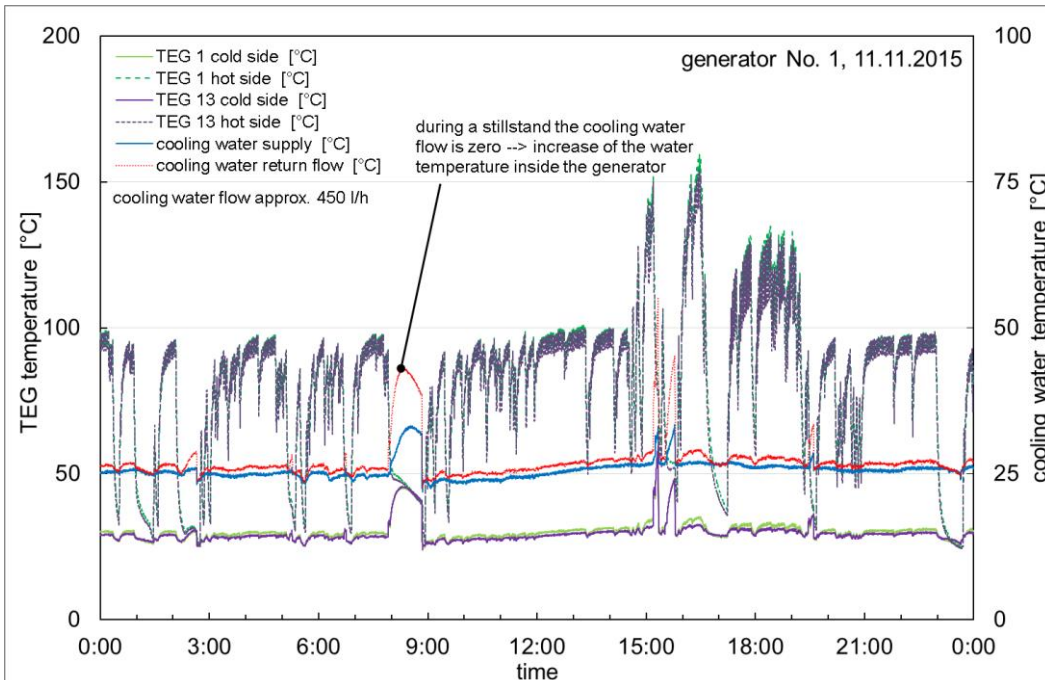
**Figure 3.5.2.2.3** - Measured profile of voltage, current and electrical power for generator No. 2 on November 11<sup>th</sup>

Figure 3.5.2.2.4 shows the temporal distribution of the electrical power of both generators over the whole testing period. The electrical power was lower than 2 W for approximately 80 % of the time, when the generators were not blacked. This value was halved with the blackening of the generators. At the same time the period with an electrical power of more than 5 W was multiplied.



**Figure 3.5.2.2.4** - Comparison of proportional produced electrical power between generators No. 1 and No. 2 of prototype B

The comparison of the temperature profiles with the electrical power of both generators show, that the measured temperature difference over the TE modules is higher for generator No. 1, while the electrical power is higher for generator No. 2 (compare Figure 3.5.2.2.2, Figure 3.5.2.2.3 with Figure 3.5.2.2.5 and Figure 3.5.2.2.6; and Figure 3.5.2.2.4 with Figure 3.5.2.2.7).



**Figure 3.5.2.2.5** - Measured temperature profile for generator No. 1 on November 11<sup>th</sup>

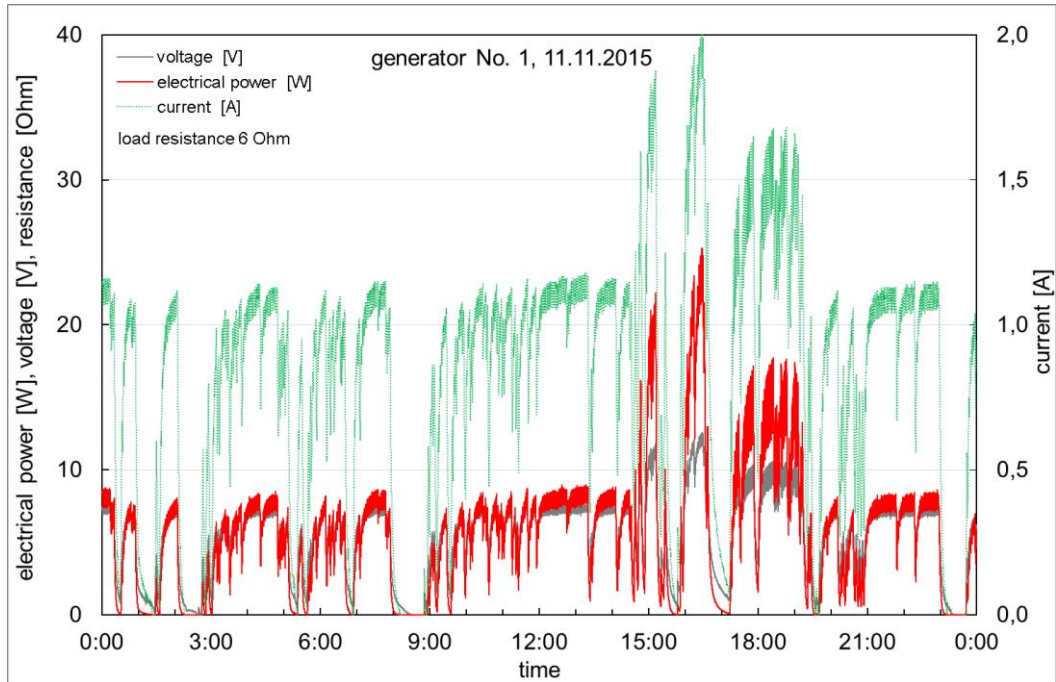


**Figure 3.5.2.2.6** - Measured profile of voltage, current and electrical power for generator No. 1 on November 11<sup>th</sup>

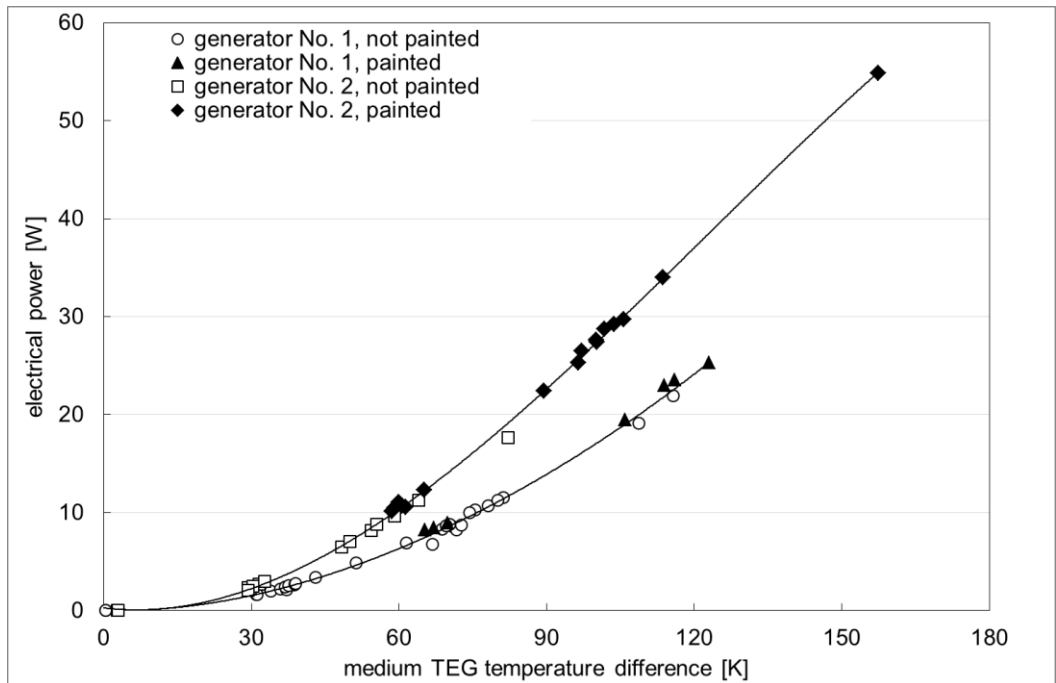


**Figure 3.5.2.2.7** - Measured electrical power as a function of the temperature difference over the TE modules

Reasons could be (see also Sec. 3.4.1.2):

- Improved heat transfer from the copper plate to the TE modules at Generator No. 2 by using more heat-conductive paste and improved contact of the TE modules to the copper plates due to using more screws
- Improved performance of TE modules in generator No. 2 due to manufacturing differences

Hence, differences in the performance of the two generators were detected, as shown in Figure 3.5.2.2.7. At the same measured temperature difference over the TE modules, the electrical power of generator No. 2 is significantly higher than the power of generator No. 1. With increasing

temperature difference, this effect continues to increase. This is reflected also in the efficiency of the generators (see Figure 3.5.2.2.8):

- The efficiency of generator No. 1 is in the range of 0,4 and 1,8 % depending on the temperature difference
- The efficiency of generator No. 2 is in the range of 0,6 and 2,8 % depending on the temperature difference

These values are well within the range of normal manufacturer's data.

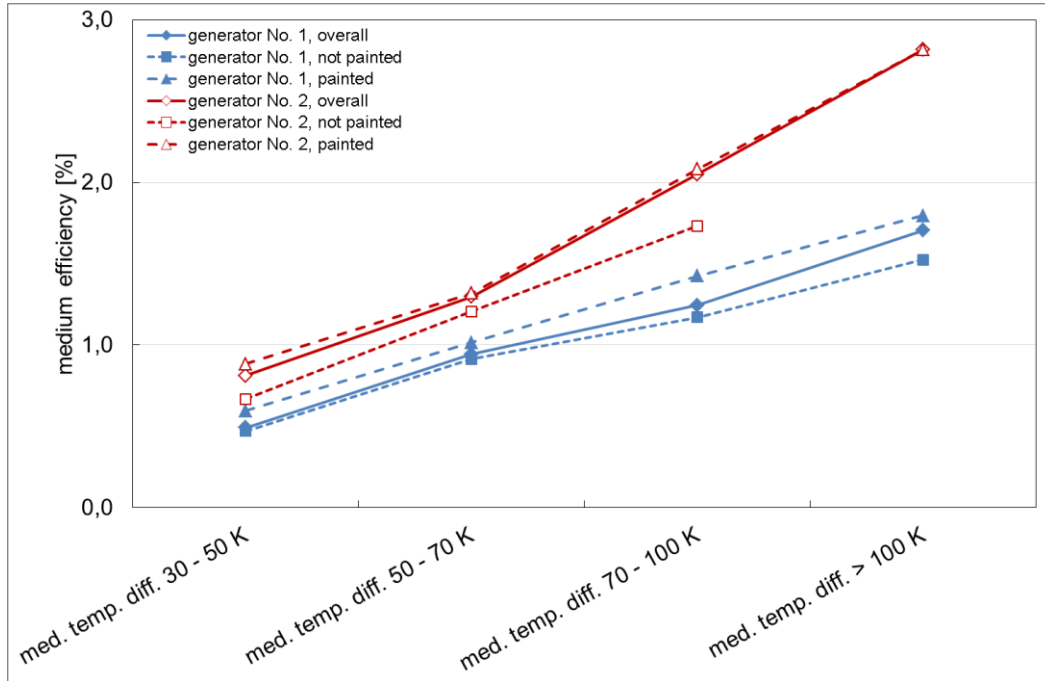


**Figure 3.5.2.2.8** - Medium efficiency of prototype B versus measured TE module temperature difference

#### **Weakness and failure analysis of prototype B**

After carrying the equipment back to the BFI a failure analysis was done by BFI staff to determine the causes of the failure of both generators (as described in Sec. 3.5.1.2). The exterior view and analysis of the generators without the protection sheets (see also ) showed several damages:

- Generator No. 1 (see Figure 3.5.2.2.9)
  - some TEG were displaced
  - loose wires of the TEG
  - flaking of the black paint
  - fouling through dust deposits
- Generator No. 2 (see Figure 3.5.2.2.10)
  - badly damaged wire of the pressure measurement
  - damaged wires due to bending
  - loose wires of the TEG
  - flaking of the black paint
  - fouling through dust deposits

Through an analysis of the data acquisition system the cause of the failure of the data recording was detected. The damaged wire of the pressure measurement of generator No. 2 caused short-circuit fault, so that the input signal of all measurement categories into the data acquisition system was 24 V (like the power supply of the pressure measurement). Since the data acquisition system needs an input signal of 0 - 10 V all data were falsified after November 17<sup>th</sup> (see Sec. 3.5.1.2).

The following disassembling of the generators showed:

- Destruction of all TEGs. Almost all soldering's that connect the wires to the modules were melted (see Figure 3.5.2.2.11)
- Black discoloration indicate damages between the insulating layer and the TE material (see Figure 3.5.2.2.12)
- The formation of verdigris on the copper plate indicates damage by water, but leak tests of the cooling system of both generators water showed no leakages. The verdigris could be accrued by water that has been released during the removal of the generators from the side panels when releasing the cooling water connections.
- Impurity of both generators

The date at which the modules have been destroyed cannot be identified exactly. Through the failure of the data recording on November 17<sup>th</sup> a damage of some or all TE modules could not be identified by the measuring data. However, the dissolution of the soldering's that connect the wires to the modules, the loosening of the wires and the black discoloration indicate overheating.

To prevent the identified damages several improvements of prototype B are possible:

- To prevent an overheating of the TE modules different measures are possible:
  - Instead of using a copper plate for the heat transfer to the hot side of the TE modules a heat storage plate could be used, filled with a phase change Material (PCM). Through the isothermal phase change (from solid to liquid) of the PCM the temperature of the plate would be limited to the melting temperature of the PCM. Thus the maximum temperature of the hot side of the TE modules can be limited regarding to the used PCM. Possible feasible materials could be tin with a melting temperature of 231°C or zinc – tin alloying with a melting temperature of about 200°C. Disadvantages of this solution are the more complex structure of the heat storage plate, heat transfer losses by using different materials and the resulting boundary layers between the materials, the costs of the PCM and that the temperature increases after the PCM is melted. This could happen, when the temperature of the heat source is higher as estimated for a longer period.
  - Extraction of the waste heat and heat transfer to the TE modules via heat pipes. Thus the maximum temperature of the hot side of the TE modules can be limited regarding to the used fluid of the heat pipes. Further the temperature of the hot side of the TEG would be more continuous by using heat pipes. Main disadvantages of this solution are the complex structure of the heat pipe heat exchanger and thus the higher costs and potentially heat transfer losses. Further the possibility of an installation of such a system depends strongly to the environmental conditions of the waste heat source (accessibility, space, vibrations, etc.).
  - Automatic distance control between the generator and the heat source. Depending on the measured temperature of the hot side of the TE modules the distance between the generator and the heat source could be altered automatically. Thus it would be possible to position the generator in such a distance to the heat source, so that the TE modules operate in their optimal design point. Main disadvantages are the complex structure of such a system including control and a propulsion system to move the generator and thus the higher investment and maintenance costs.
- To prevent a movement of the TE modules the fixation has to be improved through utilisation of more screws, like it was done for generator No. 2.
- To prevent fouling through dust deposits a housing of the generator could be necessary, depending on the environmental conditions.
- To prevent bending of the wires edges of the construction should be chamfered.
- The adhesion of the black paint has to be improved, e.g. through a prior surface treatment of the copper plate.

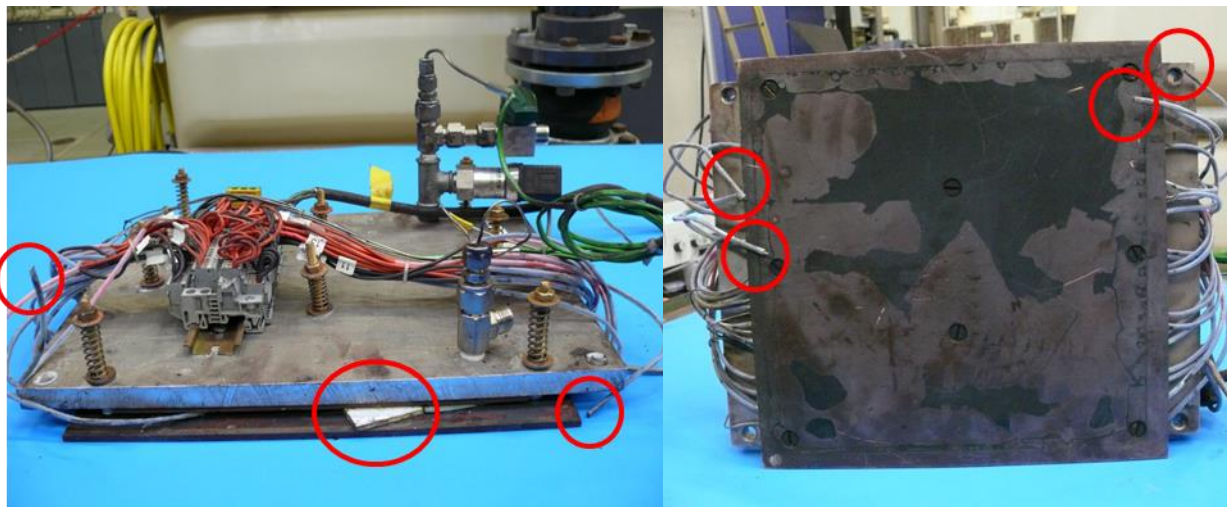


**Figure 3.5.2.2.9** – Exterior view of generator No. 1 after the on-line test

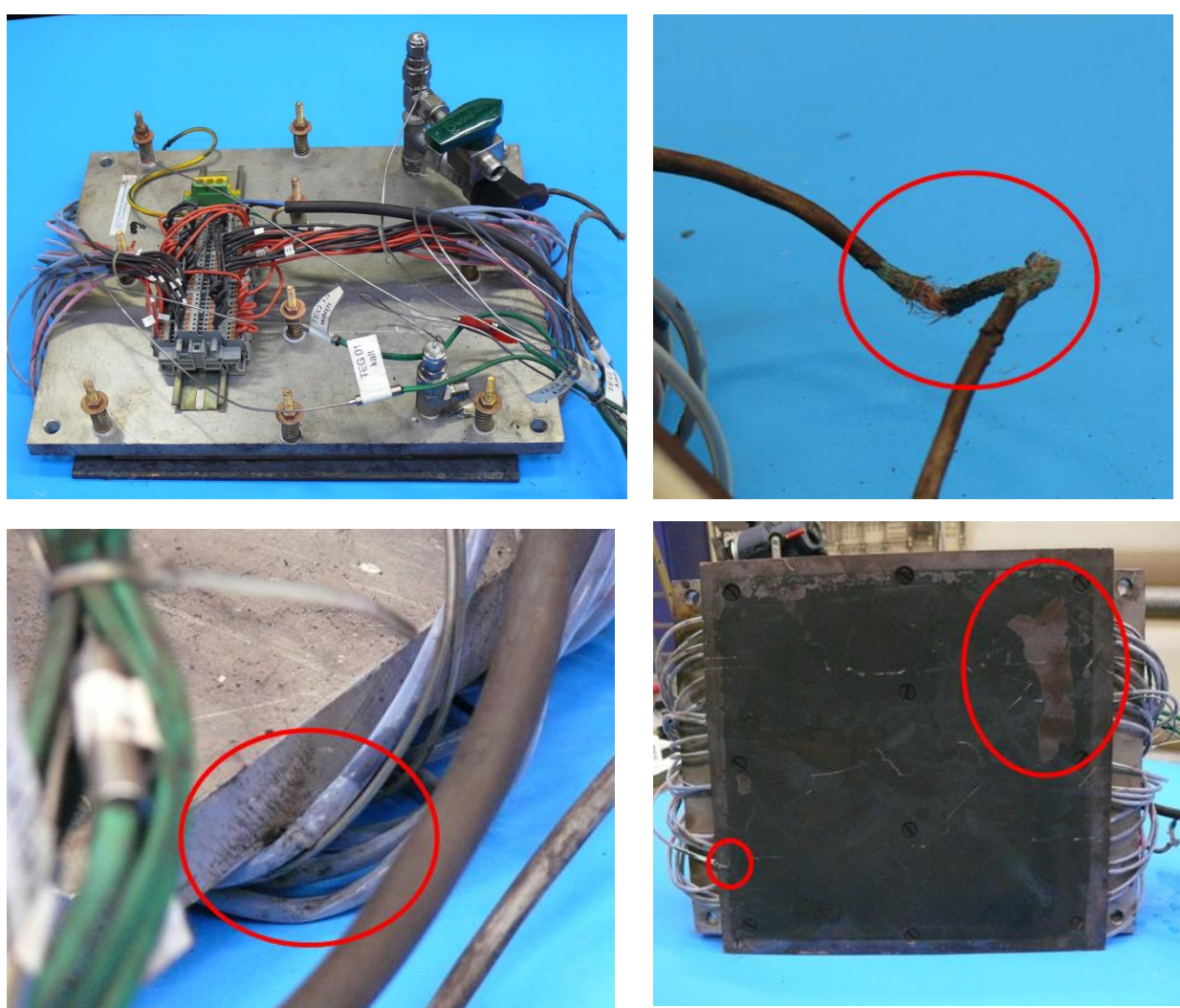


**Figure 3.5.2.2.10** - Exterior view of generator No. 2 after the on-line test

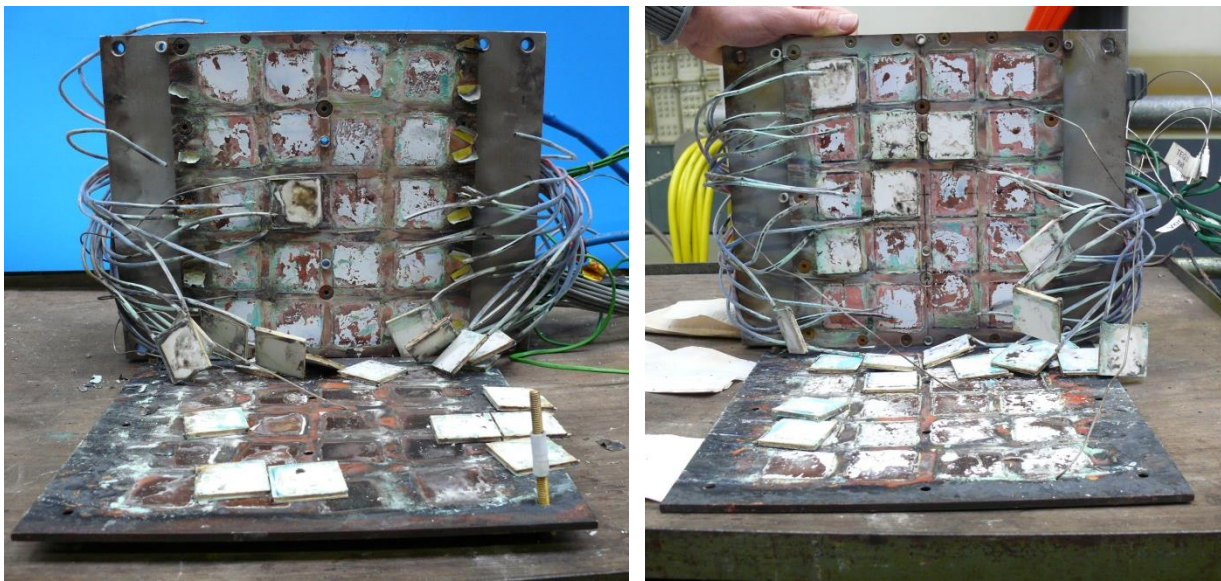


**Figure 3.5.2.2.11** - Disassembled generators after the on-line test (left - generator No. 1, right - generator No. 2)



**Figure 3.5.2.2.12** - Detailed view of TE modules after the on-line test

### 3.5.3 Task 5.3 – **Estimation of the electricity production cost (CSM, AME, CU, FENO)**

#### 3.5.1.3      **Method of electric energy cost calculation (CSM)**

Every electric power producer has the serious problem of understanding, before building a new industrial plant, what is the cost of the produced electricity for a given type of plant. The problem may seem deceptively simple to solve, but it is not. In fact, the real cost of electricity produced by a given plant derives from many factors, some of them absolutely unpredictable and highly variable during the lifetime of the production plant.

Moreover, the problem is further complicated if it is required to compare production costs of electricity supplied by plants using different primary energy sources and production technologies.

This problem has been deeply studied in recent years due to the start of exploitation of renewable energy sources. In fact, this exploitation has multiplied enormously the methods of producing electricity by introducing systems significantly different from the traditional ones with completely new features that have cost items which affect the final cost of electricity in a completely different way. For example, differently from traditional systems based on fossil fuels, in many cases the cost of the primary energy is zero (for example in PV) while the cost of plants construction per unit of electric power can be very high.

Therefore several formulas, more or less complex, have been developed over the time. The objective of these formulas is to be able to calculate the cost of the electricity produced by a given production plant taking into account all the predictable items that contribute to it.

Although waste heat is not a renewable energy source, but rather the by-product of a main production process, the cost of the electricity obtained by waste heat (as for all the other production systems) can be calculated with the same methods.

In the present study, the so-called Levelized Cost of Electricity (LCOE) has been used to compare the economic performance of power plants. The LCOE yields the discounted average cost of the produced electric energy for a specified power plant, expressed in €/kWh. It can be also considered as the price at which the produced electric energy must be sold to obtain parity between the revenue and the expenditure accumulated at the end of the plant lifetime assuming the constancy of the quantity and the production costs. It must be considered that the LCOE is only a simplified parameter and therefore not completely suitable for determining an effective power plant financing calculation, which must take into account also any investment risk (both market and technological risks). However, it is reliable for the present study and widely used to assess the cost of electricity production from different production technologies.

The LCOE [€/kWh] formula adopted in the present study is given as follows [6]:

$$LCOE = \frac{I_0 + \sum_{t=1}^N A_t (1+i)^{-t}}{\sum_{t=1}^N M_{t,el} (1+i)^{-t}} \quad \text{Eq. 3.5.1.1.1}$$

where  $I_0$  = initial plant cost (investment expenditure) [€];  $t$  = generic year of plant operation from the beginning (1, 2, 3... N) [-];  $N$  = number of years of the system in operation [-];  $A_t$  = annual total costs in Euro at the generic year  $t$  [€];  $M_{t, el}$  = produced quantity of electricity during the generic year  $t$  [kWh];  $i$  = discount rate (interest rate in %) [-].

For simplicity, two parameters in this formula have been omitted, which can sometimes be important. One is the residual value (RV) of the plant at the end of lifetime (after  $N$  years), and the second the reduction of electric energy production of the plant caused by the wear of the industrial plant itself (SDR, system degradation rate). However, the expression of Eq. 3.5.1.1.1 can be considered adequate for the present study.

The term  $A_t$  includes several expenditures and can be expressed as the following summation:

$$A_t = C_{O\&M,t} + C_{C,t} \quad \text{Eq. 3.5.1.1.2}$$

where  $C_{O\&M,t}$  = operative & maintenance (O&M) costs for the year  $t$ , [€];  $C_{C,t}$  = combustible costs for the year  $t$ , [€].

The term  $C_{O\&M,t}$  contains several costs depending on the type of plant, including: staff costs, ordinary maintenance costs, supplementary maintenance costs, accounting provisions, assurance provisions, waste disposal costs, loan costs, taxes and rental costs, etc.

The term  $M_{t, el}$  [kWh] is the net electricity generated in the year  $t$ , and can be calculated by the following formula:

$$M_{t,el} = CF_t M_{max,yr} \quad \text{Eq. 3.5.1.1.3}$$

where  $CF_t$  = net capacity factor of the plant during the year  $t$  [-];  $M_{max,yr}$  = maximum net electric energy generation of the plant for one year of production [kWh].

Sometimes the term  $M_{t,el}$  is also calculated by a similar formula:

$$M_{t,el} = Hr_t P_{max} \quad \text{Eq. 3.5.1.1.4}$$

where  $Hr_t$  = plant operation hours for the year  $t$  (max value = 8760) [h];  $P_{max}$  = maximum net electric power generation of the plant [kW].

It is important to observe that LCOE factor, as reported in Eq. 3.5.1.1.1, do not consider the value of the thermal heat produced by the heat engine. This by-product may be sold (for example as district heating) increasing the revenue of the overall system and therefore reducing the production cost of the electricity.

### **3.5.1.4 Comparison with different competing technologies (CSM, CU)**

In this section different technologies for the production of electrical energy are compared. For each technology the calculation of the LCOE parameter and other important plant factors are shown.

Eight different methods of electricity production have been compared taking into account, when possible, systems which have both a similar electric power capacity and the temperature of the heat source. The possible impact of cogeneration, using output thermal heat, are not considered here. However it is important to consider that cogeneration could have very important effect when applied.

Input data and results of the LCOE and the other parameters are shown in Table 3.5.1.4.1. It is important to remember that the results shown the table depend directly on the data used, and that they may change according to the typical conditions of the electrical production site.

The first two columns refer to the TEG prototypes developed in this research. The next three columns refer to ORC and Kalina systems, based on Rankine cycle technologies, using both low enthalpy geothermal and biomass sources. Subsequent column refers to data of a small photovoltaic plant (PV) and the last columns refer to two different types of internal combustion engines: a 4 stroke Otto cycle (spark fired) engine filled with biogas fuel, and a Diesel cycle engine filled with liquid biofuel.

The LCOE parameters have been calculated on the basis of the formula shows in Eq. 3.5.1.1.1.

The final result, under the assumed data, is:

- Prototype A: 10 years of operation, net electricity 175 kWh/Y -> LCOE = 4.12 €/kWh
- Prototype A: 20 years of operation, net electricity 175 kWh/Y -> LCOE = 3.61 €/kWh
- Prototype B: 10 years of operation, net electricity 175 kWh/Y -> LCOE = 3.50 €/kWh
- Prototype B: 20 years of operation, net electricity 175 kWh/Y -> LCOE = 3.24 €/kWh

Comparison with the other considered methods of electricity production shows that the LCOE is much higher for the TEG (multiple of the LCOE of all other considered systems). Thus it can be concluded that the use of thermoelectric energy production systems, based on the two prototypes developed in this research cannot be used for large electricity production, due to the high cost of electricity produced. This "high cost" is even more sensitive in the steel industry where typically, for various reasons, the cost of electricity available is particularly low, lower than in other industrial plants.

<b>Input data</b>	<b>symbol</b>	<b>unit</b>							
<i>Plant description</i>			TEG, THERELEXPRO Project, Prototype A	TEG, THERELEXPRO Project, Prototype B	ORC Geothermal plant, Chena Hot Springs, Alaska, PureCycle™200	ORC Biomass plant, 10 CHP Turboden	KALINA Geothermal plant, Husavik, Iceland, KCS-34	PV, Photovoltaic plant	Internal Combustion Engine, Biogas plant, Otto cycle
<i>Heat Source temperature</i>		[°C]	77	800	73	300	120	-	600
<i>Heat Source thermal flow rate</i>		[kW]	6.5	4.4	2580	5140	15800	-	280
<i>Heat Sink temperature</i>		[°C]	11	26	4	60	5	-	20
<i>Heat Sink thermal flow rate</i>		[kW]	6.2	4.0	2380	4081	13500	-	127
<i>Average gross electric power generation</i>		[kW]	0.04	0.03	250	1016	1820	100	110
<i>Average net electric power generation</i>	P <sub>max</sub>	[kW]	0.02	0.02	210	968	1700	100	100
<i>Plant operation hours per year</i>	Hr	[h/Y]	8760	8760	8322	8000	8000	1257	8000
<i>Net electricity generated</i>	Mt,el	[kWh/Y]	175	175	1747620	7744000	13600000	125700	800000
<i>Investment expenditure</i>	I <sub>0</sub>	[€]	1800	920	550000	4000000	7100000	127000	500000
<i>Staff costs</i>		[€/Y]	0	0	36000	5200	5200	0	36000
<i>Ordinary maintenance cost</i>		[€/Y]	500	500	27500	40000	40000	10000	36000
<i>Assurance costs</i>		[€/Y]	0	0	3000	20000	35500	2500	3000
<i>Operative &amp; Maintainance cost</i>	C <sub>O&amp;M,t</sub>	[€/Y]	500	500	66500	65200	80700	12500	75000
<i>Combustible cost</i>	C <sub>C,t</sub>	[€/Y]	0	0	0	540000	0	0	156000
<i>Annual total cost</i>	At	[€/Y]	500	500	66500	605200	80700	12500	75000
<i>Discount rate</i>	i	[%]	4	4	4	4	4	4	4
<b>Results:</b>									
<i>Total energy produced (10 years)</i>		[kWh]	1752	1752	17476200	7744000	13600000	1257000	800000
<i>Total energy produced (20 years)</i>		[kWh]	3504	3504	34952400	154880000	272000000	2514000	16000000
<i>Investment expenditure per power</i>		[€/W]	90.00	46.00	2.62	4.13	4.18	1.27	5.00
<i>Investment expenditure per total energy produced (10 years)</i>		[€/kWh]	1.03	0.53	0.03	0.05	0.05	0.10	0.06
<i>Investment expenditure per total energy produced (20 years)</i>		[€/kWh]	0.51	0.26	0.02	0.03	0.03	0.05	0.03
<i>Gross conversion efficiency</i>		[%]	0.62	0.68	9.69	19.77	11.52	-	39.29
<i>Net conversion efficiency</i>		[%]	0.31	0.45	8.14	18.83	10.76	-	31.25
<i>LCOE (10 years of operation)</i>		[€/kWh]	4.12	3.50	0.08	0.08	0.07	0.22	0.17
<i>LCOE (20 years of operation)</i>		[€/kWh]	3.61	3.24	0.06	0.05	0.04	0.17	0.14

**Table 3.5.1.4.1** - Comparison of different electric power production plants

In the following it is reported a brief discussion regarding the input data used for each plant analysed. Since it was not possible to find from the literature all the necessary data for calculating the LCOE, the data have been divided in two groups: those available from the literature and those estimated in this report.

### **TEG (THERELEXPRO Project, prototype A)**

Data refers to Prototype A manufactured in the present research program. Most measured data are reported in Sec. A.11.1. For calculation of the investment expenditure (1800 €) has been considered the cost of the TEMs (600 € total TEMs cost, 10€/TEM), the cost for the aluminium boxes (200 €), the cost for valves, pumps and components (500 €), assembling (250 €) and installation/transportation (250 €). Furthermore, has been considered a maintenance cost of about 500 €/year. This cost is mainly due to washing operations required to clean the TEG pipes.

*Available data (from measures):* average gross electric power generation  $n = 40$  W; average net electric power generation = 20 W (gross minus 20 W for water pumping and auxiliaries).

*Estimated data:* plant operation hours per year = 8760 h (100% of one year); investment expenditure = 1800 €; O&M costs = 500 €/Y; number of years of the system in operation = 10 or 20; discount rate 4%.

### **TEG (THERELEXPRO Project, prototype B)**

Data refers to Prototype B manufactured in the present research program. Most measured data are reported in Sec. A.11.2. For calculation of the investment expenditure (920 €) has been considered the cost of the TEMs (400 € total TEMs cost, 10€/TEM), the cost for the aluminium plates (40 €), the cost for the copper plates (60 €), cost of screws, seals, wires, etc. (20 €), assembling (200 €) and installation/transportation (200 €). Furthermore, has been considered a maintenance cost of about 500 €/year.

*Available data (from measures):* maximum gross electric power = 100 W; average gross electric power generation 30 W (value averaged over one year of working time); average net electric power generation (gross minus 10 W for water pumping and auxiliaries)

*Estimated data:* plant operation hours per year 8760 (i.e. the annual time period during which the plant is ready to produce energy); unfortunately, due to the strong working discontinuity of the steel plants, the time of energy production of this TEG device is about 1300 hours per year; investment expenditure = 920 €; O&M costs = 500 €/Y; number of years of the system in operation = 10 or 20; discount rate 4%.

Scaling up of the TEG devices to large electric production plants may reduce the investment expenditure, especially concerning the cost of pipes and framework components. However it is difficult to imagine a general cost reduction, due to plant scaling up, higher than 10% of the initial investment.

### **ORC (Geothermal source)**

Data refers to a 400 kW Binary Geothermal plant built in Chena Hot Springs, Fairbanks - Alaska (USA) in 2006 [7], [8]. The plant has been built to generate electrical energy for the local Resort in substitution of a former Diesel power generator, reducing electricity cost from 0.30 \$/kWh to 0.07 \$/kWh. This plant is composed of two autonomous ORC plants generating each one 200 kW manufactured by United Technologies Corporation (UTC) and Chena Power LLC.

*Available data:* plant operation hours per year = 8322 h (95% of one year); average gross electric power generation = 250 kW; average net electric power generation = 210 (gross minus 40 kW for water pumping).

*Estimated data:* investment expenditure = 550000 € (including ORC, wells drilling, piping, well pump and civil works); O&M costs = 66500 €/Y (including staff costs, = 36000 €/Y; ORC maintaining costs = 5% of the ORC cost; assurance); number of years of the system in operation = 10 or 20; discount rate 4%.

See also, as Ref.

<http://www.chenahotsprings.com/geothermal-power/>

<http://www.chenapower.com/>

<http://www.utc.com/Pages/Home.aspx>

### **ORC (Biomass source)**

Data refers to a 1 MW size Biomass plant manufactured by Turboden®. The selected type is the Turboden 10 CHP used generally for combined heat and power production. In this report are considered only the electricity production aspects. The possibility to reuse the cooling heat of the ORC engine can modify significantly the LCOE final value. Furthermore comparing the LCOE of the various systems must be considered that this is the one of greatest electrical production plant.

*Available data:* average gross electric power generation = 1016 kW; average net electric power generation = 968 kW.

*Estimated data:* plant operation hours per year = 8000 h (91% of one year); investment expenditure = 4000000 € (including civil works); O&M costs = 65200 €/Y (including staff costs = 5200 €/Y – automatic operation plant, biomass combustible cost 0.07 €/kWh); ORC ordinary maintaining costs = 40000 € ; assurance = 20000 €); number of years of the system in operation = 10 or 20; discount rate 4%.

See also, as Ref.

<http://www.turboden.eu/en/products/products-chp.php>

### **KALINA (Geothermal source)**

Data refers to a 2 MW size Kalina (KCS-34) binary geothermal plant at Husavik, Iceland in operation from July 2000. This plant, designed by Dr. Alexander Kalina, uses as working fluid a mixture of 82% of ammonia and 18% of water, instead of organic fluid as for ORC plant. The plant uses as heat source a geothermal brine flow of 90 kg/s at 120 °C (assumed specific heat 4000 J/kgK). As investment expenditure has been assumed the same as for the ORC plant, i.e. 3900 €/kW.

*Available data:* average gross electric power generation = 1820 kW; average net electric power generation = 1700 kW.

*Estimated data:* plant operation hours per year = 8000 h (91% of one year); investment expenditure = 4000000 € (including civil works); O&M costs = 80700 €/Y (including staff costs = 5200 €/Y – automatic operation plant; ORC ordinary maintaining costs = 40000; assurance = 35500 €); number of years of the system in operation = 10 or 20; discount rate 4%.

See also, as Ref.

<http://www.globalgeothermal.com/>

<http://estl.com.au/>

### **PV**

A lot of data regarding photovoltaic systems are widely available. It was chosen to take averaged values obtained from web search and not values from a single plant. As for the other plants also PV shows a large difference in the values depending on the size of the plant. An important factor for this kind of plant is the effective annual radiation on the panels. This value depends on latitude, geographical area characteristics (rainy, sunny etc.) and effective set up of the system. It has been considered: monocrystalline modules, average radiation for year of 1540 kWh/m<sup>2</sup>, a group of 285 modules of 350 W each (maximum power), total nominal power 100 kW, modules dimension 1.91 m<sup>2</sup>, average panel efficiency of 15%; by these data can be obtained the energy produced in 1 year, i.e. 1540x1.91x285x0.15 = 125745 kWh/Y of net electricity, that means an hypothetic system working 1257 h/Y with a constant power production of 100 kW.

Furthermore, a photovoltaic plant cannot be considered a heat engine, therefore some data in Table 3.5.1.4.1 is missing.

*Estimated data:* plant operation hours per year = 8760 h (100% of one year); investment expenditure = 127000 € (assumed 1270 €/kW roof-top installation [9]); O&M costs = 65200 €/Y (including staff costs = 5200 €/Y RC plant; ORC ordinary maintaining costs = 40000 ; assurance = 20000 €); number of years of the system in operation = 10 or 20; discount rate 4%.

See also, as Ref.

<https://www.ise.fraunhofer.de/en.html>

<http://www.solaritaly.enea.it/>

### ***Internal combustion engine (Otto cycle)***

Data refers to a 100 kW Biogas plant using an internal combustion engine [10]. The plant has been built to generate electric energy from biogas produced by anaerobic digestion of organic fraction of urban solid wastes. This plant is mainly formed by one 4 stroke Otto cycle Man® engine (E0836-LE202), one plastic centrifugal separator and an anaerobic digestion system. No cost is considered for combustible supply of these kind of plants.

*Available data:* plant operation hours per year = 8000 h; average gross electric power generation = 110 kW; average net electric power generation = 100 kW; investment expenditure = 500000 € (including engine, plastic centrifugal separator, anaerobic digestion system, design); O&M costs = 75000 €/Y (including staff costs, engine maintaining costs; digest system maintaining costs; assurance).

*Estimated data:* number of years of the system in operation = 10 or 20; discount rate 4%.

See also, as Ref.

<http://www.engines.man.eu/global/en/index.html>

### ***Internal combustion engine (Diesel cycle)***

Data refers to an hypothetic 100 kW plant using an internal combustion Diesel engine [10]. The plant is assumed to be filled with palm oil and uses a Deutz® (BF4M1013FC) 4 cylinder, 4 stroke Diesel cycle engine.

*Available data:* average gross electric power generation = 110 kW; average net electric power generation = 100 kW.

*Estimated data:* plant operation hours per year = 8000 h; investment expenditure = 300000 € (including engine, plant design and components); O&M costs = 59000 €/Y (including staff costs, 3 h/day with a cost of 33€/h; maintaining costs, 200€/kW; assurance); combustible cost = 156000 €/Y (palm oil engine consumption = 300 g/kWh, palm oil cost 650 €/t, calorific value 37 MJ/kg); number of years of the system in operation = 10 or 20; discount rate 4%.

See also, as Ref.

<http://www.deutz.com/home.en.html>

### ***3.5.4 Task 5.4 – Environmental benefits analysis (CSM, AME, CU, FENO)***

#### ***3.5.2.3 Classification of thermoelectric materials (CSM, CU)***

Although almost all of electrically conductive materials exhibit thermoelectric properties to some extent, only a very limited number of materials possess adequate thermoelectric properties that can be employed in practice for energy conversation applications. They are broadly classified into Chalcogenides, Silicides, Clathrates, Skutterudites, Oxides and Half-heuslers, as shown in Table 3.5.2.3.1. The raw material cost per kilogram is also shown in the table along with the thermoelectric figure of merit, ZT [11].

Material type	Material name	Manufacturing type	Material cost (\$/kg)	ZT at low or high temp. scenario for the specified leg length (L)			
				ZT	F	L (mm)	Temp
Chalcogenides and SiGe	Bi <sub>2</sub> Te <sub>3</sub>	Bulk	110	0.74	0.18	4.53	Low
	Bi <sub>0.52</sub> Sb <sub>1.48</sub> Te <sub>3</sub>	Bulk	125	1.05	0.21	4.41	Low
	Bi <sub>0.52</sub> Sb <sub>1.48</sub> Te <sub>3</sub>	Nanobulk	125	1.52	0.29	3.47	Low
	Bi <sub>0.54</sub> Te <sub>0.46</sub> (Na <sub>0.0283</sub> Pb <sub>0.945</sub> T <sub>e<sub>0.9733</sub></sub> )	Nanowire	84	0.02	0.07	1.1	Low
	Bi-doped PbSe <sub>0.98</sub> Te <sub>0.02</sub> /PbTe	Nanobulk	81	1.45	0.34	3.01	High
	AgPb <sub>18</sub> SbTe <sub>20</sub>	Bulk	84	1.31	0.26	3.59	High
	SiGe	Bulk	679	0.8	0.07	2.66	High
	Si <sub>80</sub> Ge <sub>20</sub>	Nanobulk	371	0.53	0.13	3.39	High
	SiGe	Nanowire	679	0.22	0.06	1.59	Low
	Mg <sub>2</sub> Si <sub>0.6</sub> Sn <sub>0.4</sub>	Bulk	4.04	1.05	~1	-	High
Clathrates	Si	Nanowire	3.09	0.72	0.09	3.38	Low
	Mn <sub>15</sub> Si <sub>28</sub>	Nanobulk	1.51	0.07	~1	-	Low
	Ba <sub>8</sub> Ga <sub>16</sub> Ge <sub>28</sub> Zn <sub>2</sub>	Bulk	615	0.48	0.13	1.5	High
Skutterudites	Ba <sub>8</sub> Ga <sub>16</sub> Ge <sub>30</sub>	Bulk	644	0.36	0.11	1.65	High
	Ba <sub>7</sub> Sr <sub>1</sub> Al <sub>16</sub> Si <sub>30</sub>	Bulk	1.64	0.09	~1	-	High
	CeFe <sub>4</sub> Sb <sub>12</sub>	Bulk	37	0.77	0.28	8.34	High
Oxides	Yb <sub>0.2</sub> In <sub>0.2</sub> Co <sub>4</sub> Sb <sub>12</sub>	Bulk	24	0.93	0.31	10.6	High
	Ca <sub>0.18</sub> Co <sub>3.97</sub> Ni <sub>0.03</sub>	Bulk	13	0.77	0.39	17.6	High
	(Zn <sub>0.98</sub> Al <sub>0.02</sub> )O <sub>4</sub> O <sub>9</sub>	Bulk	2.3	0.08	0.48	-	High
	InGaZnO	Nanowire	511	0.07	0.04	1.59	Low
Half-heuslers	Na <sub>0.7</sub> CoO <sub>2-δ</sub>	Bulk	36	0.52	0.22	12.7	High
	Zr <sub>0.25</sub> Hf <sub>0.25</sub> Ti <sub>0.5</sub> NiSn <sub>0.994</sub> Sb <sub>0.006</sub>	Bulk	9.71	1.38	0.49	-	High
	Zr <sub>0.5</sub> Hf <sub>0.5</sub> Ni <sub>0.8</sub> Pd <sub>0.2</sub> Sn <sub>0.99</sub> Sb <sub>0.01</sub>	Bulk	8.51	0.69	0.46	15.4	High
	Ti <sub>0.8</sub> Hf <sub>0.2</sub> NiSn	Bulk	10.7	0.41	0.41	16.5	High

**Table 3.5.2.3.1** - A classification of thermoelectric materials along with their cost and figure of merit (ZT) [11]. It is to be noted that the fill factor (F) is the ratio of the area covered by the active thermoelectric material to the area of the substrate. The low and high temperature scenarios corresponds to ~373 K and ~1073 K hot side temperature

Chalcogenides consist of the most commonly used thermoelectric materials: Bi<sub>2</sub>Te<sub>3</sub> and PbTe. Bi<sub>2</sub>Te<sub>3</sub> based alloys, which has a peak ZT of ~1, have been widely used in cooling and power generation around room temperatures. PbTe has a ZT value of ~0.85 at 770 K, making it suitable for power generation at intermediate temperatures [12]. Both are well-established thermoelectric materials and they are the base compounds for many recently developed high ZT chalcogenides, including LASTs and TAGs.

Silicides possess unique advantages of non-toxic, low-cost and lightweight. Typical silicides include Mg<sub>2</sub>(Si,Sn) as n-type and MnSi<sub>~1.75</sub> as p-type. Recently, a number of silicides have shown ZT ~ 1 at temperatures over 700 K. There is a potential to achieve higher ZT values through optimisation of alloying and doping [1].

The Clathrates, due to their unique structure, can be synthesised to attain glass-like lattice thermal conductivity, while maintaining relatively good electronic properties. The ZT value of ~ 1.2 has been obtained at temperatures of around 700 K. However, the ZT at room temperature of these materials is only ~0.33 [13].

Skutterudites have emerged as promising thermoelectric materials over the past decade. The ZT value of >1 has been obtained in this group of materials over temperatures of 500 - 700 K and hence they are of interest for power generation using waste heat from industrial processes. Further improvement is possible due to their reasonably high power factors and potential of reduction in lattice thermal conductivity because of their open structure and presence of two large voids in their unit cell [14].

Metal oxides are a relatively new and interesting class of thermoelectric materials. Their chemical stability in air is the key reason for being considered as potential thermoelectric materials for power generation application at higher temperatures. However, challenges are encountered in module fabrication using metal oxides because the contact resistance at oxide/metal junctions is high and degradation occurs due to large differences in thermal expansion between them [12].

Half-heuslers have been identified as potential thermoelectric materials for high temperature power generation applications. Compared with silicides and skutterudites, half heuslers show better stability at high temperature. The formation of high quality junctions is found to be relatively easier.

Over the last 5-10 years, enhanced theoretical understanding, new synthesis techniques, and state of the art measurement systems have enabled the development of new materials with higher ZT values. For example, nanostructuring of Skutterudites and Half-heuslers have shown enhanced ZT values due to reduction in thermal conductivity by introducing nano-inclusions [12]. It is to be noted that the major progress in recent years is mainly associated with the materials that have large ZT values at relatively high temperature (>500K). For temperatures below 450 K,  $\text{Bi}_2\text{Te}_3$  alloys remain as the best thermoelectric materials.

### **3.5.2.4 Thermoelectric materials and their Earth's crust abundance (CSM, CU)**

With the increase in scope of thermoelectrics, it is important to consider the material consumption and environmental issues associated with this technology. The cost and abundance in earth's crust plays a vital role in assessing the suitability of an element for thermoelectric applications. The Table 3.5.2.3.2 presents a list of abundance of elements in earth's crust, which are used for the synthesis of thermoelectric materials [15]. The abundance of the most widely used thermoelectric compounds, namely Bismuth Telluride ( $\text{Bi}_2\text{Te}_3$ ), Lead Telluride ( $\text{PbTe}$ ) and Silicon Germanium ( $\text{SiGe}$ ) [1], is shown in Table 3.5.2.3.3 [16].

<b>Element</b>	<b>Abundance (ppm)</b>
Te	1.49
Bi	0.00294
Si	151200
Mg	139000
Mn	750
Pb	0.00158
Sn	0.390
Hf	0.230
Zr	7.2
Ga	3.1
Ge	7.6
Zn	74
Al	14100
Fe	320700
Ce	1.010
Ti	820
Ni	18200

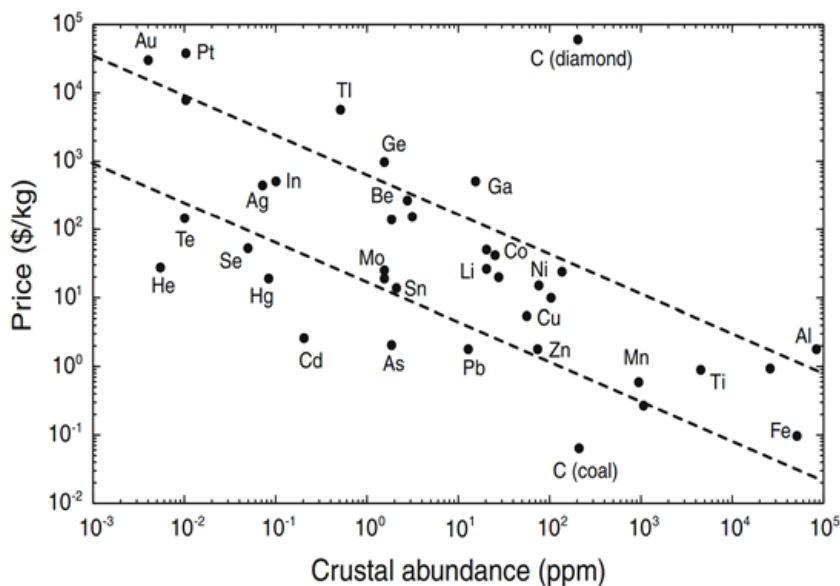
**Table 3.5.2.3.2** - Abundance of elements used for the synthesis of thermoelectric materials [15]

<b>Thermoelectric Material</b>	<b>Weighted Crustal Abundance (Metric Tons)</b>
$\text{Bi}_2\text{Te}_3$	$2.8 \times 10^{14}$
SiGe	$2.6 \times 10^{17}$
PbTe	$3.5 \times 10^{14}$

**Table 3.5.2.3.3** - Abundance of thermoelectric materials in metric tons [16]

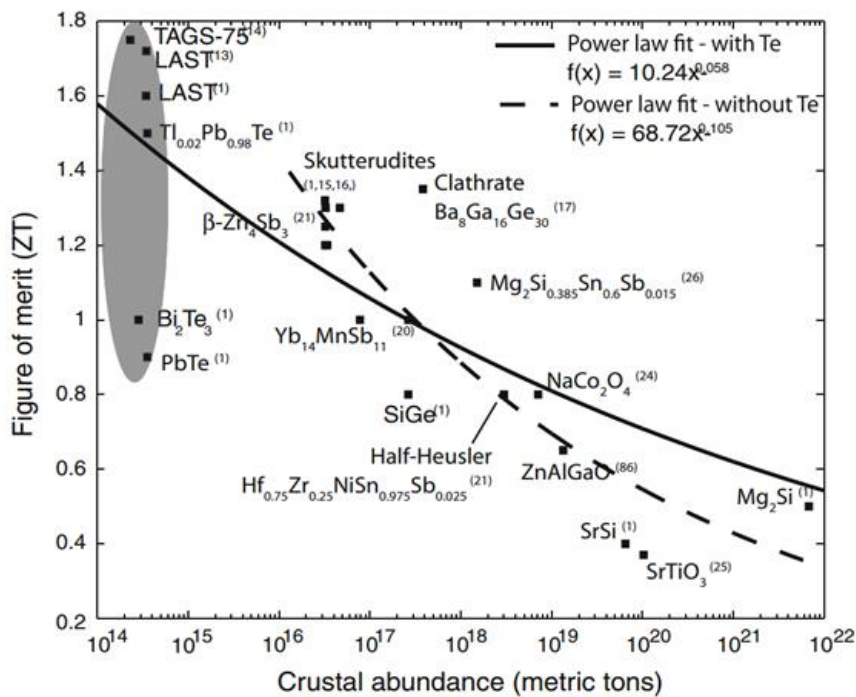
The important thermoelectric materials, such as tellurium (Te), antimony (Sb), bismuth (Bi) and germanium (Ge) have low abundance in earth's crust. Te is probably the most frequently used element in thermoelectric materials and also widely in photovoltaic technology. Its low abundance in earth's crust does not pose a threat on its supply chain at present as Te is being produced as a by-product of copper. In addition, some photovoltaic companies have a proper network of recycling and reprocessing of Te. The thermoelectric materials which are identified as having lower risk of being scarce in the near future are reported to be SiGe, silicides, half-Heuslers and cobaltates [17].

Figure 3.5.2.3.1 shows the price per kilogram versus crustal abundance of elements. The trend observed indicates that less abundant elements are more expensive [16]. The fact that some thermoelectric materials are increasingly being used in other fields too, such as Te mentioned above in photovoltaic technology, makes their price volatile. The price of Te increased from \$ 22/kg in 2004 to around \$ 440/kg at the beginning of 2011. On the other hand, there has been only 25% increase in the global production of Te [16].



**Figure 3.5.2.3.1** - Graph showing negatively slope trend between price (\$/kg) of elements and their crystal abundance. From reference [16].

Figure 3.5.2.3.2 shows the ZT values of thermoelectric materials as a function of their abundance in earth's crust in metric tons. Despite of the problems and low abundance of  $\text{Bi}_2\text{Te}_3$ , it is the most suitable material around room temperatures due to its better performance (ZT). The rest of competitors around  $\text{ZT} \approx 1$  are useful at higher temperature ranges.



**Figure 3.5.2.3.2** - ZT versus crustal abundance of thermoelectric materials [16].

### 3.5.2.5 Thermoelectric generators and their environmental impact (CSM, CU)

With the increase in emission of greenhouse gases from the use of conventional technologies for the production of electricity and from other industrial operations, efforts have been made to explore environmental friendly or green technologies. Thermoelectrics have been explored more seriously as an environmentally friendly source of electrical power in the past two decades [18]. The main advantages of thermoelectric systems include high reliability, noiseless operation, inexpensive maintenance and long life. It has been reported that thermoelectric power generation can reduce costs, lower the environmental burdens and contribute towards more sustainable energy systems [19].

Heat is generated from various industrial operations involving fuel combustion and chemical reactions. This heat is wasted if unused. Thermoelectric generators can be used to recover this unused heat which eventually leads to reduction in energy consumption and as a result, contributes to reduction in greenhouse gas emissions. A theoretical study has shown that thermoelectric generator driven by automobile exhaust can generate enough power to meet electrical requirements of a middle sized automobile [18], ultimately reducing fuel consumption and thus environmental impact. It is estimated that around 20,000 tonnes of general purpose batteries are thrown away as waste in the UK and only 2 % of them are recycled, the rest are landfilled [20]. Thermoelectric integrated combustion systems have been developed for small scale power generation applications which have the potential to replace the conventional lithium-ion batteries and hence reducing the carbon footprint. These are some of the examples of how thermoelectric generators can have a positive impact on the environment.

The materials used in thermoelectric generators can have a negative impact on the environment due to consumption of energy for material production. Hence, it is important that they are used in a sustainable way. Recycling of materials is advantageous in terms of energy consumption, lower carbon emissions to the environment and conservation of less abundant resources.

The most commonly used material in thermoelectric generators is Bi<sub>2</sub>Te<sub>3</sub>. It is rated as acutely toxic [21], and hence requires proper disposal. It is estimated that 40% tellurium is used in photovoltaic industry and 30% in thermoelectric power generation and cooling modules [22]. Recycling of Te is growing gradually, photovoltaic industry produced around ~7% of total Te production in 2010 through recycling [22]. According to official US statistics, nearly all alloys containing Bi were recycled in 2012 and contributed to 10% of US's Bi consumption [23]. Other important material currently being explored is nanostructured Mg<sub>2</sub>Si, Mg is recycled at a decent scale (In 1998, 33% of all Mg in the United States was supplied from recycling sources, a rate lower than Al and Fe, but in line with Ni and Cu [24]) whereas Si is not being recycled at a large scale due to its availability at low cost. PbTe is a high temperature thermoelectric material which has been widely used in thermoelectric generators by US army [25] and also by NASA in its space missions [26]. Pb is reported to be dangerous to environment; higher concentrations of Pb in the ecosystem can affect soil, plants, microorganisms, animals and humans; and hence, requires

careful disposal. It is reported by International Lead Association that around 90% of lead used in recyclable products is recycled [27]. Ge is another important thermoelectric material, it is non-toxic and do not possess any immediate risk to the environment [28].

The information available on manufacturing processes involved in production of thermoelectric modules is very limited. The basic process should involve cutting pellets of thermoelectric materials into individual elements of required size, followed by soldering them onto two metallised ceramic substrates. The cutting process can incur some material waste, which should not be a significant amount that would have an adverse effect on the environment as the waste material is again processed into pellets. The soldering of elements may produce fume from flux used in the soldering process. Soldering in electronic industry is generally carried out with fume extractors present in the workplace to reduce fume exposure to workers. The only exposure to the environment could be cleaning agents and the washed flux, however its impact on the environment has not been reported by any organisation.

### **3.5.2.6    Life Cycle Assessment (LCA) (all partners)**

Life cycle assessment (LCA) is a standardized international technique used to better understand and address environmental protection and impacts associated with product manufacturing and consumption (ISO 14040:2006 and ISO 14044:2006).

The objective of life cycle assessment is to assist in: 1) identifying opportunities to improve the environmental performance of products at various points in their life cycle 2) informing decision-makers in industry, government or non-government organizations 3) selecting relevant indicators of environmental performance, 4) marketing [ref. ISO 14040:2006].

LCA study is composed of four phases [ref. ISO 14040:2006]:

- a) goal and scope definition phase,
- b) inventory analysis phase,
- c) impact assessment phase, and
- d) interpretation phase.

The goal and scope definition phase is required to fix the boundaries and level of details of the study.

The life cycle inventory analysis (LCI) phase is an inventory of input/output data of the system under study, in terms of both materials and energy input/output.

The life cycle impact assessment (LCIA) phase provides additional information of environmental significance, for example in terms of climate change, acidification, resource depletion, human toxicity etc.

The life cycle interpretation phase concludes the study supplying conclusions, recommendations and decision-making argumentations. [ref. ISO 14040:2006].

In Annex A.13 (Deliverable D5.4 – Thermoelectric system environmental benefit analysis), the life cycle of the two thermoelectric generators (prototypes A and B) developed in the present research were examined. The study examined the environmental ramifications for the production and installation of a number of the two prototypes even to their disposal.

LCA analysis has been carried out considering a production of a set of 2750 TEGs of Prototype A, corresponding to an electric power of 55 kW. This number has been calculated assuming to discharge into the cold sink 18 MW of heat energy, as required by the EAF off-gas cooling system. For comparison reasons, it is also assumed that Prototype B has the same electric power (55 kW). Because both prototypes have the same average power, Prototype B was considered to require a production set of 2750 TEGs.

Based on these assumptions, the inventory of the materials required to manufacture a single TEG has been estimated and then used for the LCA calculation.

The "inventory results" showed a large difference in energy consumption (energy input) for the two prototypes. This is caused by the large amount of steel (50 kg and 1.83 kg) and aluminium (50 kg and 6.93 kg) used to manufacture Prototype A and Prototype B, respectively.

Concerning the outputs, the inventory results showed a similar conclusion that the emission caused by the production of Prototype A is approximately 70% higher than that caused by the production of Prototype B.

Concerning the "impact results", it can be noted that the first four "impact categories" are the same, and in the same order. They are: marine and aquatic ecotoxicity, depletion of abiotic resources (fossil fuels), climate change and human toxicity.

Marine and aquatic toxicity is caused by release of hydrogen fluoride (HF) into the seawater.

Depletion of fossil fuel resources has the same flow sources for both prototypes but different distribution.

Climate change is caused mainly by carbon dioxide emission, both for prototype A (91%) and prototype B (89%). Considering these figures, it is possible to obtain the carbon footprint for electricity production for Prototype A (69 gCO<sub>2</sub>eq/kWh) and Prototype B (21 gCO<sub>2</sub>eq/kWh).

Toxicity for humans is caused mainly by dioxins dispersion in water and air, and by hydrogen fluoride dispersion in air.

Main result of the LCA analysis is that Prototype A production has more impact on the environment than prototype B production for the same electric power generation. This is caused by a greater weight of Prototype A compared with Prototype B. In terms of greenhouse emissions both the prototypes can be considered low-carbon renewable power production systems. Concerning emission of toxic materials into the environment, it should be noted that electricity production using thermoelectric generators involves producing toxic materials only during the manufacturing phase, not during the working period. Therefore, assuming that every power plant has comparable impact during the manufacture phase, TEGs must be considered as a green technology similar to wind, hydro or solar production and much better, for this impact category, than production methods based on combustion technologies.

### **3.6 WP6 – Coordination and dissemination**

#### **3.6.1 Project management and description of the activities (all partners)**

Project management has been carried out by CSM in collaboration with all partners. The activities have involved three laboratories and two industrial plants where two on-site tests of the developed thermoelectric generators prototypes carried out.

#### **3.6.2 Result dissemination (all partners)**

Results of the present research have been widely disseminated through participation at national and international congress or with publication in international scientific journals. A list of activities carried out in disseminating the results of THERELEXPRO project is reported in Deliverable 6.1.

#### **3.6.3 Result exploitation (all partners)**

The results of this research have brought a large amount of data usable for subsequent studies. However, they are not sufficient to realize electricity production systems at industrial scale.

The use of thermoelectric energy production systems based on the two prototypes developed in this research cannot be used for large electricity production due to the high cost of electricity produced.

This "high cost" is even more sensitive in the steel industry where typically, for various reasons, the cost of electricity available is particularly low (lower than in other industrial plants).

However, it has been demonstrated that these systems are able to produce electricity through waste heat harvesting, producing "net electricity" under proper circumstances. They are suitable, in the near future, for small electric energy productions.

To lower the electricity production cost produced by thermoelectric systems at low temperatures, the approach of focusing only on developing "new" thermoelectric materials does not seem to be a viable route for the time being. In fact, the efficiency benefit that would be obtained by introducing new materials, different to Bi<sub>2</sub>Te<sub>3</sub>, appears to be too small to be practical. Nevertheless, scientific studies on new thermoelectric materials and their mass production remain important..

It seems more profitable to focus on improving the performances of prototypes by incorporating the thermoelectric materials (based on Bi<sub>2</sub>Te<sub>3</sub>) into the structures or components of industrial plants. This would bring in reducing the assembly and installation costs at the end user, allowing also the optimization of heat exchange of the overall thermoelectric system.

The availability of components, already fitted with a "thermal to electric" conversion systems, optimized and easily installable, could increase the interest by the end users, lowering manufacture costs by increasing the volumes.

Data obtained in this study may be used to accomplish this further objective.

## **Table of symbols**

<b>Subscripts</b>	
<b>Symbol</b>	<b>Description</b>
A	prototype A
B	prototype B
c	contact layer
C	cold side
e	electric
ef	effective
H	hot side
HE	heating element (prototype B)
i	internal
L	load
n	n-type thermoelement
oc	open circuit
out	output
p	p-type thermoelement
t	thermal
TEG	thermoelectric generator
TEM	thermoelectric module

<b>Variables</b>		
<b>Symbol</b>	<b>Unit (*)</b>	<b>Description</b>
A	[m <sup>2</sup> ]; [mm <sup>2</sup> ]	cross-sectional area
A <sub>t</sub>	[€]	annual total cost
c <sub>p</sub>	[J/(kg K)]	specific heat capacity
C <sub>O&amp;M,t</sub>	[€]	operative & maintenance (O&M) costs for the year t
C <sub>C,t</sub>	[€]	combustible costs for the year t
H <sub>r</sub>	[-]	plant operation hours per year
i	[-]	discount rate
I	[A]	current
I <sub>0</sub>	[€]	initial plant cost or investment expenditure
K	[W/(m <sup>2</sup> K)]	thermal conductance of both n- and p-type thermoelements
l	[mm]	length of the thermoelement
l <sub>c</sub>	[mm]	thickness of the contact layer
m	[kg]	mass
$\dot{m}$	[kg/s]	mass flow rate
M	[W/m <sup>2</sup> ]	specific radiation
M <sub>t,el</sub>	[kWh]	quantity of electricity produced during the generic year t
n	[mm]	electrical contact parameter [defined as = 2 $\rho_c/\rho$ ] (typical value $\sim 0.1$ mm)
N	[-]	number of thermoelements in a module

N	[ - ]	number of years of the electric generator system in operation
P	[kW], [W]	power
P <sub>e</sub>	[kW], [W]	electric power
P <sub>t</sub>	[kW], [W]	thermal power (or heat power)
Q	[J]	heat
Q/A	[J/m <sup>2</sup> ]	heat flow
$\dot{Q}$	[W]	heat power (or thermal power)
$\dot{Q}/A$	[W/m <sup>2</sup> ]	heat flux (or thermal power flow)
r	[ - ]	thermal contact parameter [defined as = $\lambda_c / \lambda$ ] (typical value $\sim 0.2$ )
R	[ $\Omega$ ]	electrical resistance
T	[K]; [ $^{\circ}$ C]	temperature
s	[ - ]	thermoelectric module resistance ratio [defined as = $R_L / R_{TEM}$ ]
U <sub>TEG</sub>	[V]	voltage of prototype B thermoelectric generator
V	[V]	voltage
Z	[K <sup>-1</sup> ]	thermoelectric figure of merit of the materials [defined as = $\alpha^2 / (\rho \lambda)$ ]
ZT	[ - ]	thermoelectric dimensionless figure of merit [defined as = Z · T]
$\alpha$	[V/K]; [ $\mu$ V/K]	Seebeck coefficient
$\Delta T$	[K]	temperature across the module
$\varepsilon$	[ - ]	emission coefficient
$\Phi$	[ - ]	conversion efficiency of a thermoelectric module
$\lambda$	[W/(m K)]	thermal conductivity of thermoelement materials
$\lambda_c$	[W/(m K)]	thermal contact conductivity
$\rho$	[ $\Omega$ cm]; [ $\Omega$ m]	electrical resistivity
$\rho_c$	[ $\Omega$ cm]; [ $\Omega$ m]	electrical contact resistivity
$\sigma$	[S/cm]; [S/m]	electrical conductivity [defined as = 1/ $\rho$ ]
$\sigma$	[W/(m <sup>2</sup> K <sup>4</sup> )]	Stefan-Boltzmann constant
(*) If not differently specified		

## **List of figures**

<b>Figure 1.1 – Ferriere Nord plant, Italy</b>	7
<b>Figure 1.2 – Arcelor Mittal plant, Spain</b>	7
<b>Figure 1.3 – General layout of Prototype A</b>	8
<b>Figure 1.4 – General layout of Prototype B</b>	8
<b>Figure 1.5 – Prototype A lab test</b>	9
<b>Figure 1.6 – Prototype B lab test</b>	9
<b>Figure 1.7 – Prototype A</b>	10
<b>Figure 1.8 – Prototype B</b>	10
<b>Figure 1.9 – Prototype A at plant site</b>	11
<b>Figure 1.10 – Prototype B at plant site</b>	11
<b>Figure 3.1.1.2.1 – FENO, EAF off gas duct and water air cooler.</b>	18
<b>Figure 3.1.1.2.2 - FENO, EAF off-gas duct and pipe path</b>	19
<b>Figure 3.1.1.2.3 – FENO, Water Air Cooler scheme and pick-up point</b>	19
<b>Figure 3.1.1.2.4 – FENO, water temperature trend at the air cooler.</b>	20
<b>Figure 3.1.1.2.5 – FENO, heat sink temperature monitoring</b>	20
<b>Figure 3.1.1.3.1 – AME, wire rod as hot source</b>	21
<b>Figure 3.1.1.3.2 – AME, slabs in cooling yard as hot source</b>	21
<b>Figure 3.1.1.3.3 – AME, hot strip mill as hot source</b>	21
<b>Figure 3.1.1.3.4 – AME, cover panels of the cooling table conveyor</b>	22
<b>Figure 3.1.1.3.5 – AME, fixed lateral panels of the cooling table conveyor</b>	22
<b>Figure 3.1.1.3.6 – AME, cooling table conveyor layout</b>	23
<b>Figure 3.1.1.3.7 - AME, air temperature and air speed at panel 6</b>	23
<b>Figure 3.1.1.3.8 – AME, air temperature and air speed at panel 3</b>	24
<b>Figure 3.1.1.3.9 - AME, position of the thermocouple for the internal side measurements</b>	24
<b>Figure 3.1.1.3.10 – AME, long term panel measurement (internal side)</b>	25
<b>Figure 3.1.1.3.11 – AME, panel temperature measurement in two points</b>	25
<b>Figure 3.1.1.3.12 – AME, panel temperature measurement in two points</b>	26
<b>Figure 3.1.1.3.13 – AME, panel temperature measurement with IR thermo-camera</b>	26
<b>Figure 3.1.1.3.14 – AME, four line temperature measurement with IR thermo-camera</b>	27
<b>Figure 3.1.1.5.1 - Prototype A, general layout</b>	28
<b>Figure 3.1.1.6.1 General layout of Prototype B.</b>	29
<b>Figure 3.1.1.6.3 - Prototype B, copper TEG plate and steel sheet geometries</b>	30
<b>Figure 3.1.1.6.4 - Electrical power as a function of surface temperature of the heating element, situation a and situation b</b>	30
<b>Figure 3.1.1.6.5 - TE module hot side temperature as a function of surface temperature of the heating element at situations a and b</b>	31
<b>Figure 3.1.1.6.6 - TE module cold side temperature as a function of surface temperature of the heating element for situations a and b</b>	31
<b>Figure 3.1.1.7.1 - Typical <math>\text{Bi}_2\text{Te}_3</math> based TE modules electric power output</b>	34
<b>Figure 3.1.1.9.1 - Cross sectional view of a thermoelectric module</b>	36
<b>Figure 3.1.1.9.2 - Thermoelectric model results for given <math>\Delta T</math></b>	36
<b>Figure 3.1.1.10.1 - Thermoelectric module subject to a given thermal input</b>	37
<b>Figure 3.1.1.10.2 - Thermoelectric model results for given thermal flux (600 W)</b>	38
<b>Figure 3.1.1.11.1 – Prototype A, electric power and conversion efficiency of one TEM vs. hot side temperature (cold side temperature =30°C)</b>	39
<b>Figure 3.1.1.11.2 – TEG power vs. hot source temperature for different thermal power cooling plant (TEMs cold side temperature =30°C)</b>	40
<b>Figure 3.1.1.12.1 – ZT of state of the art thermoelectric materials vs. temperature.</b>	41
<b>Figure 3.1.1.12.2 – Example of a regulation system to obtain the optimal distance from the radiation hot source</b>	42
<b>Figure 3.1.2.1.1 - Prototype A: on line control and monitoring software &amp; interface</b>	42
<b>Figure 3.2.1.1.1 – Lab-scale test bed for the hydraulic pressure test</b>	45
<b>Figure 3.2.1.1.2 - Lab scale test bed for single TEM test</b>	45
<b>Figure 3.2.1.1.3 – Lab-scale test bed for TEG on-site readiness test</b>	46
<b>Figure 3.2.1.2.1 - Schematic diagram of module characterisation set-up</b>	47
<b>Figure 3.2.1.2.2 - Schematic of Lab Scale Power Generator developed by CU</b>	48
<b>Figure 3.2.1.2.3 - Schematic of Cold and Hot Side Heat Exchangers and Thermoelectric modules in CU's Lab Scale Power Generator</b>	48

<b>Figure 3.2.1.2.4 - Power output from CU's Lab Scale Power Generator at various temperature difference at matched-load condition</b>	49
<b>Figure 3.2.2.1.1 – Water box hydraulic test</b>	50
<b>Figure 3.2.2.1.2 – Manual pressure calibrator</b>	51
<b>Figure 3.2.2.2.1 - Power Generation at some temperature differences for samples A and B</b>	51
<b>Figure 3.2.2.2.2- Figure of Merit (ZT) at different temperature differences for samples A and B</b>	52
<b>Figure 3.2.2.2.3 - Characterization results of CSM modules- Open circuit voltage comparison for different cases.</b>	52
<b>Figure 3.2.2.2.4 - The power output as a function of temperature difference for modules of different suppliers</b>	53
<b>Figure 3.2.2.3.1 – Laboratory testing device: power vs. load pressure test</b>	53
<b>Figure 3.2.2.3.2 – TEM electric power vs. load pressure test</b>	54
<b>Figure 3.2.2.4.1 - 15 Nm torque applied to screws that push (via copper plate) TE modules to heat sink</b>	54
<b>Figure 3.2.2.4.2 - Power output and <math>\Delta T_{\text{module}}</math> as a function of the applied torque on screws as shown in Figure 3.2.2.4.1 (two TE module, supplier 2)</b>	55
<b>Figure 3.2.2.5.1 – Prototype B test bed set-up</b>	55
<b>Figure 3.2.2.5.2 – Laboratory V-I test results (supplier 2)</b>	56
<b>Figure 3.2.2.5.3 - TE power output as a function of the load resistance (<math>R_L</math>)</b>	56
<b>Figure 3.2.2.6.1 - TE power output and <math>\Delta T_{\text{module}}</math> as a function of the temperature of the heating element (one TE module, supplier 2)</b>	57
<b>Figure 3.2.2.6.2 - TE power output as function of <math>\Delta T_{\text{module}}</math> (one TE module, supplier 2)</b>	57
<b>Figure 3.2.2.7.1 – Prototype A during final laboratory set up</b>	58
<b>Figure 3.2.2.8.1 – Prototype B: V-I and P-I characteristic curves of generator No. 1 recorded at the BFI testing facility</b>	59
<b>Figure 3.2.2.8.2 – Prototype B: V-I and P-I characteristic curves of generator No. 2 recorded at the BFI testing facility</b>	59
<b>Figure 3.3.1.1.1 – TE module after maximum compression test</b>	60
<b>Figure 3.3.1.2.1 - Module manufactured by traditional manufacturing method</b>	61
<b>Figure 3.3.1.2.2 - Module manufactured by non-traditional manufacturing method</b>	61
<b>Figure 3.3.1.2.3 - Comparison of the open-circuit voltage generated by modules fabricated using traditional and non-traditional methods.</b>	62
<b>Figure 3.3.1.3.1 – Thermoelectric module exposed to high temperature</b>	62
<b>Figure 3.3.1.3.2 – type K thermocouple clamped in the hot side</b>	63
<b>Figure 3.3.2.1.1 - Clean and covered TE module surfaces</b>	63
<b>Figure 3.3.2.1.2 - V-I relation for TE module (supplier 2) that were tested with graphite foil and thermal conductive paste</b>	64
<b>Figure 3.3.2.2.1 – Potentiometer for the tuning of the TEG load resistance</b>	64
<b>Figure 3.3.2.2.2 – Prototype A: V-I and P-I characteristic curves of column 1, TEMs 1 to 5.</b>	65
<b>Figure 3.3.3.1.1 - Prototype A, simplified model for TEG design</b>	66
<b>Figure 3.3.3.2.1 - V-I relations at <math>T_{HE} = 750^\circ\text{C}</math></b>	68
<b>Figure 3.3.3.2.2 - P-I relations at <math>T_{HE} = 750^\circ\text{C}</math></b>	68
<b>Figure 3.4.1.1.1 - Prototype A, in its final configuration</b>	69
<b>Figure 3.4.1.2.1 - Design of 1 (of 2) TE generator of the prototype B</b>	70
<b>Figure 3.4.1.2.2 - Front view of the Al-heat sink of 1 (of 2) TEG of the prototype B</b>	70
<b>Figure 3.4.2.1.1 - Prototype A connections with EAF plant hot and cold water</b>	72
<b>Figure 3.4.2.1.2 – Prototype A installed at Ferriere Nord plant</b>	72
<b>Figure 3.4.2.1.3 - Prototype A, hot water connection with EAF off-gas cooling water duct</b>	73
<b>Figure 3.4.2.2.1 - Prototype B at installation plant area</b>	73
<b>Figure 3.4.2.2.2 – Prototype B, drawing of side panel at the AME cooling table</b>	74
<b>Figure 3.4.2.2.3 – Prototype B, general overview of layout at AME plant</b>	74
<b>Figure 3.4.2.2.4 - Prototype B, possible multiple installation</b>	74
<b>Figure 3.5.1.1.1 – Snapshot of measured data during on-line tests of Prototype A</b>	75
<b>Figure 3.5.1.1.2 – Prototype A, control interface</b>	76
<b>Figure 3.5.1.2.1 - Front view of prototype B, copper plate of generator No. 2 painted black, copper plate of generator No. 1 not painted</b>	77
<b>Figure 3.5.1.2.2 - Measured temperature profile for generator No. 1 on November 17<sup>th</sup>, most likely overheating of the TE modules from approximately 17:30 to 19:30; unusable data after 19:30</b>	77
<b>Figure 3.5.1.2.3 - Measured temperature profile for generator No. 2 on November 17<sup>th</sup>; most likely overheating of the TE modules from approximately 17:30 to 19:30; unusable data after 19:30</b>	78
<b>Figure 3.5.1.2.4 - Flaking of the black paint from the generators</b>	78
<b>Figure 3.5.2.1.1 – Prototype A, electric power versus hot water temperature</b>	79

<b>Figure 3.5.2.1.2 - Power production and power consumption (<math>T_{hot}=73^{\circ}C</math>)</b>	80
<b>Figure 3.5.2.1.3 - Power production and power consumption (<math>T_{hot}=77^{\circ}C</math>)</b>	80
<b>Figure 3.5.2.1.4 - Characteristic curves (V-I) and (P-I) of five TEMs of the first TEG column</b>	81
<b>Figure 3.5.2.1.5 – Disassembling of prototype A</b>	82
<b>Figure 3.5.2.1.6 – Small damages on the thermoelectric modules caused by sticking</b>	82
<b>Figure 3.5.2.1.7 – Some thermoelectric modules stick on the water box</b>	83
<b>Figure 3.5.2.2.1 - Maximum measured temperature difference of selected TE modules from both generators during the full scale tests at AME plant site</b>	83
<b>Figure 3.5.2.2.2 - Measured temperature profile for generator No. 2 on November 11<sup>th</sup></b>	84
<b>Figure 3.5.2.2.3 - Measured profile of voltage, current and electrical power for generator No. 2 on November 11<sup>th</sup></b>	84
<b>Figure 3.5.2.2.4 - Comparison of proportional produced electrical power between generators No. 1 and No. 2 of prototype B</b>	85
<b>Figure 3.5.2.2.5 - Measured temperature profile for generator No. 1 on November 11<sup>th</sup></b>	85
<b>Figure 3.5.2.2.6 - Measured profile of voltage, current and electrical power for generator No. 1 on November 11<sup>th</sup></b>	86
<b>Figure 3.5.2.2.7 - Measured electrical power as a function of the temperature difference over the TE modules</b>	86
<b>Figure 3.5.2.2.8 - Medium efficiency of prototype B versus measured TE module temperature difference</b>	87
<b>Figure 3.5.2.2.9 – Exterior view of generator No. 1 after the on-line test</b>	89
<b>Figure 3.5.2.2.10 - Exterior view of generator No. 2 after the on-line test</b>	89
<b>Figure 3.5.2.2.11 - Disassembled generators after the on-line test (left - generator No. 1, right - generator No. 2)</b>	90
<b>Figure 3.5.2.2.12 - Detailed view of TE modules after the on-line test</b>	90
<b>Figure 3.5.2.3.1 - Graph showing negatively slope trend between price (\$/kg) of elements and their crystal abundance. From reference [16].</b>	99
<b>Figure 3.5.2.3.2 - ZT versus crustal abundance of thermoelectric materials [16].</b>	100
<b>Figure A.9.2.1 – Prototype B: generator No. 1 (left), generator No. 2 (right) after installation on the plant</b>	160
<b>Figure A.9.2.2 - Prototype B: generators and protected measuring lines after installation on the plant</b>	160



## **List of tables**

<b>Table 3.1.1.2.1 - FENO, hot source and cold sink heat carrier characteristics</b>	18
<b>Table 3.1.1.3.1 - AME, hot source temperature measurement</b>	22
<b>Table 3.1.1.6.1 – Prototype B, TE power production properties using a heating element with a surface temperature of 700°C</b>	32
<b>Table 3.1.1.6.2 – Prototype B, TE power production properties at a surface temperature of the heating element of 880°C.</b>	33
<b>Table 3.1.1.7.1 - TE modules purchased in the project</b>	34
<b>Table 3.1.1.8.1 - Model variables definitions</b>	35
<b>Table 3.1.1.11.1 – Operative water temperature in the pipeline with a safety temperature gap of 70°C</b>	39
<b>Table 3.1.1.11.2 – Prototype A, TEM parameters</b>	40
<b>Table 3.3.3.1.1 – Prototype A final main specifications</b>	67
<b>Table 3.4.1.2.1 - Prototype B design parameters</b>	71
<b>Table 3.5.1.4.1 - Comparison of different electric power production plants</b>	93
<b>Table 3.5.2.3.1 - A classification of thermoelectric materials along with their cost and figure of merit (ZT) [11]. It is to be noted that the fill factor (F) is the ratio of the area covered by the active thermoelectric material to the area of the substrate. The low and high temperature scenarios corresponds to ~373 K and ~1073 K hot side temperature</b>	97
<b>Table 3.5.2.3.2 - Abundance of elements used for the synthesis of thermoelectric materials [15]</b>	98
<b>Table 3.5.2.3.3 - Abundance of thermoelectric materials in metric tons [16]</b>	99



## **List of acronyms and abbreviations**

<b>Acronym</b>	<b>Definition</b>
AC	Alternate Current
AME	Arcelor Mittal España
BFI	VDEh-Betriebsforschungsinstitut
BOF	Basic Oxygen Furnace
CCGT	Combined Cycle Gas Turbines
CH	Channels
CHP	Combined Heat and Power
CPU	Central Processing Unit
CSM	Centro Sviluppo Materiali
CU	Cardiff University
DC	Direct Current
DEER	Directions in Engine-Efficiency and Emissions Research
DIN	Deutsches Institut fur Normung
DN	Diametro Nominale
DOE	Department Of Energy (US)
DRI	Direct Reduced Iron
DS	Dry Steam
EAF	Electric Arc Furnace
EC	External Combustion (engine)
ECS	Evaportive Cooling Systems
ECT	European Conference on Thermoelectrics
ELCD	European reference Life Cycle Database
EN	European Norm
FENO	Ferriere Nord
FSP	Flash Steam Power (plant)
GJ	Giga Joule
GM	General Motors®
GTD	Ground Test Demonstrator
HC	Hydrocarbons
HFC	Hydrofluorocarbons
HTPEM	High Temperature Polymer Electrolyte Membrane
Hz	Hertz
IBC	Inverted Brayton Cycle
IC	Internal Combustion (engine)
IR	Infra-red
ISE	Fraunhofer Institute for Solar Energy Systems
JFE	Jeiefuī Hōrudingusu Kabushiki-gaisha
LAST	Lead Antimony Silver Telluride
LCA	Life Cycle Assessment
LCIA	Life Cycle Impact Assessment
LCOE	Levelized Cost of Electricity

<b>Acronym</b>	<b>Definition</b>
LLC	Limited Liability Company
LPG	Liquefied Petroleum Gas
MGT	Micro-Gas Turbine
MPT	Metallurgical Plant and Technology (magazine)
MSDS	Material Safety Data Sheet
MW	Mega-watt
NASA	National Aeronautics and Space Administration (USA)
ORC	Organic Rankine Cycle
PCM	Phase Change Material
PED	Pressure Equipment Directive
PGEC	Photon Glass Electron Crystal
PV	Photo-Voltaic
RFSR	Research Fund for Coal and Steel (EU)
RTG	Radioisotope Thermoelectric Generators
RV	Residual Value
SDR	System Degradation Rate
SETIS	Strategic Energy Technologies Information System (EU)
SPS	Spark Plasma Sintering
SRC	Steam Rankine Cycle
SSSA	Scuola Superiore Sant'Anna (Pisa)
STG	Solar Thermal Generator
SZFG	Salzgitter Flachstahl GmbH
TE	Thermoelectric
TEG	Thermoelectric Generator
TELPG	Thermoelectric Liquefied Petroleum Generator
TEM	Thermoelectric Module
TGS	Technical Group for Steel
UTC	United Technologies Corporation®
WAC	Water Air Cooler
WP	Work Package

**Note:** in this report the term "TEG" refers to an "engineering equipment" that produces electricity by means of thermoelectric modules and the term "TEM" refers to the thermoelectric module. Unfortunately, in the literature, the term "thermoelectric generator" is used sometimes (by our point of view incorrectly) to indicate also the single thermoelectric module.

## **List of references**

- [1] M. Gao and D. M. Rowe, "Thermoelectric Handbook: Macro to Nano," in *Thermoelectric Handbook: Macro to Nano*, D. M. Rowe, Ed. CRC Press, 2006.
- [2] O. Bubnova *et al.*, "Optimization of the thermoelectric figure of merit in the conducting polymer poly(3,4-ethylenedioxothiophene).," *Nat. Mater.*, vol. 10, no. 6, pp. 429–433, 2011.
- [3] H. Zhao *et al.*, "High thermoelectric performance of MgAgSb-based materials," *Nano Energy*, vol. 7, pp. 97–103, Jul. 2014.
- [4] A. Montecucco, J. Siviter, and A. R. Knox, "The effect of temperature mismatch on thermoelectric generators electrically connected in series and parallel," *Appl. Energy*, vol. 123, pp. 47–54, 2014.
- [5] Gao Min, "Thermoelectric Energy Harvesting," in *Energy Harvesting for Autonomous Systems*, S. Beeby and N. White, Eds. Artech House, 2010, pp. 135–157.
- [6] C. Kost, J. N. Mayer, J. Thomsen, and S. Nold, "Levelized Cost of Electricity - Renewable Energy Technologies," *Fraunhofer ISE*, no. November, 2013.
- [7] G. Holdmann, "Chena Geothermal Power Plant, Project Final Report, Prepared for the Alaska Energy Authority," Fairbanks, AK (USA), 2007.
- [8] G. Holdmann and K. List, "The Chena Hot Springs 400kW geothermal power plant: experience gained during the first year of operation," *GRC Trans.*, vol. 31, pp. 515–519, 2007.
- [9] H. Wirth, "Recent facts about photovoltaics in Germany," *Fraunhofer ISE*, 2017.
- [10] Renzo Marchesi, Paola Bombarda and A. R. Andrea Casalegno, Luigi Colombo, Manfredo Gulizzoni, Andrea Lucchini, Angelo Gino Manfredi, Fabio Rinaldi, "Costi di produzione di energia elettrica da fonti rinnovabili," *Politecnico di Milano*. 2013.
- [11] S. Leblanc, S. K. Yee, M. L. Scullin, C. Dames, and K. E. Goodson, "Material and manufacturing cost considerations for thermoelectrics," *Renew. Sustain. Energy Rev.*, vol. 32, pp. 313–327, 2014.
- [12] J. R. Sootsman, D. Y. Chung, and M. G. Kanatzidis, "New and old concepts in thermoelectric materials," *Angewandte Chemie - International Edition*, vol. 48, no. 46. pp. 8616–8639, 2009.
- [13] G. S. Nolas, "Clathrate Thermoelectrics," in *Chemistry, Physics, and Materials Science of Thermoelectric Materials - Beyond Bismuth Telluride*, Springer, 2003, pp. 107–120.
- [14] C. Uher, "Skutterudites: Prospective Novel Thermoelectrics," in *Recent Trends in Thermoelectric Materials Research: Part I*, T. Tritt, Ed. London: Academic Press, 2001, pp. 139–247.
- [15] J. W. Morgan and E. Anders, "Chemical composition of Earth, Venus, and Mercury.," *Proc. Natl. Acad. Sci. U. S. A.*, vol. 77, no. 12, pp. 6973–6977, 1980.
- [16] R. Amatya and R. J. Ram, "Trend for thermoelectric materials and their earth abundance," *J. Electron. Mater.*, vol. 41, no. 6, pp. 1011–1019, 2012.
- [17] M. W. Gaulois, T. D. Sparks, C. K. H. Borg, R. Seshadri, W. D. Bonificio, and D. R. Clarke, "Data-driven review of thermoelectric materials: Performance and resource onsiderations," *Chemistry of Materials*, vol. 25, no. 15. pp. 2911–2920, 2013.
- [18] D. M. Rowe, "Thermoelectrics, an environmentally-friendly source of electrical power," *Renewable Energy*, vol. 16, no. 1–4. pp. 1251–1256, 1999.
- [19] A. Patyk, "Thermoelectric generators for efficiency improvement of power generation by motor generators - Environmental and economic perspectives," *Appl. Energy*, vol. 102, pp. 1448–1457, 2013.
- [20] "Batteries," *Scottish Environment Protection Agency*. [Online]. Available: [http://www.sepa.org.uk/waste/waste\\_regulation/producer\\_responsibility/batteries.aspx](http://www.sepa.org.uk/waste/waste_regulation/producer_responsibility/batteries.aspx). [Accessed: 26-Mar-2015].
- [21] "Material Safety Data Sheet," *University of Minnesota*, 1994. [Online]. Available: [http://www.nfc.umn.edu/assets/pdf/msds/bismuth\\_telluride.pdf](http://www.nfc.umn.edu/assets/pdf/msds/bismuth_telluride.pdf).
- [22] M. R. Ernst Worrell, "Recycling of Rare Metals," in *Handbook of Recycling*, V. W. Y. Tam, Ed. Elsevier, 2014, p. 139.
- [23] J. James F Carlin, "USGS Minerals Information: Bismuth." [Online]. Available: <http://minerals.usgs.gov/minerals/pubs/commodity/bismuth/>. [Accessed: 26-Mar-2015].
- [24] S. F. Sibley, Ed., *Flow Studies for Recycling Metal Commodities in the United States* -

*Circular 1196-A-M.* U.S. Department of the Interior U.S. Geological Survey, 2004.

- [25] Z. H. Dughaish, "Lead telluride as a thermoelectric material for thermoelectric power generation," *Phys. B Condens. Matter*, vol. 322, no. 1–2, pp. 205–223, 2002.
- [26] A. D. Lalonde, Y. Pei, H. Wang, and G. Jeffrey Snyder, "Lead telluride alloy thermoelectrics," *Mater. Today*, vol. 14, no. 11, pp. 526–532, 2011.
- [27] "Lead Recycling," *International Lead Association*. [Online]. Available: <http://www.ilalead.org/lead-facts/lead-recycling>. [Accessed: 26-Mar-2015].
- [28] "GERMANIUM METAL MATERIAL SAFETY DATA SHEET," *Lattice Materials LLC*, 2003. [Online]. Available: <http://wcam.engr.wisc.edu/Public/Safety/MSDS/Germanium.pdf>.
- [29] G. Schierning, R. Chavez, R. Schmechel, B. Balke, G. Rogl, and P. Rogl, "Concepts for medium-high to high temperature thermoelectric heat-to-electricity conversion: a review of selected materials and basic considerations of module design," *Transl. Mater. Res.*, vol. 2, no. 2, p. 25001, 2015.
- [30] G. Min, D. M. Rowe, and K. Kontostavlakis, "Thermoelectric figure-of-merit under large temperature differences," *J. Phys. D-Applied Phys.*, vol. 37, no. 8, pp. 1301–1304, 2004.
- [31] G. Min, "Principle of determining thermoelectric properties based on I – V curves," *Meas. Sci. Technol.*, vol. 25, no. 8, p. 85009, 2014.
- [32] J. B. Guinée *et al.*, *Handbook on life cycle assessment: operational guide to the ISO standards*. Kluwer Academic Publishers, 2002.
- [33] L. van Oers, A. de Koning, J. B. Guinée, and G. Huppes, "Abiotic resource depletion in LCA Improving characterisation factors for abiotic resource depletion as recommended in the new Dutch LCA Handbook." Road and Hydraulic Engineering Institute, 2002.
- [34] L. van Oers and J. Guinée, "The Abiotic Depletion Potential: Background, Updates, and Future," *Resources*, vol. 5, no. 1, p. 16, Mar. 2016.
- [35] O. Barbier, L. Arreola-Mendoza, and L. M. Del Razo, "Molecular mechanisms of fluoride toxicity," *Chem. Biol. Interact.*, vol. 188, no. 2, pp. 319–333, 2010.
- [36] US Environmental Protection Agency - EPA42, "Emission factors," *Compilation of Air Pollutant Emission Factors*. 1998.
- [37] "Carbon footprint of electricity generation," *POSTnote Updat.*, no. 383, pp. 1–4, 2011.
- [38] "Carbon footprint Factsheet." Center for Sustainable Systems, University of Michigan, 2016.

## Appendices

### Annex A.1

#### **Deliverable D1.1: Procedure of manufacturing the thermoelectric systems prototypes (CU):**

This deliverable reports how a thermoelectric system is manufactured.

##### **A.1.1 Procedure of manufacturing the thermoelectric systems prototypes**

The fabrication of TE devices is typically achieved by connecting a large number of TE legs (alternating n and p-type semiconductor materials) electrically in series and thermally in parallel (Figure A.1.1(a)). The legs are connected by metallic strips (usually Cu or Ni) that are attached to an electrical insulator layer or ceramic (typically aluminium oxide or aluminium nitride). The ceramic layers are the parts that enter into direct contact with the heat source and the heat sink, so they have to be mechanically robust and possess high thermal conductivities.

A basic unit (unicouple) could be identified in the device, which is formed by the connection of a p-type and an n-type element (Figure A.1.1(b)). This connection is one of the crucial aspects of module fabrication and is the main reason for the device efficiency being smaller than the prediction from the ZT of the materials [29]. The electrical connection requires the use of a thin metal barrier in order to prevent the diffusion of atoms from the solder into the TE element and vice versa, which could cause poisoning and degradation of the thermoelectric properties. Then, an adequate solder, with a melting point suitable for the operating temperature range of the device and chemically compatible, should be used to connect the thermoelement to the electrode. It is also important to match the thermal expansion coefficients of the different materials involved in the junction in order to avoid the apparition of cracks under the mechanic-thermal stress. Finally, the thermal resistance rising from the solder/electrode/ceramic part should be minimised as much as possible to achieve the maximum temperature difference across the TE materials.

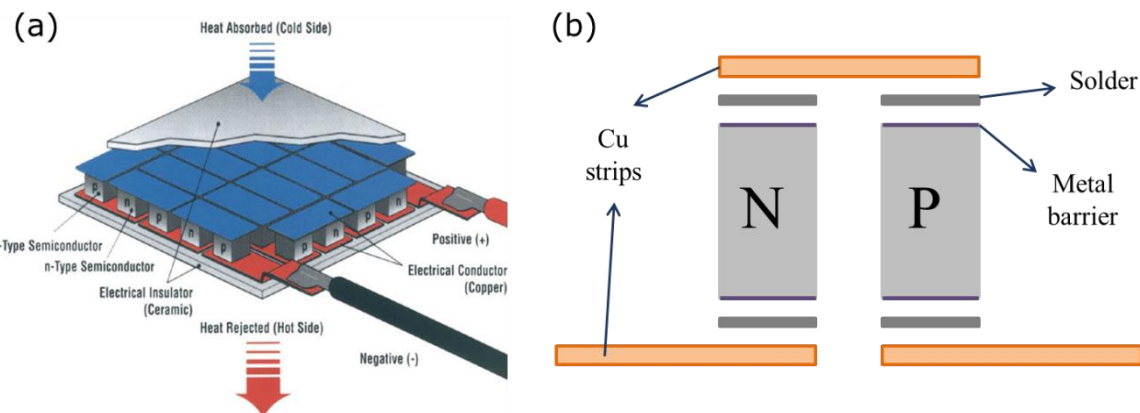


**Figure A.1.1** - Diagram of a thermoelectric module (a) and elements that integrate a unicouple basic unit (b).

All the requirements mentioned above make the fabrication of devices very challenging, especially for high temperature applications [29], where the thermo-mechanical stress is quite significant, the interdiffusion of atoms at the junctions becomes more likely and suitable commercial solders are not abundant in the market. In addition to this, some thermoelectric materials (such as skutterudites or Mg<sub>2</sub>Si) require surface treatments to avoid sublimation and corrosion reactions.

Usually the fabrication process consists of several steps:

1. **Polishing and dicing of the ingot material:** TE materials are typically provided in ingot form with a disc shape (similar to a coin). First, it is very important to polish both top and bottom surfaces in order to achieve a completely uniform thickness. In this way, legs with exactly the same length will be obtained. By polishing and subsequent cleaning, oxide and/or layers of dirtiness that could be present in the areas to be electrically contacted are removed. Once polished, the ingot is diced at the desired sizes to obtain the thermoelements. An example of a machine used for dicing is shown in Figure A.1.2(a).

2. ***Metallisation***: In this step, the areas of the thermoelements to be electrically contacted are coated with a thin metallic layer (the use of more than one metallic layer is also common). This serves to prevent inter-diffusion as mentioned above and it could also be performed before dicing for a more time-effective fabrication. Figure A.1.2(b) shows a collection of diced and metallised thermoelements.

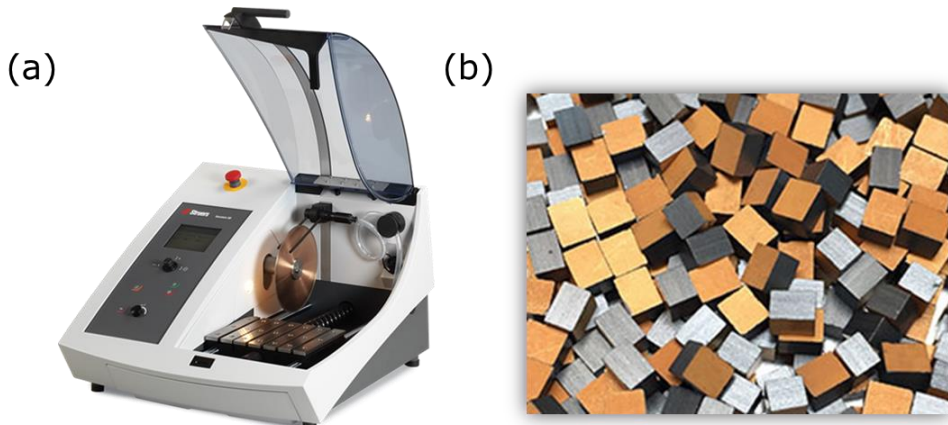


**Figure A.1.2** - Dicing machine (a) and diced and metallised thermoelements (b). Credits to Struers and Alphabet Energy respectively.

3. ***Assembling***: The metallised thermoelements, solder or brazing material pieces, and the ceramics with the attached electrodes, are assembled using a properly designed rig that keeps all the elements in place (Figure A.1.3 (a)).
4. ***Soldering***: Once assembled, the soldering process is performed at the required temperature. Different soldering procedures can be used (furnace, induction heating, etc.). Very short soldering times are usually required to minimise sublimation or degradation of the thermoelectric materials. The process is commonly carried out under vacuum or inert atmosphere for the same reason. A tube furnace used for the soldering process at Cardiff University can be seen in Figure A.1.3 (b).
5. ***Leads connection***: Finally, leads are soldered at the initial and final electrodes for the electrical connection of the device. These leads are typically of large cross-sectional area to provide low electrical resistance and keep the total resistance of the system as low as possible.

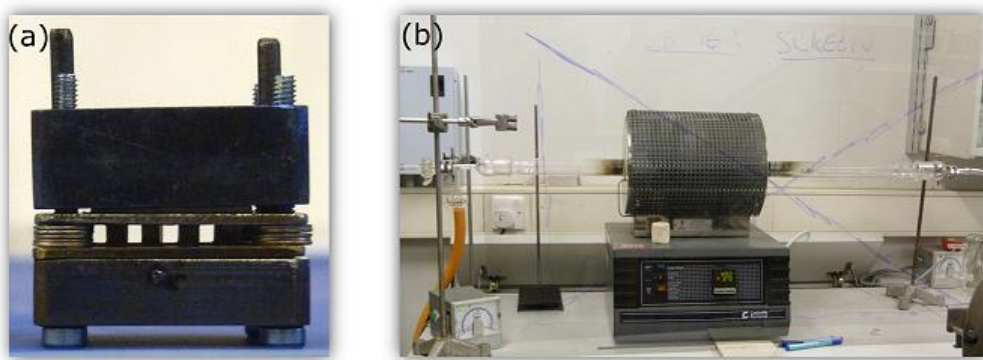


**Figure A.1.3** - Assembled module (a) and tube furnace (b) for the soldering process.

Nowadays, different manufacturers across the globe are able to provide reliable and robust thermoelectric modules for hot side operation around 200 or 250 °C. They are all based on  $\text{Bi}_2\text{Te}_3$  materials. On the other hand, for operation at higher temperature is less common to find commercially available devices, although a lot of efforts are currently in progress and some devices start to become commercialised. A number of module suppliers is shown in Table A.1.1.

<b>Manufacturer/Supplier</b>	<b>Materials used</b>	<b>Country</b>
Custom Thermoelectrics	Bi <sub>2</sub> Te <sub>3</sub>	USA
Marlow	Bi <sub>2</sub> Te <sub>3</sub>	USA
Alphabet Energy	Tetrahedrites	USA
Gentherm	PbTe	USA
Tellurex	Bi <sub>2</sub> Te <sub>3</sub>	USA
TE Technology	Bi <sub>2</sub> Te <sub>3</sub>	USA
Melcor	Bi <sub>2</sub> Te <sub>3</sub>	USA
European Thermodynamics	Bi <sub>2</sub> Te <sub>3</sub>	UK
Quick Ohm	Bi <sub>2</sub> Te <sub>3</sub>	Germany
Kelk	Bi <sub>2</sub> Te <sub>3</sub>	Japan
Thermion	Bi <sub>2</sub> Te <sub>3</sub>	Ukraine
Kryotherm	Bi <sub>2</sub> Te <sub>3</sub>	Russia
Thermonamic	Bi <sub>2</sub> Te <sub>3</sub>	China
Eureca	Bi <sub>2</sub> Te <sub>3</sub>	Germany
Ferrotec NORD	Bi <sub>2</sub> Te <sub>3</sub>	Russia

**Table A.1.1** - List of several thermoelectric module suppliers around the world



## Annex A.2

### **Deliverable D1.2: Description of the tools for modules control and monitoring (CSM, CU, BFI)**

This deliverable reports the description of the control and monitoring tools the systems and their main components of prototype A and B.

#### **A.2.1 Prototype A: description of the tools for modules control and monitoring**

Figure A.2.1.1 shows a technical drawing of the whole system of prototype A, including both connections with hot source, cold sink, ancillaries and TEG system.

Table A.2.1.1 reports the list of components and their description on the basis of the reference code reported in the Figure A.2.1.1.

Table A.2.1.2 reports the technical characteristics of the components used for control & monitoring of prototype A.

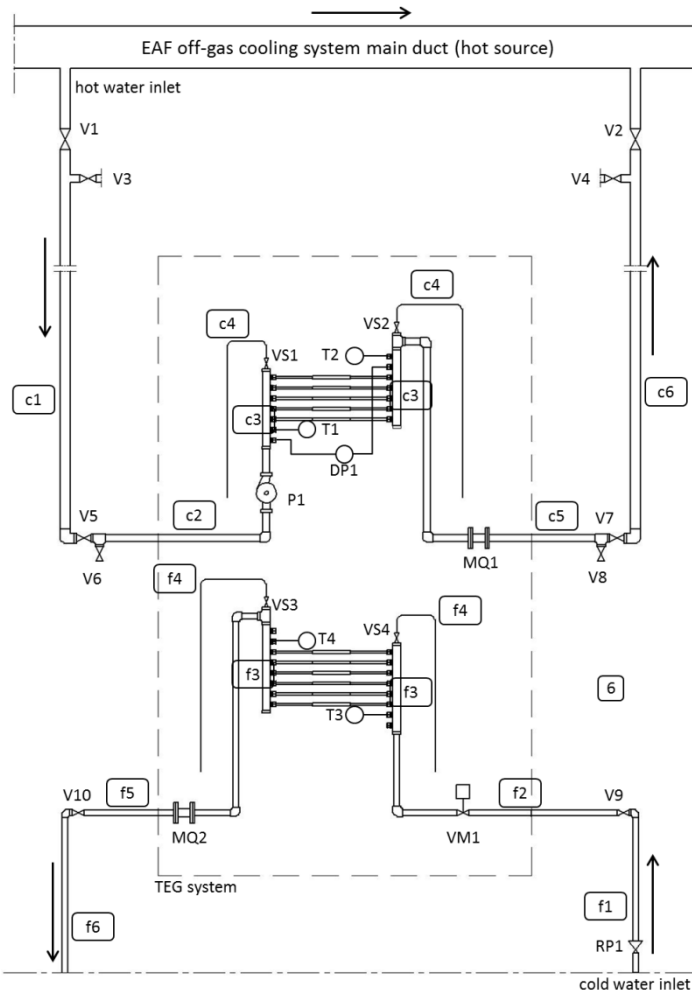


**Figure A.2.1.1 – Prototype A, hydraulic and monitoring scheme**

<b>Code</b>	<b>Description</b>	<b>Code</b>	<b>Description</b>
c1	hot water inlet line	T2	thermoresistance
c2	hot water connector	T3	thermoresistance
c3	hot water collector	T4	thermoresistance
c4	vent	V1	hand stop valve
c5	hot water connector	V2	hand stop valve
c6	hot water outlet line	V3	purge valve
DP1	differential pressure meter	V4	purge valve
f1	cold water inlet line	V5	hand stop valve
f2	cold water connector	V6	purge valve
f3	cold water collector	V7	hand stop valve
f4	vent	V8	purge valve
f5	cold water connector	V9	hand stop valve
f6	cold water outlet line	V10	hand stop valve
MQ1	electromagnetic flow rate meter	VM1	motor operated valve
MQ2	electromagnetic flow rate meter	VS1	purge valve
P1	water pump	VS2	purge valve
RP1	pressure reducer	VS3	purge valve
T1	thermoresistance	VS4	purge valve

**Table A.2.1.1** – Prototype A, list of components as shown in Figure A.2.1.1.

<b>Measure /Control</b>	<b>Picture</b>	<b>Manufacturer</b>	<b>Characteristics / Remarks</b>
Hot water flow rate		Endress & Hauser®; PROLINE PROMAG 50	<ul style="list-style-type: none"> <li>• DN 25</li> <li>• Range: 10 – 150 l/min</li> <li>• Output type: 4 – 20 mA</li> <li>• Measurement error: &lt; 1 % of measured value</li> <li>• Selected for use in both test bed- and on-line application</li> </ul>
Cold water flow rate		Endress & Hauser®; PROLINE PROMAG 50	<ul style="list-style-type: none"> <li>• DN 15</li> <li>• Range: 10 – 150 l/min</li> <li>• Output type: 4 – 20 mA</li> <li>• Measurement error: &lt; 1 % of measured value</li> <li>• Selected for use in both test bed- and prototype application</li> </ul>

Temperature of hot and cold water, in & out flow		Italcoppie® sensori srl	<ul style="list-style-type: none"> <li>• Type: PT100</li> <li>• Range: -50°C – 120°C: Output type: 4 – 20 mA</li> <li>• Accuracy: ± 0,3°C</li> <li>• DIN IEC 751</li> <li>• Selected for use in both test bed- and prototype application</li> </ul>
Differential pressure measurement of hot source and cold sink water circuit		Endress & Hauser®; Deltabas S	<ul style="list-style-type: none"> <li>• Type: PMD75</li> <li>• Range: -500...500 mbar</li> <li>• Maximum error: ±0.075%</li> <li>• Output type: 4 – 20 mA</li> <li>• Selected for use in both test bed- and prototype application</li> </ul>
Cold water electrovalve		Enolgas® Bonomi SpA	<ul style="list-style-type: none"> <li>• Type: S2281N05</li> <li>• Range: -20...80°C</li> <li>• Bidirectional valve</li> <li>• 230V 50 HZ</li> <li>• Selected for use in both test bed- and prototype application</li> </ul>
Hot water circuit pump		Lowara®	<ul style="list-style-type: none"> <li>• Type: ecocirc 25-6/180</li> <li>• Power: 4-42 W</li> <li>• Range: -10...110°C</li> <li>• Max pressure: 10 bar</li> <li>• Max flow rate: 3200 l/h</li> <li>• Max head: 5.7m</li> <li>• Selected for use in both test bed- and prototype application</li> </ul>

Analog I/O module		Seneca®	<ul style="list-style-type: none"> <li>Type: Z-8AI</li> <li>Description: 8-CH analog input module / RS485</li> <li>Range: ±2,5 Vdc, ±5 Vdc, ±10 Vdc, ± 20 mA</li> <li>Selected for use in both test bed- and prototype application</li> </ul>
-------------------	--	---------	---

**Table A.2.1.2 – Prototype A, description of control & monitoring tools**

### A.2.2 **Prototype B: description of the tools for modules control and monitoring**

Table A.2.2.1 describes tools characteristics used for control & monitoring of prototype B.

Measurement	Picture	Manufacturer	Characteristics / Remarks
Flow rate of cooling water		Endress & Hauser®; PROMAG 10 D	DN 25 Range: 10 – 150 l/min Measurement error: < 1 % of measured value Selected for use in both test bed- and prototype application
Temperature of cooling water		TC Mess- und Regeltechnik® GmbH	Type: PT100 Range: 0 – 100°C: 4 – 20 mA Accuracy: 1/10B according to DIN EN 60751: ± 0,12°C Selected for use in both test bed- and prototype application
Surface temperature (picture shows thermocouple on inside surface of hot side heat exchanger = TE module's hot side)		TC Mess- und Regeltechnik® GmbH	Range: 0 – 100°C: 4 – 20 mA Accuracy: ± 2,5°C Selected for use in both test bed- and prototype application Using Knick thermocouple transmitters

Variable load control		Elektro-Automatik® GmbH	<p>Range (DC): 400 V, 400 W, 25 A, 0 – 40 / 40 – 800 <math>\Omega</math></p> <p>Accuracy: &lt; 0,08 <math>\Omega</math></p> <p>Selected for use in both test bed- and prototype application</p> <p>Output Signals for current and voltage additionally</p>
Electrical current		Ziehl®	<p>Type: Minipan 352V</p> <p>Range: 0 – 5 A</p> <p>Accuracy: 5·10-3 A</p>

**Table A.2.2.1** - Prototype B, description of control & monitoring tools



## Annex A.3

### **Deliverable D2.1: Design of the lab-scale test bed (CSM, CU, BFI)**

The present deliverable shows a collection of photographs with explanations of the developed lab-scale test beds components realized by CSM, Cardiff University and BFI specifically for the present research project. Furthermore tables summarize the main characteristics of the equipment used.

#### **A.3.1 Design of CSM lab-scale test bed**

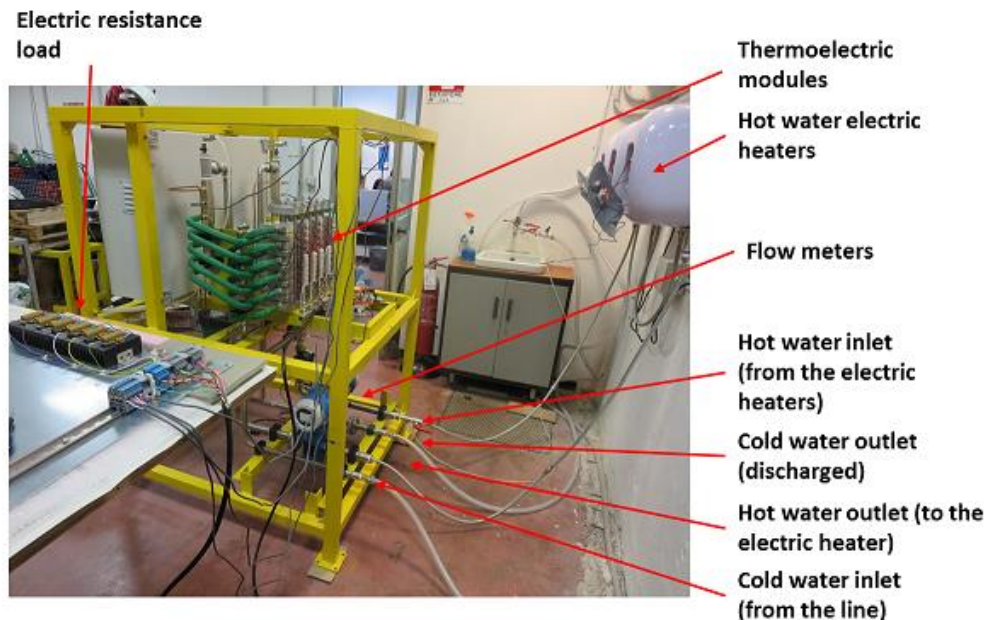


**Figure A.3.1.1** - Prototype A, lab scale test bed main components

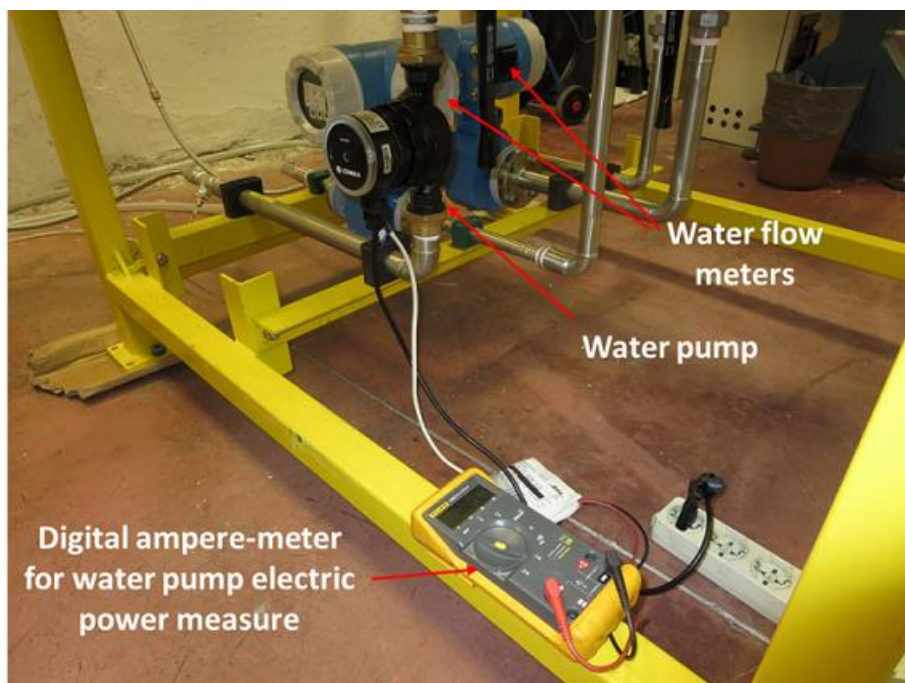


**Figure A.3.1.2** – Prototype A, hot water pump lab test measurement

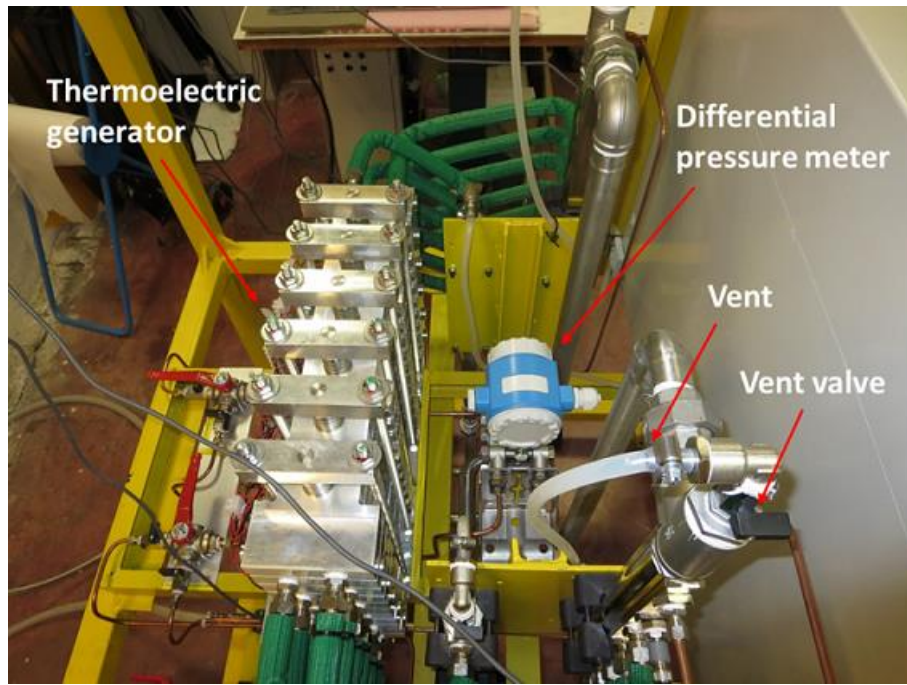


**Figure A.3.1.2 – Prototype A, differential pressure meter**

Equipment and tools	Picture	Manufacturer	Characteristics / Remarks
Electric resistance load		(6x)Vishay® RH050 (6x)Welwyn® WH5 33R	Resistance: 3.3 Ω Power( 25°C):50 W Accuracy: ±1 % Temperature coeff.(100 mΩ): 100 ppm/°C  Resistance: 33 Ω Power( 25°C):10 W Accuracy: ±5% Temperature coeff.(100 mΩ): 50 ppm/°C
Hot water electric heater		GruppoLazio®	Type: SG15SVE1.5V Water capacity: 15 L Rated power: 1.5 kW Factory temperature range: 35-75°C

Manual pressure calibrator		Druck®	Type: DPI600 Pressure range: 0-34 bar Error: 0.1 %
Electric hot plate electronically controlled		Ero-electronic® controller	Power: 600 W 230 V, 50 Hz

**Table A.3.1.1** - Prototype A, lab-scale test bed equipment and tools

### A.3.2 Design of CU lab-scale test bed

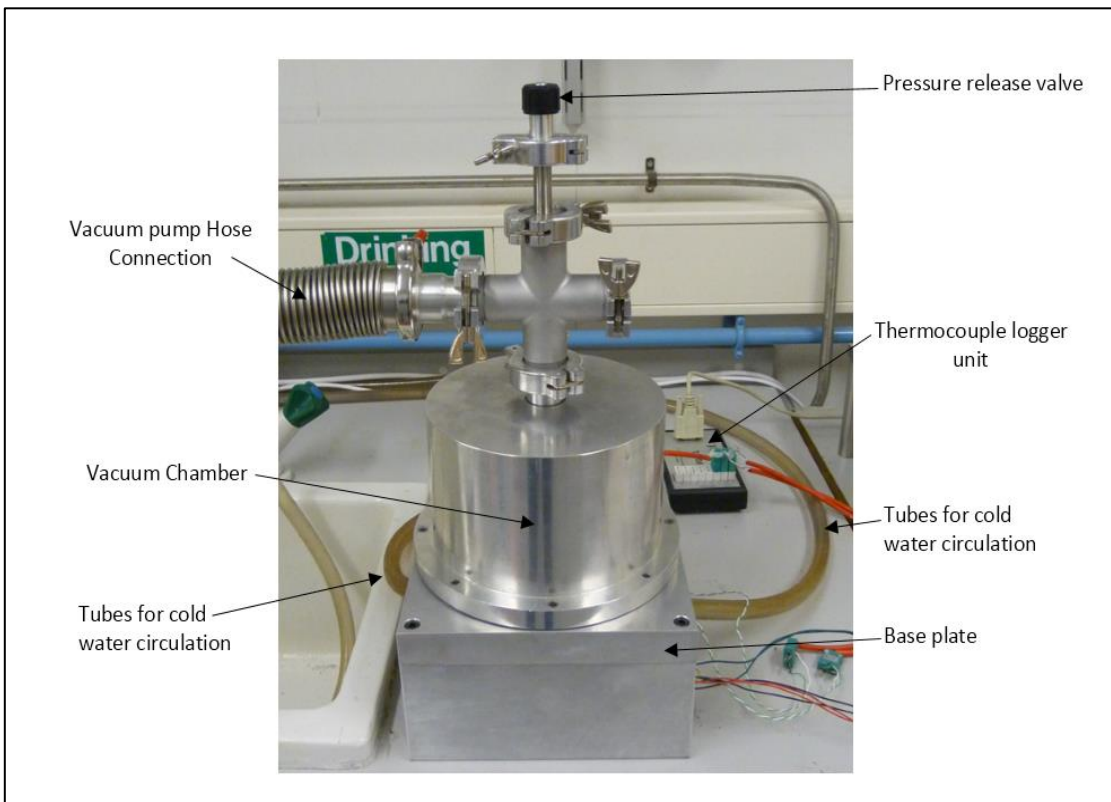


**Figure A.3.2.1** - CU lab scale test-bed, The photograph shows the vacuum chamber set up for characterisation of thermoelectric modules

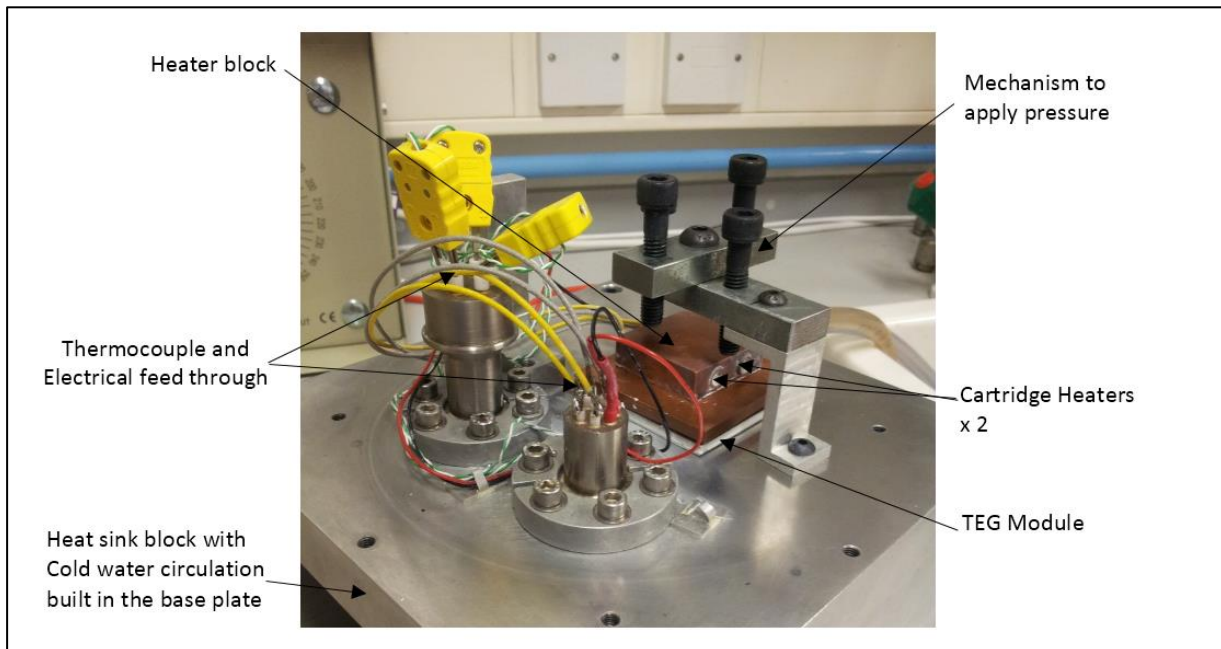


**Figure A.3.2.2** - CU lab scale test-bed, Internal view of the vacuum chamber showing main components.

Description	Specification
Module size range	up to 62 mm <sup>2</sup>
Min. achievable pressure in the vacuum chamber	$\sim 4 \times 10^{-5}$ torr
Cartridge heater power rating	200 W
Number of cartridge heaters	2 or 3 (depending on the size of TE)
Max. achievable temperature difference	$\sim 250$ °C
Max. achievable hot side temperature	$\sim 300$ °C
AC voltage supply range to the heaters	0-270 V

**Table A.3.2.1** - Specifications of CU lab scale test-bed

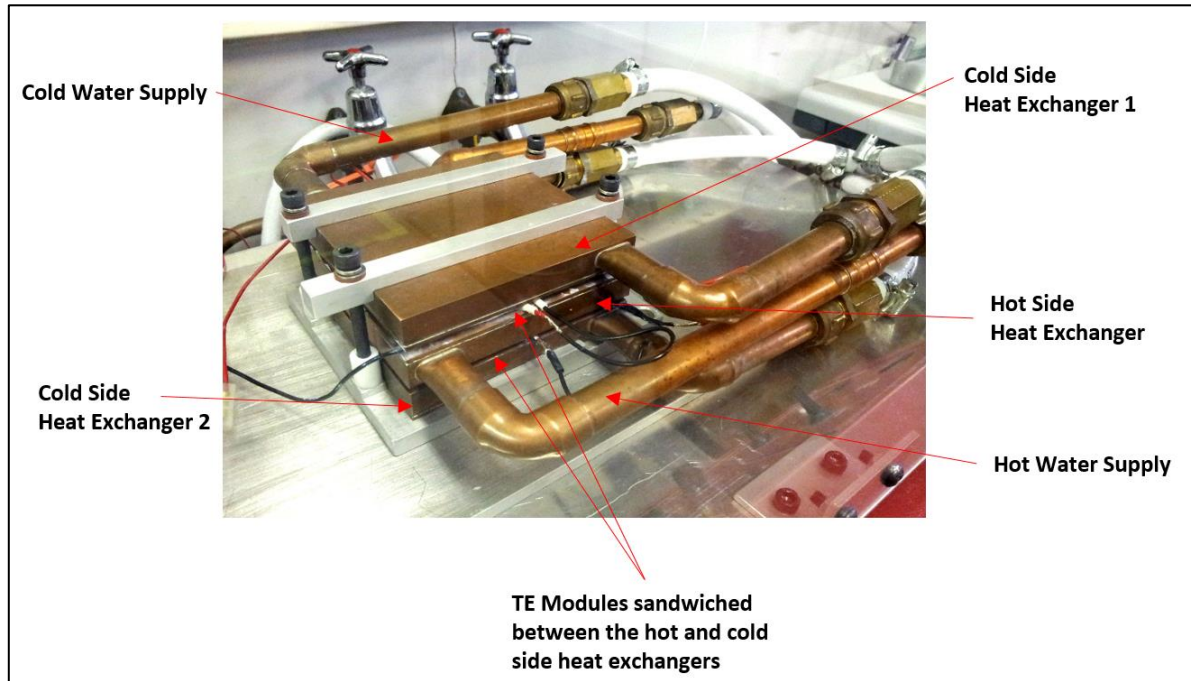
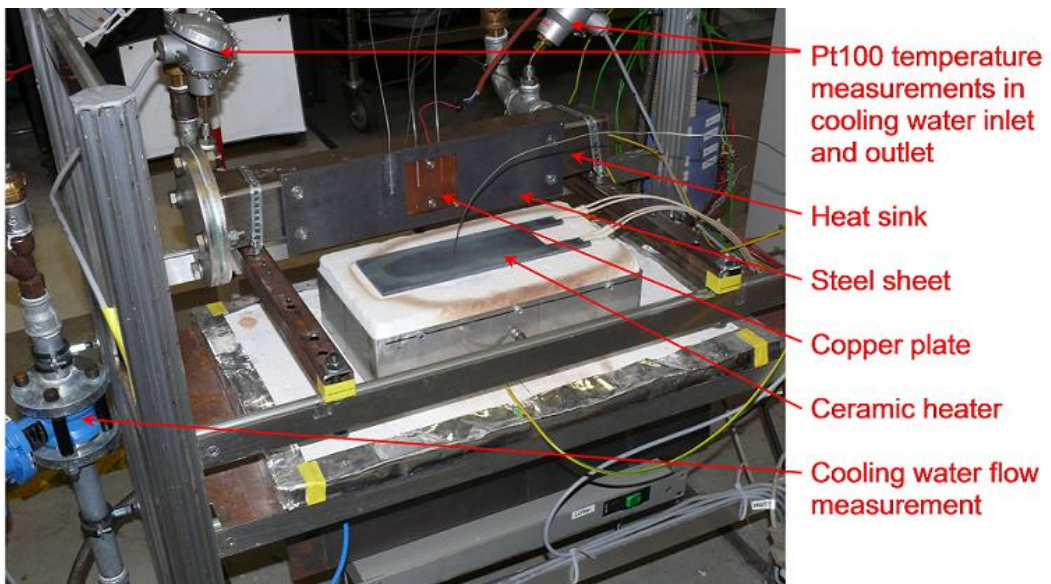


**Figure A.3.2.3** - CU lab scale power generator, The photograph shows the power generator developed for studying the behaviour of thermoelectric modules connected in series and parallel

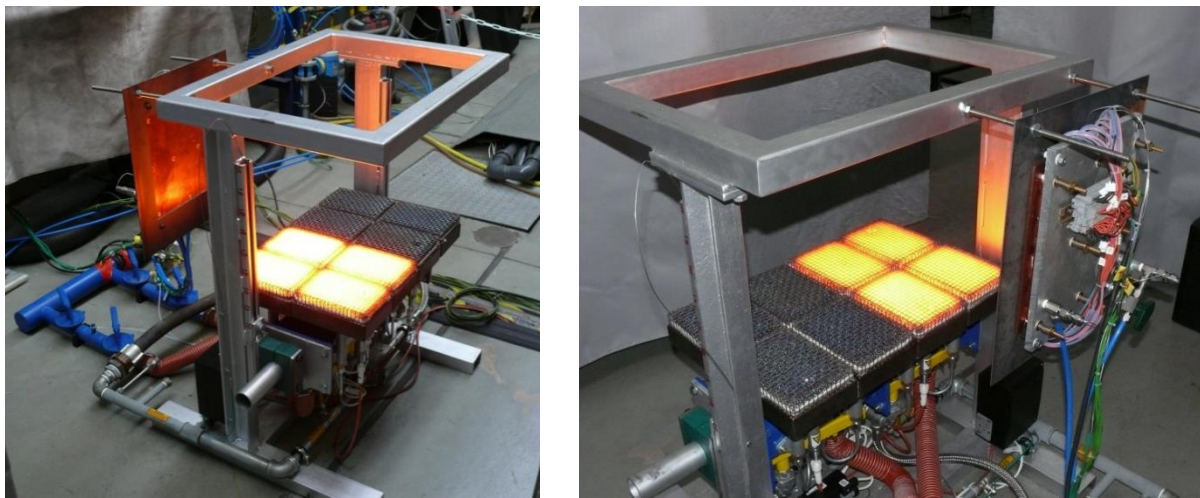
Description	Specification
Number of modules	up to 8 (40 mm <sup>2</sup> module size)
TE Connection	Series or Parallel
Max. achievable temperature difference	100 °C
Max. achievable hot side temperature	130 °C
Hot water pumping capacity	3 gpm, 60 psi

**Table A.3.2.2** - Characteristics of CU lab scale power generator

### A.3.3 Design of BFI lab-scale test bed

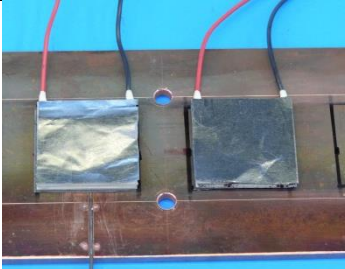


**Figure A.3.3.1** – Prototype B, main components of lab-scale test bed for single TE modules



**Figure A 3.3.2 – Prototype B, test bed for functionally tests of Prototype B**

Equipment and tools	Picture	Manufacturer	Characteristics / Remarks
Data acquisition system		MeasX® using Daisylab software (V 11.0.0) installed on Intel Core 2 CPU 2,4 GHz 2,4 GHz using MS XP (2002) operating system	Selected for use in both test bed- and prototype application Sampling rate 2/s Input (32) and output (5) signal: 0 – 10 V
Heat sink (picture shows test-bed heat sink incl. assembled hot side heat exchanger and (2) TE modules)		Buchwald	Stainless steel (1.4301) Thickness: 4 mm For test-bed use only Cooling water inlet and outlet diameter: 3/4"
Heat source (ceramic (silicon nitride) heating element)		Bach RC	Surface of heating element is temperature (thermocouple type K) controlled; Max. surface temperature: 1.000°C

			For test-bed use only
Graphite foil		Quick-Ohm Küpper® & Co. GmbH	To decrease resistance to heat flow between components of the installation
Heat sink compound		RS components®	To decrease resistance to heat flow between components of the installation
DC power supply			For Pt100 temperature measurement

**Table A.3.3.1** – Prototype B, lab-scale test bed equipment and tools for TE module tests

Equipment and tools	Picture	Manufacturer	Characteristics / Remarks
Data acquisition system		MeasX® using Daisylab software (V 11.0.0) installed on Intel Core 2 CPU 2,4 GHz 2,4 GHz using MS XP (2002) operating system	Selected for use in both test bed- and prototype application Sampling rate 2/s Input (32) and output (5) signal: 0 – 10 V
8 porous burners		GoGas Ecothermal Engineering	8 – 25 kW each, combustion gas: natural gas
DC power supply			For Data acquisition system

**Table A.3.3.2** – Prototype B, equipment and tools for test bed functionally tests of prototype B



## Annex A.4

### **Deliverable D2.2: Description of lab-scale performance test results (CSM, CU, BFI)**

The present deliverable summarizes the main results of the thermoelectric modules and components laboratory tests. These tests have performed in the three lab-scale "test-bed" at the following sites: CSM laboratories in Rome, Cardiff University laboratories in Cardiff and BFI laboratories in Dusseldorf.

#### A.4.1 ***CSM lab-scale performance test results***

Type of lab-scale test performed at CSM	Description	Results summary
Hydraulic pressure test	Cooling and heating aluminium boxes have been filled with high pressure water to verify possible leakages of the TEG hydraulic circuit	The experiment has shown the capability of the water boxes connections to maintain a pressure of 10 bars without any pressure reduction for more than one hour. Therefore the water boxes can be considered adequately designed for the TEG working conditions which are approximately 4 bar for the cold water circuit and 6 bar for the hot water circuit.
Thermoelectric Module Test	TEMs electric power has been measured under different load pressures, hot side temperatures and cooling water fluxes.	The variability of thermoelectric module performance with temperature and water flow rate was well known, while less predictable was the substantial variability from the applied pressure. This test showed a great variability of the electric power generated by a single TEM under different load pressure. The result of the test was that it is required to press the TEM heavily, close to the maximum load (1 MPa), to achieve a good electric behaviour. However, this behaviour is a specific characteristic of the particular modules used for the prototype A.

**Table A.4.1.1 – CSM lab-scale performance test results**

#### A.4.2 ***Cardiff University lab-scale performance test results***

Type of lab-scale test performed at CU	Description	Results summary
Initial module testing on lab-scale test bed	These are the initial experiments carried out on the CU lab-scale test bed. Two modules, sample A and B, were characterised with the aim of determining maximum power output and figure of merit (ZT).	The maximum power output of sample A was higher than B. The ZT determined was in the range of commercially available modules, however it was higher for sample A than B.
Characterisation of CSM modules	The modules provided by CSM were characterised with the aim of comparing the results with the datasheet provided by the manufacturer and get an indication of their performance under actual operating conditions.	The characterisation results showed disagreement with the results mentioned in the datasheet. The open circuit voltage was found to be low, 0.47 V at 50 K temperature difference. On application of pressure on the module, the open circuit voltage was observed to increase but was still below the theoretical value of open circuit voltage. It was concluded that

		<p>in order to achieve reasonable performance from these modules, huge amount of pressure is required.</p>
Characterisation of BFI modules	<p>The modules provided by BFI were characterised for power generation and figure of merit at different temperature differences. The modules were procured from different suppliers: Quick Ohm (Quick Ohm_A and Quick Ohm_B), Eureca (Eureca_A and Eureca_B), RS components and PSI. All modules were 40x40 mm<sup>2</sup>, except the module from RS which was 62x62 mm<sup>2</sup> in size.</p>	<p>The module from RS generated the largest power output due to the large area. However, it was the module Eureca_A that produced the largest power per unit area, whereas the module from PSI generated the lowest.</p> <p>The figure of merit of Eureca_A was highest, while the lowest was for PSI.</p>
Determination Of Thermoelectric Figure-of-merit using 'open/short-circuit' Technique And I-V Curves	<p>Experimental investigation of two methods for determination of effective figure of merit (<math>Z_{efT}</math>) of commercially available modules was carried out.</p> <p>The first method is the 'open/short-circuit' technique, which considers the ratio of temperature differences during open and short-circuit conditions [30] and the second method is based on the current-voltage (I-V) curves obtained at two different operating conditions of the module: 'constant <math>\Delta T</math>' and 'constant heat flux (Q)' [31].</p> <p>The two techniques were compared to study their reliability in determining <math>Z_{efT}</math>.</p>	<p><math>Z_{efT}</math> is one of the most important parameters of a thermoelectric module as it gives information about the thermoelectric material quality and an indication of the performance of the module under actual operating conditions. The conversion efficiency of a module depends upon the <math>Z_{efT}</math>, therefore it is necessary to determine its value accurately.</p> <p>The experimental investigation showed that the <math>Z_{efT}</math> obtained using the two methods were in the expected range for commercially available Bi<sub>2</sub>Te<sub>3</sub> modules. Results are shown in Figure A.4.2.1 and Figure A.4.2.2.</p> <p>The techniques investigated in the research can be used to determine the <math>Z_{efT}</math> by the project partners in the future, and the selection of the modules for integration into the power generation system can be made accordingly. The open/short circuit technique is very quick and requires only the measurement of temperatures. It does not require complex electronic gadgets and therefore can be recommended for measurement of <math>Z_{efT}</math>. Along with the determination of <math>Z_{efT}</math>, the I-V curve method is very useful to gain insights into the performance of the module under different operating conditions. More details on the two methods can be found in the publications [30] and [31].</p>
Investigation into thermal interface materials	<p>A good thermal contact between TE module and the hot and cold sources is very important as the performance of a module can be significantly affected by any air gaps present in the assembly.</p> <p>There are various types of interface materials commercially available in the market; and can be identified as silicon paste, gel based pads, graphite sheets and other 'branded' thermal gap pads. Experiments were conducted to evaluate the performance of a TE module using</p>	<p>The highest power output was achieved with Silicon thermal paste (Figure A.4.2.3), whereas with VO Ultimate thermal pad the power output was lowest. Graphite sheet with <math>\lambda=10\text{ W}\cdot\text{m}^{-1}\cdot\text{K}^{-1}</math> showed the second highest power output followed by graphite sheet with <math>\lambda=8\text{ W}\cdot\text{m}^{-1}\cdot\text{K}^{-1}</math>. Gel passed gap pad and VO Ultimate showed significantly lower performance when compared with silicon and graphite based interface materials. The highest power output using silicon paste can be explained</p>

	<p>different types of thermal interface materials. These materials were procured from RS components, UK. The specifications of the materials are shown Table A.2.2.2.</p>	<p>by the 'fluid' nature of the paste which allows it to reach even the microscopic imperfections in the coupled parts. On the other hand, materials in the form of a sheet have high resistance to change in shape due to their solid state, and therefore they do not fill in the air gaps effectively. Based on the experimental investigation, silicon paste does not require great pressure, whereas graphite sheet requires huge amount of pressure to achieve good thermal contact, this again can be attributed to the physical state of the two.</p>
--	---	---

**Table A.4.2.1** - Cardiff University lab-scale performance test results

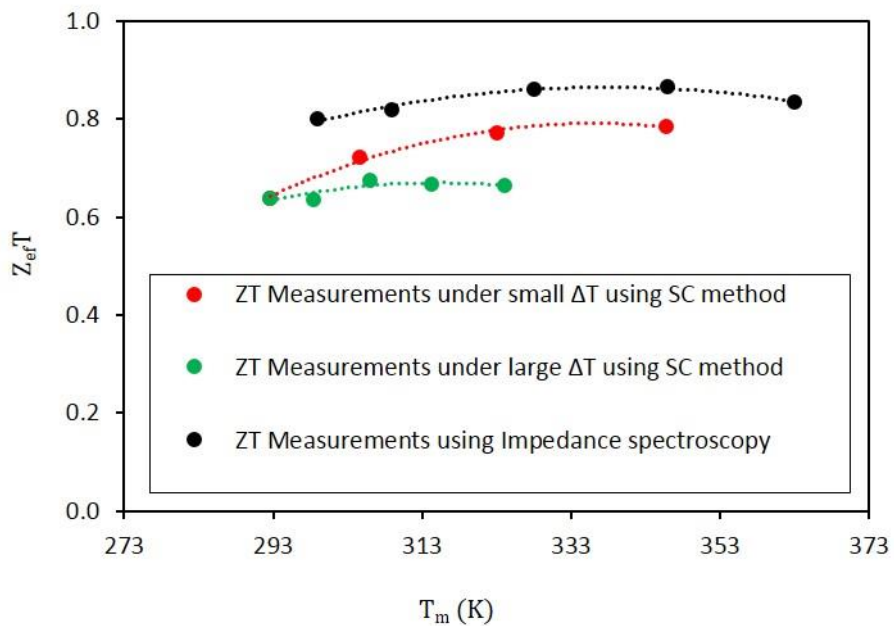


**Figure A.4.2.1** -  $Z_{\text{eff}}T$  measurements using open/short-circuit technique as a function of mean temperature

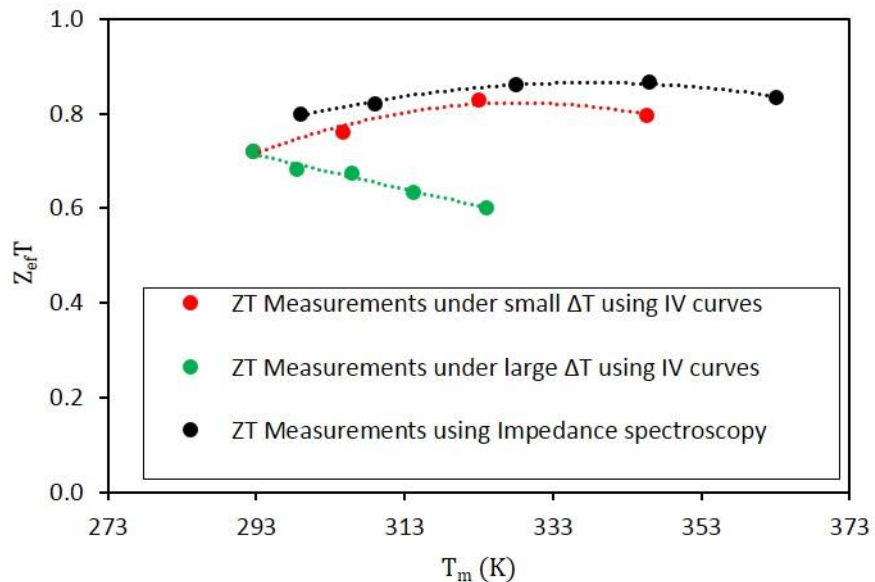


**Figure A.4.2.2** -  $Z_{\text{eff}}T$  measurements using I-V technique as a function of mean temperature

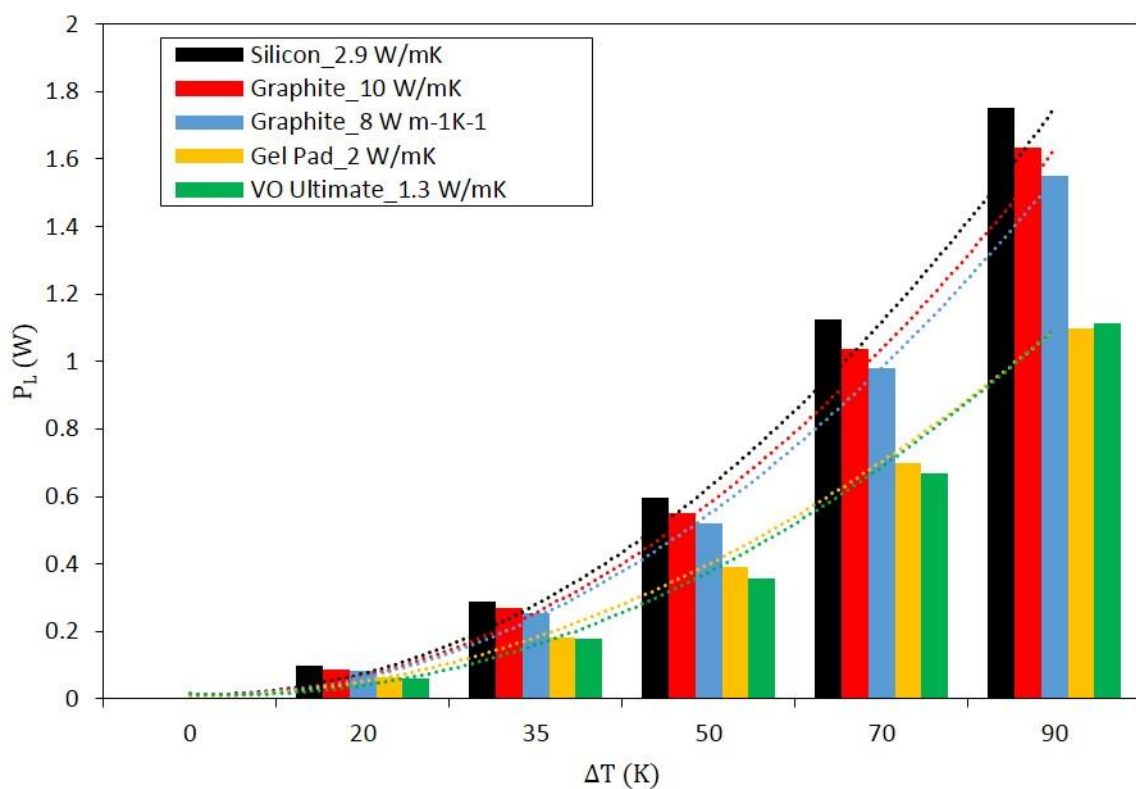


**Figure A.4.2.3** - Power generation using difference interface materials at various temperature differences. Silicon paste showed highest power generation while VO ultimate showed the lowest.

Type	Thickness mm	Thermal conductivity [W·m <sup>-1</sup> ·K <sup>-1</sup> ]	Temperature range [°C]	Cost €/m <sup>2</sup>
Silicon based paste	-	2.9	-100 to +200	25 (100 g tube)
Graphite sheet	0.5	8	-50 to +150	230
Graphite sheet	0.5	10	-50 to +150	433
VO Ultimate thermal gap pad	0.5	1.3	-60 to +200	1700
Gel based thermal gap pad	0.5	2	-45 to +200	700

**Table A.2.2.2** - Specifications of interface materials

#### A.4.3 BFI lab-scale performance test results

Type of lab-scale test performed at BFI	Description	Results summary
TEM electric power vs. modules pressure (torque) and thermal interface material	TE modules positioned between the heat sink and a copper plate which was heated by radiation from the heat source	Bending of the copper plate with increasing torque of the screws. This resulted in a non-complete contact between the surfaces of the module and their corresponding heat exchangers. At increased torques, the $\Delta T$ module increases as a result of the decreased heat flow as a result of the diminishing contact. Thus, the power generated by the TE modules also decreases.
TEM electric power vs. electric resistance load	Because the power output of a TE module is at its maximum when $R_i = R_L$ , a external load has been purchased by BFI which can be manually controlled ( $0 \Omega - 40 \Omega / 40 \Omega - 800 \Omega$ ). V-I and P-I relationships of single TE modules were determined with the variation of the external load resistance.	Maximum power first increases with increasing load resistance, reaches a maximum, then decreases with increasing load resistance. Maximum power at 4 – 8 Ohm depending on the supplier of the TE module.  Power output should increase parabolically with increasing temperature.  This can be seen from Figure 3.5.2.2.7.
TEM electric power vs. module temperature difference	Variation of the temperature of the heating element and thus variation of the radiation.	Nearly linear increasing TE module power output with increasing module temperature difference. Increasing efficiency of the TE module with increasing temperature difference.

**Table A.4.3.1** – BFI lab-scale performance test results



## Annex A.5

### **Deliverable D3.1: Weaknesses analysis of thermoelectric devices and the causes/mechanisms of degradation/failures (CSM, CU, BFI)**

The present deliverable summarizes the main results achieved during laboratory tests performed to determine the weakness point of the thermoelectric generators and their components. All the tests have been carried out in the three lab-scale "test-bed" at three sites: CSM laboratories in Rome, Cardiff University laboratories in Cardiff and BFI laboratories in Dusseldorf. More details can be found in WP3 Task 3.1 "Identification of the equipment weakness points".

#### A.5.1 CSM weakness analysis

Type of weakness	Description	Degradation/failure	Causes/mechanism
TEM maximum mechanical compression	Some thermoelectric modules require a high value of mechanical compression to allow a good level of heat exchange between their hot and cold surfaces. The level of compression load must not exceed the values defined by the manufacturer. This test was performed pressing a single TEM up to its breaking point.	The failure is caused by the excessive levels of compression which lead to module breaking.	The first element of the thermoelectric module that breaks is the ceramic layer (upper or lower). The breaking of the ceramic layer does not produce loss of functionality of the system immediately, but only a reduction in performance. Subsequently, by increasing the compression force, the electrical connections and the semiconductor can be damaged, generating the out of service of the whole component. The mechanism of the failure is associated with brittle fracture of the ceramic layers. The main causes of these failures are associated to the uncorrect assembling of the device or unexpected thermal stress.

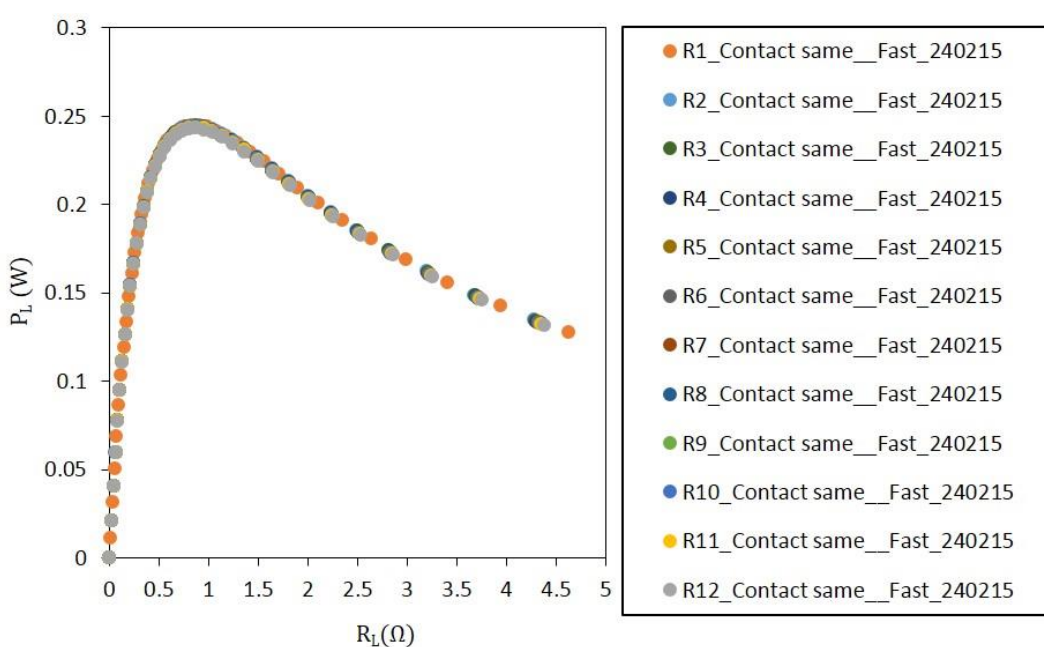
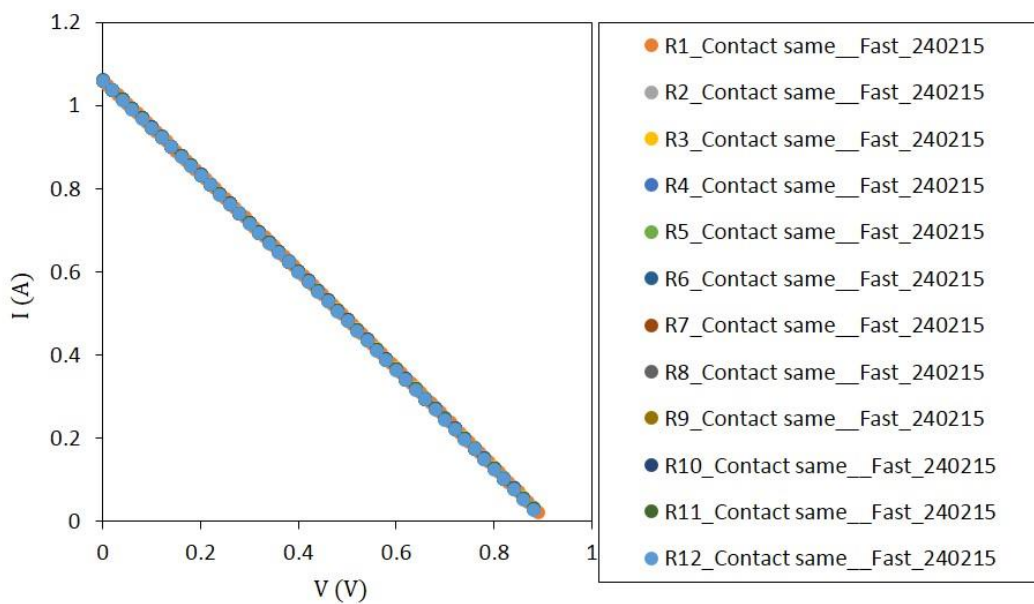
**Table A.5.1. 1 – CSM weakness analysis summary**

#### A.5.2 Cardiff University weakness analysis

Type of weakness	Description	Degradation/failure	Causes/mechanism
Poor heat transfer due to non-conventional module construction	An investigation was carried out to analyse the performance of modules manufactured by traditional and non-traditional methods.	The open circuit voltage of the module manufactured using non-traditional method was observed to be 0.6 V, which is significantly lower than the theoretical value. By applying pressure to the module, the open circuit voltage is increased significantly but still below the theoretical value.  On the other hand, the module manufactured using tradition method	The thermoelements of the hot side are not soldered to the ceramic plate, which is held in place by the silicone sealant. Therefore, the heat transfer to the thermoelements is very poor due to air gaps present in the module assembly. However, under the application of pressure the heat transferred is increased and hence, the load voltage obtained is

		<p>showed predictable performance without the need of high pressure.</p>	higher.
Degradation of interface material	<p>The aim of these experiments was to observe any change in performance of thermoelectric generator system after it has been under operation for extended duration. Three sets of experiments were carried out: (a) a series of fast I-V scans with an interval of 2 minutes between each one of them, (b) fast measurements with an interval of 8 hours, and (c) fast measurements with an interval of 8 hours and replacing the thermal interface material after each measurement.</p> <p>The experiments were conducted using a Potentiostat, which is capable of a scan rate of less than a second, hence it is called 'fast measurement'. The thermal interface material used was silicon paste of <math>\lambda=2.9 \text{ W}\cdot\text{m}^{-1}\cdot\text{K}^{-1}</math>. The hot and cold side temperatures were 338 K and 318 K respectively. The experiments were conducted in a vacuum pressure of <math>4.5 \times 10^{-4} \text{ mbar}</math>. It is important to note that for experiments (a) and (b), the silicon paste was not replaced after each measurement, whereas for the experiment (c) the paste was replaced after each measurement.</p>	<p>Following are the results from each set of experiments:</p> <p>It can be seen (Figure A.5.2.1 and Figure A.5.2.2) that all the curves, I-V and power generation, superimpose on top of each other.</p> <p>When the duration between each measurement was increased to 8 hours, the performance of the generator can be seen decreasing. There was around 10 % decrease in the power generation from Run 1 to 2 (Figure A.5.2.3 and Figure A.5.2.4).</p> <p>When the silicon paste was replaced after carrying out Run 1, the power generation was very similar in Run 1 and Run 2. The Run 2 in-fact generated slightly higher power, which can be expected when new thermal contacts are made (Figure A.5.2.5 and Figure A.5.2.6).</p>	<p>The investigation suggested that the duration of operation seems to have an effect on the performance of the generator. When the duration between any two measurements was only 2 minutes, the power output was same, however when the duration was increased to 8 hours, the power generation decreased. The results of (c) showed that when the thermal interface material was replaced before carrying out the next measurement, the generator produced almost identical power. This indicates that the module did not deteriorate but it was the thermal interface material which degraded and reduced the power generation in the case of (b).</p> <p>So, it can concluded from this investigation that a decrease in performance of the generator system can be expected with the use of silicon paste as interface material.</p> <p>A further investigation on degradation of other interface materials, such as graphite sheets, needs to be investigated.</p>

**Table A.5.2.1** – Cardiff University weakness analysis summary



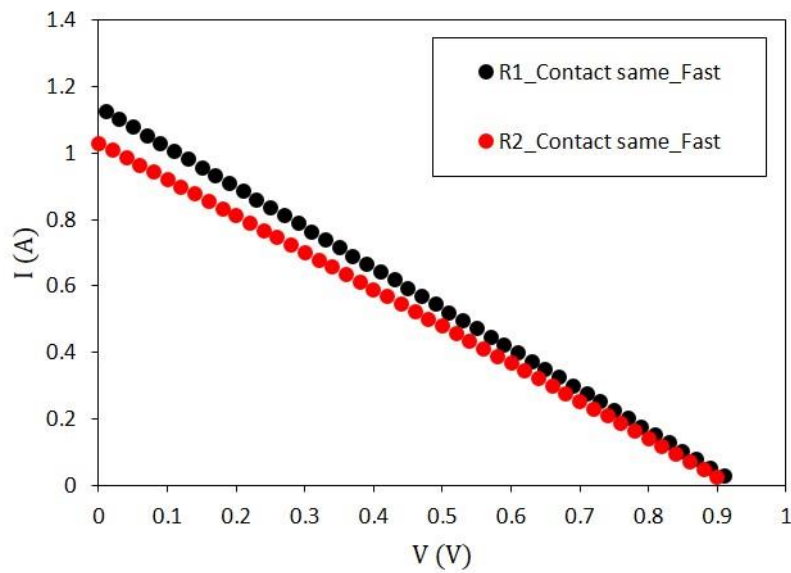


**Figure A.5.2.3** - I-V curves obtained at a constant temperature difference of 20 K. Measurement R2 was done after the module has been operating for 8 hours. A decrease in performance can be seen.

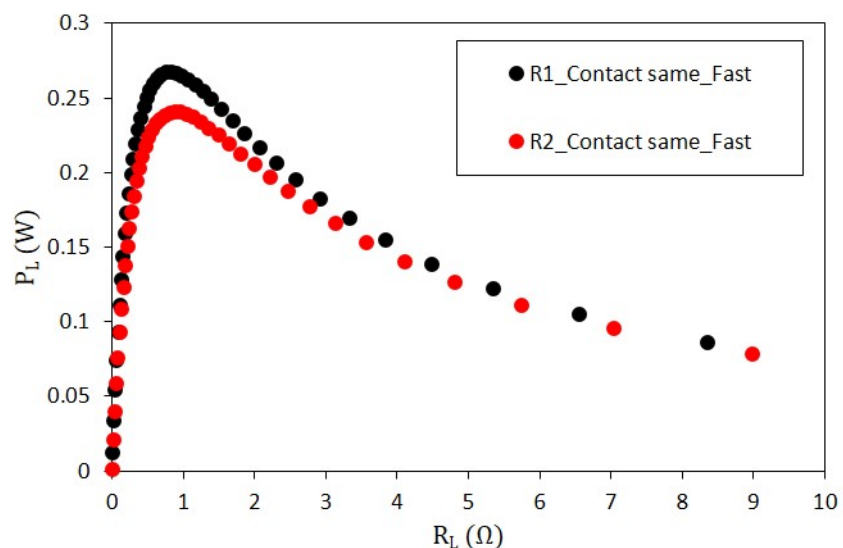


**Figure A.5.2.4** - Power generation as a function of load resistance at a temperature difference of 20 K. The module was under operation for 8 hours before taking measurement R2.

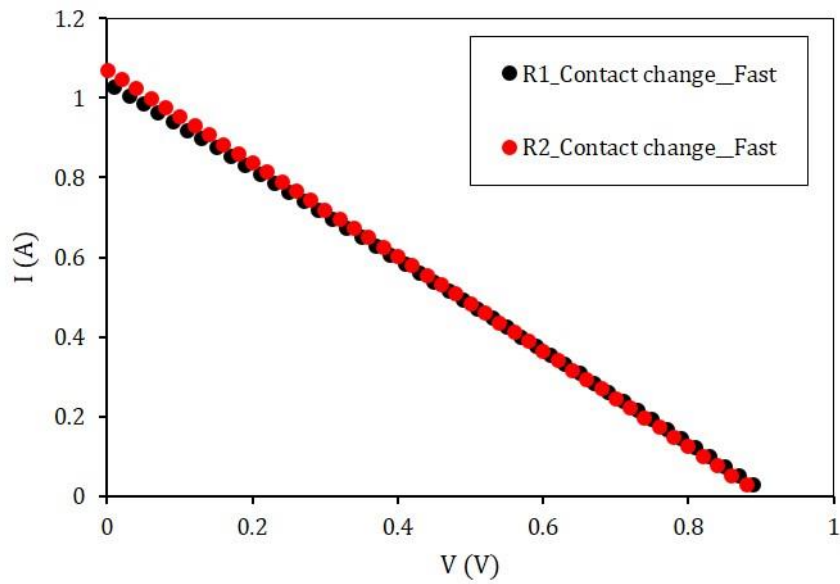


**Figure A.5.2.5** - I-V curves obtained at a constant temperature difference of 20 K. The thermal contacts were changed or in other words the silicon paste was replaced and the module was operated for 8 hours before carrying out measurement R2.

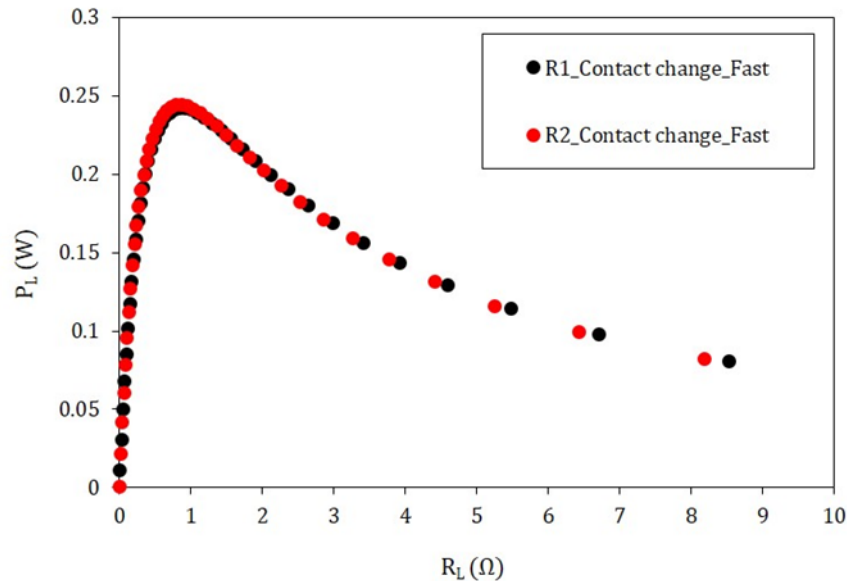


**Figure A.5.2.6** - Power generation as a function of load resistance at a constant temperature difference of 20 K. The thermal contacts were changed or in other words the silicon paste was replaced and the module was operated for 8 hours before carrying out measurement R2.

### A.5.3 BFI weakness analysis

Type of weakness	Description	Degradation/failure	Causes/mechanism
Thermoelectric modules wires soldering	A correct determination of the temperature of the hot side of the module is required in order to be able to guarantee a long operating live	Overheating of TE module: Solder at the TE module liquefied and re-solidified, thus putting the TE module out of operation	TE module has been exposed to too high temperatures (>200°C)
Thermal bridges	No heat sink compound was used to bridge the tip of the thermocouple (which measures the TE modules hot side) to the copper plate at the very first laboratory tests	Overheating of TE module: Solder at the TE module liquefied and re-solidified, thus putting the TE module out of operation	Too low temperature measurement, thus exposing the module to too high temperatures.

**Table A.5.3.1** – BFI weakness analysis summary

## Annex A.6

### **Deliverable D3.2: Description of the technological solutions to be implemented for improving the reliability and the performance of the systems (CSM, CU, BFI)**

The present deliverable summarizes the work done looking for technological solutions to improve the reliability and performance of the developed thermoelectric units. More details can be found in WP3 Task 3.2 "Identification of the technological improvements".

#### **A.6.1 CSM identification of technological improvements (CSM)**

Topic	Description	Technological solution
Optimize the energy fluxes inside the TEG unit	A thermoelectric generator needs to transfer heat to the thermoelectric modules hot side and then to remove part of it from the cold side. To do this fast, the prototype A uses fluid carriers which require the consumption of electricity for their motion. Therefore the maximum net power of the unit (produced power minus consumed power) is obtained minimizing the electric consumption required for fluid motion and contemporary maintaining the highest possible the heat exchange efficiency.	The first requirement is a correct calculation of the section of each pipeline of the whole device, including the pipelines from the hot and cold source and sink. Too large pipeline sections lead to insulating problems and also to very expensive components, while too small sections leads to an increase of the energy lost due to friction. Another important point is to reduce as much as possible thermal barriers using suitable materials with high thermal conductivity and small thickness.
Optimize the electric load matching	A thermoelectric module has its own internal electric resistance depending on the actual thermal conditions. Furthermore none TEMs of a TEG units will work under the same thermal conditions. Therefore the external electric load is always unmatched with each single TEMs, leading to the impossibility to draw from the system the maximum electric power.	The optimal solution should be to control electronically the matched load resistance of each TEM of a TEG unit. This is now possible using specific electronic control systems. However this solution gives an increase of the costs which have to be carefully analysed.

**Table A.6.1.1 – CSM summary of possible technological improvements**

**A.6.2      Cardiff University identification of technological improvements (CU)**

<b>Topic</b>	<b>Description</b>	<b>Technological solution</b>
Developing new TE materials that are low cost and can operate to a higher temperature range	Bi <sub>2</sub> Te <sub>3</sub> based alloys are currently the best materials for application around room temperatures. However, they are expensive and the performances decrease quickly with increasing temperature over 150 °C. Developing new, low cost and high efficiency materials is crucial to improve the economic potential.	MgAgSb based materials has recently reported to have ZT of 1.4 at 200 °C. This provides a new promising material candidate for prototype two application where operating temperature has been shown to be over 200 °C. However, this material is only available with p-type. In order to be technological feasible for module fabrication, it is necessary to have n-type. The search of n-type to match this material is important.
Fabricate modules using advanced materials and optimized geometry	Commercial modules available from manufacturer are designed for general purposes. The property and geometry are not optimized for the applications of this study.	The system performance and efficiency could be improved by tuning the material properties to corresponding operating temperature range. Advanced material structures such as segmented thermoelements may be employed to further increase the TE module efficiency. Optimized geometry of thermoelements is also crucial to achieve high efficiency of the system. The optimization can be achieved by using COMSOL simulation.
Developing thermal interface materials for improved performance and long-term stability	Current thermal interface materials present challenges in achieving the both requirements for performance and long-term stability. It appears that the thermal paste that shows good performance at room temperature but has long-term stability issue.	Recent progress in carbon nanotube, graphene materials have led to some work in study of their suitability as thermal interface materials. In-depth research on how to minimize thermal contact resistance is getting increasing attention in scientific community. We are developing a novel high resolution characterisation technique to determine thermal contact resistance using Infrared Microscopy.

**Table A.6.2.1** – Cardiff University summary of possible technological improvements

**A.6.3 BFI identification of technological improvements (BFI)**

Topic	Description	Technological solution	Results
Hot side heat exchanger magnification	Increase of the heat transport to (from heat source) and from (to heat sink) the module surfaces.	Two different conditions have been tested. TE module covered with a thermal conductive paste ( $\text{Al}_2\text{O}_3$ compound, heat conductivity: 2,9 W/mK) and a TE module covered with graphite foil (thickness: 125 $\mu\text{m}$ ; heat conductivity: 16 W/mK).	Increased performance (despite the lower heat conductivity of the thermal paste compared to that of the graphite foil) when using the thermal paste between the TE module and the copper plate and the heat sink. All tested TE modules showed the same power output improvement when using the thermal conductive paste

**Table A.6.3.1** - BFI summary of possible technological improvements



## Annex A.7

### **Deliverable D3.3: Description of the final configuration of the thermoelectric modules (CSM, CU, BFI)**

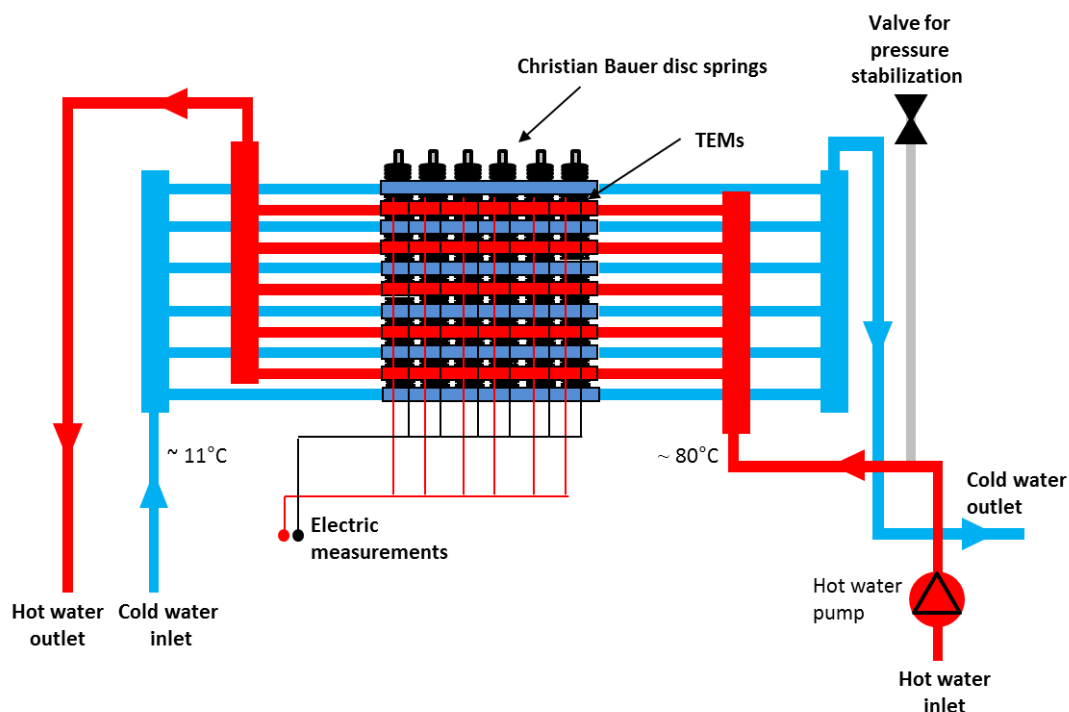
The present deliverable summarises the final configuration of the thermoelectric modules arrangements and characteristics as used for the manufacturing of the two prototypes. More details can be found in WP3 Task 3.3 "Design of the final specification".

#### **A.7.1 Prototype A: thermoelectric modules assembling and characteristics**

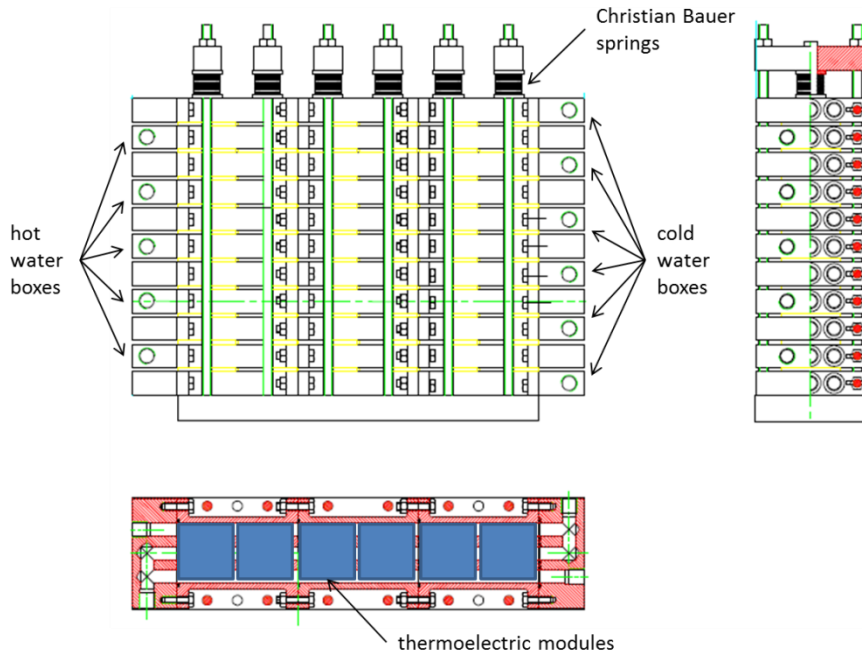
Figure A.7.1.1 shows the final layout of prototype A. The device can be considered as a liquid-liquid counter current heat exchanger which transfer the heat through a matrix of thermoelectric modules.

Figure A.7.1.2 shows a detailed final drawing of the unit. As is possible to observe in the figure, the prototype A has six water boxes for the cold water circulation and five water boxes for the hot water, alternated and forming a stack. Each water box is in contact with six thermoelectric modules on the top side and six on lower side, except for the first and the last water box which are in contact only with six modules. Therefore the modules on the top and on below has a better cooling and then show better electric conversion performance. Each water box is made of three channels so that the water flow is forced to run back and forth inside the whole length of the water box making as much as possible uniform the water box sides. The water boxes are made of aluminium. On the top of the TEG six Christian Bauer springs press the water boxes and the TEMs together to regulate the correct pressure over the TEMs.

Table A.7.1.1 shows the main characteristics concerning the thermoelectric module selected for prototype A.



**Figure A.7.1.1 – Prototype A: TEG unit final layout**



**Figure A.7.1.2** – Prototype A: TEG unit final drawing

Manufacturer	European Thermodynamic Limited
Type	GM250-127-28-10
Photo	
Dimension (width, length, thickness) [mm]	62x62x4 mm
Total number of TEMs used in prototype A	60
Electrical configuration	6 independent column made each of 10 TEMs connected in series
Average electrical load for each column	3 Ω
Matched load output power for each module (hot side 250°C, cold side 30°C). From manufacturer datasheet.	28.3 W
Calculated matched load output power for each module of prototype A (hot water 80°C, cold water 12°C)	0.85 W

**Table A.7.1.1** – Prototype A, selected thermoelectric module characteristics

### A.7.2 Prototype B: thermoelectric modules assembling and characteristics

Figure A.7.2.1 shows the thermoelectric modules arrangement of prototype B. The modules are fixed over a copper plate forming four rows and five columns. The copper plates are used to uniform the heat as much as possible on the modules. More details on the assembling method can be found in WP3 Task 3.3.

Table A.7.2.1 shows the main characteristics of the thermoelectric module selected for manufacturing the prototype B.

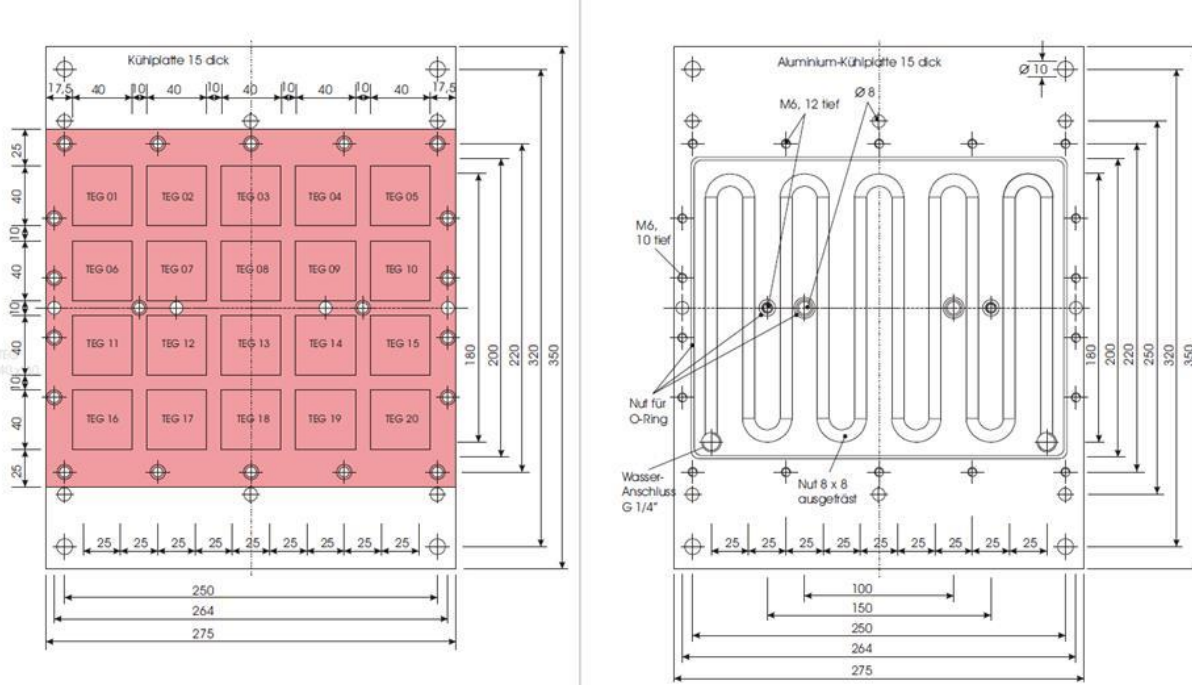


**Figure A.7.2.1 - Prototype B: TEG unit modules assembling**

Manufacturer of TE module	Quick Ohm
Type	$\text{Bi}_2\text{Te}_3$ , QM – 127-1.4-6.0
Photo TE module	
Dimension (width, length, thickness)	40 x 40 x 3,8 mm
Total number of TEMs used in prototype B	Two generators, each 20 modules
Electrical configuration	4 rows, each row counting 5 modules
Average electrical load for each column	7 W at $dT_{\text{module}} = 95 \text{ K}$
Matched load output power for each module (hot side 147°C, cold side 34°C). From manufacturer datasheet.	2.82 W
Calculated matched load output power for each module of prototype B ( $dT_{\text{module}} = 95 \text{ K}$ )	1.4 W

**Table A.7.2.1** - Prototype B, selected thermoelectric module characteristics

## Annex A.8

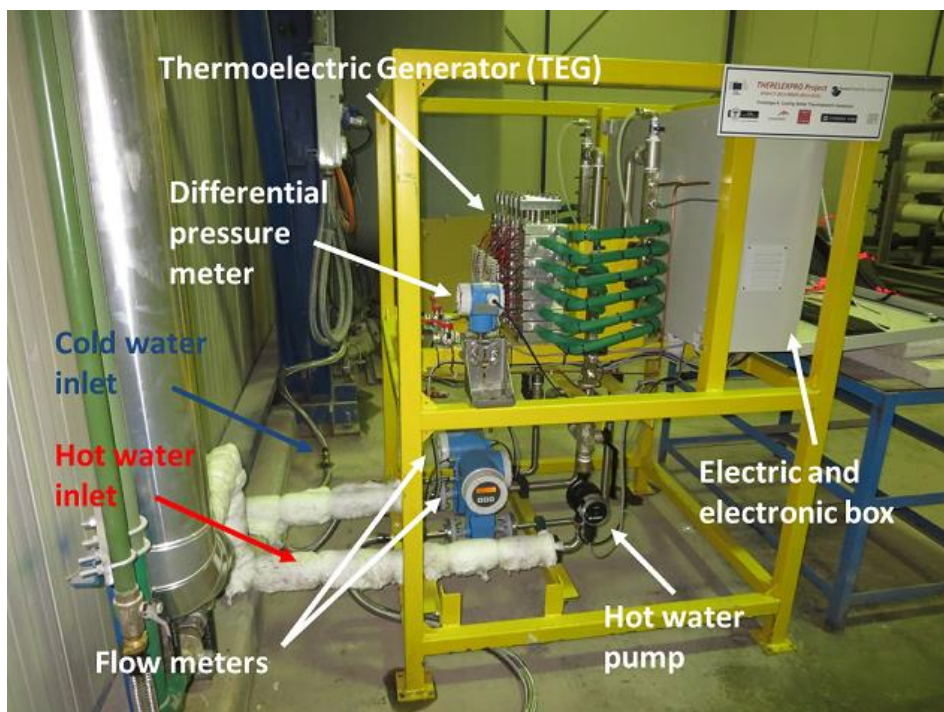
### **Deliverable D4.1: Design of the final configuration of the thermoelectric system (all partners)**

The present deliverable shows the final layout configuration of the two developed TEG prototypes. More details can be found in WP4 Task 4.1 "Design of the final specification".

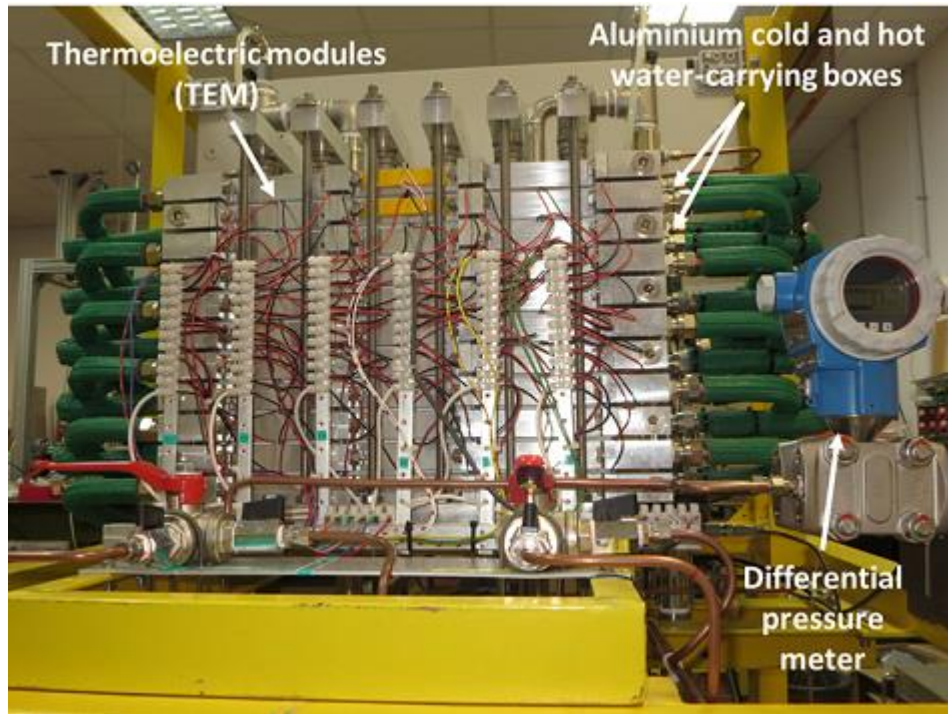
#### **A.8.1      Prototype A: final configuration**

Figure A.8.1.1 shows a photograph of prototype A in its final configuration at plant site. In the photo can be seen the main body of the TEG unit (Thermoelectric generator), the differential pressure meter used to measure the water pressure drop inside the unit, the two flow meters, the hot water pump, the electronic box and the connections with the hot water source and cold water sink. Figure A.8.1.2 shows a detail of the main body of the TEG unit.

Table A.8.1.1 shows the final specifications of the prototype A used for the design of the TEG unit.



**Figure A.8.1.1 – Prototype A: TEG unit final layout configuration**



**Figure A.8.1.2** – Prototype A: detail of the main body of the TEG unit

Variable	Unit	Value
Hot water flow rate & cold water flow rate	[m <sup>3</sup> /h]	0-2.5
Hot water inlet temperature at TEG	[°C]	70-85
Cold water inlet temperature at TEG	[°C]	10-20
Aluminium hot water box temperature at TEG central row and central vertical line.	[°C]	0-85
Aluminium cold water box temperature at TEG central row and central vertical line.	[°C]	0-85
Pressure drop through the TEG hot water circuit	[mbar]	0-100
Thermal power lost by hot water crossing the TEG	[W]	5000-10000
Thermal power absorbed by cold water crossing the TEG	[W]	5000-10000
Electric power produced by the TEG	[W]	0-100
Hot water electric pump power consumption	[W]	0-50

**Table A.8.1.1** – Prototype A: main design specifications

#### A.8.2      *Prototype B: final configuration*

Prototype B consists of 2 generators with 20 TE modules each. Figure A.8.2.1 to Figure A.8.2.4 show the assembly of a generator of prototype B. Figure A.8.2.1 shows the copper plate for the cold side of generator No. 1 with the marked fields for the installation of the TE modules. At the TE modules No. 1 and 13 the thermocouples for temperature measurement of the cold side of the modules can be seen. Figure A.8.2.2 shows the aluminium cooling plate/heat sink of generator No.

1 with the channel for the cooling water. Figure A.8.2.3 shows the copper plate for the cold side with the 20 TE modules. To increase the heat transfer from the TE modules to the copper plate a heat-conductive paste was used. Figure A.8.2.4 shows the completed generator No. 1, consisting of 20 TE modules, wiring and cooling water supply.

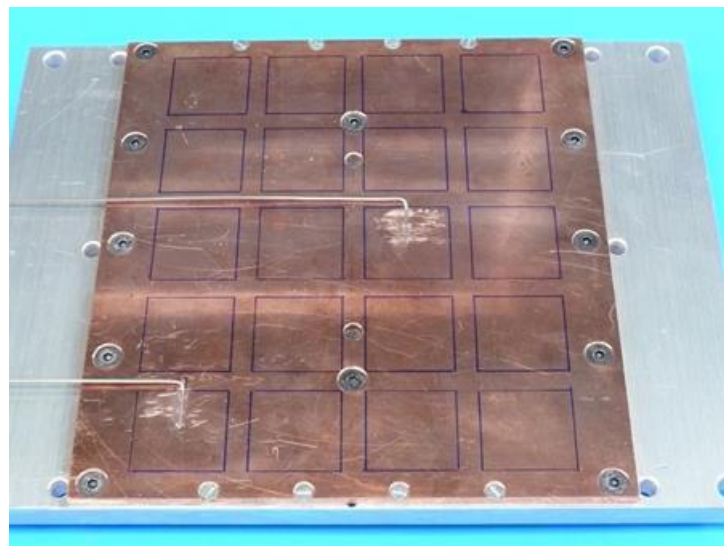


**Figure A.8.2.1** – Prototype B copper plates



**Figure A.8.2.2** – Prototype B: cooling plate/heat sink

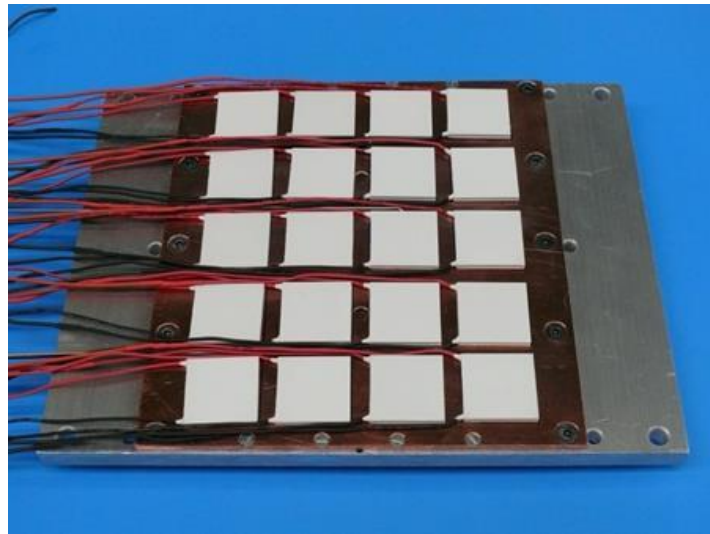


**Figure A.8.2.3** – Prototype B: thermoelectric modules assembling

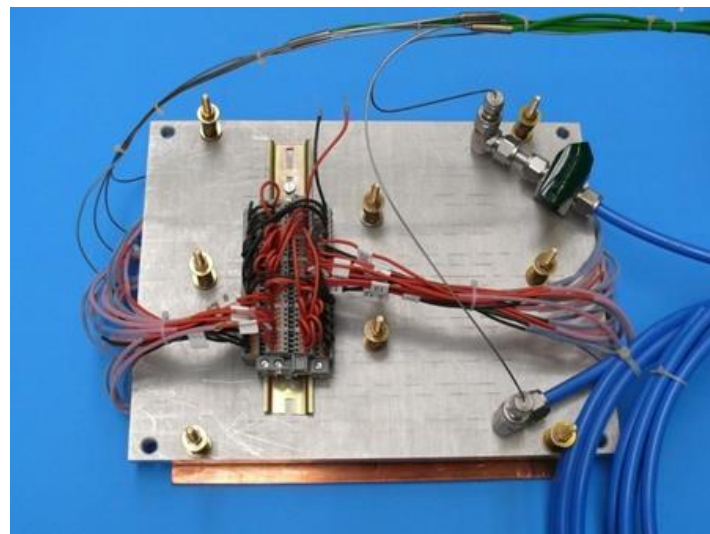


**Figure A.8.2.4** – Prototype B: thermoelectric generator completed

## **Annex A.9**

### **Deliverable D4.2: Description of the activities for the plant test set up (all partners)**

*The present deliverable shows a set of pictures taken during TEG prototypes installation at plant site. More details can be found in WP4 Task 4.2 "Plant installation of the full-scale thermoelectric systems modules".*

#### **A.9.1      Prototype A: set up of the TEG at plant site**

Prototype A was installed at Ferriere Nord plant in Osoppo (Udine) in January 2016. The installation of this prototype was very fast and simple. The installation do not requires any stop of the production plant. It requires only to flush water into the plant circuit before the connection with the device (to empty the pipelines from air) and then to connect the prototype water circuit with the plant water circuit.

Figure A.9.1.1 to Figure A.9.1.4 show the prototype A inside the service building after the connection with the pipelines.

Figure A.9.1.5 and Figure A.9.1.6 shows details of the pipeline connections.



**Figure A.9.1.1 – Prototype A: installed at Ferriere Nord plant site.**



**Figure A.9.1.2** - Prototype A: installed at Ferriere Nord plant site



**Figure A.9.1.3** - Prototype A: installed at Ferriere Nord plant site



**Figure A.9.1.4** - Prototype A: installed at Ferriere Nord plant site



**Figure A.9.1.5** - Prototype A: hot and cold water connections detail



**Figure A.9.1.6** - Prototype A: hot and cold water connections detail

#### **A.9.2      Prototype B: set up of the TEG at plant site**

Prototype B was installed at Arcelor Mittal plant in Gijon in October 2015. The installation of this prototype was much more complicated than the prototype A installation and required a stop of the production plant.

The entire installation was done during one day. First the equipment (prototype B, data acquisition system, wires and tubes, etc.) had to be transported to the plant, which is located several meters above ground level. Next steps were the installation of cooling water supply for the prototype as well as the power supply for the data acquisition system. The installation of the two generators of prototype B was done during a short standstill of the plant (approx. two hours). Before restarting the plant the generators were connected to the cooling water supply to avoid an overheating of the TE modules during the following connection of prototype measuring devices (thermocouples, cooling water flow measurement) to the data acquisition system. After that the commissioning of the data acquisition system and measuring equipment followed. A remote data transmission was installed, so that it was possible to continuously check the performance of the prototype. Last steps of the prototype commissioning were the installation of protecting sheets for the two generators and the protection of the measuring lines with tubes.

Below a set of pictures shows prototype B installed at plant site.

Figure A.9.1.1 and Figure A.9.2.2 show the prototype B generator No. 1 (left) and generator No. 2 (right) after installation on the plant ready to work. Figure A.9.2.3 shows the data acquisition system of prototype B. Figure A.9.2.4 shows the installed generators with the protecting sheets. Figure A.9.2.5 shows the front view of the prototype B with the copper plates of both generators painted black.

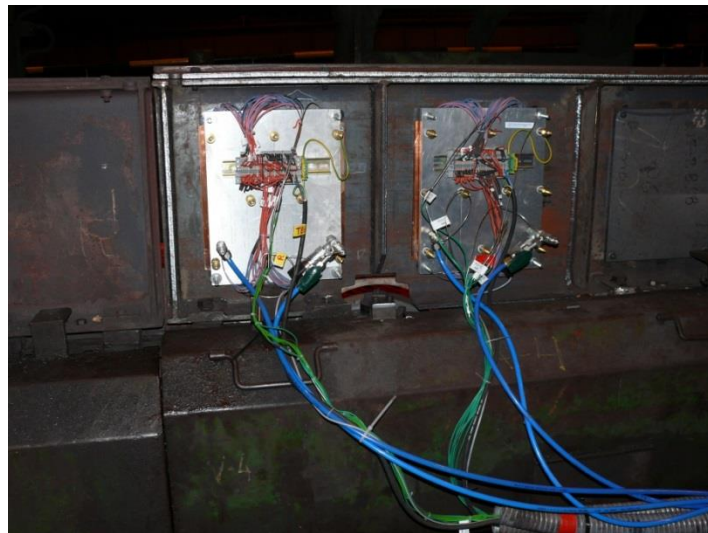


**Figure A.9.2.1** – Prototype B: generator No. 1 (left), generator No. 2 (right) after installation on the plant



**Figure A.9.2.2** - Prototype B: generators and protected measuring lines after installation on the plant

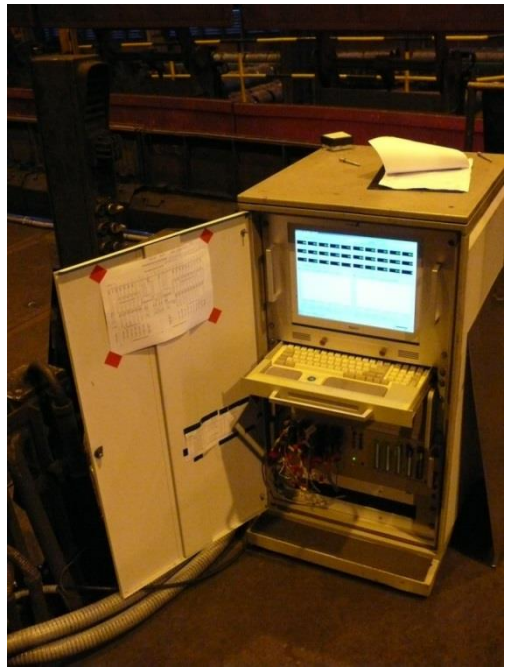


**Figure A.9.2.3** - Prototype B: data acquisition system



**Figure A.9.2.4** – Prototype B: protecting sheets



**Figure A.9.2.5** – Prototype B: front view during normal operation

## **Annex A.10**

### **Deliverable D5.1: Description of the full-scale test results (AME, FENO, CSM, BFI)**

The present deliverable summarizes within a table the main results obtained by means of the on-line full-scale tests. More details can be found in WP5 Task 5.1 "On-line full-scale test of the thermoelectric system prototypes" and WP5 Task 5.2 "Assessment of the thermoelectric system performance".

#### **A.10.1 Prototype A: full-scale test results table**

<b>Prototype A: full scale test main results</b>
At standard conditions prototype A works as a heat exchanger which transfers about 6500 W of thermal energy from the hot source to the cold sink producing about 40 W of electric power.
Considering the TEG as an heat engine, with a distance of the hot and cold source from the TEG unit of about 50 m (as in the case study), the measured electric conversion efficiency of prototype A is 0.33 % (40 W produced by the thermoelectric modules and 20 W consumed by the pumps).
Prototype A shows an electric energy conversion efficiency of about 0.61% when no energy is required to pump the water.
Assuming the distance of the hot and cold source from the TEG unit of about 100 m, the electric conversion efficiency of prototype A is 0 %.
A linear dependence of the TEG power with respect to the water temperature difference has been observed.
The power output of the thermoelectric system can be easily controlled through the control of the cold and hot water flow rate.
Thermoelectric power production and pump power consumption have a parabolic dependence with respect to the hot and cold water flow rate
Up to flow rates of 1.6-1.8 m3/h the system is able to produce net power. At higher values the pumps have a power consumption higher than the TEG power production.
The maximum net power was obtained at about 1 cubic meter per hour.
The Maximum Power Point (maximum electrical power) of each column was obtained with an electric resistance load of $3 \Omega$ (10 thermoelectric modules in series).
No particular damage was observed after disassembling of the device.

#### **A.10.2 Prototype B: full-scale test results table**

<b>Prototype B: full scale test main results</b>
Blackening of the hot generator surface (copper plate) resulted in a substantial increase in the achievable performance by up to 200%.
With generators not painted the electrical power was lower than 2 W for approximately 80 % of the time, with generators painted the period with an electrical power below 2 W was halved and the period with an electrical power of more than 5 W was multiplied.
Heat transfer from the copper plate to the TE modules was improved at Generator No. 2 by using more heat-conductive paste.
Electric contact of the TE modules to the copper plates was improved due to using more screws
Automatic stop of the cooling water supply during longer standstills of the hot wire rod resulted in an increase of the cooling water temperature inside of the generators occurred by absorbing residual heat.
Overheating of both generators with temperatures $> 300^\circ\text{C}$ caused several damages, resulting in the slump of the generators performance and the termination of the full scale test after a testing period of 6 weeks; main damages:

- Melting of all soldering's that connect the wires to the modules → destruction of all TEGs.
- black discoloration indicate damages between the insulating layer and the TE material
- flaking of the black paint

Derived major improvements for prototype B:

- overheating protection by using for the heat transfer to the hot side of the TEG a heat storage plate which is filled with a PCM, extraction of the waste heat and heat transfer to the TEG via heat pipes or automatic distance control system between the generator and the heat source
- improvement of the adhesion of the black paint through a prior surface treatment of the copper plate
- to prevent fouling through dust deposits a housing of the generator could be necessary

## Annex A.11

### **Deliverable D5.2: Thermoelectric system performance analysis (AME, FENO, CSM, CU)**

The present deliverable summarizes within a table the most important thermoelectric systems performance analysis. Other details can be found in WP5 Task 5.1 "On-line full-scale test of the thermoelectric system prototypes" and WP5 Task 5.2 "Assessment of the thermoelectric system performance".

#### **A.11.1 Prototype A: performance analysis table**

Variable	Unit	Value	Variable	Unit	Value
Hot water flow rate & cold water flow rate	[m <sup>3</sup> /h]	1	Pressure drop through the TEG hot water circuit	[mbar]	22.5
Hot water inlet temperature at TEG	[°C]	76.9	Thermal power lost by hot water crossing the TEG	[W]	6463
Hot water outlet temperature at TEG	[°C]	70.1	Thermal power absorbed by cold water crossing the TEG	[W]	6154
Cold water inlet temperature at TEG	[°C]	11.5	Electric power produced by the TEG	[W]	38.8
Cold water outlet temperature at TEG	[°C]	17.5	TEG electric conversion efficiency (without electric pump power consumption)	[%]	0.6
Aluminium hot water box temperature at TEG central row and central vertical line.	[°C]	65.4	Hot water electric pump power consumption	[W]	8.7
Aluminium cold water box temperature at TEG central row and central vertical line.	[°C]	29.9	Lost thermal power (mainly radiation)	[W]	270.1
Aluminium hot water box temperature at TEG upper row and central vertical line.	[°C]	62.8	Net electric power produced by the TEG (assuming total pump power consumption as double of hot water electric power consumption)	[W]	21.3
Aluminium cold water box temperature at TEG upper row and central vertical line (extemal box)	[°C]	20.2	TEG electric conversion efficiency (including electric pumps power consumption)	[%]	0.33

**Table A.11.1.1** – Summary of prototype A performances

#### **A.11.2 Prototype B: performance analysis table**

Measurement type	Unit	Value	Test description
Electric power	W	12	Generator No.1, temperature difference 80°C, not painted
Electric power	W	12	Generator No.1, temperature difference 80°C, painted
Electric power	W	18	Generator No.2, temperature difference 80°C, not painted
Electric power	W	18	Generator No.2, temperature difference 80°C, painted
Electric power	W	22	Generator No.1, temperature difference 120°C, not painted
Electric power	W	22	Generator No.1, temperature difference 120°C, painted
Electric power	W	-	Generator No.2, temperature difference 120°C, not painted
Electric power	W	35	Generator No.2, temperature difference 120°C, painted
Electric power	W	25	Generator No. 1, maximum measured electric power:, temperature difference 125°C, painted
Electric power	W	56	Generator No. 2, maximum measured electric power:, temperature difference 160°C, painted
Efficiency	%	0.4	Generator No. 1, average temperature difference 30 -

			50°C, not painted
Efficiency	%	0.5	Generator No. 1, average temperature difference 30 - 50°C, painted
Efficiency	%	0.6	Generator No. 2, average temperature difference 30 - 50°C, not painted
Efficiency	%	0.8	Generator No. 2, average temperature difference 30 - 50°C, painted
Efficiency	%	1.2	Generator No. 1, average temperature difference 70 - 100°C, not painted
Efficiency	%	1.4	Generator No. 1, average temperature difference 70 - 100°C, painted
Efficiency	%	1.7	Generator No. 2, average temperature difference 70 - 100°C, not painted
Efficiency	%	2.1	Generator No. 2, average temperature difference 70 - 100°C, painted
Efficiency	%	1.8	Generator No. 1, maximum reached efficiency, average temperature difference > 100°C, painted
Efficiency	%	2.8	Generator No. 2, maximum reached efficiency, average temperature difference > 100°C, painted
Voltage	V	12.6	Generator No. 1, maximum measured voltage, temperature difference 125°C, painted
Voltage	V	18.6	Generator No. 2, maximum measured voltage, temperature difference 160°C, painted
Current	A	2.0	Generator No. 1, maximum measured current, temperature difference 125°C, painted
Current	A	3.0	Generator No. 2, maximum measured current, temperature difference 160°C, painted

**Table A.11.2.1** - Summary of prototype B performances

## Annex A.12

### **Deliverable D5.3: Thermoelectric system economic viability analysis (AME, FENO, CSM, CU)**

#### **A.12.1 “cost-per-watt” analysis of TEG modules**

Economic analysis of commercially available thermoelectric power generation modules was performed. The aim of this analysis was to determine “cost-per-watt” of modules from several different suppliers which gives an indication of their performance in terms of module fabrication cost. These results can be used as a reference for selection of modules for thermoelectric power generation systems for waste heat recovery from steel production processes.

Firstly, experiments were carried out to evaluate the performance of modules from major suppliers around the world at various different  $\Delta T$ s. The experiments involved obtaining I-V characteristics and determining the  $P_{max}$  and  $Z_{eff}T$  at different  $\Delta T$ s. The measurements were done in the vacuum chamber at a pressure of around  $1 \times 10^{-6}$  mbar. The interface material used was silicon thermal paste,  $\lambda = 2.9 \text{ W}\cdot\text{m}^{-1}\cdot\text{K}^{-1}$ . All the modules were  $40 \times 40 \text{ mm}^2$  in size, the thermoelectric material was  $\text{Bi}_2\text{Te}_3$  and the number of thermoelements (legs) was 254 in each module. The modules were procured from Custom Thermoelectric (US), European Thermodynamics Ltd. (ETL) (UK), Ferrotech Nord (Germany), Eureka (Germany), Melcor (Russia) and Quick Ohm (Sweden). Unlike all other manufacturers, Custom Thermoelectric only sell modules which are made up using the non-conventional method which is explained in Sec. 2.1.3.4.

The  $P_{max}$  as a function of  $\Delta T$  for all the modules tested is shown in Figure A.12.1.1. It can be seen that the module supplied by Eureca generated the highest power, followed by Ferrotech Nord, ETL, Quick Ohm and Melcor. The low power output of the module from Custom Thermoelectric can be attributed to the non-conventional construction of the module resulting in poor heat transfer. The Custom Thermoelectric module showed a trend of increasing power output with temperature which was further confirmed by performing a comparison of power output of ETL (constructed using traditional method) and Custom Thermoelectric (constructed using non-traditional method) at high  $\Delta T$ s.

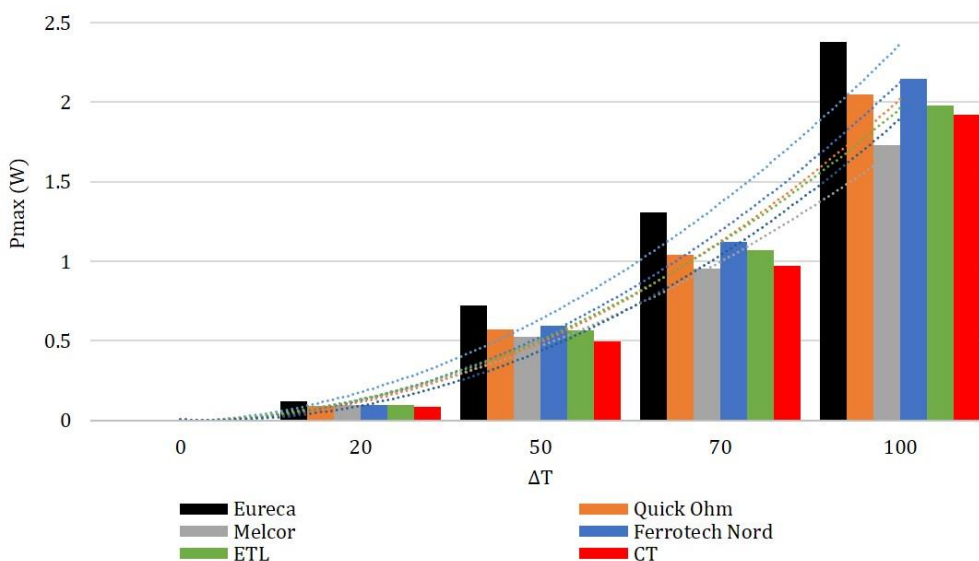


**Figure A.12.1.1 – Maximum power output as a function of temperature difference for various suppliers in EU and US**

Figure A.12.1.2 shows power generated by Custom Thermoelectric and ETL modules, it is clear from this graph that the ETL module generated more power than Custom Thermoelectric at  $\Delta T$  of up to 150 K. However, as the  $\Delta T$  was further increased, the Custom Thermoelectric module outperformed ETL. The reason of higher performance from Custom Thermoelectric module can be attributed to the fact that at higher temperatures the thermal expansion of the thermoelements resulted in improved thermal contacts by elimination of the air gaps.

The  $Z_{eff}T$  of these modules was also determined at different temperature differences using the open-short circuit technique, the results are shown in Figure A.12.1.3. The values of  $Z_{eff}T$  of module from Ferrotech nord and ETL was highest among all - between 0.6 and 0.7. The  $Z_{eff}T$  measured of Melcor, Quick Ohm and Eureka was between 0.5 and 0.6. The lowest value of  $Z_{eff}T$  was shown by Custom Thermoelectric module. (It should be noted that the  $Z_{eff}T$  measurement of module from Custom

Thermoelectric is unreliable due to inaccuracy in  $\Delta T$  measurements because of air gaps in the module structure due to its unconventional design. Using I-V curve method ( $Z_{efT} = \frac{I_A}{I_Q} - 1$ ), this module's  $Z_{efT}$  is around 0.50).

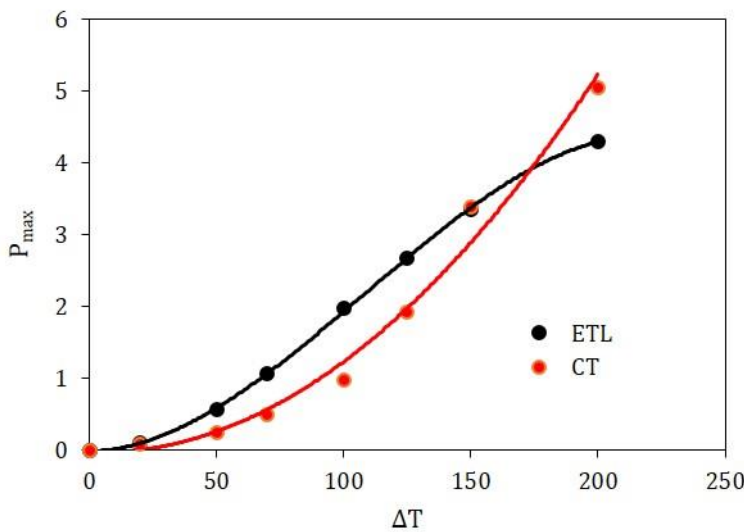


**Figure A.12.1.2** – Maximum power output as a function of temperature difference for ETL and Custom thermoelectric modules

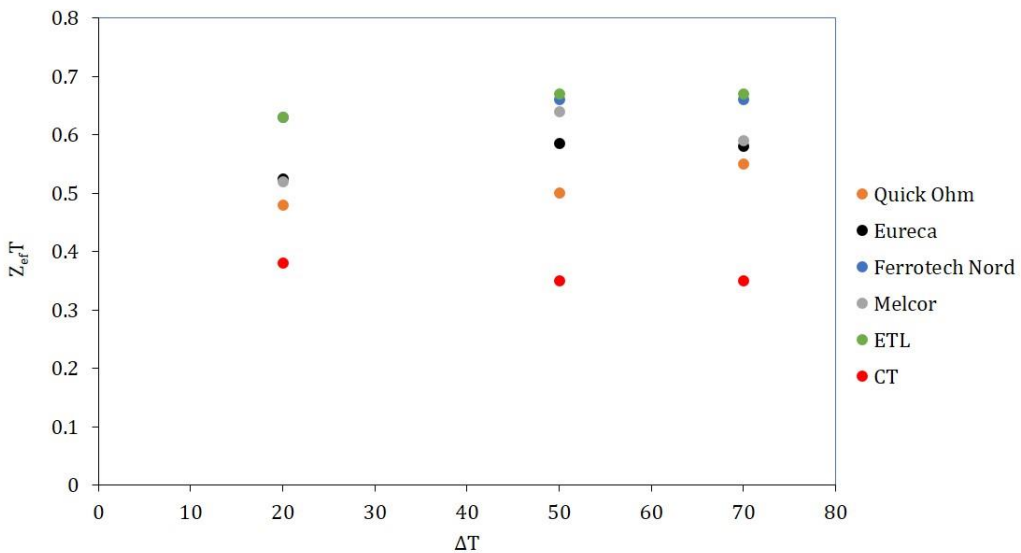


**Figure A.12.1.3** – Effective figure-of-merit at different temperature differences

It can be concluded from the results reported above that the modules from ETL and Ferrotech nord seems to generate electrical power which is in the high end of the range and also have the highest  $Z_{efT}$  among other modules, therefore these modules are ideal candidates for waste heat recovery at low temperatures ( $\Delta T < 150$  K). The performance of Eureca module is also promising, it showed the highest power output and a reasonable  $Z_{efT}$ . Higher  $Z_{efT}$  of these modules indicate good thermoelectric material quality and also suggests that these modules should have high efficiency as compared to modules with low  $Z_{efT}$ . Also, these three modules are constructed with conventional method, and hence does not require huge compression force which makes their implementation in the system simple. The modules from Custom Thermoelectric seems to be ideal for high temperature applications,  $\Delta T$  above 150 K, because of their high power output at elevated temperatures and reduced probability of mechanical breakdown of legs due to thermal expansion. The gap between the legs and ceramic plate facilitates the thermal expansion of the elements, making them more reliable at higher temperatures than the modules which are constructed with traditional method.

Secondly, after obtaining performance data of modules, their manufacturing cost was considered. The TEG modules from major suppliers based in Europe, US and China have been evaluated. Quotation of modules were obtained for different order quantities. The table below shows the unit price of modules for different order quantities. It should be noted that additional costs, such as shipping and taxes, have not been considered in this analysis.

Supplier	Supplier based in:	Price (€/TEM)				
		OQ=1	OQ=10	OQ=50	OQ=100	OQ=300
Eureca	Germany	66.27	46.97	34.06	21.58	18.48
Quick Ohm	Sweden	33.33	28.84	19.63	16.74	16.74
Ferrotech Nord	Germany	53.18	42.76	36.42	31.22	27.31
Custom Thermoelectrics	US	36.34	31.02	27.7	26.37	26.37
European Thermodynamics Ltd	UK	46.26	44.47	38.15	33.63	33.63
Wellentech	China	5.23	4.52	4.52	4.34	4.34
Everredtronics	China	10.37	10.37	9.75	8.86	8.86
Z-max	China	14.32	14.32	8.6	8.6	6.02

**Table A.12.1.1** - Cost per unit of modules from different suppliers around the world

It can be seen in the Table A.12.1.1 that the unit cost of modules differ significantly with the number of units ordered. For instance, the cost of Eureca module is around 2.5 times lower when the order quantity is increased from 10 to 300, similar trend can be seen in all suppliers. There is a significant difference in the unit cost of module from suppliers based in China and other EU/US. Wellentech, based in China, has quoted the lowest unit price among other Chinese suppliers, whereas Z-max has quoted the highest price. The supplier Quick Ohm have quoted the lowest price among EU suppliers. It is interesting to note that many EU/US based suppliers sell modules which are made in China. Based on the high cost of modules from EU/US suppliers and the fact that these suppliers obtain the modules from Chinese manufacturers, it would be economic to procure the modules directly from a reliable Chinese manufacturer.

The cost-per-watt of modules for different order quantities and temperature differences is shown in the Figure A.12.1.4. In this analysis, three order quantities have been considered: 10, 100 and 300; and the  $\Delta T$ s considered are 100 K, 125 K, 150 K and 200 K. It should be noted here that the modules from China have not been characterised by us. The power generation data for these Chinese origin modules is taken from the average of EU and US modules for each  $\Delta T$ . For instance, the power output considered for Z-max module at 100 K  $\Delta T$  is the average power output of ETL, Ferrotech nord, Eureca, Custom Thermoelectric and Quick Ohm modules at 100 K  $\Delta T$ . Also, the modules from Eureca, Quick Ohm and Ferrotech are rated for low temperature applications and hence, their performance data above 125 K  $\Delta T$  is not available.

It can be seen in the graph that the cost-per-watt of modules is highly dependent on the order quantity (OQ) and  $\Delta T$ . It decreases with increase in the order quantity and  $\Delta T$ . For instance, the cost-per-watt of ETL module decreases from 22.49 to 17.01 €/W when the order quantity is increased from 10 to 300. Similarly, the cost-per-watt for ETL module decreases from 17.01 to 7.82 €/W (for order quantity 300) when the  $\Delta T$  is increased from 100 to 200 K. The ETL module seems to have the highest cost-per-watt among the EU and US modules. Up-to a temperature difference of 125 K and order quantity of 300 units, the modules from Eureca and Quick Ohm have the lowest. Overall, the cost-per-watt seems to be high for the modules from EU and US suppliers and might not be ideal candidates for waste heat recovery when compared with modules from Chinese suppliers. The cost-per-watt of modules from China is the lowest, in-fact it is less than a euro for the modules from Wellentech. The modules from Z-max have the highest cost-per-watt among the Chinese suppliers, which is lower than the EU and US modules. It can be recommended from the cost-per-watt analysis that the modules should be procured from a reliable Chinese manufacturer directly, and if possible in large quantities, and efforts should be made to improve the power output from the system which would result in lower cost-per-watt of modules.

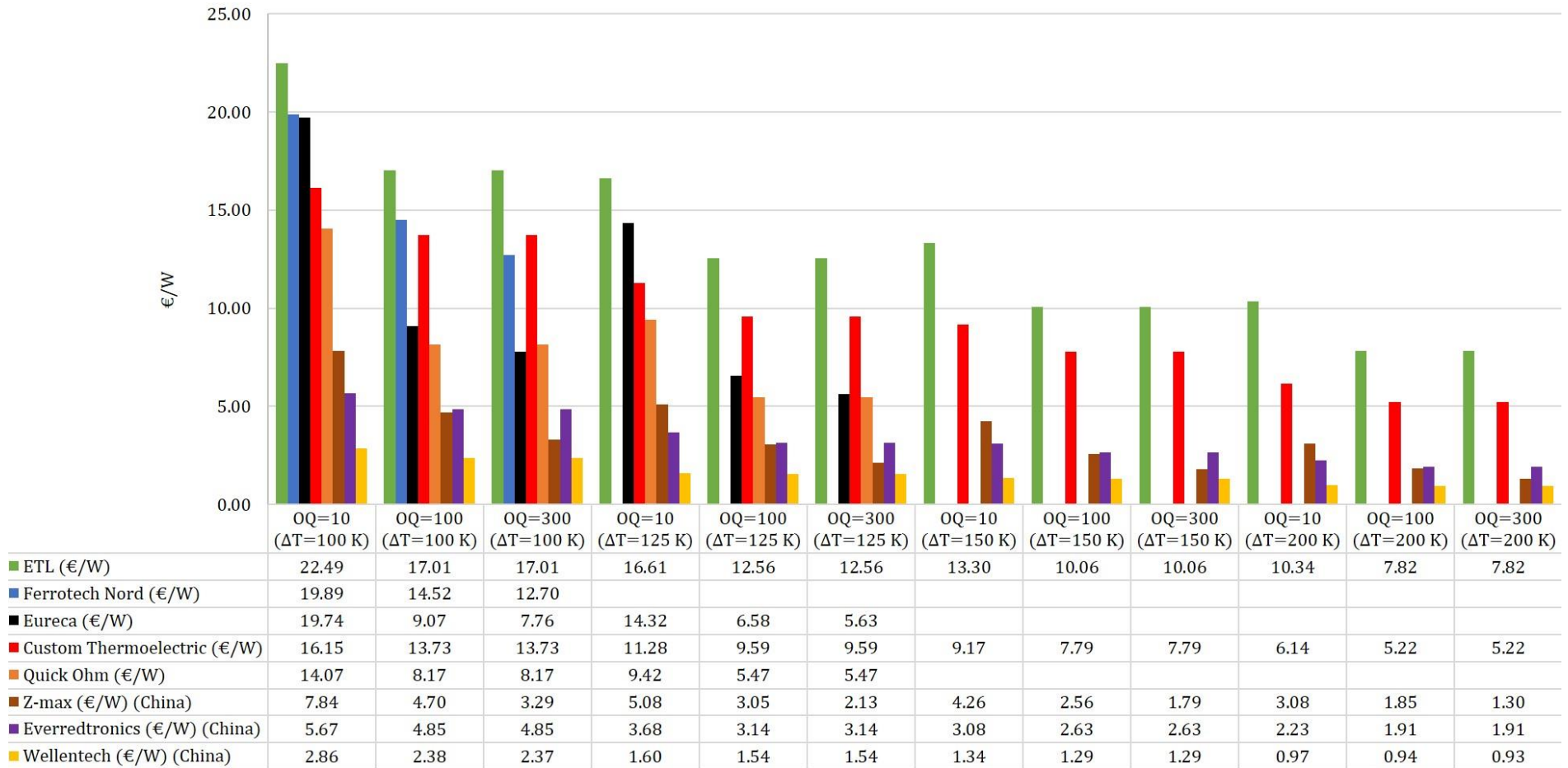


**Figure A.12.1.4** - cost-per-watt of modules at different temperature differences and order quantities for various different suppliers

## Annex A.13

### **Deliverable D5.4: Thermoelectric system environmental benefit analysis (AME, FENO, CSM, CU)**

The present deliverable reports the Life Cycle Analysis (LCA) carried out to evaluate the environmental benefit and impact related with the production of a number of thermoelectric generators, similar to the prototype A and B, manufactured in large number to produce electric energy.

#### **Goal definition**

The goal of this study is to determine the environmental cost, in terms of climate change, fossil depletion, acidification potential, eutrophication, human toxicity, and ozone layer depletion, of a massive production of the two prototypes developed in the present research.

#### **Scope definition**

The functional unit for this study was set differently for the two prototypes.

Prototype A can be considered a cooling system in substitution of a traditional heat exchanger and fan coolers. This cooling system must be able to discharge 18 MW of thermal heat from EAF off-gases, as required by Ferriere Nord plant. Starting from this assumption, the number of prototype A, required to discharge 18 MW into the cooling water, is 2750. These TEGs are able, at once, to produce 55 kW of electric power.

For comparison reasons, it has been assumed to produce the same electric power (55 kW) using a number of TEGs of prototype B. Therefore, without any relationship with a particular plant requirement. As the average net power of the two TEG system is the same, also the number of TEGs of type B, required to produce 55 kW, is the same, i.e. 2750 TEGs.

Therefore, the LCA analysis has been carried out considering the production of a set of 2750 TEGs of each type, i.e. the "target amount" of the LCA analysis is 2750.

Table A.13.1 shows the main data concerning each group of TEGs assumed as "production".

Prototype A	
Total thermal energy dissipati	[MW]
Thermal energy dissipated by	[W]
Number of TEGs required	
Electric power of each TEG	[W]
Total electric power available	[kW]

Prototype B	
Total thermal energy dissipati	[MW]
Thermal energy dissipated by	[W]
Number of TEGs required	
Electric power of each TEG	[W]
Total electric power available	[kW]

**Table A.13.1** - Main data concerning each group of TEGs used as "target amount" to carry out the Life Cycle Assessment analysis.

The transport processes were assumed similar for both the groups of devices. Thermoelectric modules were assumed manufactured in China, and then transported to Europe for their assembling with the whole TEGs devices, and their consequent installation. Even the disposal of the devices is assumed in Europe.

#### **Inventory analysis**

OpenLCA software version 1.5.0 (<http://www.openlca.org/>) was used to model the inventory analysis and impact assessment. All the data used in this study are from the ELCD (European reference Life Cycle Database) 3.2 database (<https://nexus.openlca.org/databases>). Data were selected to represent the average market consumption mix.

Each TEG prototype has been deeply analysed to define material, electricity and transportation used for their manufacture. Table A.13.2 shows the result of this analysis. At first, the flows making up a single thermoelectric module (TEM) was analysed. Both the two types of TEM used in the different TEG devices have been sectioned to verify materials and weight of each component (tables on the top). Then it was done a similar analysis considering the whole thermoelectric generator (tables on the bottom).

These data have been used to fill the "flows" in the openLCA software (see Figure A.13.1 for prototype A, and Figure A.13.2 for prototype B). After definition and quantification of "flows", a

new “process” was set up, defining the characteristics of the production method. After that was set the “target amount”, that is the number of items (TEGs) that will be manufactured during the production. In our case the number of TEGs that must be produced is 2750 items for each production set.

Flow	Unit	Amount
<i>Prototype A</i>		
<i>Materials required to manufacture 60 TEMs</i>		
Bismuth (TEMs)	[kg]	0.433
Tellurium (TEMs)	[kg]	0.4
Copper sheet (TEMs)	[kg]	0.717
Zinc (TEMs)	[kg]	0.826
Ceramic (TEMs)	[kg]	1.77
Silicone rubber (TEMs)	[kg]	0.06
copper wires (TEMs)	[kg]	0.15
PVC wires (TEMs)	[kg]	0.05

Flow	Unit	Amount
<i>Prototype B</i>		
<i>Materials required to manufacture 40 TEMs</i>		
Bismuth (TEMs)	[kg]	0.1276
Tellurium (TEMs)	[kg]	0.1178
Copper sheet (TEMs)	[kg]	0.2408
Zinc (TEMs)	[kg]	0.0000
Ceramic (TEMs)	[kg]	0.3037
Silicone rubber (TEMs)	[kg]	0.0198
copper wires (TEMs)	[kg]	0.3122
PVC wires (TEMs)	[kg]	0.1041

Materials requires to manufature 1 TEG		
Aluminium extrusion profile	[kg]	50
Bismuth	[kg]	0.433
Copper sheet	[kg]	0.717
Copper tube	[kg]	10
Copper wire	[kg]	5
electricity Mix	[MJ]	172.8
Polyethylene (PE-HD)	[kg]	1.5
Polyvinylchloride (PVC)	[kg]	1.5
Steel sections	[kg]	50
Tellurium (TEMs)	[kg]	0.4
Transport (t*km)	[t*km]	1500
Water desalinated	[kg]	100
Zinc (TEMs)	[kg]	0.826

Materials requires to manufature 1 TEG		
Aluminum plate	[kg]	6.9372
Bismuth	[kg]	0.12761
Copper sheet	[kg]	0.240753
Copper plates	[kg]	13.5208
Copper wire	[kg]	0.3122
electricity Mix	[MJ]	172.8
Polyethylene (PE-HD)	[kg]	0.52
Polyvinylchloride (PVC)	[kg]	
Steel sections	[kg]	1.831
Tellurium (TEMs)	[kg]	0.1178
Transport (t*km)	[t*km]	1500
Water desalinated	[kg]	100
Zinc (TEMs)	[kg]	0

**Table A.13.2** – Flows definition of Prototype A and B

## Process: TEG Production - type A

### ▼ Inputs

Flow	Category	Amount	Unit
F <sub>0</sub> aluminium extrusion profile	Materials production/Metals and semi...	50.00000	kg
F <sub>0</sub> Aluminum oxide (alumina)	Production residues in life cycle/Waste ...	1.77000	kg
F <sub>0</sub> Bismuth	Resource/in ground	0.43300	kg
F <sub>0</sub> Copper sheet	Materials production/Metals and semi...	0.71700	kg
F <sub>0</sub> copper tube	Materials production/Metals and semi...	10.00000	kg
F <sub>0</sub> Copper wire	Metals and semimetals/Metals	5.15000	kg
F <sub>0</sub> electricity mix	Energy carriers and technologies/Electri...	172.80000	MJ
F <sub>0</sub> polybutadiene granulate (PB)	Materials production/Plastics	0.06000	kg
F <sub>0</sub> polyethylene high density granul...	Materials production/Plastics	1.50000	kg
F <sub>0</sub> polyvinylchloride resin (B-PVC)	Materials production/Plastics	1.55000	kg
F <sub>0</sub> process water	Materials production/Water	100.00000	kg
F <sub>0</sub> Steel sections	Materials production/Metals and semi...	50.00000	kg
F <sub>0</sub> Tellurium	Resource/in ground	0.40000	kg
F <sub>0</sub> transport in t*km	Transport services/Other transport	1500.00000	t*km
F <sub>0</sub> Zinc	Resource/in ground	0.82600	kg

**Figure A.13.1** – Flows input for production of one TEG, prototype A

## Process: TEG Production - type B

### ▼ Inputs

Flow	Category	Amount	Unit
F <sub>0</sub> aluminium sheet	Materials production/Metals and semi...	6.93720	kg
F <sub>0</sub> Aluminum oxide (alumina)	Production residues in life cycle/Waste...	0.30370	kg
F <sub>0</sub> Bismuth	Resource/in ground	0.12760	kg
F <sub>0</sub> Copper sheet	Materials production/Metals and semi...	0.24075	kg
F <sub>0</sub> copper sheet	Materials production/Metals and semi...	13.52080	kg
F <sub>0</sub> copper wire	Materials production/Metals and semi...	0.31220	kg
F <sub>0</sub> electricity mix	Energy carriers and technologies/Elect...	172.80000	MJ
F <sub>0</sub> polybutadiene granulate (PB)	Materials production/Plastics	0.01980	kg
F <sub>0</sub> polyethylene high density granulat...	Materials production/Plastics	0.52000	kg
F <sub>0</sub> polyvinylchloride resin (B-PVC)	Materials production/Plastics	0.10410	kg
F <sub>0</sub> process water	Materials production/Water	100.00000	kg
F <sub>0</sub> Steel sections	Materials production/Metals and semi...	1.83100	kg
F <sub>0</sub> Tellurium	Resource/in ground	0.11794	kg
F <sub>0</sub> transport in t*km	Transport services/Other transport	1500.00000	t*km

**Figure A.13.2** – Flows input for production of one TEG, prototype B

## Impact assessment

The Life Cycle Impact Assessment (LCIA), or “impact assessment” only, is that part of the Life Cycle Assessment deputy to understand and evaluate the impact of the production system, throughout its life cycle, on the environment. OpenLCA software calculates the “impact assessment” on the basis of the “flows” and the “production sets” defined. In this section is required to define a specific “method” to make this calculation, i.e. the “Impact Assessment Method” (LCIA method). In this project the CML method has been used which was created by the University of Leiden in the Netherlands in 2001 and continuously updated. After this step, if the software has been correctly filled with all the required data, the calculation is very fast and results are shown in form of data tables and pie charts.

Figure A.13.3 shows the general information concerning the calculation properties used for the two production systems. As can be observed from this figure, both simulations have been carried out using the same “target amount” of TEG production (2750 items) and CML impact assessment method.

Results of TEG Production - type A		Results of TEG Production - type B	
▼ General information		▼ General information	
Product system	TEG Production - type A	Product system	TEG Production - type B
Allocation method	None	Allocation method	None
Target amount	2750.0 Item(s) TEG_PrototypeA	Target amount	2750.0 Item(s) TEG_PrototypeB
Impact assessment method	CML (baseline)	Impact assessment method	CML (baseline)

**Figure A.13.3 – General information on LCA calculation**

### Life cycle interpretation

In this phase of LCA, the “inventory analysis” and the “impact assessment” results are evaluated in relation with the “goal” and “scope definitions”. This part also contains conclusions and recommendations.

Figure A.13.4 and Figure A.13.5 shows the result of the “inventory analysis” concerning the production of 2750 TEGs of type A and B. The figures are shown in order of amounts (due to space reason only the first are shown). These data show the amount of materials or energy required or produced to carry out the production of the whole set of TEGs.

Flow	Inputs	Category	Sub-category	Unit	Amount
F <sub>o</sub> hard coal; 26.3 MJ/kg		Resource	in ground	MJ	2.92965E6
F <sub>o</sub> natural gas; 44.1 MJ/kg		Resource	in ground	MJ	2.89836E6
F <sub>o</sub> Water, surface		Resource	in water	kg	2.57851E6
F <sub>o</sub> crude oil; 42.3 MJ/kg		Resource	in ground	MJ	2.41745E6
F <sub>o</sub> Air		Resource	in air	kg	1.81142E6
F <sub>o</sub> Uranium		Resource	in ground	MJ	1.75327E6
F <sub>o</sub> Metamorphous rock, graphite cont...		Resource	in ground	kg	1.56226E6
F <sub>o</sub> Energy, primary, from water power		Resource	in water	MJ	1.54004E6
F <sub>o</sub> Water, ground		Resource	in water	kg	8.16124E5
F <sub>o</sub> Water		Resource	in water	kg	6.47924E5
F <sub>o</sub> brown coal; 11.9 MJ/kg		Resource	in ground	MJ	4.25289E5
F <sub>o</sub> Water (fresh water)		Resource	in water	kg	1.88047E5
F <sub>o</sub> Energy, primary, from solar energy		Resource	in air	MJ	1.05389E5
F <sub>o</sub> Bauxite		Resource	in ground	kg	8.51810E4
F <sub>o</sub> Iron		Resource	in ground	kg	6.76732E4
F <sub>o</sub> Energy, primary, from wind power		Resource	in air	MJ	3.86815E4
F <sub>o</sub> Carbon dioxide, in air		Resource	in air	kg	1.19747E4
F <sub>o</sub> Sodium chloride		Resource	in ground	kg	9274.30538
F <sub>o</sub> Calcium carbonate, in ground		Resource	in ground	kg	9053.68209
F <sub>o</sub> Dolomite, in ground		Resource	in ground	kg	7076.22529
Flow	Outputs	Category	Sub-category	Unit	Amount
F <sub>o</sub> Krypton-85		Emission to air	unspecified	kBq	1.32658E8
F <sub>o</sub> Hydrogen-3, Tritium		Emission to water	fresh water	kBq	5.24284E6
F <sub>o</sub> Heat, waste		Emission to air	unspecified	MJ	2.70852E6
F <sub>o</sub> Radon-222		Emission to air	unspecified	kBq	1.93227E6
F <sub>o</sub> Overburden (deposited)		Deposited goods	Stockpile goods	kg	1.75598E6
F <sub>o</sub> Air, used		Emission to air	unspecified	kg	1.59075E6
F <sub>o</sub> Water vapour		Emission to air	unspecified	kg	8.45296E5
F <sub>o</sub> Carbon dioxide		Emission to air	unspecified	kg	6.67367E5
F <sub>o</sub> Heat, waste		Emission to water	fresh water	MJ	3.70767E5
F <sub>o</sub> Radium-226		Emission to water	fresh water	kBq	5.84968E4
F <sub>o</sub> Red mud (dry)		Production residue...	Hazardous waste f...	kg	2.47595E4
F <sub>o</sub> Xenon-133		Emission to air	unspecified	kBq	1.76833E4
F <sub>o</sub> Hydrogen-3, Tritium		Emission to air	unspecified	kBq	1.52722E4
F <sub>o</sub> Water for industrial use		Materials production	Water	kg	1.08977E4
F <sub>o</sub> slag (unspecified)		Wastes	Production residues	kg	8127.23921
F <sub>o</sub> Argon-41		Emission to air	unspecified	kBq	7831.98005
F <sub>o</sub> Xenon-135		Emission to air	unspecified	kBq	5832.22497
F <sub>o</sub> Carbon-14		Emission to air	unspecified	kBq	3580.70616
F <sub>o</sub> spoil (unspecified)		Wastes	Mining waste	kg	3231.05377
F <sub>o</sub> Carbon monoxide		Emission to air	unspecified	kg	3151.02056

**Figure A.13.4** - Inventory result input/output of prototypes A production

Flow	Inputs	Category	Sub-category	Unit	Amount
F <sub>o</sub> crude oil; 42.3 MJ/kg		Resource	in ground	MJ	1.66836E6
F <sub>o</sub> Water, surface		Resource	in water	kg	1.05050E6
F <sub>o</sub> Energy, primary, from water power		Resource	in water	MJ	8.45721E5
F <sub>o</sub> natural gas; 44.1 MJ/kg		Resource	in ground	MJ	6.26422E5
F <sub>o</sub> Air		Resource	in air	kg	4.66549E5
F <sub>o</sub> Uranium		Resource	in ground	MJ	4.53290E5
F <sub>o</sub> Metamorphous rock, graphite conta...		Resource	in ground	kg	3.59878E5
F <sub>o</sub> hard coal; 26.3 MJ/kg		Resource	in ground	MJ	3.55293E5
F <sub>o</sub> Water, ground		Resource	in water	kg	3.52064E5
F <sub>o</sub> brown coal; 11.9 MJ/kg		Resource	in ground	MJ	1.37387E5
F <sub>o</sub> Water		Resource	in water	kg	2.13411E4
F <sub>o</sub> Bauxite		Resource	in ground	kg	2.03791E4
F <sub>o</sub> Energy, primary, from solar energy		Resource	in air	MJ	9028.20780
F <sub>o</sub> Water (fresh water)		Resource	in water	kg	6886.27059
F <sub>o</sub> Calcium carbonate, in ground		Resource	in ground	kg	5406.34147
F <sub>o</sub> wood; 14.7 MJ/kg		Resource	biotic	MJ	5179.01876
F <sub>o</sub> Energy, primary, from wind power		Resource	in air	MJ	4709.80658
F <sub>o</sub> Aggregate, natural		Resource	in ground	kg	2840.83645
F <sub>o</sub> Sodium chloride		Resource	in ground	kg	2712.15366
F <sub>o</sub> Iron		Resource	in ground	kg	2659.31831
			11		
Flow	Outputs	Category	Sub-category	Unit	Amount
F <sub>o</sub> Krypton-85		Emission to air	unspecified	kBq	3.49550E7
F <sub>o</sub> Hydrogen-3, Tritium		Emission to water	fresh water	kBq	1.36734E6
F <sub>o</sub> Heat, waste		Emission to air	unspecified	MJ	7.00177E5
F <sub>o</sub> Radon-222		Emission to air	unspecified	kBq	5.05256E5
F <sub>o</sub> tailings (unspecified)		Wastes	Mining waste	kg	4.59062E5
F <sub>o</sub> Air, used		Emission to air	unspecified	kg	3.64656E5
F <sub>o</sub> Water vapour		Emission to air	unspecified	kg	2.48104E5
F <sub>o</sub> Overburden (deposited)		Deposited goods	Stockpile goo...	kg	2.07613E5
F <sub>o</sub> Carbon dioxide		Emission to air	unspecified	kg	2.05840E5
F <sub>o</sub> Heat, waste		Emission to water	fresh water	MJ	1.09236E5
F <sub>o</sub> Radium-226		Emission to water	fresh water	kBq	1.53546E4
F <sub>o</sub> slag (unspecified)		Wastes	Production re...	kg	8481.44027
F <sub>o</sub> Red mud (dry)		Production resid...	Hazardous w...	kg	5923.55752
F <sub>o</sub> Xenon-133		Emission to air	unspecified	kBq	4425.04779
F <sub>o</sub> Nitrogen, atmospheric		Emission to air	unspecified	kg	4378.54231
F <sub>o</sub> Hydrogen-3, Tritium		Emission to air	unspecified	kBq	3905.08821
F <sub>o</sub> Argon-41		Emission to air	unspecified	kBq	1972.29516
F <sub>o</sub> Nitrogen dioxide		Emission to air	unspecified	kg	1962.74745
F <sub>o</sub> spoil (unspecified)		Wastes	Mining waste	kg	1756.00726
F <sub>o</sub> Chloride		Emission to water	ocean	kg	1672.68340

**Figure A.13.5 - Inventory result input/output of prototypes B production**

Figure A.13.6 and Figure A.13.7 show the results of the “impact assessment” concerning the production of 2750 TEGs of type A and B. The figures are shown in order of resulting amounts for each impact categories. These data show the impact on the environment caused by the production of the defined set of TEGs [32] [33].

Toxicity is expressed in terms of equivalent mass of 1,4-Dichlorobenzene ( $C_6H_4Cl_2$ ). Toxicity is calculated for different impact categories: marine environment (Marine Aquatic Ecotoxicity); human health (Human Toxicity); surface Earth water, as river, groundwater in aquifers, ice sheets, glaciers etc. (Freshwater Aquatic Ecotoxicity); terrestrial ecosystems (Terrestrial Ecotoxicity).

Depletion of non-renewable resources, in terms of fossil fuels energy consumption, is evaluated calculating the total energy consumed (Depletion of Abiotic Resources – fossil fuels). This data is expressed in terms of MJ.

Depletion of non-renewable resources, in terms of extraction of elements and ultimate reserves fossil fuels (natural gas, crude oil, coal and the non-conventional reserves), is evaluated calculating the total mass consumption (expressed in kg); the total mass, multiplied by a characterization factor (in kg of antimony equivalents/kg of extraction), gives an indicator, in kg of antimony equivalents, concerning the total depletion of abiotic resources (Depletion of abiotic resources –

elements, ultimate reserves). The choice of "antimony" to calculate the impact category indicator, for the impact category "abiotic depletion", is arbitrary. Choosing another substances will not change the relative result. Antimony was chosen because it is the first element in the alphabet for which is available a complete set of the required information [34].

Climate change effect is expressed in terms of kg of CO<sub>2</sub> equivalent mass, potentially dispersed into the environment and increasing greenhouse gases into the atmosphere (Climate Change – GWP100).

Average acidification of air, land and water in Europe, caused by various acid producers, is evaluated in terms of kg of SO<sub>2</sub> equivalent (Acidification potential – average Europe).

Enrichment of land and water with nutrients, especially compounds of nitrogen and phosphorus, is evaluated through kg of PO<sub>4</sub> equivalent (Eutrophication – generic).

Secondary air pollution caused by the chemical reaction of oxygen with emissions from fossil fuel combustion, activated by photochemical reactions, and producing other chemicals (as ozone, for example), is evaluated through kg of ethylene equivalents (Photochemical oxidation – high Nox).

Depletion of the Earth ozone layer, caused by emission of CFC or analogous contributory substances able to destroy stratospheric ozone, is evaluated through kg of CFC-11 equivalent (Ozone layer depletion – ODP steady state).

## LCIA Results

### ▼ LCIA Results

Impact category	Result	Reference unit
Marine aquatic ecotoxicity - MAETP inf	5.17332E8	kg 1,4-dichlorobenzene eq.
Depletion of abiotic resources - fossil fuels	8.67517E6	MJ
Climate change - GWP100	7.32364E5	kg CO <sub>2</sub> eq.
Human toxicity - HTP inf	4.56862E5	kg 1,4-dichlorobenzene eq.
Freshwater aquatic ecotoxicity - FAETP inf	5.36906E4	kg 1,4-dichlorobenzene eq.
Depletion of abiotic resources - elements, ultimate...	4.47355E4	kg antimony eq.
Terrestrial ecotoxicity - TETP inf	8075.14024	kg 1,4-dichlorobenzene eq.
Acidification potential - average Europe	3397.65129	kg SO <sub>2</sub> eq.
Eutrophication - generic	421.11810	kg PO <sub>4</sub> --- eq.
Photochemical oxidation - high Nox	266.91240	kg ethylene eq.
Ozone layer depletion - ODP steady state	0.04823	kg CFC-11 eq.

**Figure A.13.6** - Impact assessment result as function of the impact categories for prototypes A production

## LCIA Results

### ▼ LCIA Results

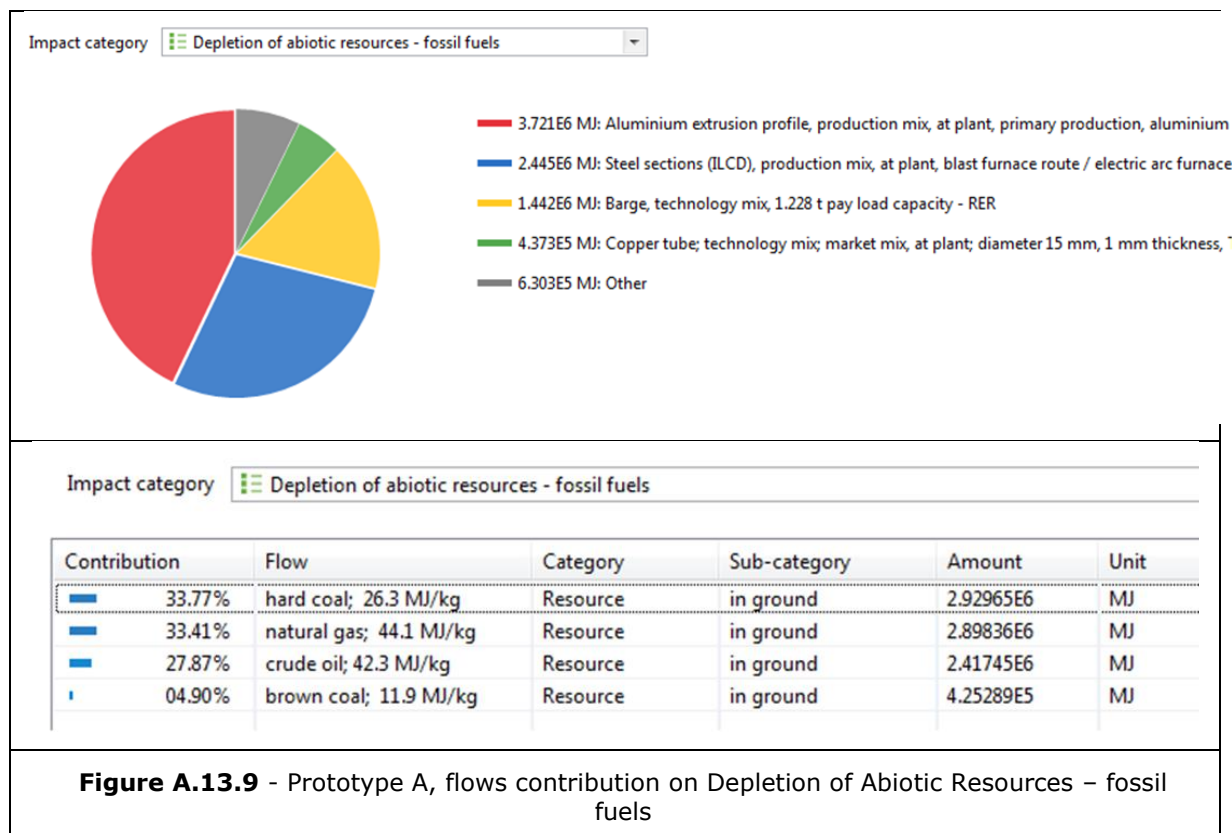
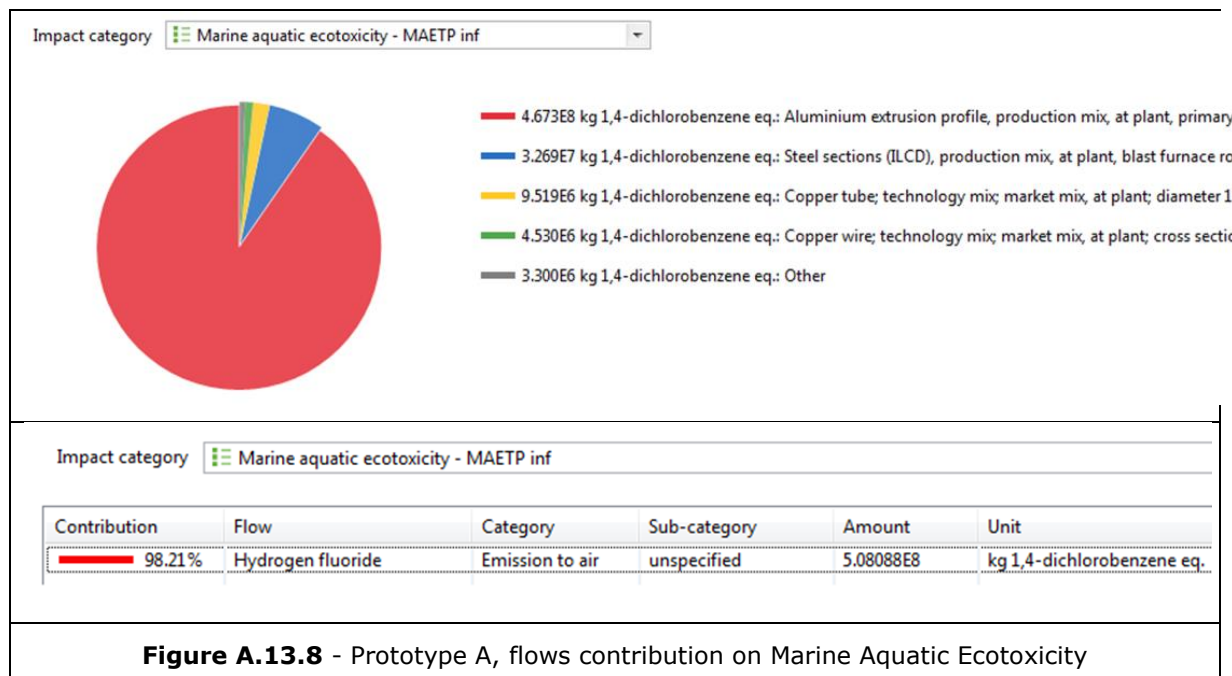
Impact category	Result	Reference unit
Marine aquatic ecotoxicity - MAETP inf	1.19885E8	kg 1,4-dichlorobenzene eq.
Depletion of abiotic resources - fossil fuels	2.78800E6	MJ
Climate change - GWP100	2.30107E5	kg CO <sub>2</sub> eq.
Human toxicity - HTP inf	6.08767E4	kg 1,4-dichlorobenzene eq.
Depletion of abiotic resources - elements, ultima...	1.31901E4	kg antimony eq.
Freshwater aquatic ecotoxicity - FAETP inf	4080.00973	kg 1,4-dichlorobenzene eq.
Eutrophication - generic	2111.61911	kg PO <sub>4</sub> --- eq.
Acidification potential - average Europe	1495.52475	kg SO <sub>2</sub> eq.
Terrestrial ecotoxicity - TETP inf	344.95482	kg 1,4-dichlorobenzene eq.
Photochemical oxidation - high Nox	97.77969	kg ethylene eq.
Ozone layer depletion - ODP steady state	0.11093	kg CFC-11 eq.

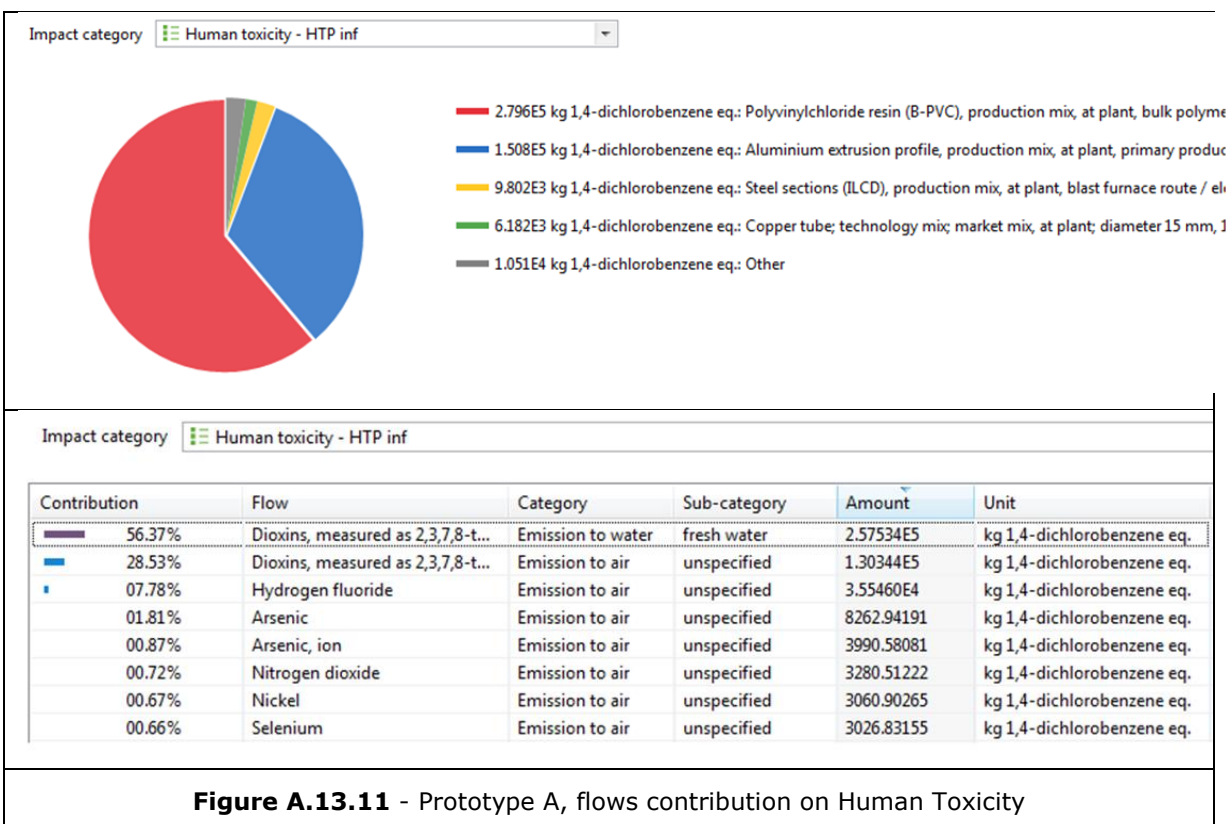
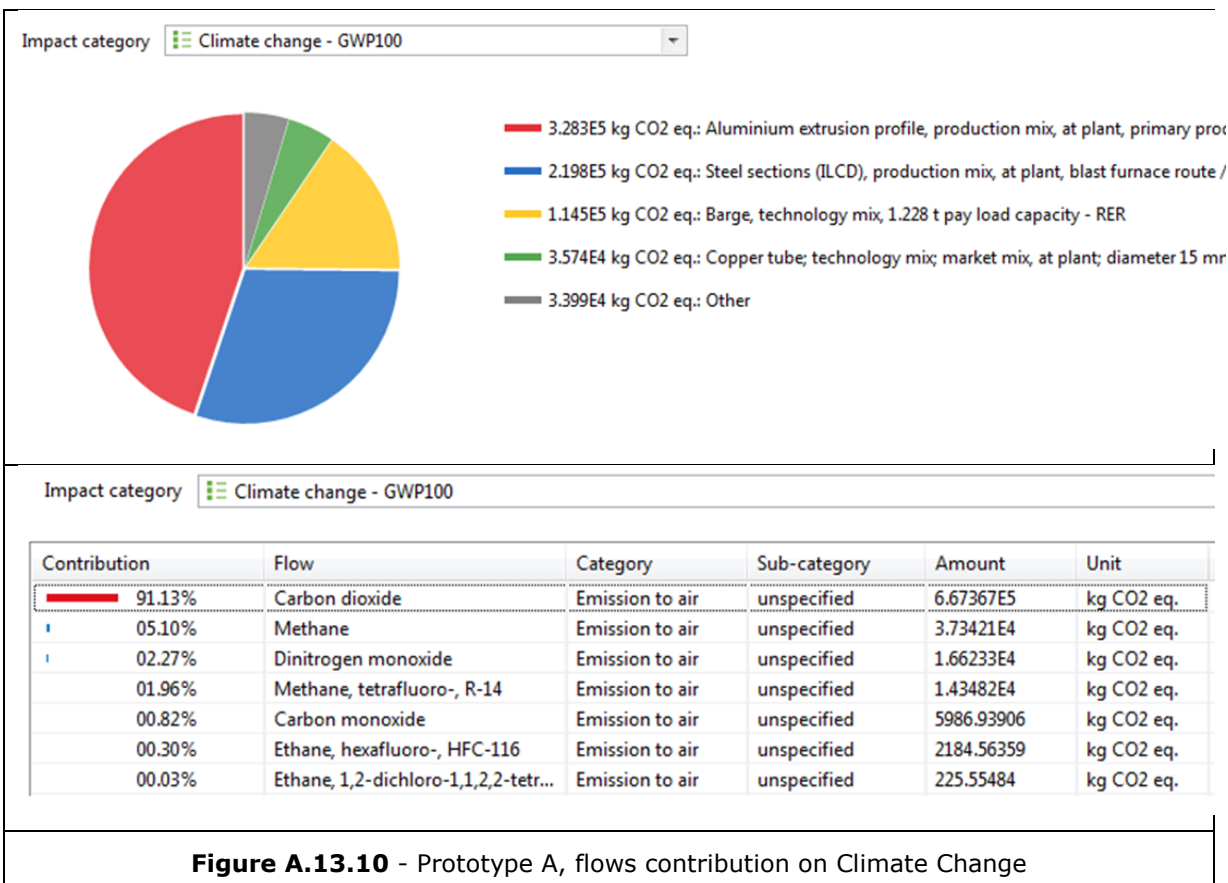
**Figure A.13.7** - Impact assessment result as function of the impact categories

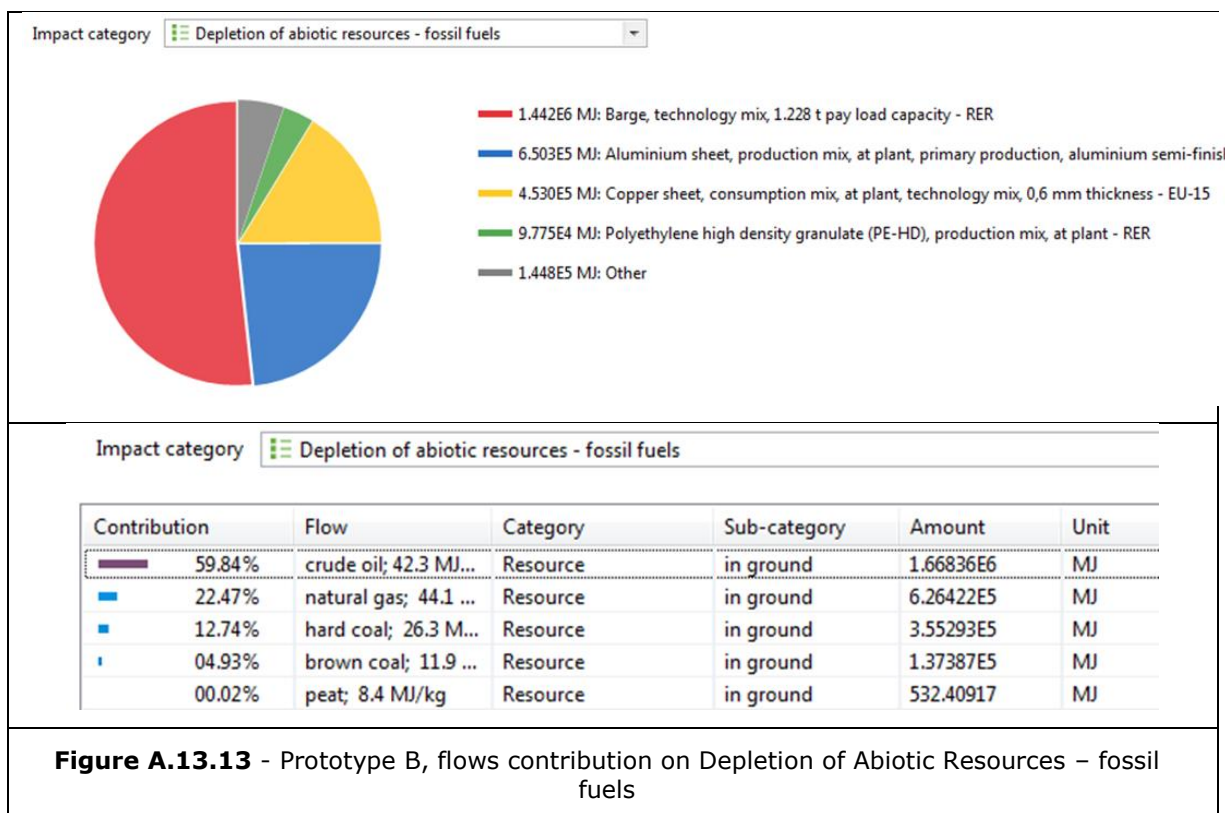
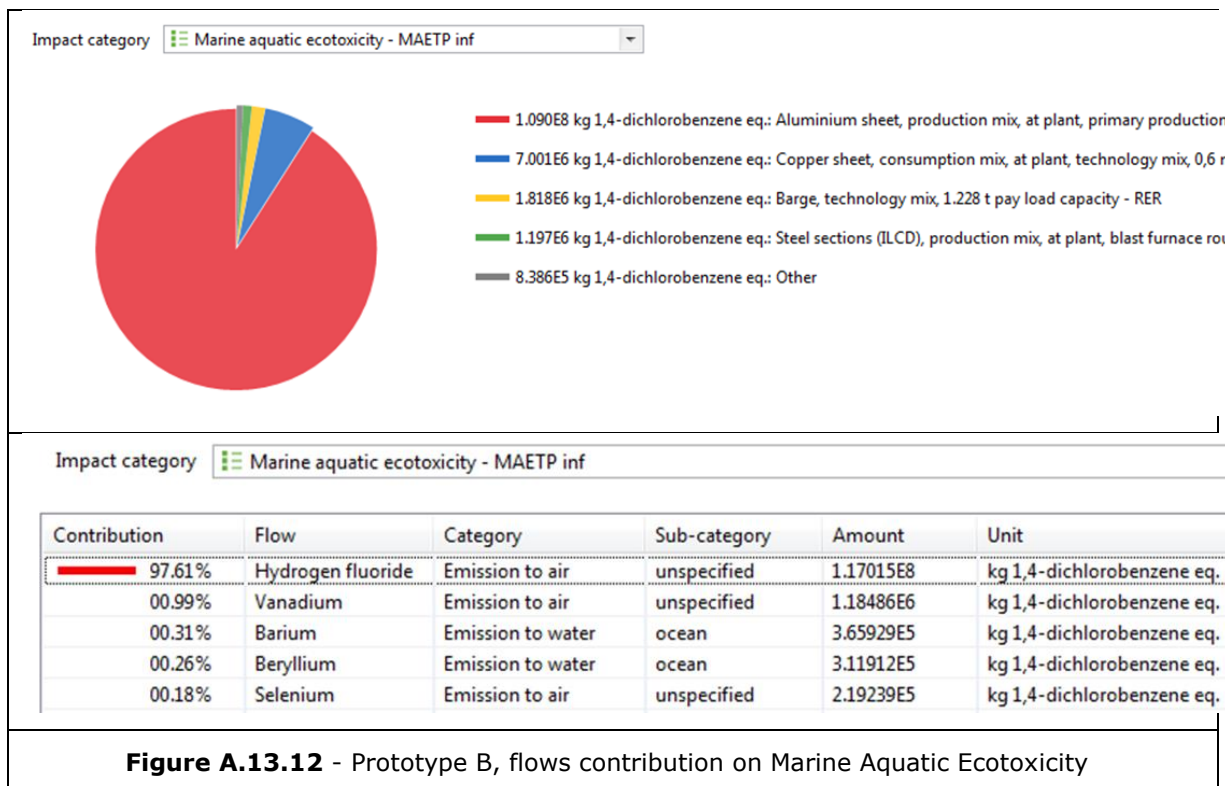
for prototypes B production

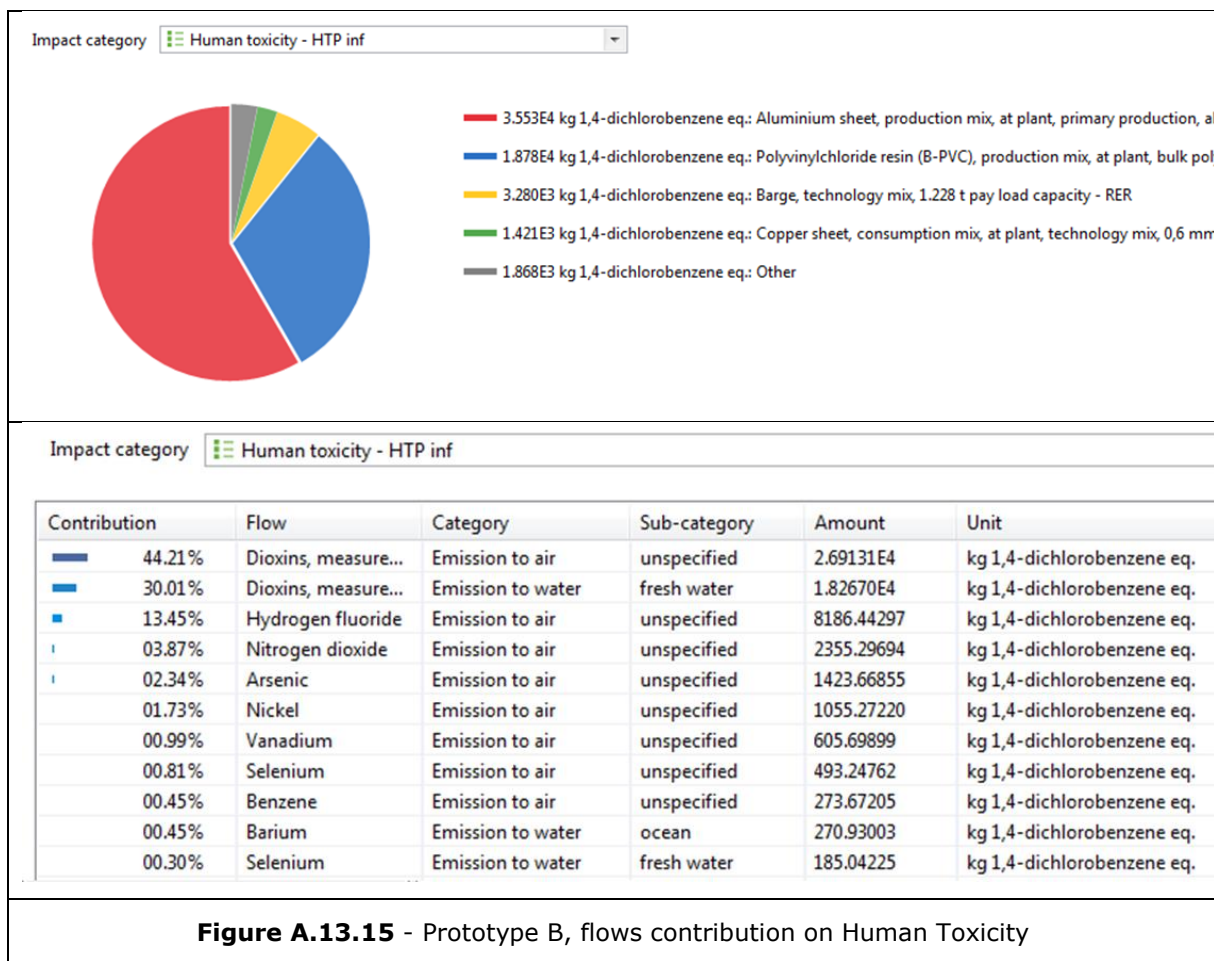
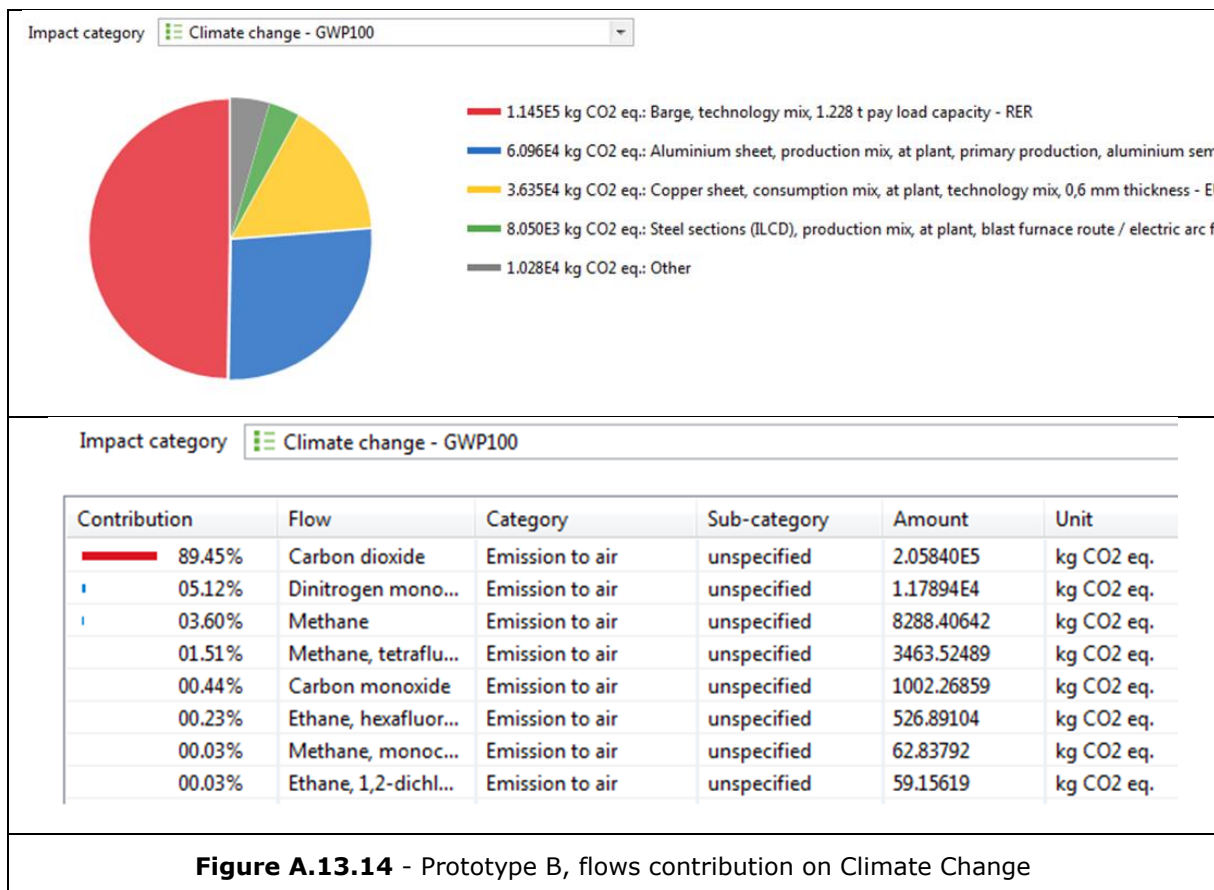
Figure A.13.8 to Figure A.13.11 reports the flows contribution to the impact categories for the case of prototype A production. These figures show both the flows, as reported in Table A.13.2, and the crisp output flows which contribute to the impact category. For space reason only the first four impact categories are shown.

Figure A.13.12 to Figure A.13.15 show the same analysis made for the prototype B production.









The “inventory results” show a large difference in energy consumption (energy input) for the two prototypes. This is caused by the large amount of steel (50 kg respect to 1.83 kg) and aluminium (50 kg respect to 6.93 kg) used to manufacture prototype A respect to prototype B. This gap is related both with the dimension of the two devices, and with the fact that prototype A includes a heavy structural frame. For the same reason, also “water” and “air” consumption of prototype A exceed more than about 60% and 70% the consumption of prototype B.

Concerning the outputs, the inventory results show a similar condition: the emissions caused by the production of the prototypes A exceed of about 70% the emissions caused by the production of prototype B.

Table A.13.3 shows the main data of flows input and output for each prototype, their difference and the percentage of the difference amount respect to the higher value. These figures show that the manufacture of prototype A requires higher flow inputs (consumption of material and energy) and flow outputs (emission into the environment) in respect to the manufacture of prototype B, and the differences of flows exceed from 59% to 77%. This gap is well related with the difference in weight between the two prototypes, which is measured in about 80% more to prototype A, as can be seen from the last raw of the table.

Concerning the “impact results” from Figure A.13.6 and Figure A.13.7 it can be noted that the first four “impact categories” are the same and in the same order. They are: marine and aquatic ecotoxicity, depletion of abiotic resources (fossil fuels), climate change and human toxicity.

Marine and aquatic toxicity is caused by release of hydrogen fluoride (HF) into the sea water. Hydrogen fluoride is very soluble in water and has deleterious effects on the cellular function of several biological systems [35]. It is possible to compare the figures obtained with the two TEGs production with that related with the emission of a coal fired plant. From literature hydrogen fluoride emission of a coal fired plant is 0.15 lb/t of coal [36]. Then, assuming the energy per mass of a coal plant 26 MJ/t, we have an emission of HF of 0.068 g/t (g of HF per tons of coal), or 2.61E-9 g/J. This value is not far from the figures obtained for the TEG prototypes, which are 4.3E-8 (prototype A) and 8.6E-9 (prototype B), assuming the MAETP conversion factor as 3.4E-2 kg of 1.4-Dichlorobenzene eq./kg [32].

Depletion of fossil fuels resources have the same flow sources for both the prototypes but different distribution. Prototype A production has the same contribution from hard coal (34%), natural gas (33%) and almost the same from crude oil (28%); instead prototype B production shows high depletion of crude oil (60%) and lower depletion for natural gas (22%) and hard coal (13%). This is caused by the different type of energy assumed (electricity mix) by the LCA database to produce steel and aluminium. In fact steel production has almost half of its worldwide production based on hard coal consumption, while aluminium production is basically based on electric power production and then on crude oil. In any case must be observed that depletion of fossil fuel, for both the prototypes, is caused by their manufactory process and not by their electric energy production, that is completely renewable. Therefore the impact of thermoelectric generators is totally not comparable with the huge impact caused by fossil fuel power generators.

Climate change is caused mainly by carbon dioxide emission, both for prototype A (91%) and prototype B (89%). It is important to note that figures refer to the manufacture of TEG systems, and not to greenhouse gases emission during electric power production. In terms of carbon footprint for electricity generation, both the thermoelectric systems have zero emissions, i.e. 0 gCO<sub>2</sub>eq/kWh, because both the systems do not produce any gas emission. However, of course there is a carbon footprint during the production and installation of the TEG systems. Considering these figures (see Table A.13.4), it is possible to obtain the carbon footprint for electricity production for prototypes A (69 gCO<sub>2</sub>eq/kWh) and prototype B (21 gCO<sub>2</sub>eq/kWh). These values are similar to other low-carbon renewable power plant systems, as Photovoltaic (75 to 116 gCO<sub>2</sub>eq/kWh), Geothermal (15 to 53 gCO<sub>2</sub>eq/kWh), Marine (15 to 40 gCO<sub>2</sub>eq/kWh), Wind (5 to 38 gCO<sub>2</sub>eq/kWh), Hydro (2 to 13 gCO<sub>2</sub>eq/kWh), Bioenergy (60 to 270 gCO<sub>2</sub>eq/kWh) or low carbon not-renewable power plant system as Nuclear (5 to 26 gCO<sub>2</sub>eq/kWh) [37]. And below average traditional household emissions as Coal (997 gCO<sub>2</sub>eq/kWh), Oil (861 gCO<sub>2</sub>eq/kWh), Natural gas (408 gCO<sub>2</sub>eq/kWh) [38]. Table A.13.4 shows also the carbon footprint per unit mass of thermoelectric system production, that is 1.99 kgCO<sub>2</sub>eq/kg for prototype A and 3.12 kgCO<sub>2</sub>eq/kg for prototype B. These figures can be interesting if compared with other production systems as, for example, food production, electronic materials production, buildings material production etc.

Toxicity for humans is caused mainly by dioxins dispersion in water and air, and by hydrogen fluoride dispersion in air. Dioxins dispersion has an impact of 84% for prototype A and 74% for prototype B of the total kg of 1.4-Dichlorobenzene equivalents emissions. Hydrogen fluorides has an impact of 7.78% in the case of prototype A and 13.45% in the case of prototype B. Also for this impact category must be observed that, for both the prototypes, dispersion of dioxins and hydrogen fluorides is caused by their manufactory process and not by their electric energy production. Therefore toxicity for humans caused by thermoelectric power production is totally

down the level of any kind of power production based on fired systems (coal fired, oil fired, biomass fired etc.).

		<b>TEG A</b>	<b>TEG B</b>	<b>difference</b>	<b>[%]</b>
<b>Flows Input (consumption)</b>					
energy input	[MJ]	1.15E+07	3.95E+06	7.59E+06	66
water surface	[kg]	2.57E+06	1.05E+06	1.52E+06	59
air	[kg]	1.81E+06	4.66E+05	1.35E+06	74
<b>Flows Output (emission)</b>					
heat waste	[MJ]	2.70E+06	7.00E+05	2.00E+06	74
krypton-85 radioactive emission	[kBq]	1.33E+08	3.50E+07	9.77E+07	74
air emission	[kg]	1.59E+06	3.64E+05	1.23E+06	77
carbon dioxide	[kg]	6.67E+05	2.06E+05	4.62E+05	69
total weight (water excluded, 2750 TEGs)	[kg]	3.36E+05	6.60E+04	2.70E+05	80

**Table A.13.3** - Flows input/output of the two prototypes production

		<b>TEG A</b>	<b>TEG B</b>
total electric energy production (2750 TEGs)	[kWh]	9636000	9636000
total weight (water excluded, 2750 TEGs)	[kg]	3.36E+05	6.60E+04
Greenhouse gas emission	[kgCO <sub>2</sub> eq.]	6.67E+05	2.06E+05
Carbon Footprint for electricity production	[gCO <sub>2</sub> eq/kWh]	69	21
Carbon Footprint for TEGs mass	[kgCO <sub>2</sub> eq/kg]	1.99	3.12

**Table A.13.4** – Climate change impact assessment results

### Conclusions and recommendations

The above findings show that Prototype A production has more impact on the environment than prototype B production, on equal electric power generation. This is caused by a greater weight of prototype A respect to prototype B. In terms of greenhouse emissions both the prototypes can be considered low-carbon renewable power production systems, with 69 and 21 gCO<sub>2</sub>eq/kWh carbon footprint. Concerning emission of toxic material into the environment, must be noted that electric production through thermoelectric generators produces these materials only during the manufactory phase, and not during the working period. Therefore, assuming that every power plant has comparable impact during the manufacture phase, TEGs must be considered as a green technology similar to wind, hydro or solar production and much better, for this impact category, than production methods based on combustion technologies.

No recommendation can be made to prefer one or the other prototype. In fact they have been designed to operate in two completely different conditions, involving their own advantages and disadvantages. Prototype A works as a cooler able to contemporarily cool water and produce electric energy, prototype B works as an heat recovery system able to convert lost radiant energy into electric energy. Therefore the two prototype have two different objectives and cannot be recommended the use of one respect the other.

The only general recommendation, that is valid for both prototypes, is to try to use thermoelectric materials consisting of less toxic materials and possibly very common on the Earth's crust, as explained in Sec. 3.5.2.5.



## **Annex A.14**

### **Deliverable D6.1: Description of the activities carried out in disseminating the results of the project (all partners)**

Below the list of the activities carried out in disseminating the results of the THERELEXPRO project:

<b>Date &amp; place, publisher</b>	<b>Congress, conference, meeting, workshop, journal</b>	<b>Type of dissemination (poster, slides paper)</b>	<b>Dissemination title</b>	<b>Authors</b>	<b>Other information</b>
22.02.2013 , Padova, Italy	Workshop: "Giornate sulla termoelettricità 2013"	Slides	Sviluppo di un prototipo per Thermoelectric Power Generation in ambiente industriale	U. Chiarotti	Oral presentation by Ugo Chiarotti
18.02.2015 , Milan, Italy	Workshop: "Giornate sulla termoelettricità 2015"	Slides	Development of a Small TEG Prototype for Energy Harvesting from low Temperature Waste Heat at Industrial Plant	F. Menchetti; U. Chiarotti; V. Moroli; R. Piancaldini; L. Bianco, A. Viotto; G. Baracchini; D. Gaspardo; F. Nazzi	Oral presentation by Fernando Menchetti
28.06.2015 , Dresden, Germany	34 <sup>th</sup> Annual International Conference on Thermoelectrics & 13 <sup>th</sup> European Conference on Thermoelectrics	Slides	Evaluation of Thermoelectric Generators by I-V Curves	G. Min, T. Singh, J. Garcia-Canadas, and R. Ellor	Oral presentation by Gao Min
28.06.2015 , Dresden, Germany	34 <sup>th</sup> Annual International Conference on Thermoelectrics & 13 <sup>th</sup> European Conference on Thermoelectrics	Poster	Determination Of Thermoelectric Figure-of-merit using 'Open/Short-circuit' Technique And I-V Curves	T. Singh; J. García-Cañadas; G. Min	
11.11.2015 , University of Reading, UK	UK Thermoelectric Network Meeting	Slides	Development of thermoelectric devices at Cardiff – design, fabrication and characterisation	G. Min	Oral presentation by Gao Min (as invited speaker)
19.11.2015 , Springer	Journal of Electronic Materials, March 2016, Volume 45, Issue 3, pp 1700–1704	Paper	Evaluation of Thermoelectric Generators by I-V Curves	G. Min, T. Singh, J. Garcia-Canadas, R. Ellor	
03.12.2015 , Hagen, Germany	Workshop: „Energierückgewinnung in Produktionsprozessen – Lösungsansätze für die	Slides	Erste Erfahrungen in der betrieblichen Umsetzung von TEG-Modulen	Mintus, F.; Stranzinger, B.	

	Massivumformung"				
11.02.2016 , Düsseldorf, Germany,	Thermoelektrika - Strom aus industrieller Abwärme	Slides	Erste Betriebserfahrungen mit TEG zur Nutzung industrieller Abwärme	B. Stranzinger, F. Mintus	
10.03.2016 , Nürnberg, Germany	ProcessNet Fachgruppe Hochtemperaturtechnik	Slides	Möglichkeiten zur Stromerzeugung aus industrieller Abwärme mittels Organic Rankine Cycle und Thermoelektrik	F. Mintus, B. Stranzinger, W. Adler	
08.06.2016 , Cologne, Germany	Thermoelektrik Kolloquium	Slides	Erste Betriebserfahrungen mit TEG zur Nutzung industrieller Abwärme in der Stahlindustrie	F. Mintus, B. Stranzinger	
01.03.2017 , American Scientific Publishers	Journal of Nanoscience and Nanotechnology, Volume 17, Number 3, March 2017, pp. 1586-1591(6)	Paper	Development of a Small Thermoelectric Generators Prototype for Energy Harvesting from Low Temperature Waste Heat at Industrial Plant	U. Chiarotti; V. Moroli; F. Menchetti; R. Piancaldini; L. Bianco; A. Viotto; G. Baracchini; D. Gaspardo; F. Nazzi; M. Curti; M. Gabriele	

## Getting in touch with the EU

### In person

All over the European Union there are hundreds of Europe Direct information centres. You can find the address of the centre nearest you at: [https://europa.eu/european-union/contact\\_en](https://europa.eu/european-union/contact_en)

### On the phone or by email

Europe Direct is a service that answers your questions about the European Union. You can contact this service:

- by freephone: 00 800 6 7 8 9 10 11 (certain operators may charge for these calls),
- at the following standard number: +32 22999696 or
- by email via: [https://europa.eu/european-union/contact\\_en](https://europa.eu/european-union/contact_en)

## Finding information about the EU

### Online

Information about the European Union in all the official languages of the EU is available on the Europa website

at: [https://europa.eu/european-union/index\\_en](https://europa.eu/european-union/index_en)

### EU publications

You can download or order free and priced EU publications at:

<https://publications.europa.eu/en/publications>. Multiple copies of free publications may be obtained by contacting Europe Direct or your local information centre (see [https://europa.eu/european-union/contact\\_en](https://europa.eu/european-union/contact_en)).

### EU law and related documents

For access to legal information from the EU, including all EU law since 1952 in all the official language versions,

go to EUR-Lex at: <http://eur-lex.europa.eu>

### Open data from the EU

The EU Open Data Portal (<http://data.europa.eu/euodp/en>) provides access to datasets from the EU. Data can be downloaded and reused for free, for both commercial and non-commercial purposes.

The project was devoted to develop and improve thermoelectric technology to recover waste heat from steel plants available at low temperature ( $T < 350^{\circ}\text{C}$ ) and convert it into electricity.

The main project objective was to verify the real economic feasibility of this energy harvesting system and identify which technological developments are needed to make this technology cost-effective.

Two thermoelectric generators, using the most common (and of different nature) hot sources at steel plants have been designed, manufactured and then installed at industrial plant site for testing. On the basis of the measured data, the electric conversion efficiency, the manufacturing best practices, and the estimation of electricity production cost have been analysed.

Furthermore it was investigated and compared the thermoelectric technology with different competing technologies and it was studied the effects on the environment of a large production of thermoelectric devices.

*Studies and reports*

